Stellar Structure and Evolution

Course at the Technische Universität München

Winter semester 2017/18

Prof. W. Hillebrandt,

Max-Planck-Institut für Astrophysik, Garching, Room 304

Tel.: 089 30000 2200

Email: wfh@mpa-garching.mpg.de

Web: www.mpa-garching.mpg.de/~wfh/

Stellar evolution – in brief

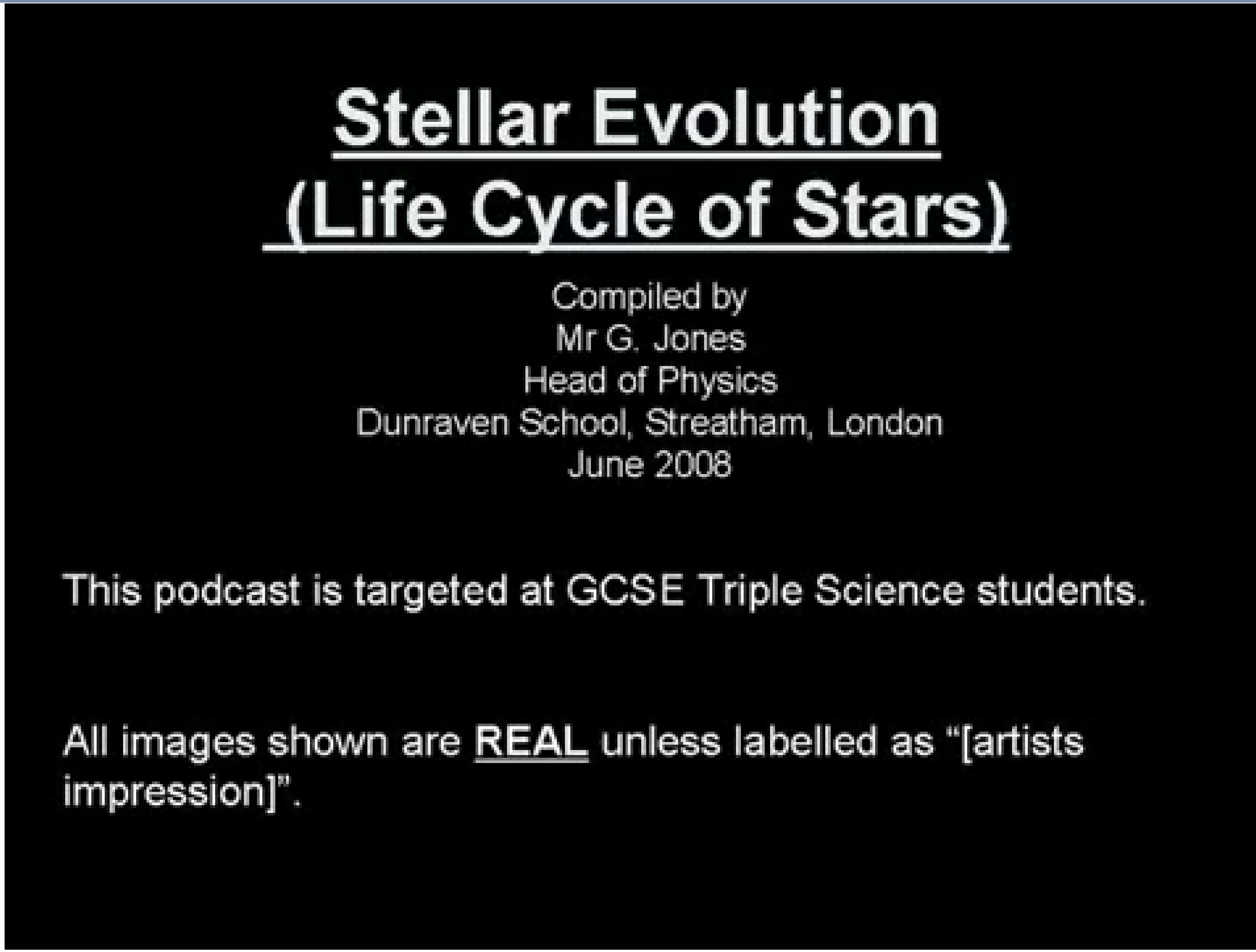

Stellar evolution - the HR diagram

Ejnar Hertzsprung (1873 – 1967)

Henry Norris Russel (1877 – 1957)

Stellar evolution - the HR diagram

The ‘Jewel Box’ cluster (credit: M. Bessel, MSSSO)

Stellar evolution - the HR diagram

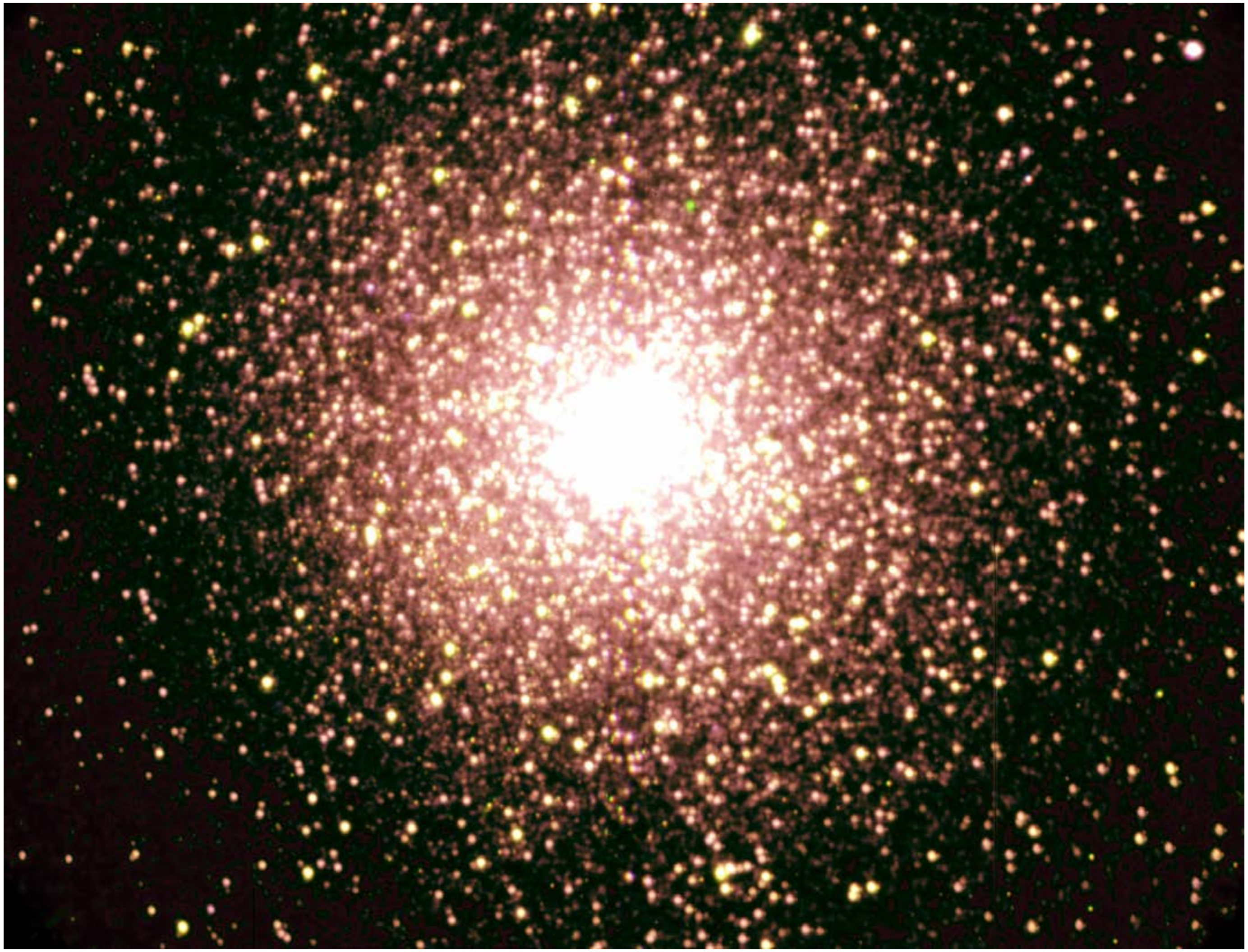

The globular cluster 47 Tucanae (credit: SALT)

Stellar evolution - the HR diagram

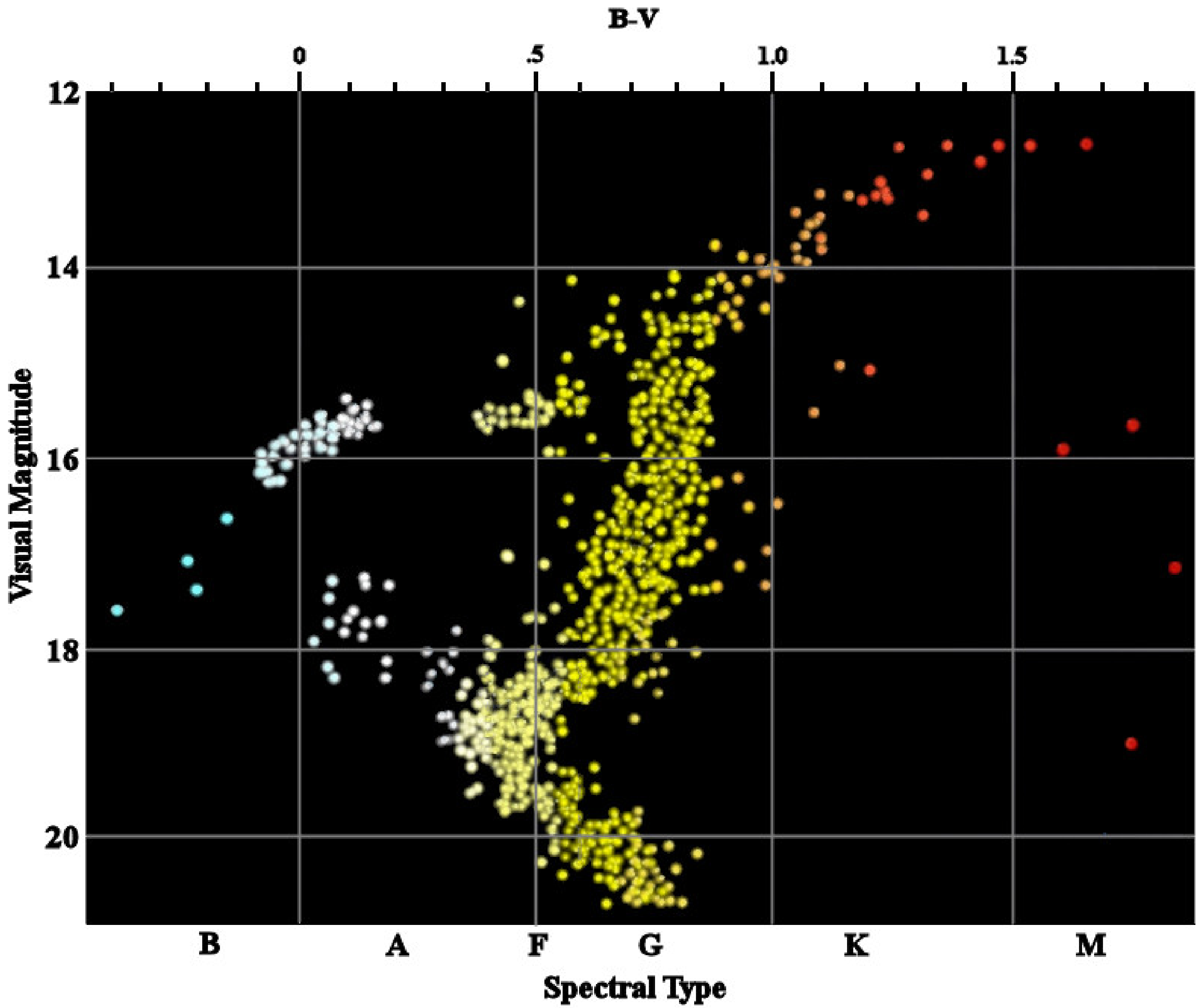

Stellar evolution - the HR diagram

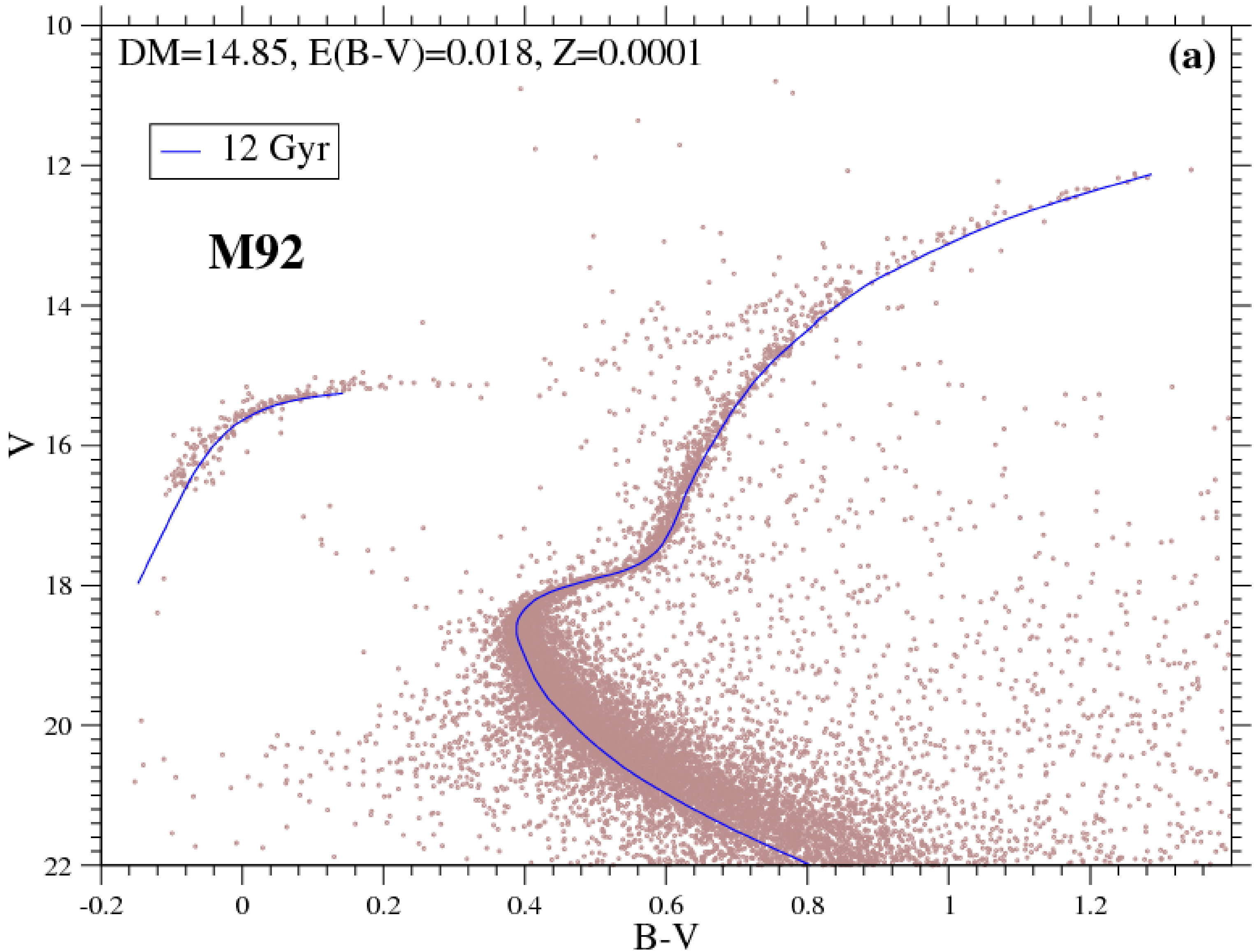

Stellar evolution - the HR diagram

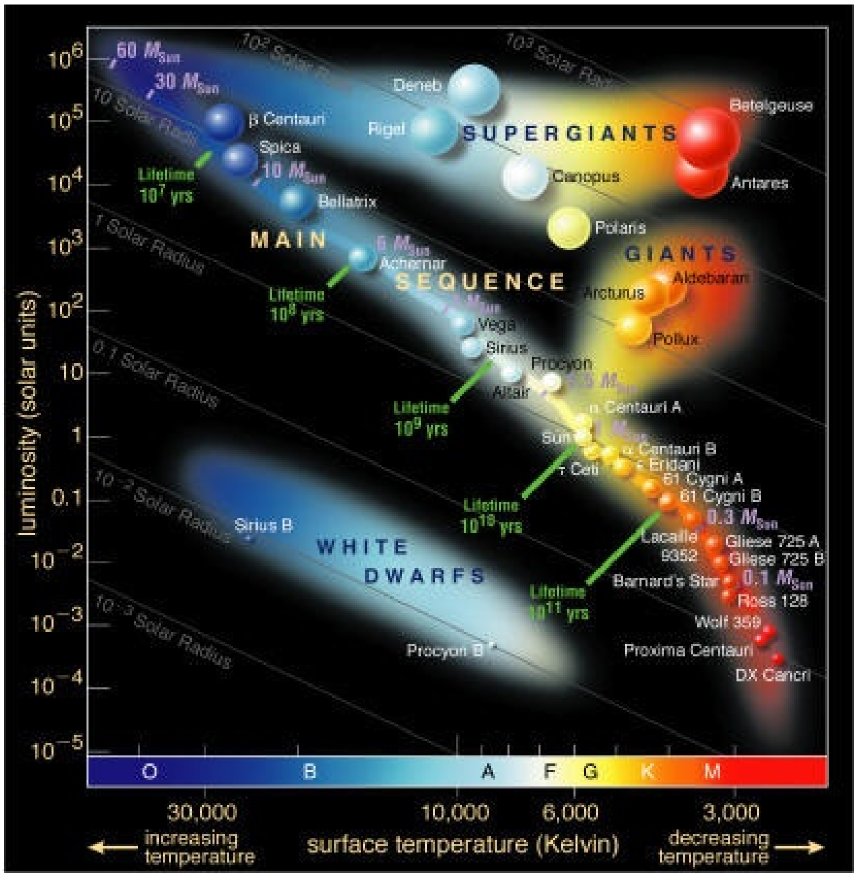

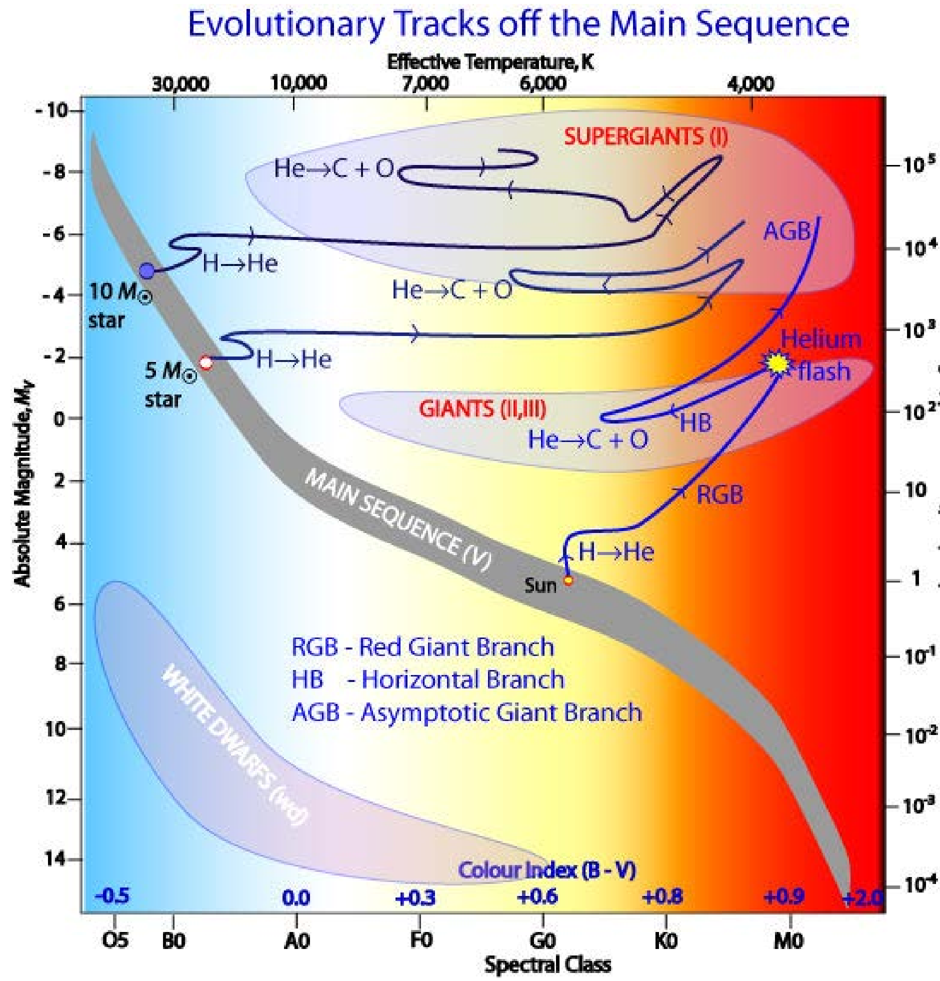

Content

I. Equations of stellar structure

1. The viral theorem and relevant timescales
2. Hydrostatic equilibrium
3. Energy generation in stars - thermonuclear reactions
4. Energy transport in stars
   - by radiation and heat conduction
   - by convection

II. Stellar evolution

1. Stellar models
2. Main-sequence evolution
3. Late stages of stellar evolution
4. Evolution of binary stars

Content

III. Stars as laboratories for fundamental physics

- Binary Black Hole merger & gravitational waves

IV. Stars and cosmology

- Stars as distance indicators

Suggested reading

1. R. Kippenhahn, A. Weigert & A. Weiss: *Stellar Structure and Evolution (Second Edition),* Springer Berlin (2012)
2. C.J. Hansen & S.D. Kwaler: *Stellar Interiors – Physical Principles, Structure and Evolutuion,* Springer Berlin (1994)
3. R.Q. Huang & K.N. Yu: *Stellar Astrophysics,* Springer Singapore (1998)
4. A. Weiss, W. Hillebrandt, H.-C. Thomas, & H. Ritter: *Cox & Giuli's Principles of Stellar Structure,* Cambridge Scientific Publishers (CSP) (2004)
5. M. Salaris & S. Cassisi: *Evolution of Stars and Stellar Populations,* J. Wiley & Sons Chichester (2005)
6. On MPA webpage (mostly in German!): http://www.mpa-garching.mpg.de/mpa/lectures/lectures-en.html

1. The virial theorem and relevant timescales

(i) Thermal energy (ideal gas)

$E_T = \frac{3}{2}\frac{\mathcal{R}}{\mu} \langle T \rangle M$ ($\mathcal{R}$=8.314·10^7 (erg/K·mol), μ= mean mol. weight)

(ii) Gravitational binding energy

$E_G = -\alpha \frac{G\,M^2}{R}$ $\quad \alpha \sim O(1)$

(iii) Nuclear energy

$E_N = 1.3 \cdot 10^{52} f X_H \frac{M}{M_{sun}}$

- $E_G \approx E_T << E_N$; Sun: $E_T \approx 5 \cdot 10^{48}$erg, $E_N \approx 10^{52}$erg

The virial theorem (in its simplest form)

1-atomic ideal gas:

$E_G = -2E_T$

In case of contraction:

$-\delta\, E_G > 0 \Rightarrow \delta\, E_T = -\frac{1}{2}\delta\, E_G > 0 \Rightarrow E_T \uparrow$

$-\frac{1}{2}\delta\, E_G > 0$ radiated away

Relevant timescales

(i) Dynamical timescale: $\tau_D = \sqrt{\frac{3}{8\pi G\rho}}$; sun: $\approx$ 3000 s

(ii) Kelvin-Helmholtz/thermal timescale: $\tau_{KH} := E_G/L$; $\tau_{th} := E_T/L$;

sun: $L = 4 \cdot 10^{33}$ erg/s $\Rightarrow \tau_{KH} \approx \tau_{th} \approx 3 \cdot 10^7$ years ($>> \tau_D$)

(iii) Nuclear timescale: $\tau_N = E_N/L = 1.3 \cdot 10^{52}\ f X_H M/M_{sun}/L$

sun: $\tau_N \approx 10^{10}$ years

Lord Kelvin (1824-1907), H.v.Helmholtz (1821-94)

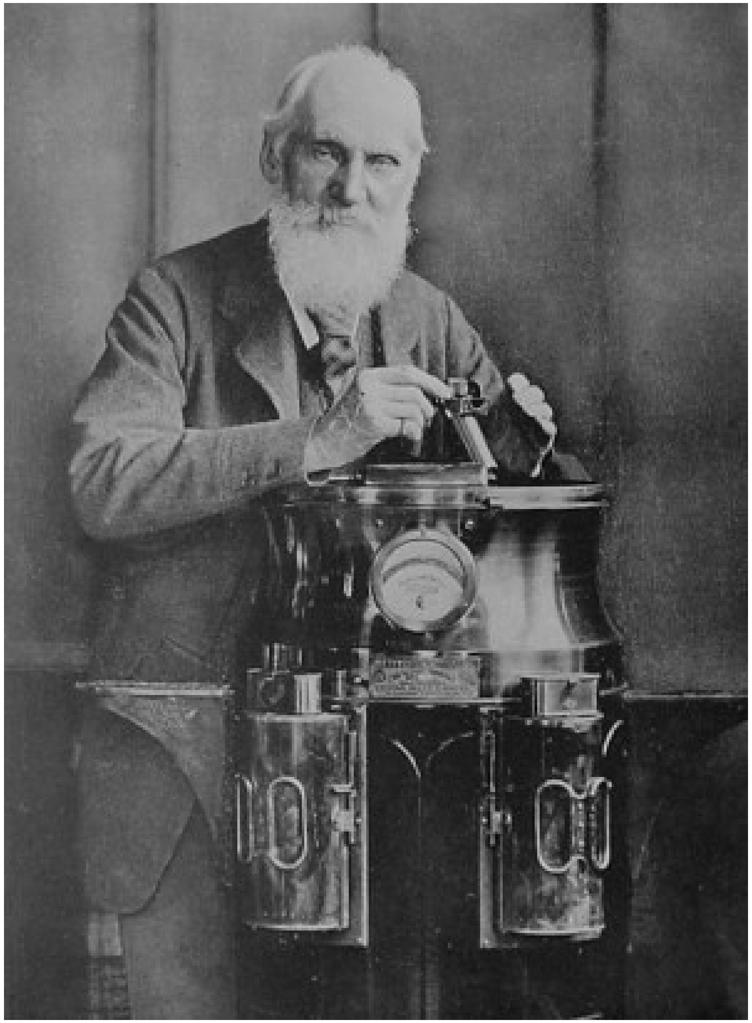

Sir Arthur S. Eddington (1882 – 1944)

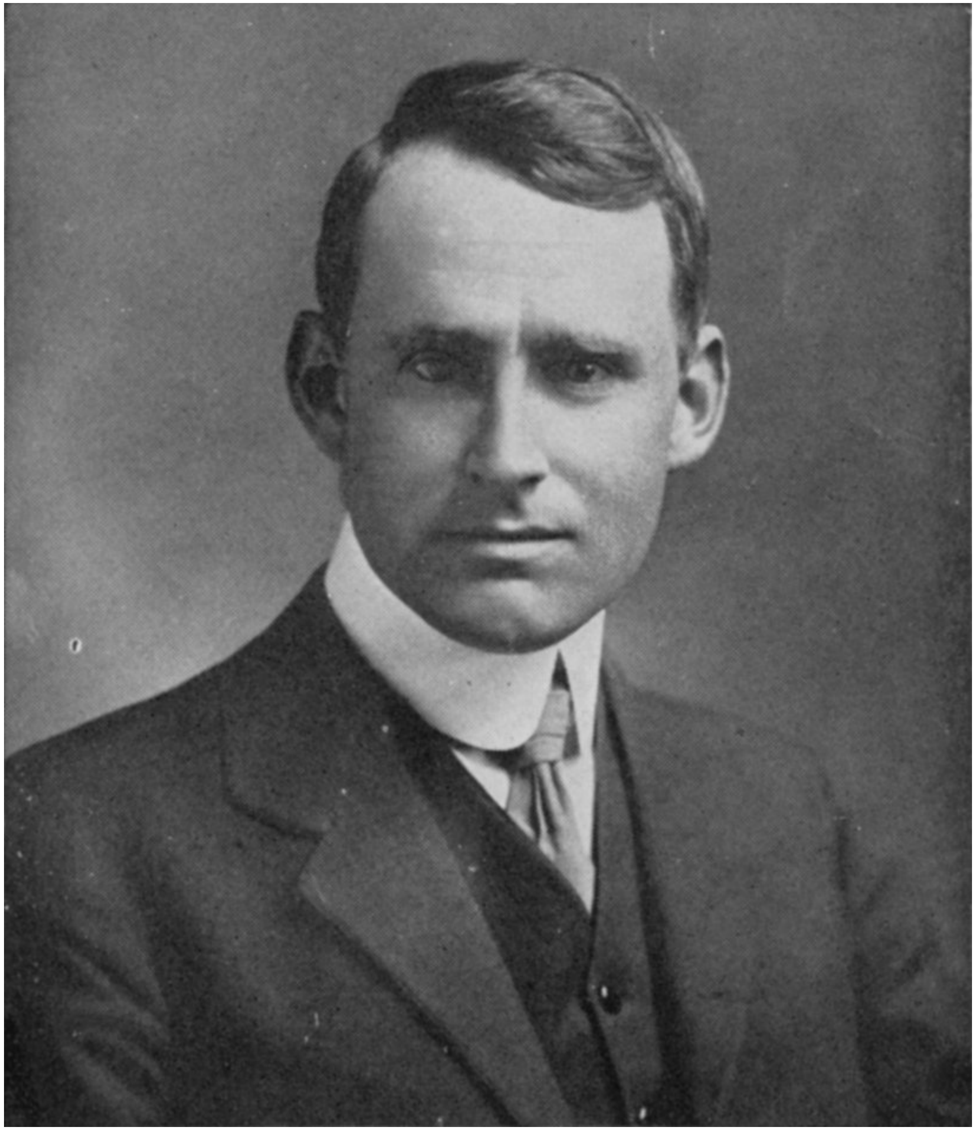

Stellar structure equations

$$\frac{\mathrm{d}m}{\mathrm{d}r} = 4\pi r^2 \rho.$$

mass conservation
($m = m(r) = M_r$)

$$\frac{\mathrm{d}P}{\mathrm{d}r} = -\frac{Gm\rho}{r^2}$$

momentum conservation
(ρ: density; P: pressure)

$$\frac{dL}{dr} = 4\pi r^2 \rho \left(\epsilon - \epsilon_\nu\right)$$

energy conservation
($L = L(r) = L_r$: luminosity,
$\varepsilon = \varepsilon_N$: nuclear energy generation rate)

Closure equations

(i) Equation of state (EoS)

a) Ideal gas equation of state:

$P/\rho = (\gamma-1)u$; $\gamma = C_P/C_V$ ('adiabatic index'); u = energy/gram

1-atomic ideal gas:

$P = nk_BT$, $\rho u = 3/2\ nk_BT \Rightarrow P/\rho = 2/3\ u$, $\gamma = 5/3$

Photon gas:

$P_{rad} = 1/3\ aT^4$, $\rho u_{rad} = aT^4$; $P_{rad}/\rho = 1/3\ u_{rad}$, $\gamma = 4/3$

$k_B = 1.380 \bullet 10^{-16}$ erg/K; $a = 7.565 \bullet 10^{-15}$ erg/cm^{3}K^4

Closure equations

(ii) Energy transport equation (see Section I.4)

Example: diffusion of radiation, black body

$$\frac{dT}{dr} = -\frac{3}{4ac}\frac{\kappa\varrho}{T^3}\frac{L}{4\pi r^2}\ ;\ \kappa = mean\ opacity$$

(iii) Nuclear energy generation rates (see Section I.3)

Example: Hydrogen burning

$$\varepsilon_N = \varepsilon_0 \rho T^\alpha, \qquad \alpha \sim 4\ (pp)\ or \sim 17 - 20\ (CNO)$$

Stellar evolution- schematically

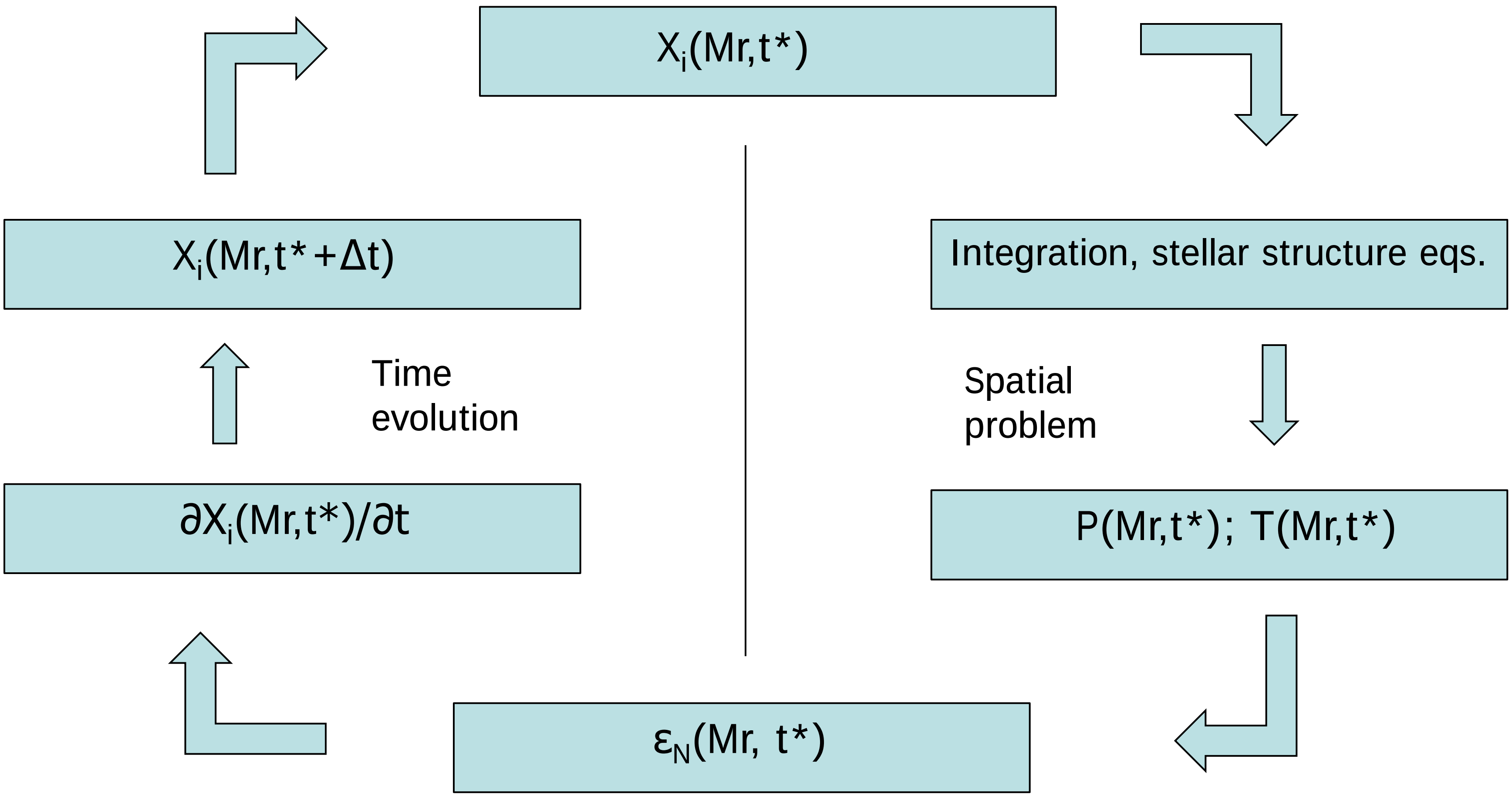

The MESA code

Go to:

http://mesa.sourceforge.net

The MESA code

My Shots

code capabilities

mesa.sourceforge.net 1 minute ago expires in 14 days

Download

MESA
Modules for Experiments in Stellar Astrophysics

- MESA home
- code capabilities
- prereqs & installation
- getting started
- using pgstar
- using MESA output
- beyond inlists (extending MESA)
- troubleshooting
- FAQ
- star_job defaults
- controls defaults
- pgstar defaults
- binary_controls defaults
- news archive
- documentation archive

MESA

Contents

What kinds of things can MESA do?

For a brief summary of the capabilities of MESA, take a look at this **presentation by Matteo Cantiello**. (He has also provided a **Keynote version**.)

The full capabilities of MESA are documented in the instrument papers. Looking through the figures will give you a feel for the broad range of problems that can be studied using MESA.

- **Paper 1 (Paxton et al. 2011)**
- **Paper 2 (Paxton et al. 2013)**
- **Paper 3 (Paxton et al. 2015)**

Additional capabilities are documented by MESA users in their publications

- **Citations to Instrument Paper 1**
- **Citations to Instrument Paper 2**
- **Citations to Instrument Paper 3**

To give you yet more flavor of what MESA can do, here are some movies made using png output from mesa/star.

Evolve a 1 Msun star

Latest News

- 21 Sep 2017
  » **New MESA SDK Version**
- 12 Sep 2017
  » **Release 10000**
- 01 Sep 2017
  » **Docker, Python and Web**
- 14 Aug 2017
  » **New mesa-users list**
- 02 Aug 2017
  » **New MESA SDK Version**
- 31 May 2017
  » **Release 9793**
- 08 Apr 2017
  » **MESA Marketplace**
- 17 Feb 2017
  » **Release 9575**
- 25 Jan 2017
  » **Diffusion Updates**
- 08 Jan 2017
  » **Summer School 2017**

H. Bethe (1906-2005), C.F.v.Weiszäcker(1912-2007)

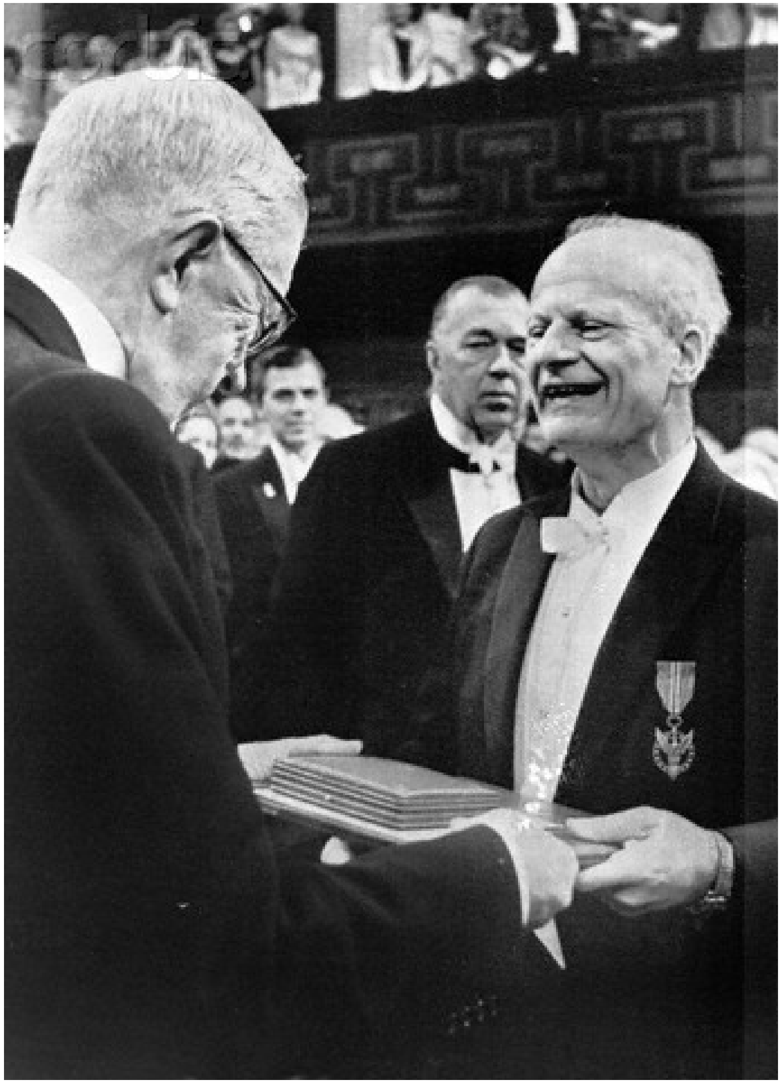

Reaction network equations

$$\frac{\mathrm{d}Y_i}{\mathrm{d}t} = \sum_j N_i \lambda_j Y_j + \sum_{j,k} \frac{N_i}{N_j! N_k!} \rho N_\mathrm{A} \langle \sigma v \rangle_{j,k} Y_j Y_k + \sum_{j,k,l} \frac{N_i}{N_j! N_k! N_l!} \rho^2 N_\mathrm{A}^2 \langle \sigma v \rangle_{j,k,l} Y_j Y_k Y_l .$$

$Y_i = X_i/A_i$: abundance od species i; N_i: number of species i produced in the reaction; N_A: Avogadro number; $<\sigma v>$: Maxwell averaged cross section

CNO cycles

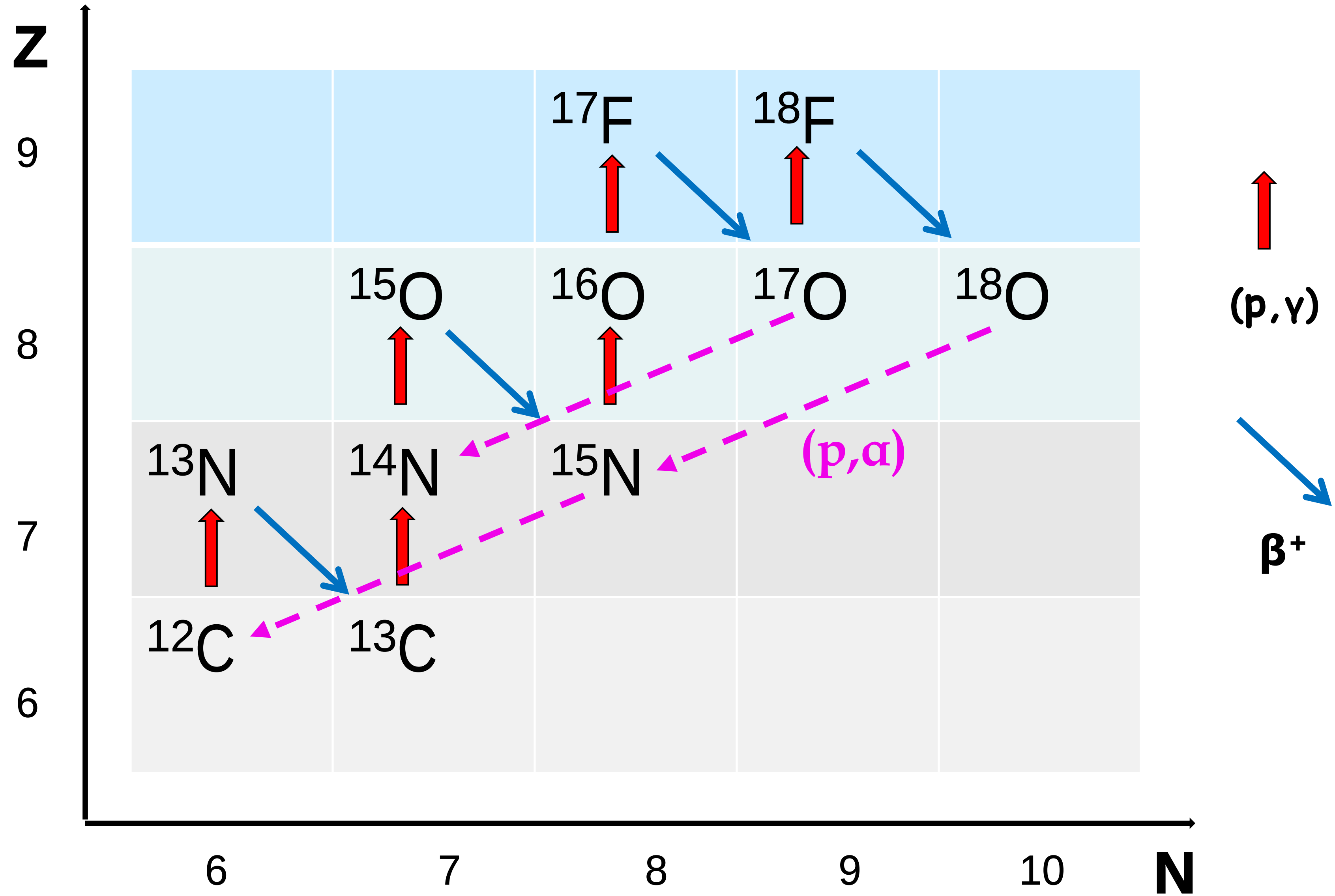

Z
9
8
7
6
^{17}F
^{18}F
^{15}O
^{16}O
^{17}O
^{18}O
^{13}N
^{14}N
^{15}N
^{12}C
^{13}C
(p,α)
(p,γ)
β+
6
7
8
9
10
N

CNO-bicycle – reaction equations

$dY_{^{12}C}/dt = -\lambda_{p^{12}C}\, Y_p Y_{^{12}C} + \alpha_1 \lambda_{p^{15}N} Y_p Y_{^{15}N}$ (p,α)

$dY_{^{13}N}/dt = -\lambda_{e+^{13}N} Y_{^{13}N} + \lambda_{p^{12}C} Y_p Y_{^{12}C}$

$dY_{^{13}C}/dt = +\lambda_{e+^{13}N} Y_{^{13}N} - \lambda_{p^{13}C} Y_p Y_{^{13}C}$

.

.

.

$dY_{^{16}O}/dt = -\lambda_{p^{16}O}\, Y_p Y_{^{16}O} + \alpha_2 \lambda_{p^{15}N} Y_p Y_{^{15}N}$ (p,γ) ($\alpha_1+\alpha_2=1$)

<u>Net result: $4p \Rightarrow {}^4He + 2e^+ + 2\nu_e$; $Q \approx 26$ MeV</u>

Maxwell-averaged reaction rates

$$< \sigma v >$$

$$= \left(\frac{8N_A}{A_{ij}\pi}\right)^{1/2} (k_B T)^{-3/2} \int_0^\infty E\sigma(E) \exp\left(-\frac{E}{k_B T}\right) dE$$

$N_A = 6.0247 \bullet 10^{23}\ g^{-1}$

$$r_{ij} \coloneqq (1 + \delta_{ij})^{-1} n_i n_i < \sigma v >$$

Nuclear reaction cross sections

Incoming particle `sees` (repulsive) potential:

$$V_l = \frac{l(l+1)\hbar^2}{2\mu r^2} + \frac{Z_1 Z_2 e^2}{r} \quad \text{(angular momentum + Coulomb barrier)}$$

In general: $< E_{kin} > \ll E_C \Rightarrow QM\ tunneling\ through\ barrier$

Two possibilities:

- Non-resonant reactions: no state in compound nucleus at E_{kin}
- Resonant reactions: state at or near E_{kin}

Non-resonant reactions (l=0 only):

$$V_c = \frac{Z_1 Z_2 e^2}{r} = \frac{1.44\ Z_1 Z_2}{r(fm)}\ (\text{MeV})$$

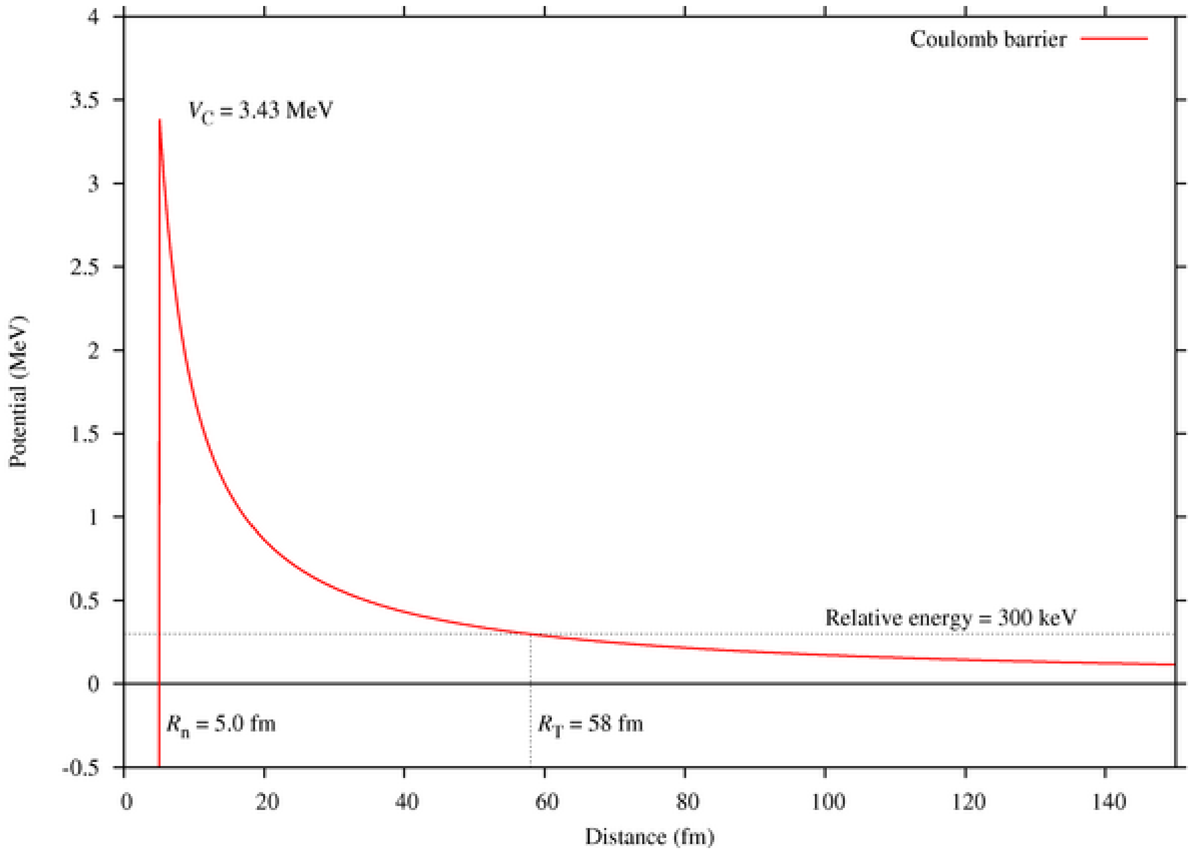

Coulomb barrier 12C + 4He

Nuclear reaction cross sections

Barrier penetrability: $P_C \propto e^{\frac{-2\pi Z_1 Z_2 e^2}{\hbar v}}$

Effective cross section:

$\propto \lambda^2\pi$; $\lambda = de\ Broglie\ wavelength = \frac{\hbar}{m_0 v}\left(1-\frac{v^2}{c^2}\right)^{1/2} \cong \frac{\hbar}{p}$

$$\Rightarrow \pi\lambda^2 \propto \left(\frac{1}{p}\right)^2 \propto \frac{1}{E}$$

$$\Rightarrow \sigma(E) =: \frac{S(E)}{E} exp\left\{-\frac{2\pi Z_1 Z_2 e^2}{\hbar v}\right\}$$

(defines S(E), \`astrophysical S-factor\`)

Advantage: less energy dependent than $\sigma(E)$!

Reaction rates and S-factor

Reaction rate versus Temperature
for some astrophysical deuteron reactions

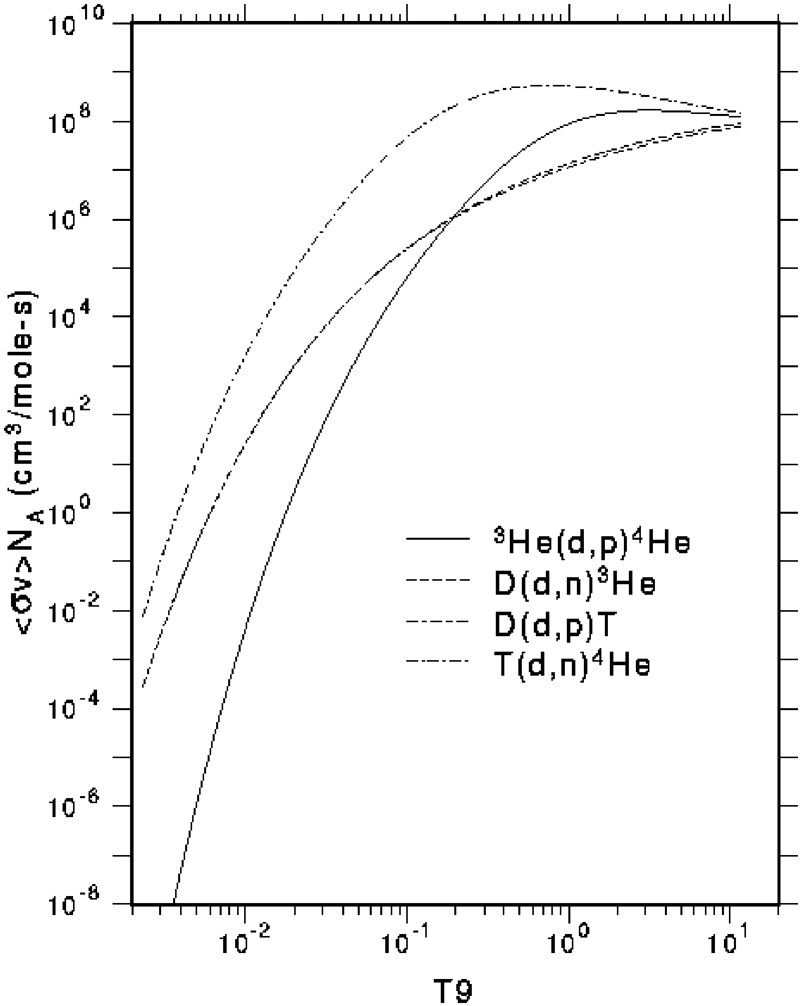

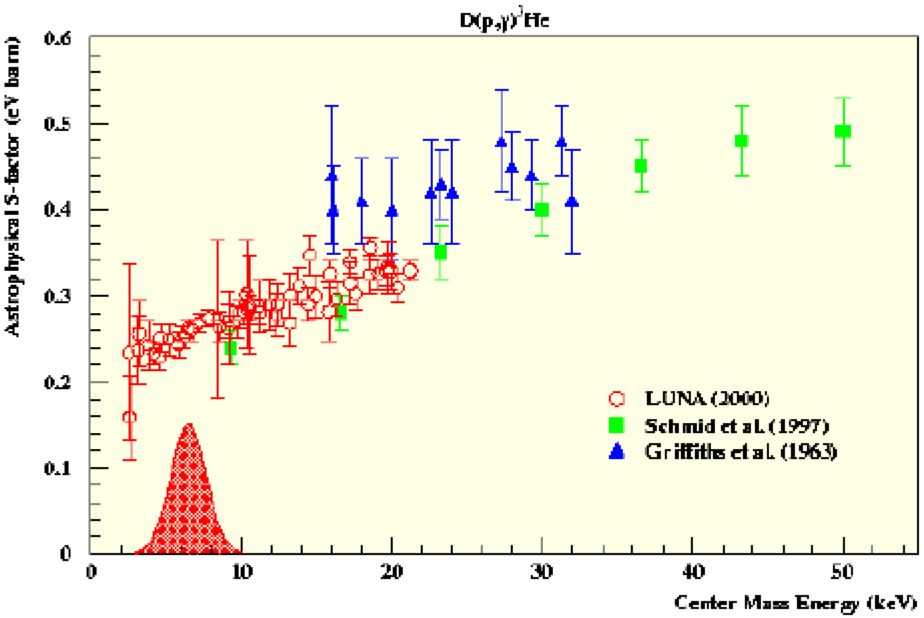

Effective stellar energies-Gamov peak

Write cross section as:

$$\sigma(E) = \frac{S(E)}{E} exp\left(-bE^{-1/2}\right),$$

where b=31.28•$Z_1 Z_2 A^{1/2}$, $A = A_1 A_2/(A_1+A_2) = \mu/M_u$

In <σv>: Integral over product of Maxwell-distribution $\left(\propto \exp\left(-\frac{E}{k_B T}\right)\right)$ and coss section $(\propto \exp(-bE^{-\frac{1}{2}})$.

Peaks at: $E_0 = 1.220(Z_1^2 Z_2^2 A T_6^2)^{1/3}$ *(`effective` stellar energy)*

(typically ~ $10 k_B T$)

Gamov peak

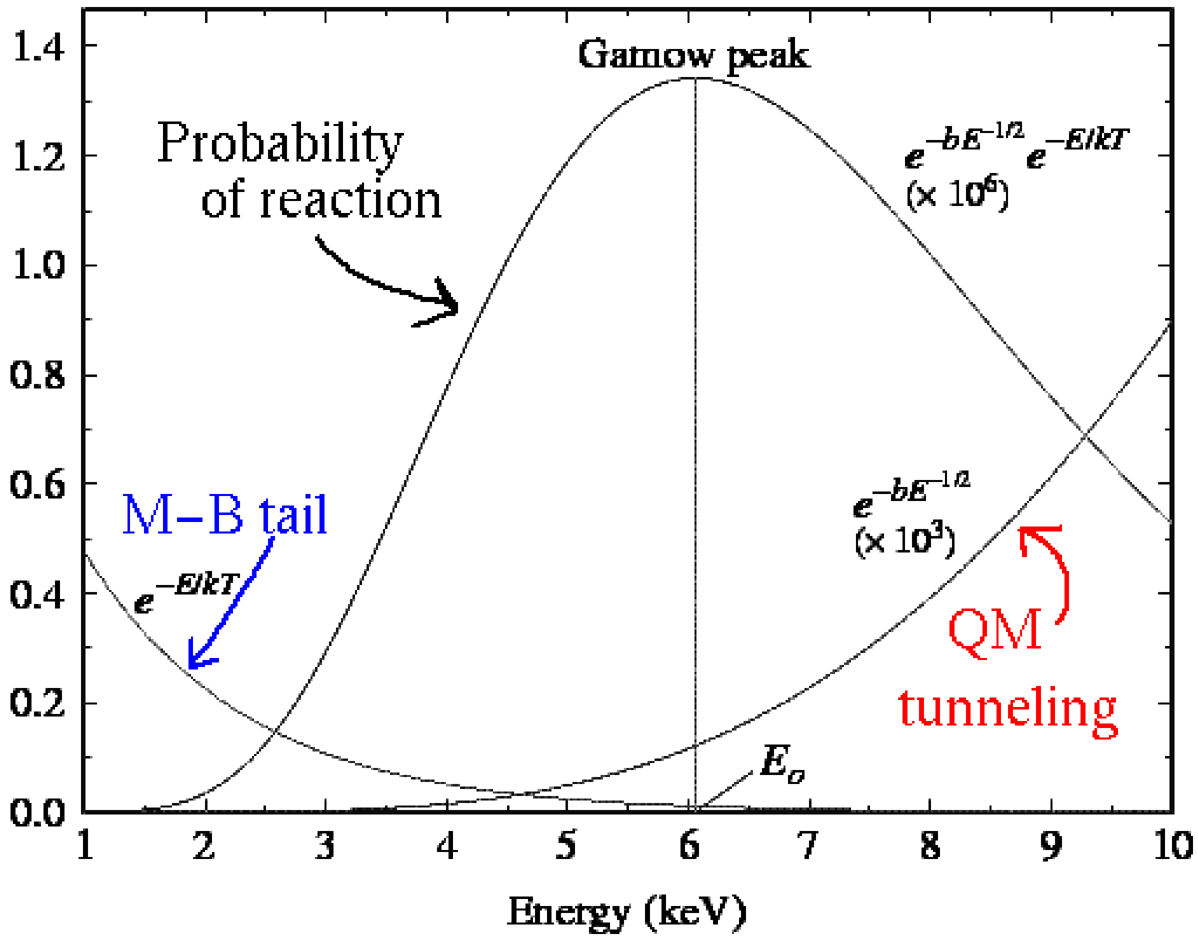

Gamow peak
Probability of reaction
$e^{-bE^{-1/2}} e^{-E/kT}$
($\times 10^6$)
$e^{-bE^{-1/2}}$
($\times 10^3$)
M–B tail
$e^{-E/kT}$
QM tunneling
E_o
1.4
1.2
1.0
0.8
0.6
0.4
0.2
0.0
1
2
3
4
5
6
7
8
9
10
Energy (keV)

Gamov peak for ^{12}C + ^{4}He

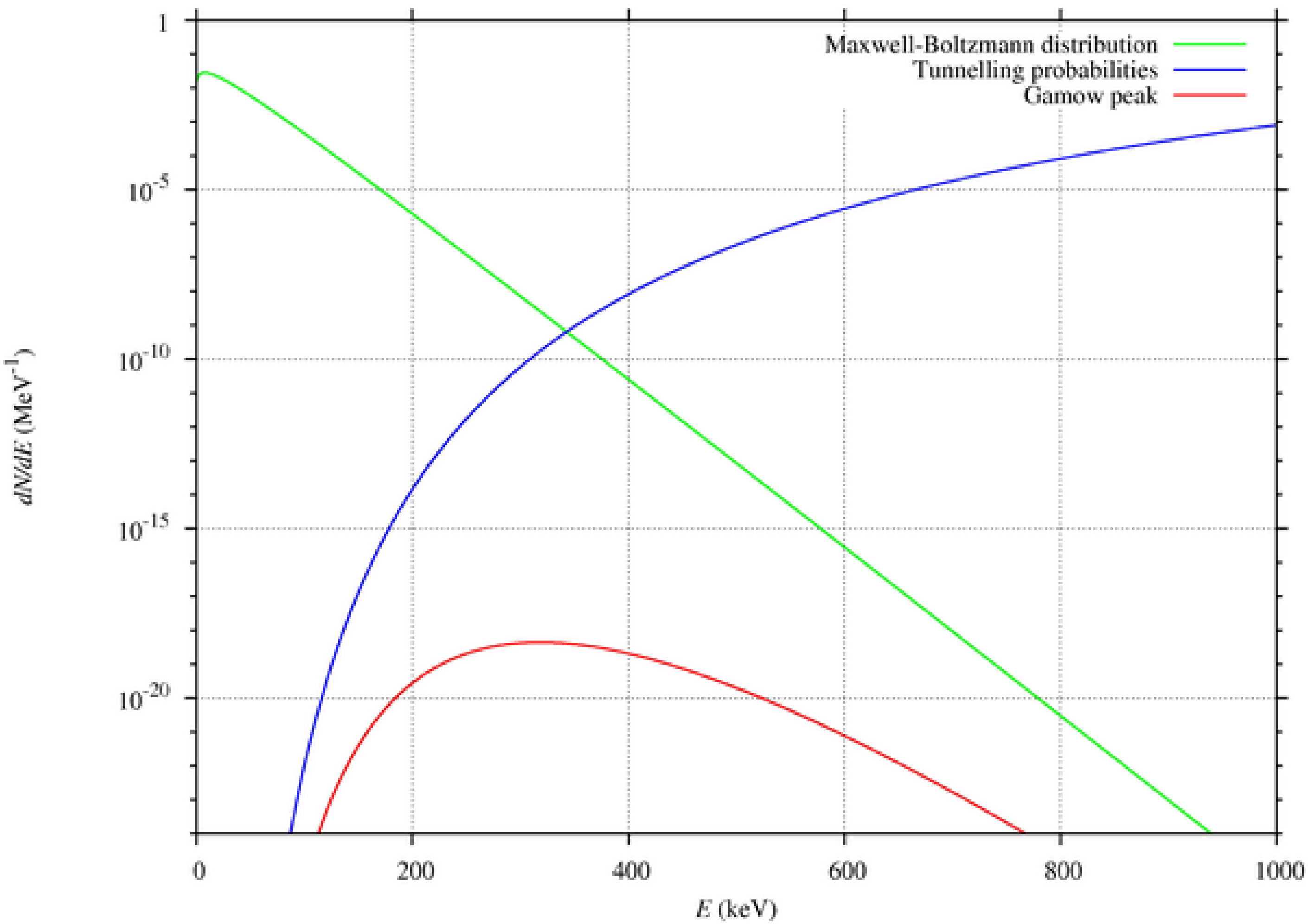

`Astrophysical` S-factor

S(E) from extrapolations of experimental data (if available) or from theory

<u>Examples:</u>

- *Statistical model (good for rather heavy nuclei)*
- *Direct captures, optical potential*

<u>Reference:</u>

C. Iliadis: *Nuclear Physics of Stars; Wiley-VCH, Berlin (2007) (contains resonant reactions also)*

Resonant reaction rates (in brief)

- Mostly relevant for ligth nuclei ($A \leq 30$)
- A particular state in the compound nucleus is at E_i:
  `resonant reaction’
- No problem for broad resonances, but:

  $\rightarrow$ Narrow resonances

  $\rightarrow$ Sub-threshold resonances

- Apply Breit-Wigner resonance formula
  (Blatt & Weisskopf: Theoretical Nuclear Physics, Dover (1991))

Examples, sub-threshold reactions

S-factor for α+^{12}C E1 capture (from an *R*-matrix fit)

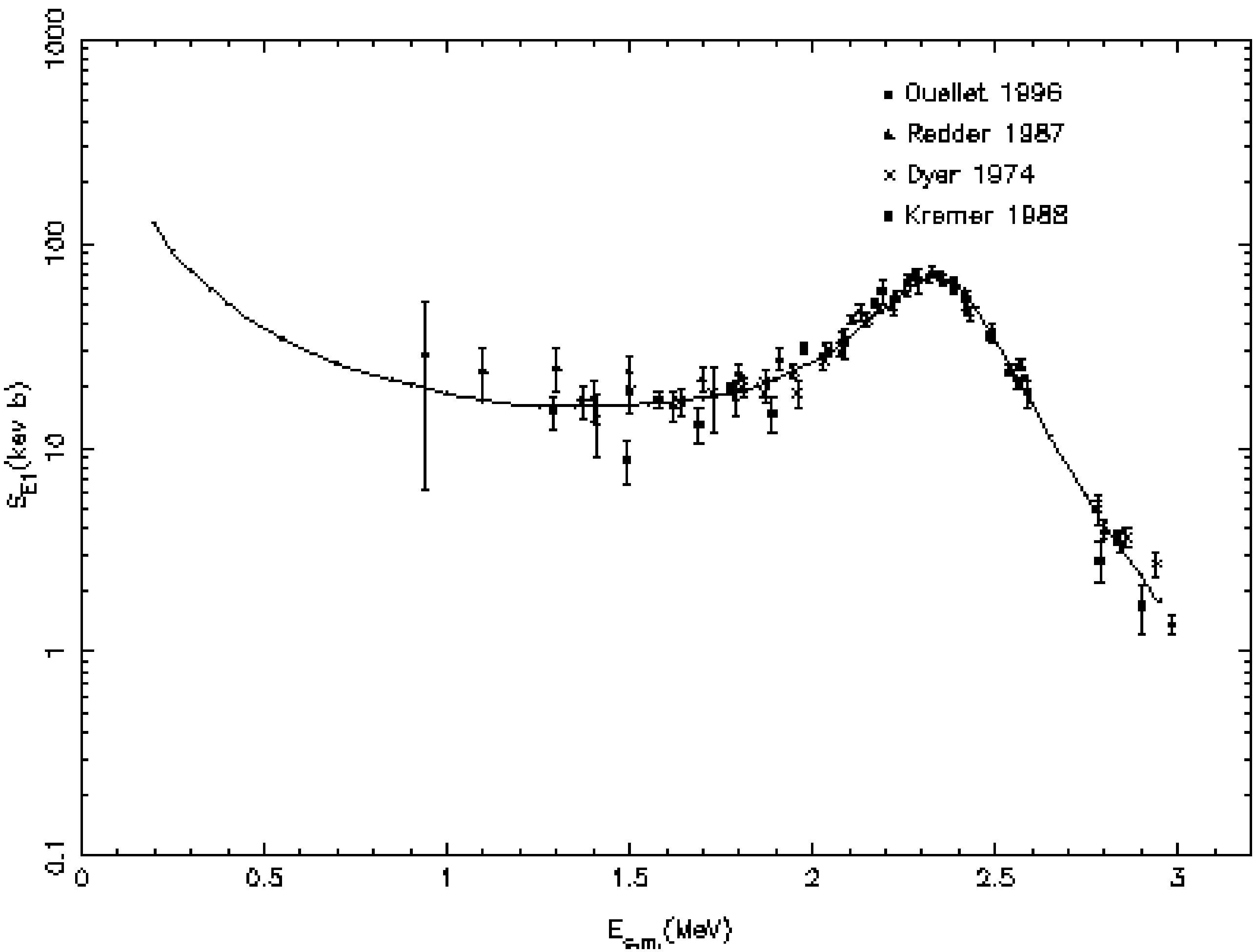

Examples, sub-threshold reactions

S-factor for α+^{12}C E2 capture (from a cluster-model fit)

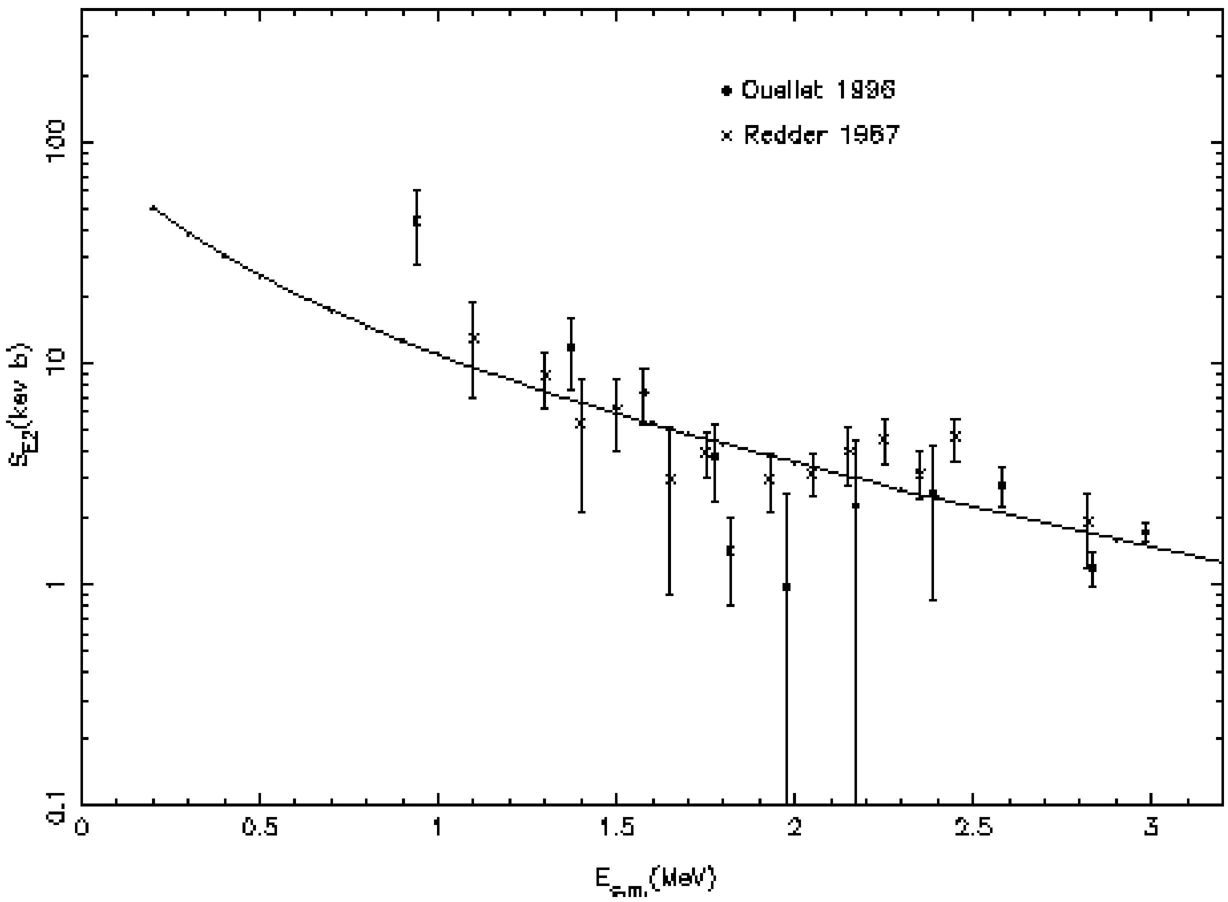

Examples, sub-threshold reactions

$$\sigma(p,\alpha) = \left(\frac{\pi}{k^2}\right)\left[\frac{2J_B+1}{(2J_p+1)(2J_{Be}+1)}\right]\left[\frac{\Gamma_p\Gamma_\alpha}{(E-E_r)^2+(\Gamma/2)^2}\right]$$

(p,α)-reaction, ^{9}Be(p,α)^{6}Li (E. Brown, ApJ 905, **495**, 1998)

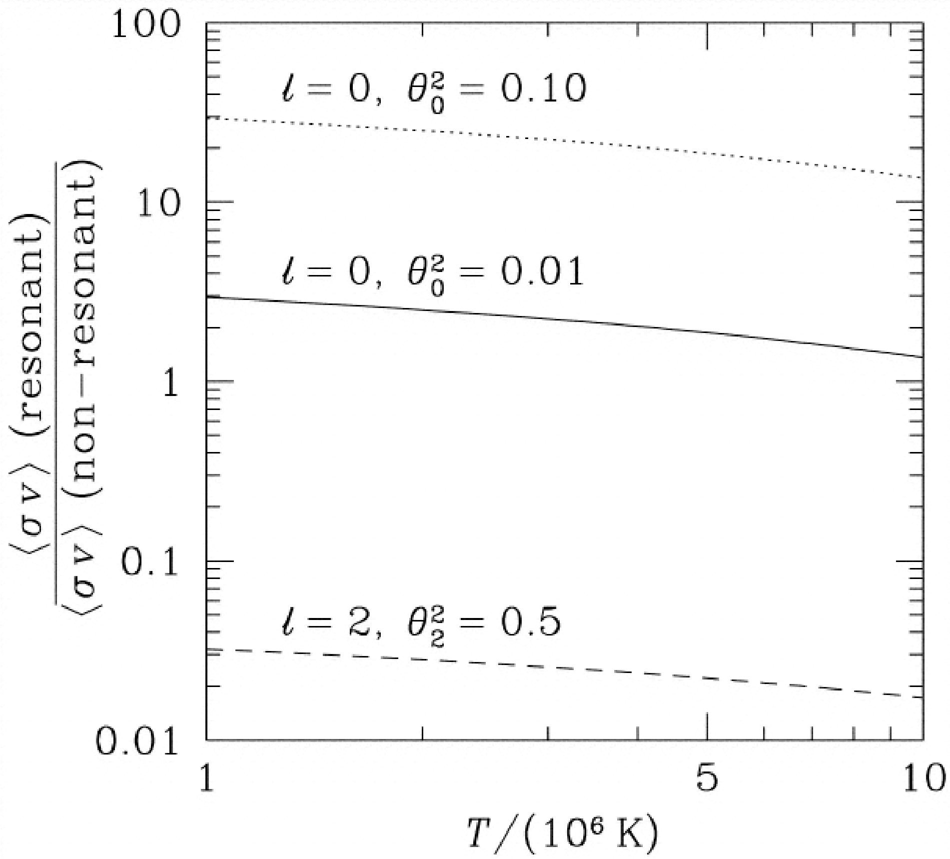

$$S(0) = 47.0\left(\frac{\theta_0^2}{0.01}\right)\ \text{MeV barns}\ .$$

Reaction rate tables: NON_SMOKER

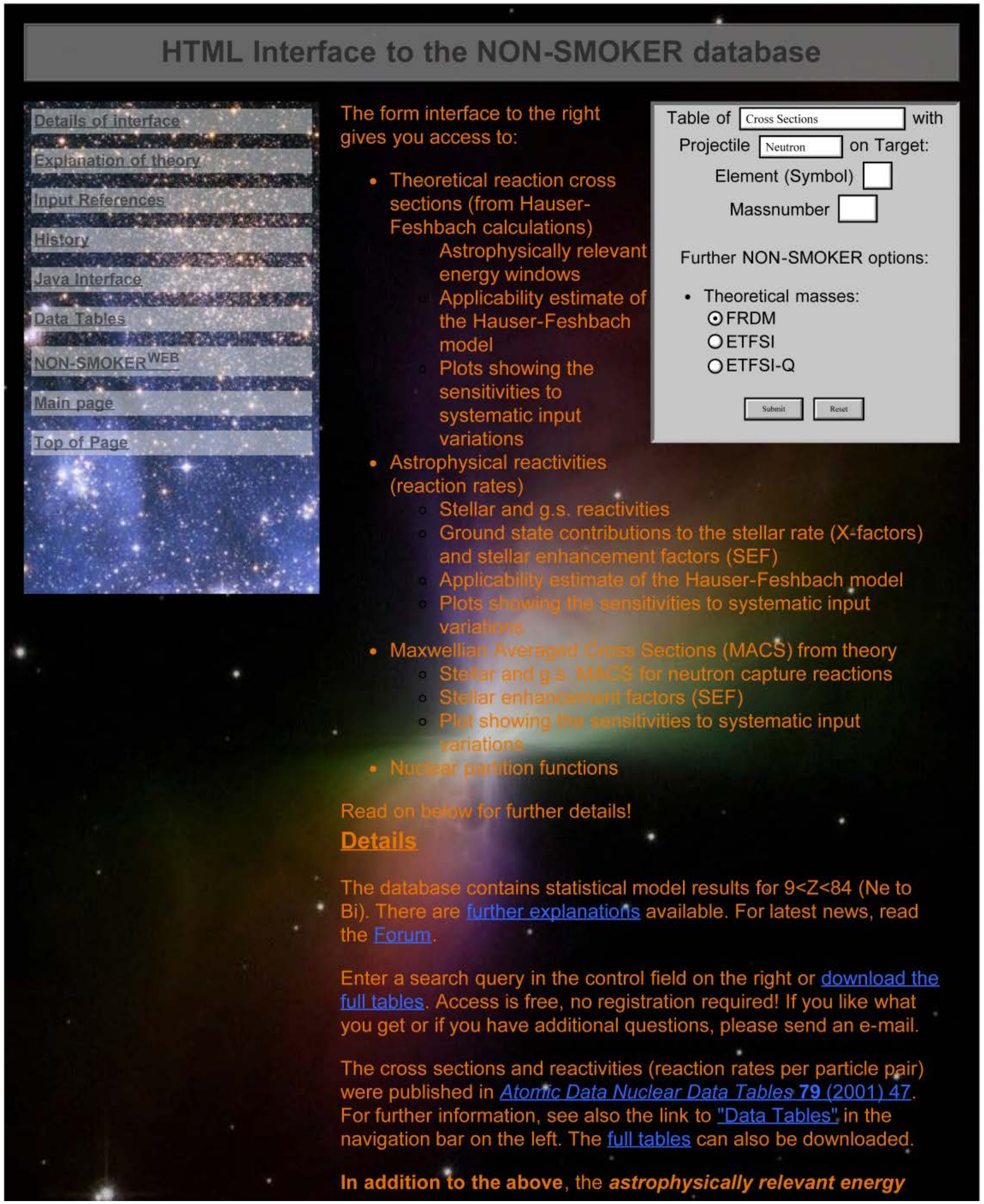

www.nucastro.org/
nonsmoker.html

Nucelar burning phases in stars

burning phase	fuel	ash	ignition temperature [10^{9} K]	energy release [10^{18} erg/g]	cooling due to
D-burning	^{2}H	^{3}He	0.0004	~0.0001	γ
H-burning	^{1}H	^{4}He, ^{14}N	0.003	5—8	γ
He-burning	^{4}He	^{12}C, ^{16}O, ^{22}Ne	0.2	0.7	γ
C-burning	^{12}C	^{20}Ne, ^{24}Mg, ^{16}O, ^{23}Na	0.8	0.5	ν
Ne-burning	^{20}Ne	^{16}O, ^{24}Mg,^{28}Si,...	1.5	0.1	ν
O-burning	^{16}O	^{28}Si, ^{32}S	2	0.5	ν
Si-burning	^{28}Si	^{56}Ni, A ¼ 56	3.5	0.1—0.3	ν
photo disintegration	^{56}Ni	n, ^{4}He, p	6—10	¬ 8	ν

$$d\mathcal{E}_\nu = I_\nu(\vec{x}, t; \vec{n}, \nu) dA \cos\vartheta d\Omega d\nu dt$$

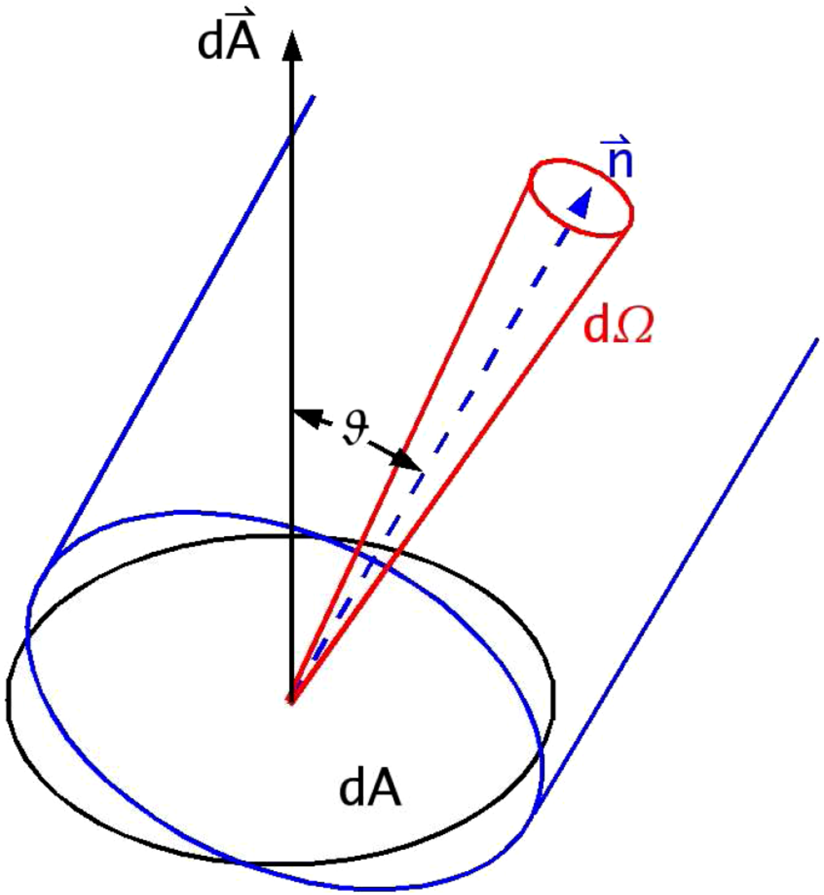

Quantities of the radiation field

- specific intensity

$$\mathrm{d}\mathcal{E}_\nu = I_\nu(\vec{x}, t; \vec{n}, \nu)\mathrm{d}A\cos\vartheta\mathrm{d}\Omega\mathrm{d}\nu\mathrm{d}t$$

- radiation flux

$$F_\nu \mathrm{d}\sigma = \int I_\nu \cos\theta \mathrm{d}\sigma\mathrm{d}\Omega$$

- total (bolometric) flux

$$F = \int F_\nu \mathrm{d}\nu$$

- luminosity

$$L = AF$$

$$F_\nu(r) = -\frac{4\pi}{3}\frac{1}{\kappa_\nu}\frac{dB_\nu}{dT}\frac{dT}{dr}$$

$$F(r) = \int F_\nu d_\nu = \int -\frac{4\pi}{3}\frac{1}{\kappa_\nu}\frac{dB_\nu(T)}{dT}\frac{dT}{dr}d\nu = -\frac{4\pi}{3}\frac{1}{\kappa_R}\frac{dB(T)}{dT}\frac{dT}{dr}$$

$$\frac{1}{\kappa_R} = \frac{\int \frac{1}{\kappa_\nu}\frac{dB_\nu(T)}{dT}d\nu}{\frac{dB(T)}{dT}}$$

<u>with</u>

$$B_\nu(T) \;=\; \frac{2h\nu^3}{c^2}[e^{h\nu/kT} - 1]^{-1}$$ <u>and</u> $$B(T) = \int B_\nu(T)d\nu$$

Stellar opacities

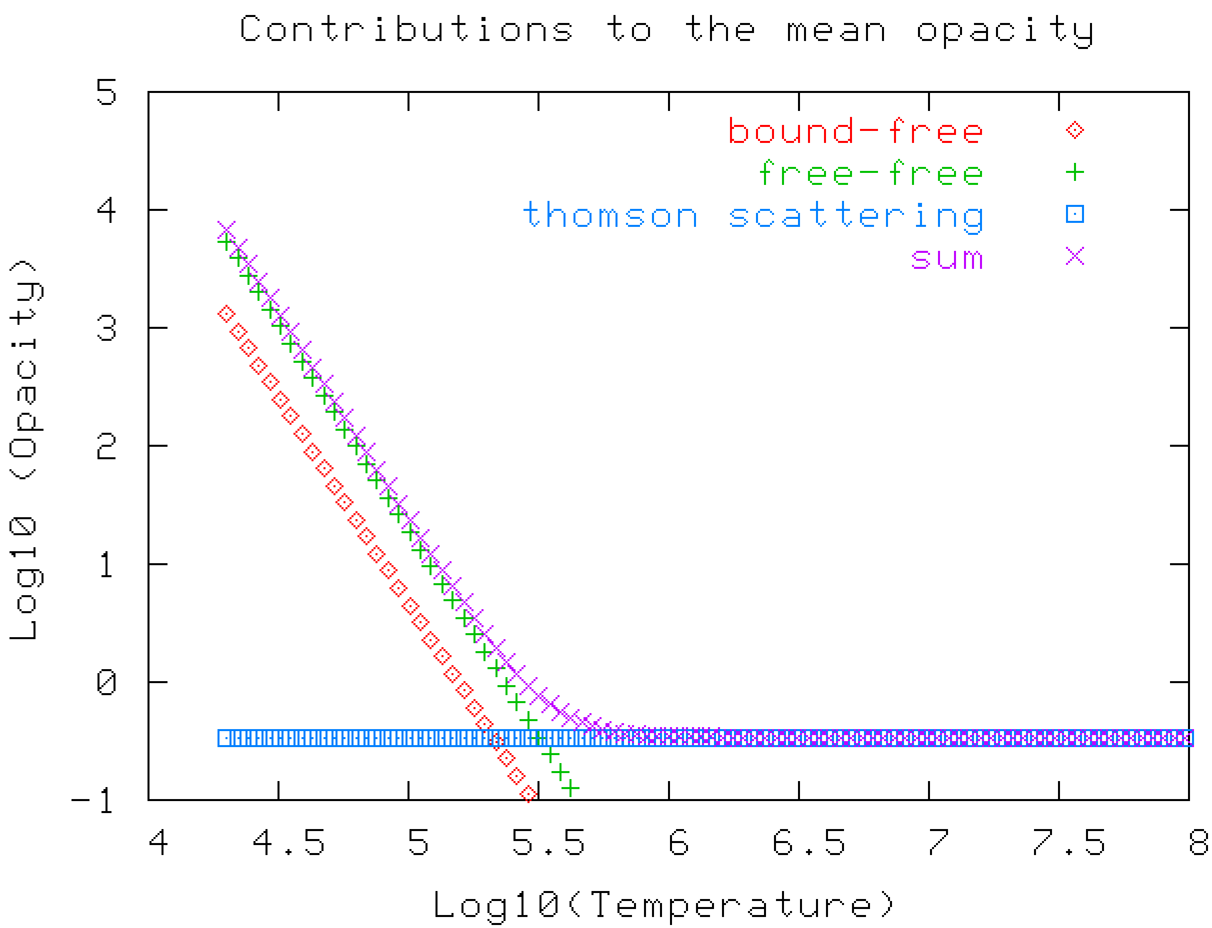

Schematic; density: 10^{-4} g/cm^3, ~solar composition

Stellar opacities

(see, e.g., D.D. Clayton: Principles of Stellar Evolution and Nucleosynthesis; University of Chicago Press (1984)

1. Bound-bound transitions (trans. between bound states)

$$\sigma_{bb}(\nu) \propto 1/\nu^2$$

2. Photoionization (`bound-free opacities`)

$$\sigma_{bf}(Z,\nu) \propto \frac{Z^4}{n^5\nu^3}$$

3. Inverse bremsstrahlung (`free-free` opacities)

$$\gamma + e^- + (Z,A) \longrightarrow e^- + (Z,A)$$

$$\sigma_{ff}(Z,\nu) \propto \frac{Z^2 ne}{T^{1/2}\nu^3} \quad \text{and} \quad \bar{\sigma}_{ff} \propto (Z,\nu) \propto n_e Z^2 T^{-7/2}$$

(2nd order contributions; 1st order = 0)

4. Electron scattering
(non-relativistic: Thomson scattering)

$$\sigma_T = \frac{8\pi}{3}\mathrm{r_e}^2 = 0.665(\mathrm{barn})$$

(valid up to T $\approx 5 \bullet 10^8$ K)

Stellar opacities

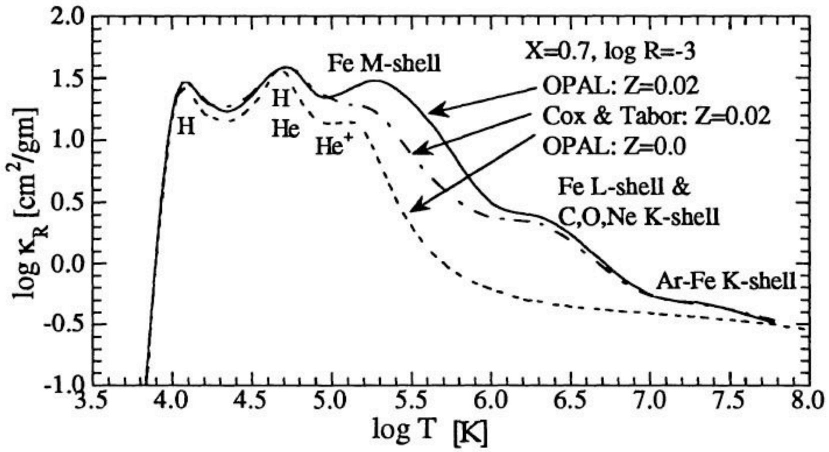

Fig. 3. Opacity versus temperature for the 12 element King4a mixture.

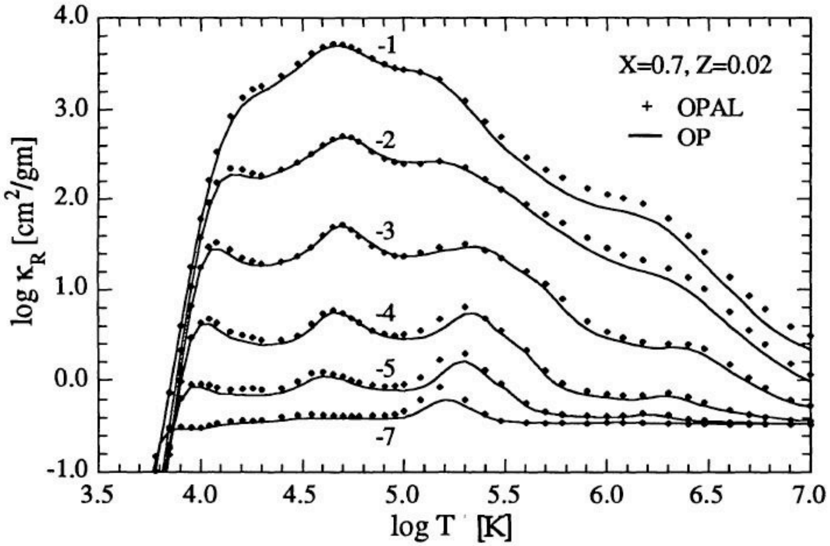

Fig. 4. Comparison of OPAL and OP for the same 14 element mixture. The results are shown for constant tracks of log R.

Heat conduction

Energy transport by conduction of heat:

Only relevant in degenerate matter (white dwarfs, neutron stars)

In white dwarfs: electrons
In neutron stars: neutrons

States $p < p_{Fermi}$ are blocked $\Rightarrow$ large mean free path
$\Rightarrow$ high (thermal) conductivity

$$\kappa_c = \frac{4ac}{3\rho} T^3 \frac{1}{\lambda_c}; \ \lambda_c = mean\ free\ path\ (electrons, neutrons)$$

$$\frac{1}{\kappa_{tot}} = \frac{1}{\kappa_R} + \frac{1}{\kappa_c}$$

Opacities: further references

New opacities (past ~ 15 years)

"OPAL" opacities (Lawrence Livermore National Laboratory):

Iglesias & Rogers: Astrophysical Journal 464 (1996) 943

Also:

http://www.cita.utoronto/~boothroy/kappa.html

"Opacity Project (OP)" (Hummer, Michalas, Seaton, ...)

See:

http://cdsweb.u-strasbg.fr/topbase/op.html

Opacities: analytic approximations

`Kramer's opacity`

bound-free: $\bar{\kappa}_{\mathrm{bf}} = 4.34 \cdot 10^{25} cm^2 g^{-1} Z(1 + X)\varrho T^{-7/2}$

free-free: $\bar{\kappa}_{\mathrm{ff}} = 3.68 \cdot 10^{22} cm^2 g^{-1} (X + Y)(1 + X)\varrho T^{-7/2}$

X: hydrogen mass fraction
Y: helium mass fraction
Z: heavy element mass fraction ("metals")

Karl Schwarzschild (1873 – 1916)

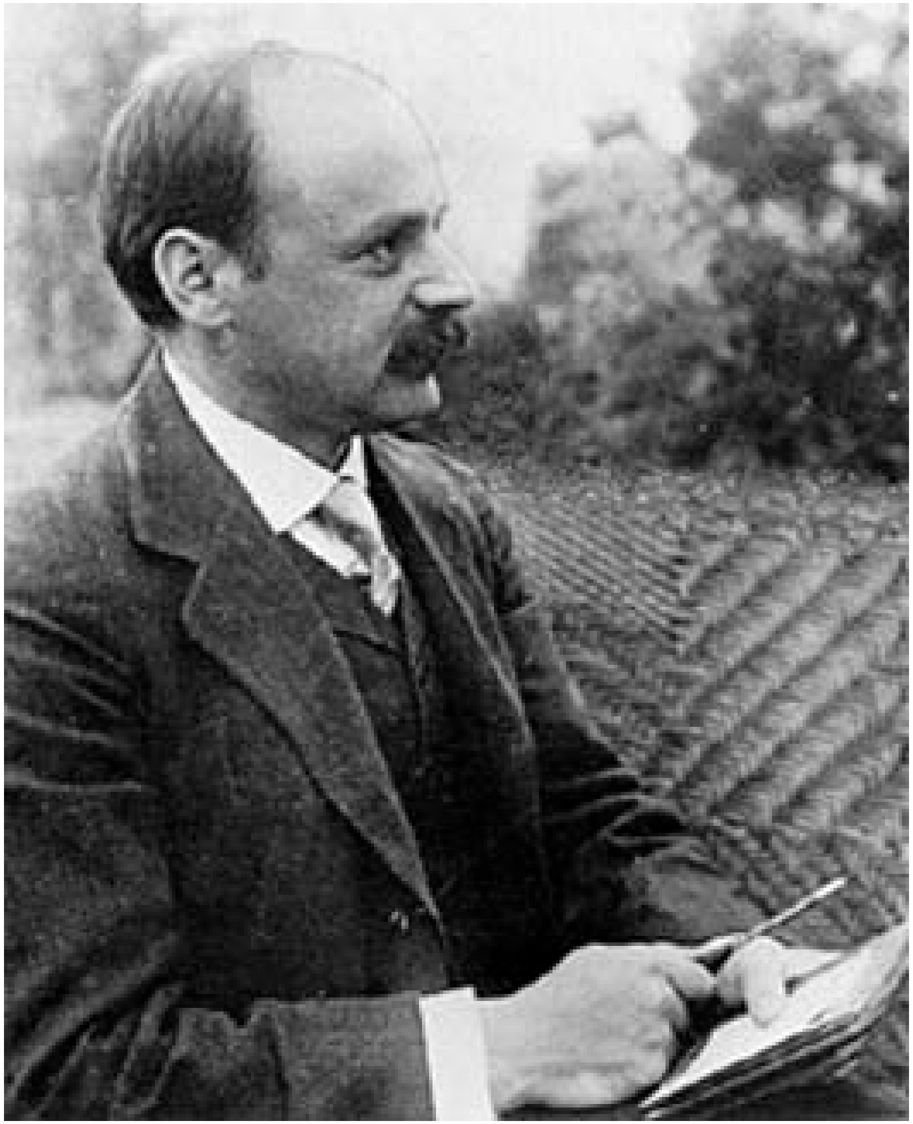

Inside mass element		Outside mass element
$\tilde{\rho}$	p - dp	p - dp, ρ(r + dr), T(r + dr)
dS = 0		(adiabatic, pressure equilibrium)
ρ	p(r)	p(r), ρ(r), T(r)

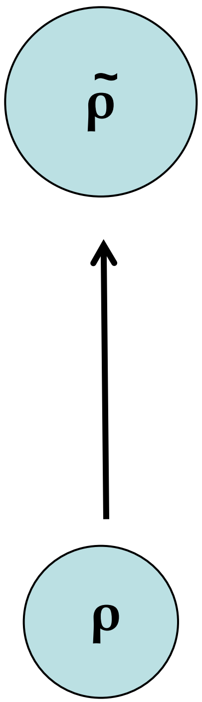

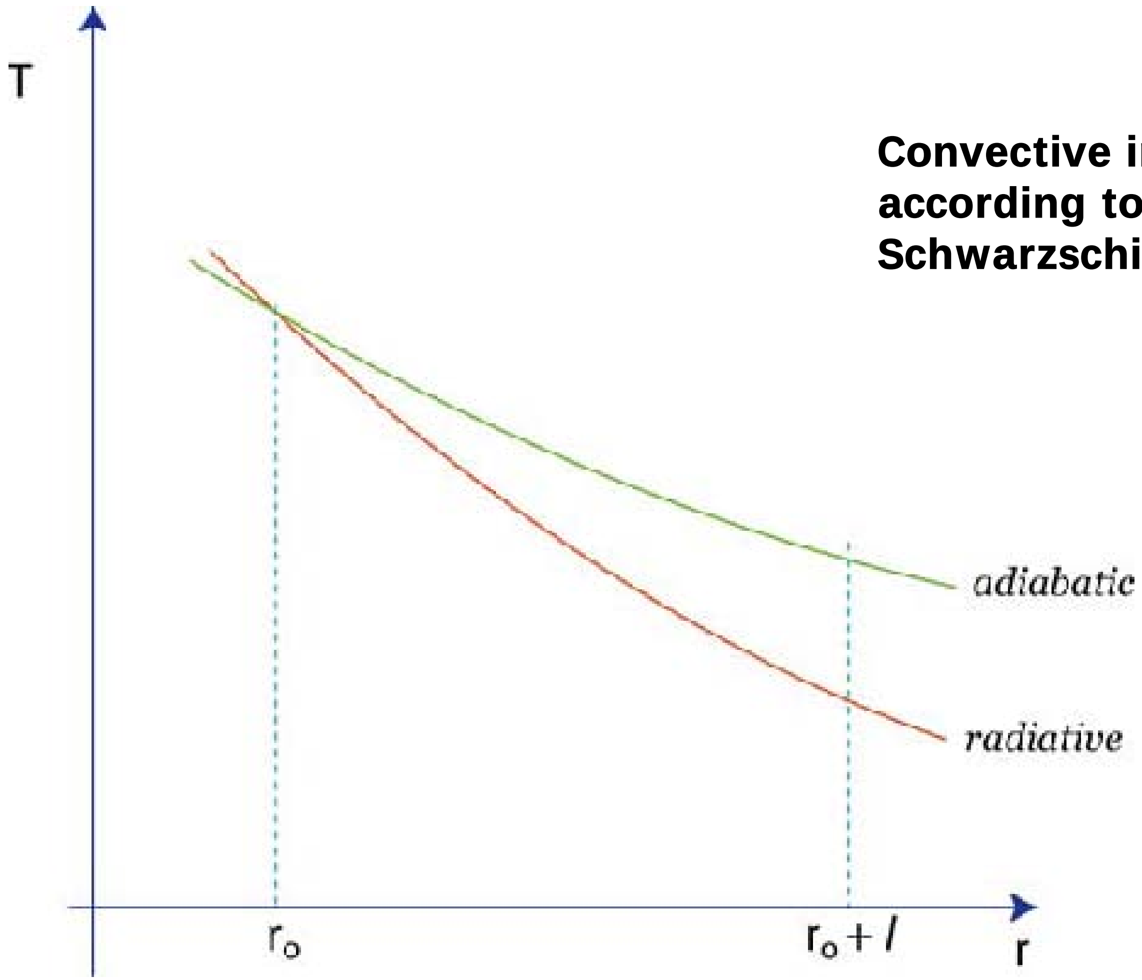

Convective instability according to the Schwarzschild criterion

Schwarzschild criterion

$$Instability\ if:\quad \frac{1}{\Gamma_1}\frac{\varrho}{P}\left(\frac{dP}{dr}\right)_* < \left(\frac{d\varrho}{dr}\right)_*$$

Or:
$$\left|\left(\frac{dT}{dr}\right)_{ad}\right| < \left|\left(\frac{dT}{dr}\right)_{rad}\right|$$

$$Good\ approximation\ for\ stellar\ structure:$$

$$\left(\frac{dT}{dr}\right)_* \cong \left(\frac{dT}{dr}\right)_{ad}$$

Mixing-length `theory`

$$Convective\ flux:\ F_c = \frac{1}{2}\bar{\varrho}\overline{c_p}\bar{w}l\left(\frac{dT}{dz} - \overline{\frac{dT}{dz}}\right)\cdot\omega$$

In practice: $\omega = 1; l = \alpha\left(\frac{dlnP}{dr}\right)^{-1}; \alpha = O(1);$

$$\bar{w}^2 = \frac{g}{T}\left(\frac{dT}{dz} - \overline{\frac{dT}{dz}}\right)\frac{l^2}{4}$$

l: `mixing length`, w: convective velocity

Improvements/modifications

- Non-adiabatic effects (radiation losses)
- Time dependence
- Non-locality (“over-” and “under-shooting”)
- Ledoux criterion (takes abundance gradients into account)

Rayleigh-Taylor instability

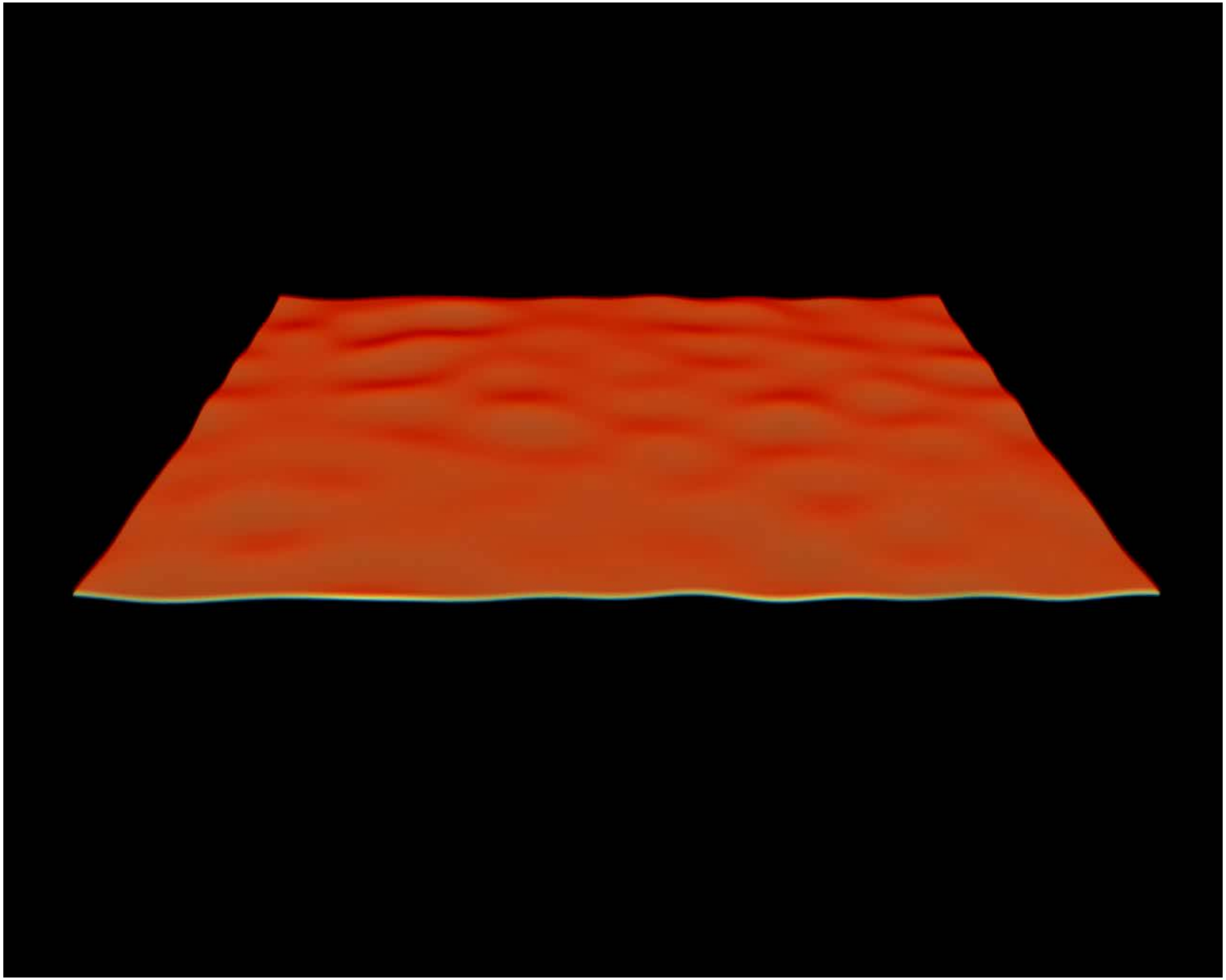

Rayleigh-Taylor instability

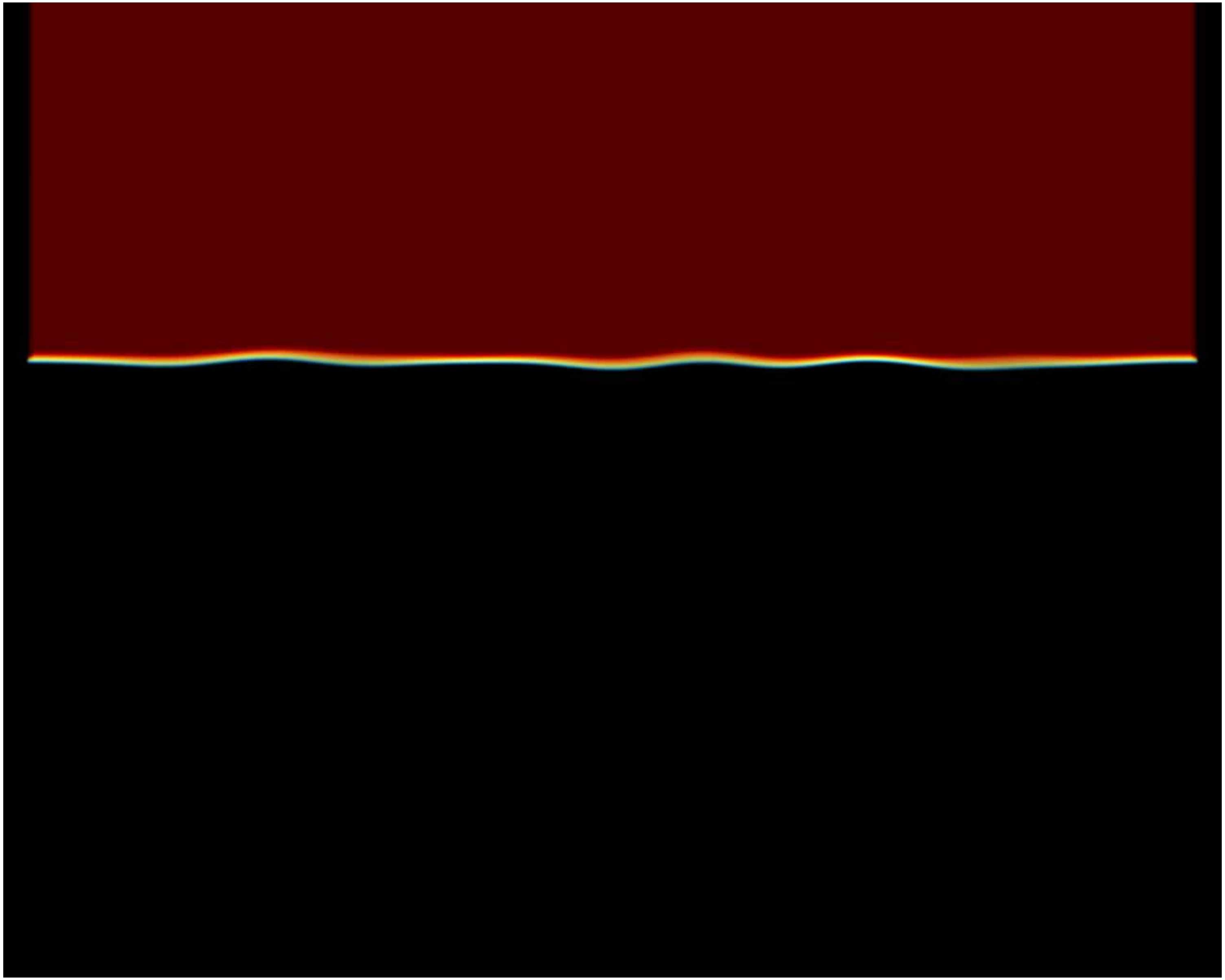

Stellar convection: evolved stars

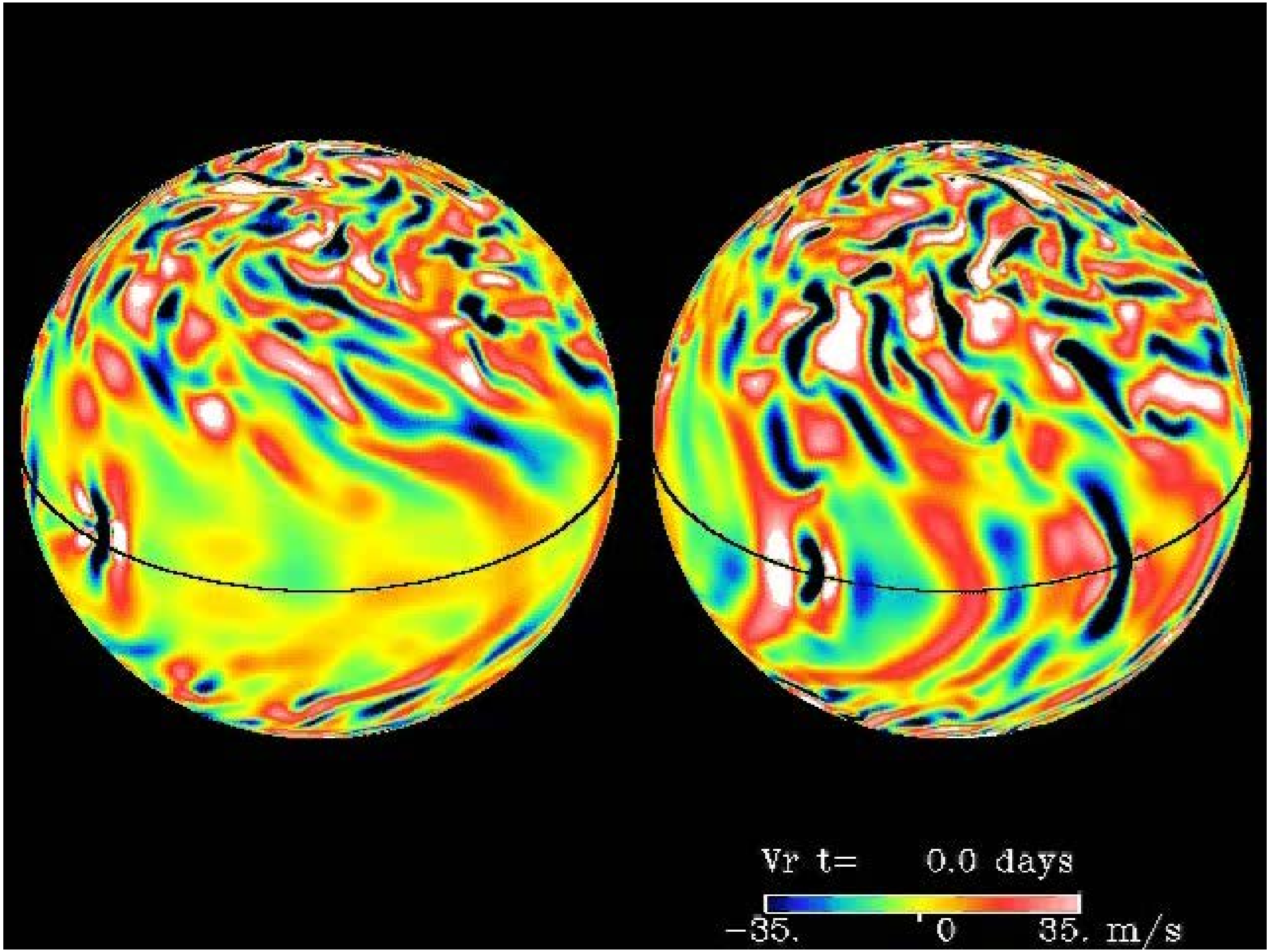

Stellar convection: classical novae

m is the Lagrangian coordinate;
r, P, T, L_r are the dependent variables;
X_i are the composition variables;
$\rho, \kappa, \epsilon, \ldots$ are physical functions, all depending on $(P, T, \vec{X})$.

The four structure equations to be solved are:

$$\frac{\partial r}{\partial m} = \frac{1}{4\pi r^2 \rho} \tag{9}$$

$$\frac{\partial P}{\partial m} = -\frac{Gm}{4\pi r^4} - \cancel{\frac{1}{4\pi r^2}\frac{\partial^2 r}{\partial t^2}} \tag{10}$$

$$\frac{\partial L_r}{\partial m} = \epsilon_n - \epsilon_\nu - \cancel{c_P \frac{\partial T}{\partial t} + \frac{\delta}{\rho}\frac{\partial P}{\partial t}} \tag{11}$$

$$\frac{\partial T}{\partial m} = -\frac{GmT}{4\pi r^4 P}\nabla \tag{12}$$

with ∇ depending of the type of energy transport:

$$\nabla = \nabla_{\mathrm{rad}} = \frac{3}{16\pi acG}\frac{\kappa L_r P}{mT^4} \tag{13}$$

$$\nabla = \nabla_{\mathrm{con}} \, (\approx \nabla_{\mathrm{ad}}) \tag{14}$$

Finally, for the composition, we have (schematically)

$$\frac{\partial X_i}{\partial t} = \frac{m_i}{\rho}\left(\sum_j r_{ji} - \sum_k r_{ik}\right) \tag{15}$$

which may include a diffusive term (here: representative for concentration diffusion)

$$\frac{\partial X_i}{\partial t} = \frac{\partial}{\partial m}\left[(4\pi r^2 \rho)^2 D \frac{\partial X_i}{\partial r}\right] \tag{16}$$

Boundary conditions

at **center**: $M_r = 0 \rightarrow \qquad r(0) = 0, \quad L_r(0) = 0$

at **surface**: different possibilities

(1) "zero" b.c.: for $M_r = M$: $P(M) = 0$, $T(M) = 0$; gives inner parts of stars approximately correct, but outer parts are unrealistic; cannot be compared to observations

(2) **photospheric b.c.**: b.c. taken at photosphere, i.e. at *optical depth* $\tau_{\mathrm{ph}} = 2/3$, where $T = T_{\mathrm{eff}}$

Boundary-value problem!

"Stellar evolution" :
sequence of stellar models

Scheme for numerical solutions

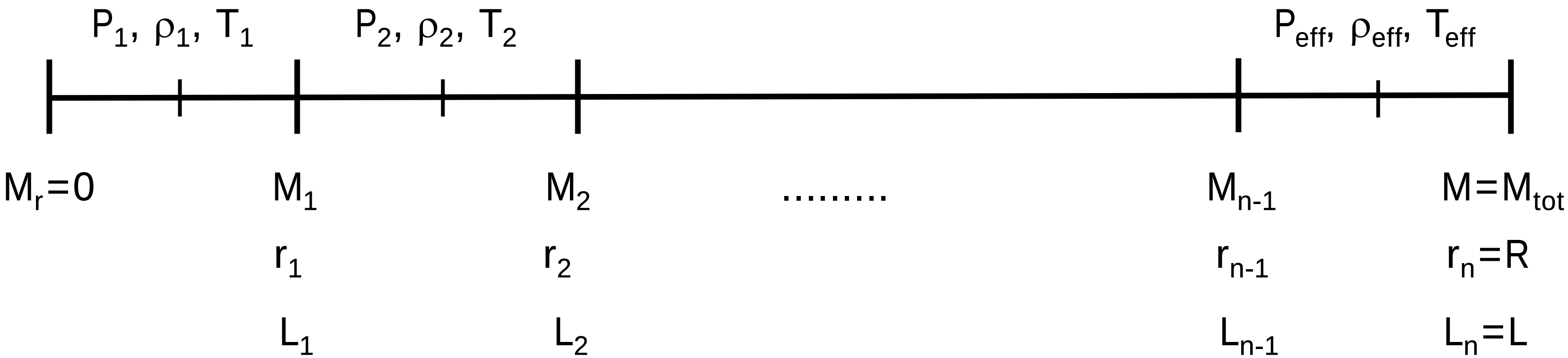

$$\frac{r_i - r_{i-1}}{M_i - M_{i-1}} = \frac{1}{4\pi r_i^2}\ \frac{1}{\varrho_i}$$

$$\frac{P_i - P_{i-1}}{\frac{1}{2}[(M_i - M_{i-1}) + (M_{i-1} - M_{i-2})]} = \frac{GM_{i-1}}{4\pi r_{i-1}^4}$$

$$\frac{L_i - L_{i-1}}{M_i - M_{i-1}} = \varepsilon_i - \varepsilon_\nu \left(-T_i \frac{dS_i}{dt}\Big|_{t_0}\right)$$

$$\frac{T_i - T_{i-1}}{\frac{1}{2}[\dots\dots]} = \frac{3}{4ac}\ \frac{\frac{1}{2}(\kappa_i + \kappa_{i-1})}{\frac{1}{2}(T_i + T_{i-1})}\ \frac{L_{i-1}}{16\pi^2 r_i^4}$$

Non-linear system of equations for discrete "i".

<u>Solution:</u>

Newton-Raphson

Structure of evolved massive stars

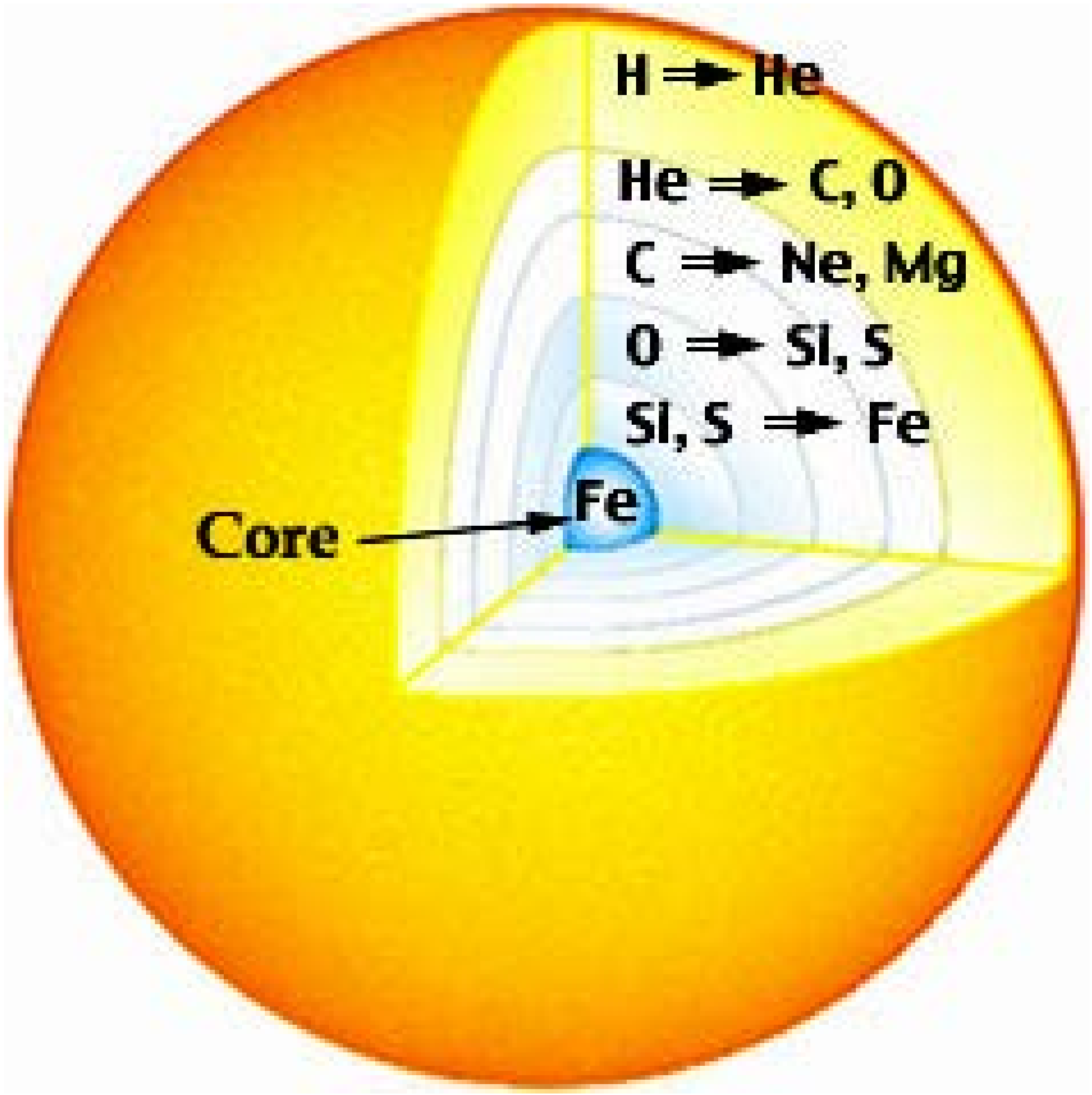

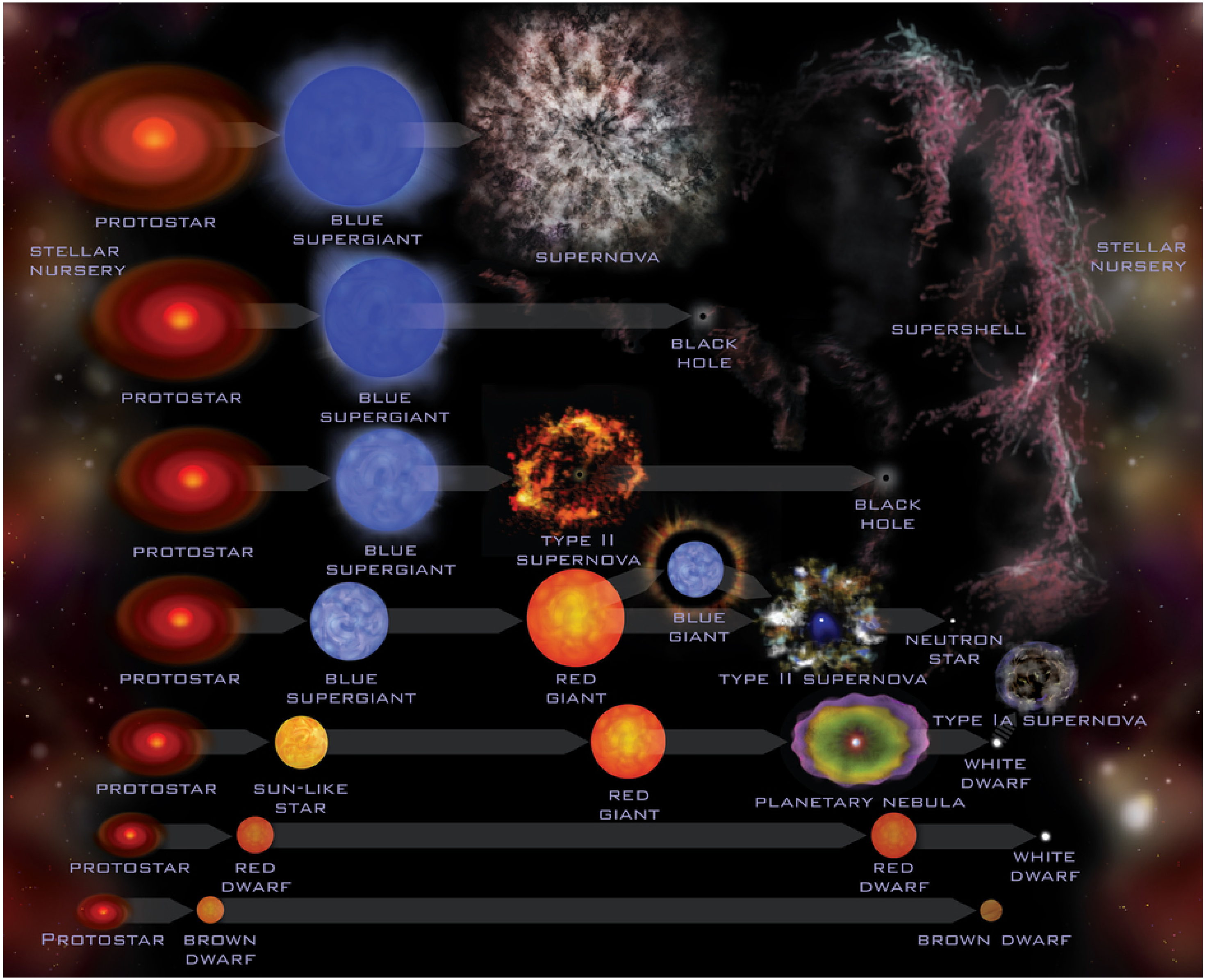

PROTOSTAR
BLUE SUPERGIANT
SUPERNOVA
STELLAR NURSERY
STELLAR NURSERY
PROTOSTAR
BLUE SUPERGIANT
BLACK HOLE
SUPERSHELL
PROTOSTAR
BLUE SUPERGIANT
TYPE II SUPERNOVA
BLACK HOLE
BLUE GIANT
PROTOSTAR
BLUE SUPERGIANT
RED GIANT
NEUTRON STAR
TYPE II SUPERNOVA
TYPE IA SUPERNOVA
PROTOSTAR
SUN-LIKE STAR
RED GIANT
PLANETARY NEBULA
WHITE DWARF
PROTOSTAR
RED DWARF
RED DWARF
WHITE DWARF
PROTOSTAR
BROWN DWARF
BROWN DWARF

Stellar evolution (and the HR diagram)

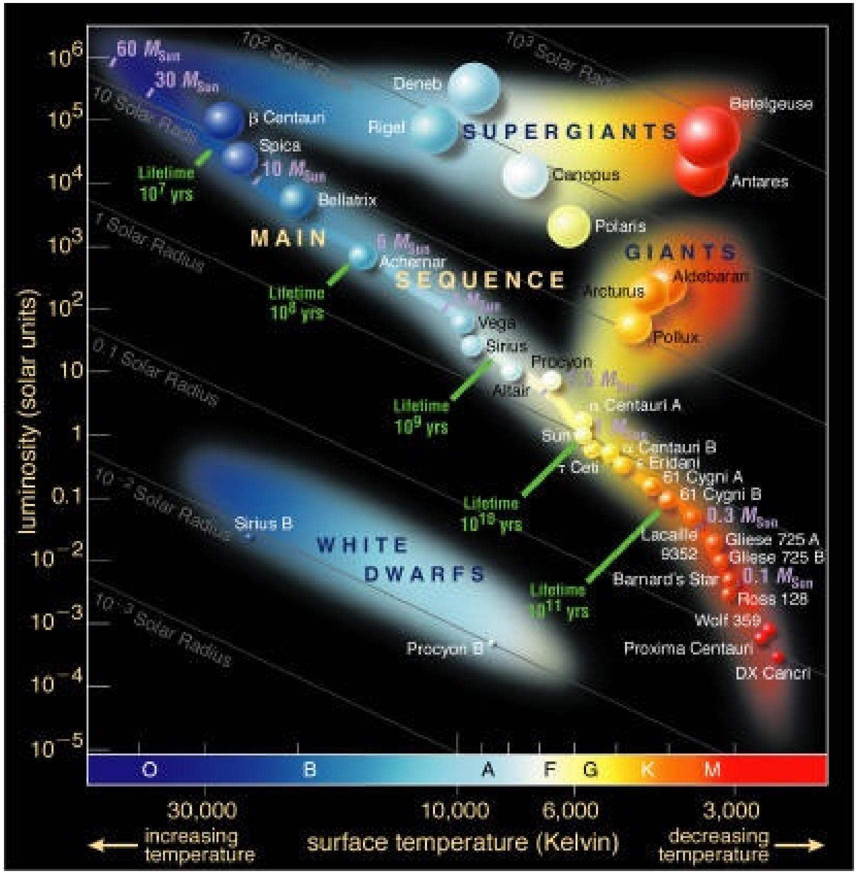

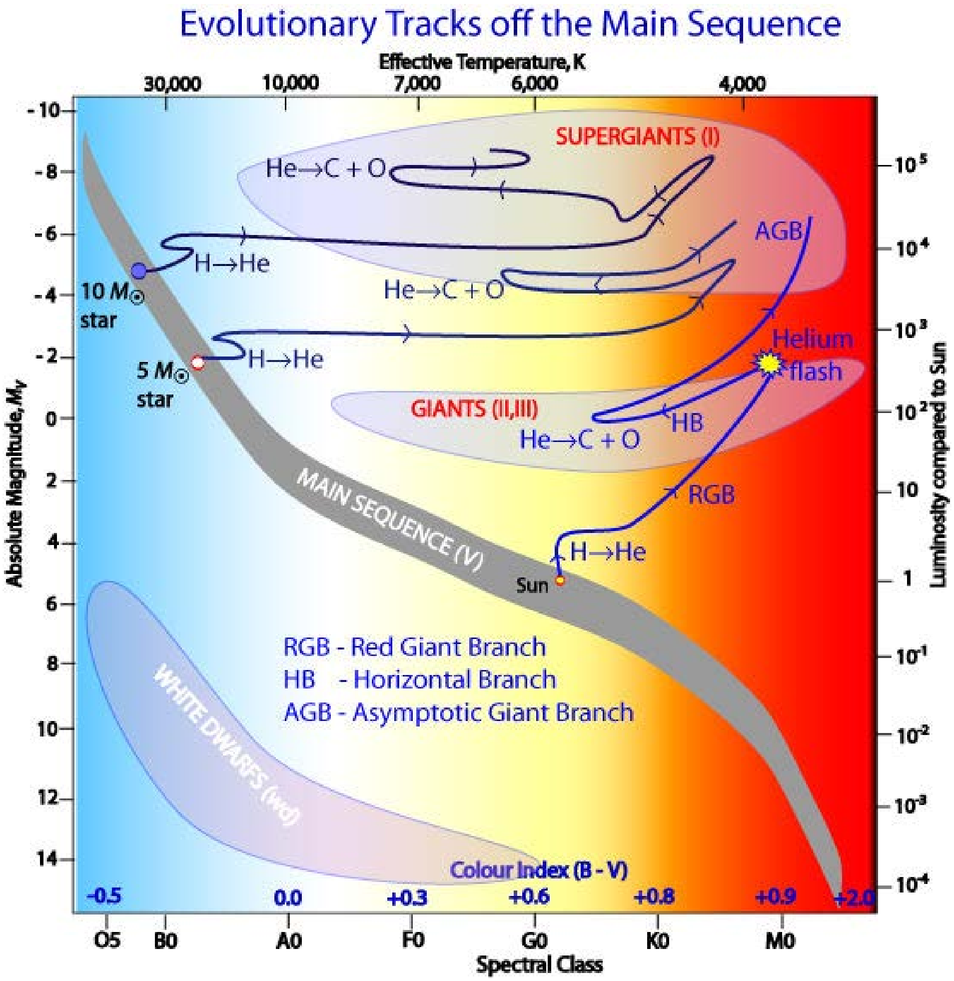

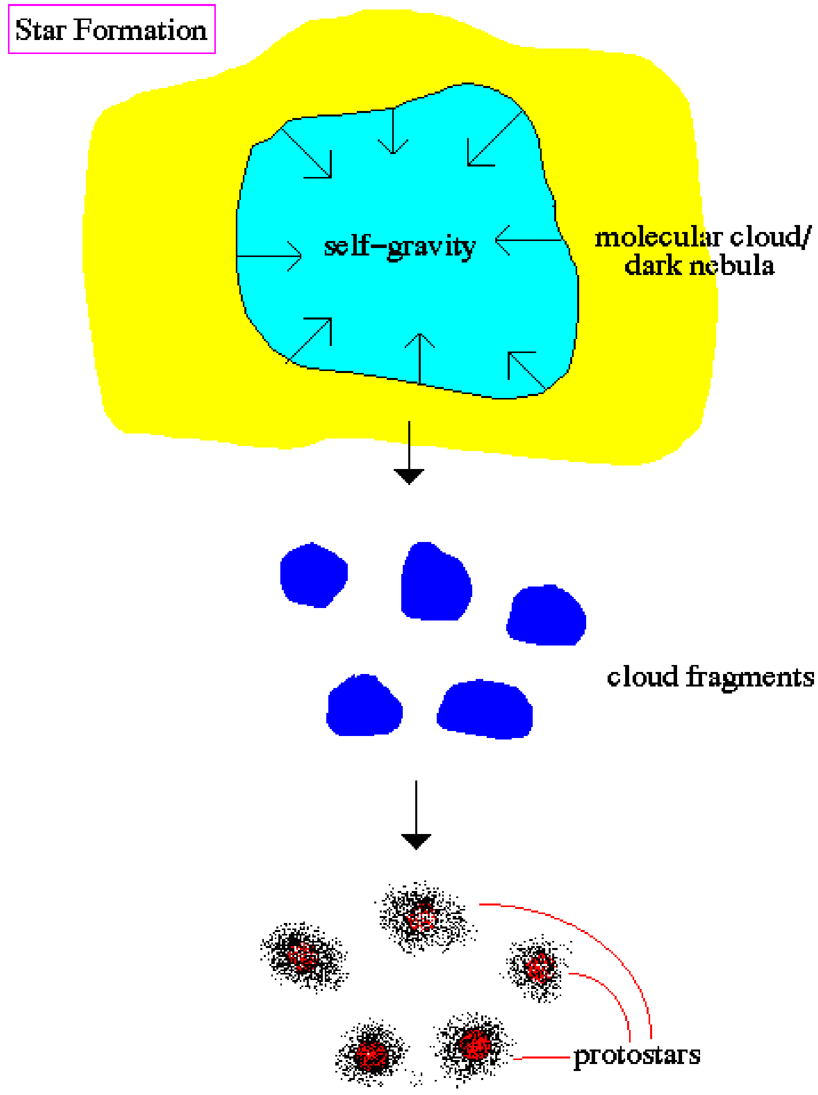
Star Formation
self−gravity
molecular cloud/
dark nebula
cloud fragments
protostars

Condition for collapse:

$$t_{ff} < t_{sound} \Rightarrow M > M_{Jeans} := \left(\frac{4\pi}{3}\right) \varrho_0 \lambda_{Jeans}{}^3$$

$$\lambda_{Jeans} := \left(\frac{\pi}{G\varrho_0}\right)^{1/2} c_s$$

$$M_{Jeans} = 1.2 \bullet 10^5 M_{sun} \left(\frac{T}{100K}\right)^{3/2} \left(\frac{10^{-24} g/cm^3}{\varrho_0}\right)^{1/2} \mu^{-3/2}$$

Star formation

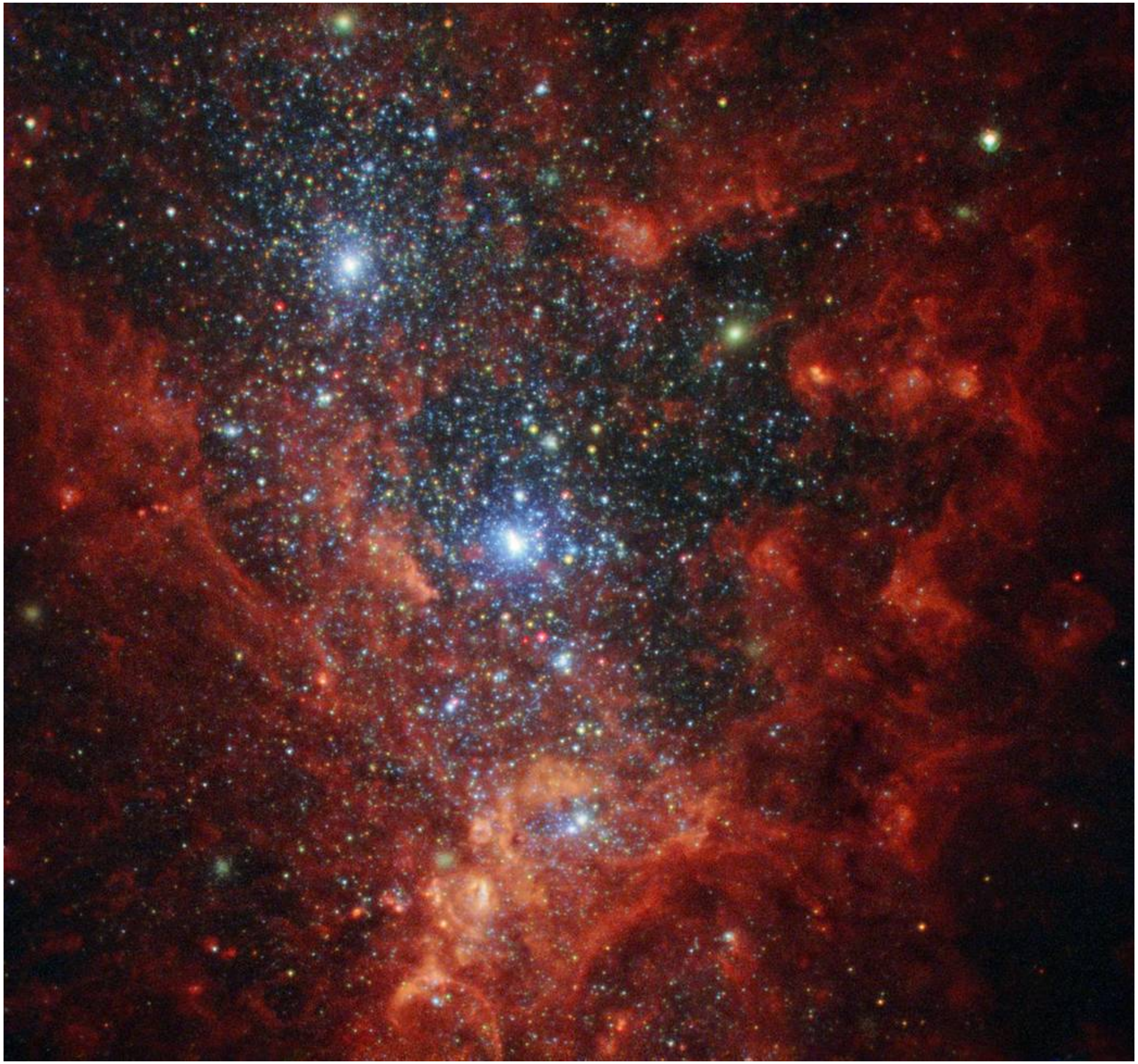

Star burst galaxy NGC 1569 (©*NASA*)

Star formation

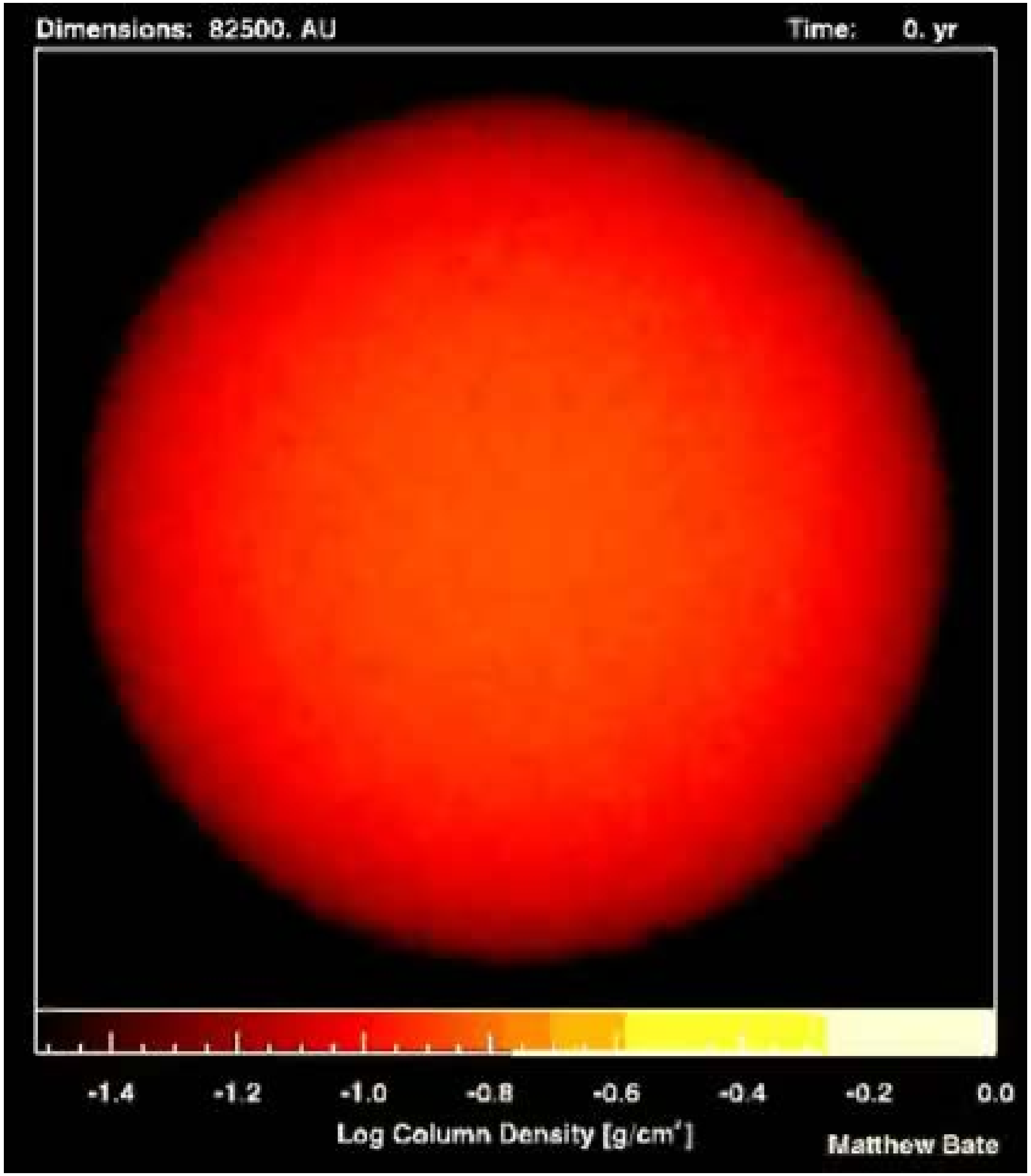

Primordial stars

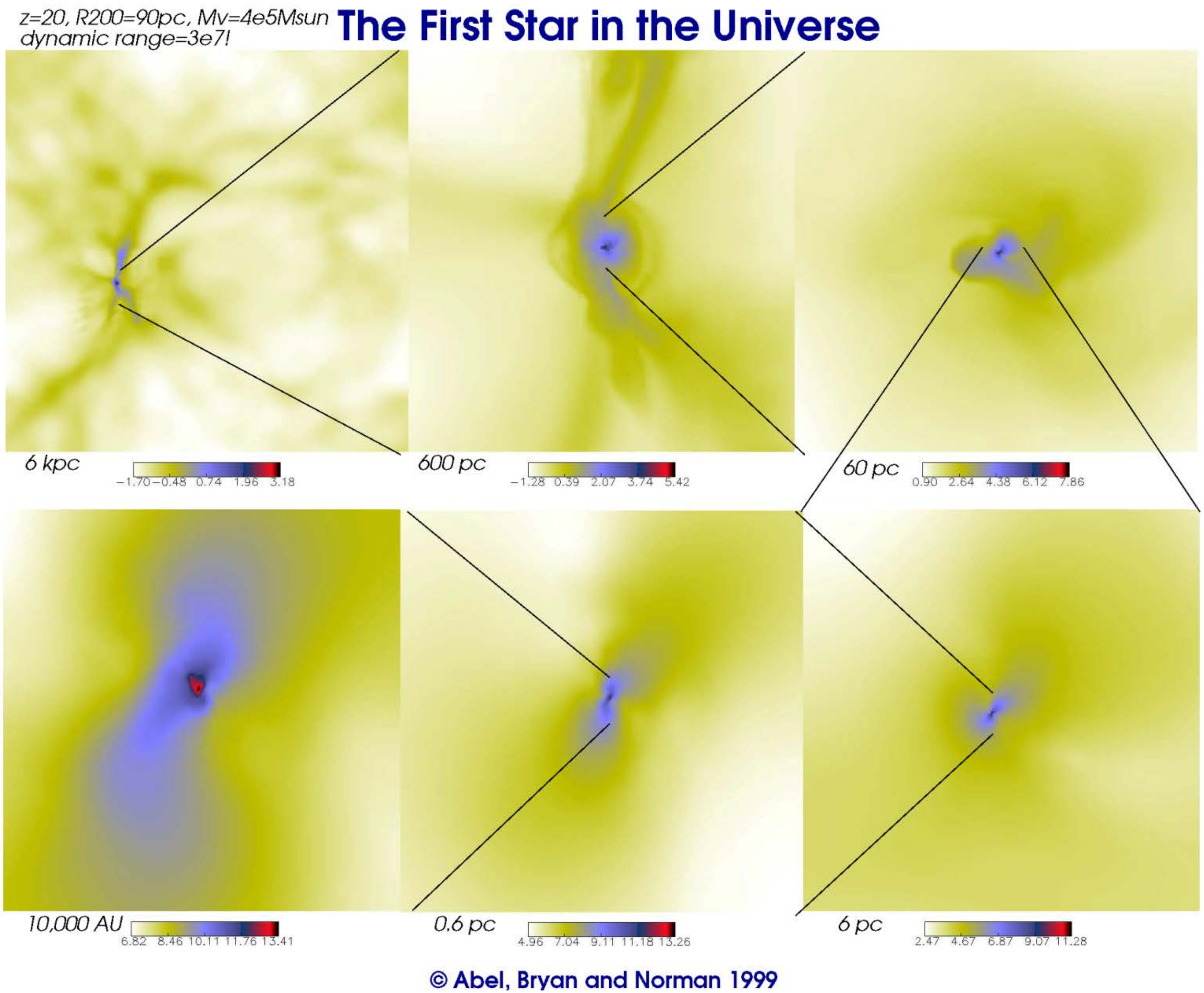

Initial mass function

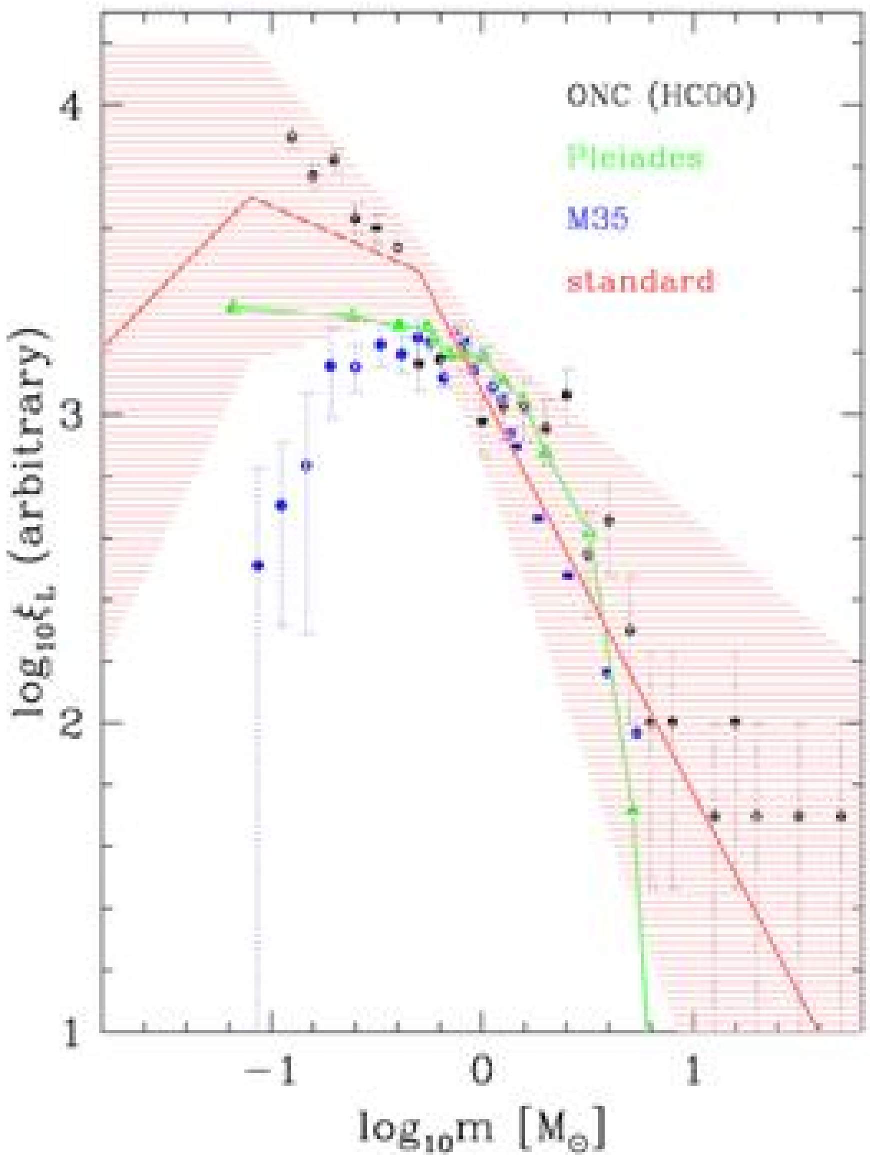

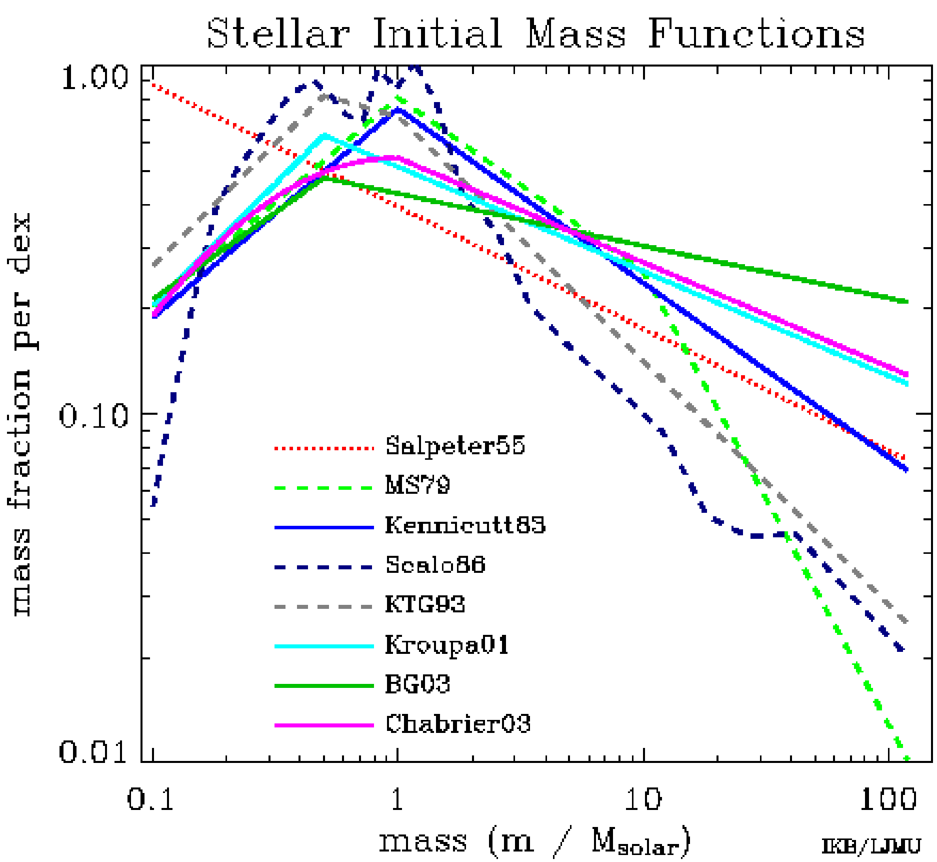

Pre-main sequence evolution

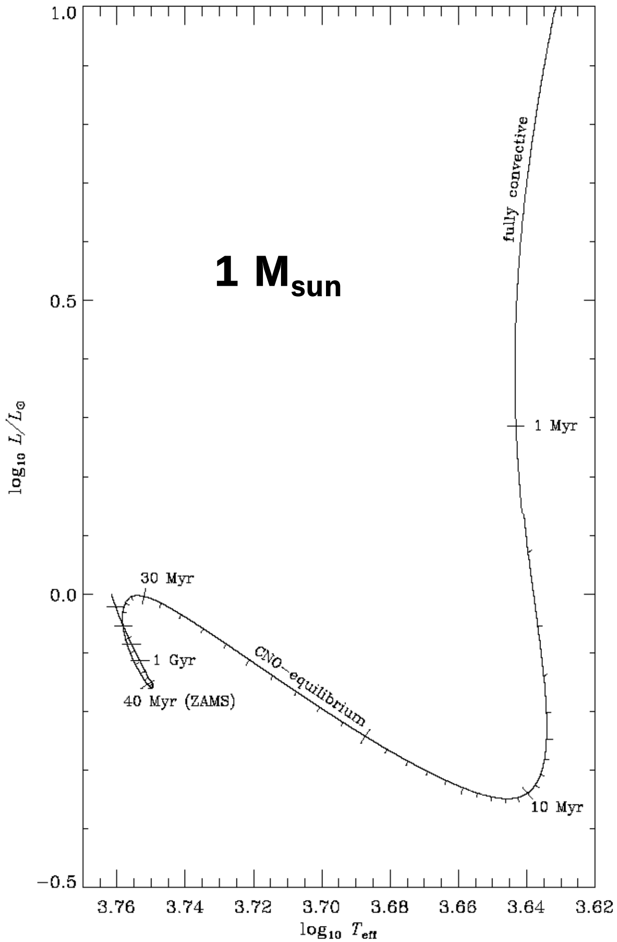

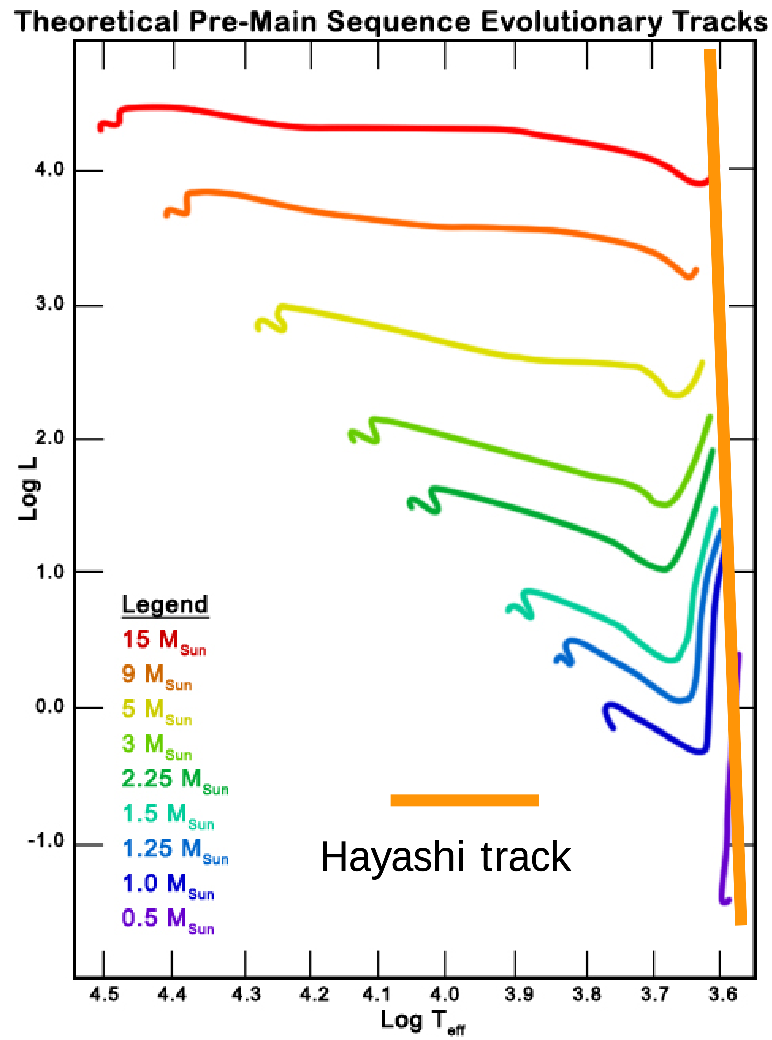

Hayashi track: fully convective (S=const) configurations (n=3/2, γ=5/3 polytropes)
(*see wwwmpa.mpa-garching.mpg.de/~weiss/Vorlesung_WS1617/index.html*)

MS mass-luminosity relation (data)

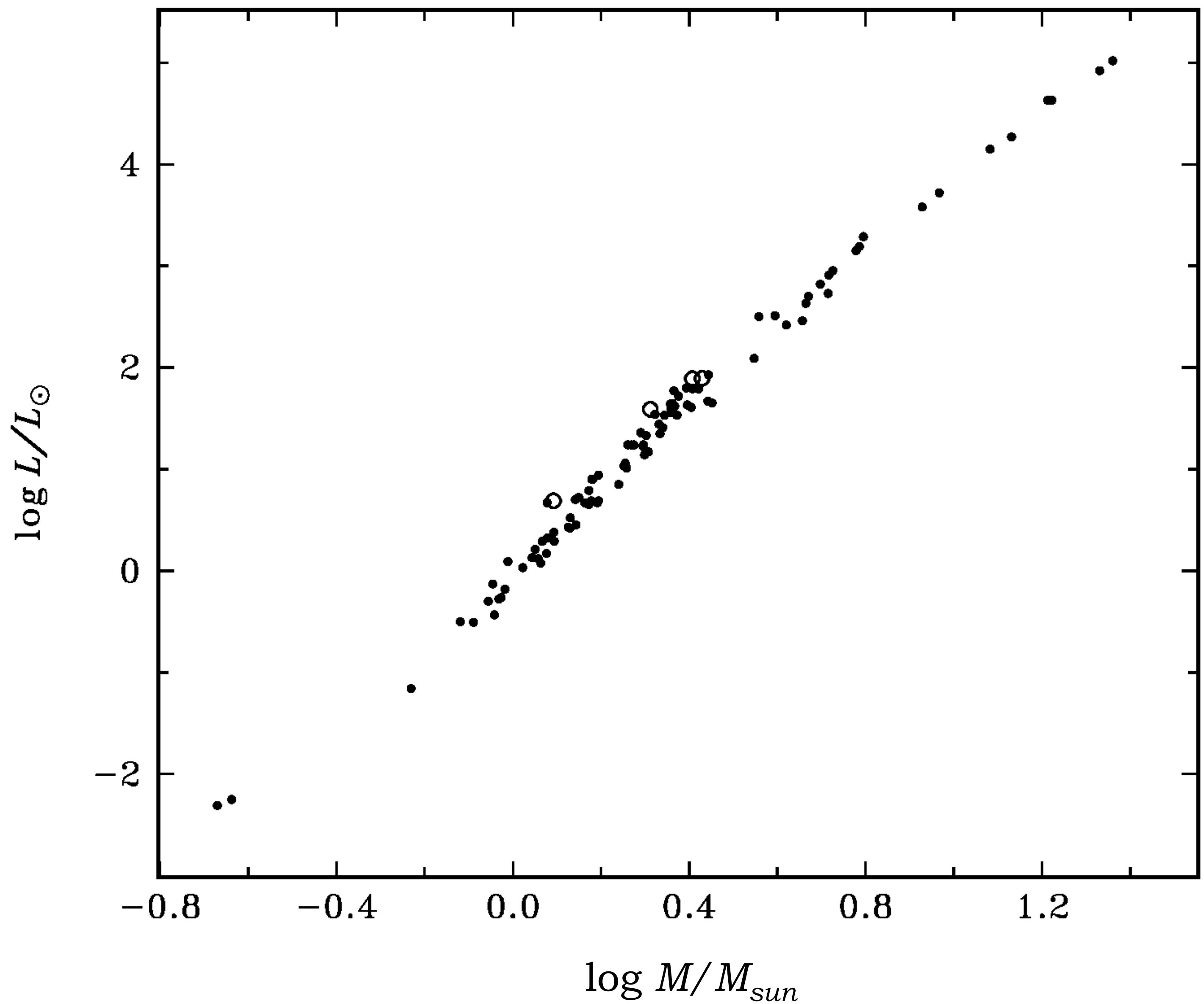

MS mass-radius relation (data)

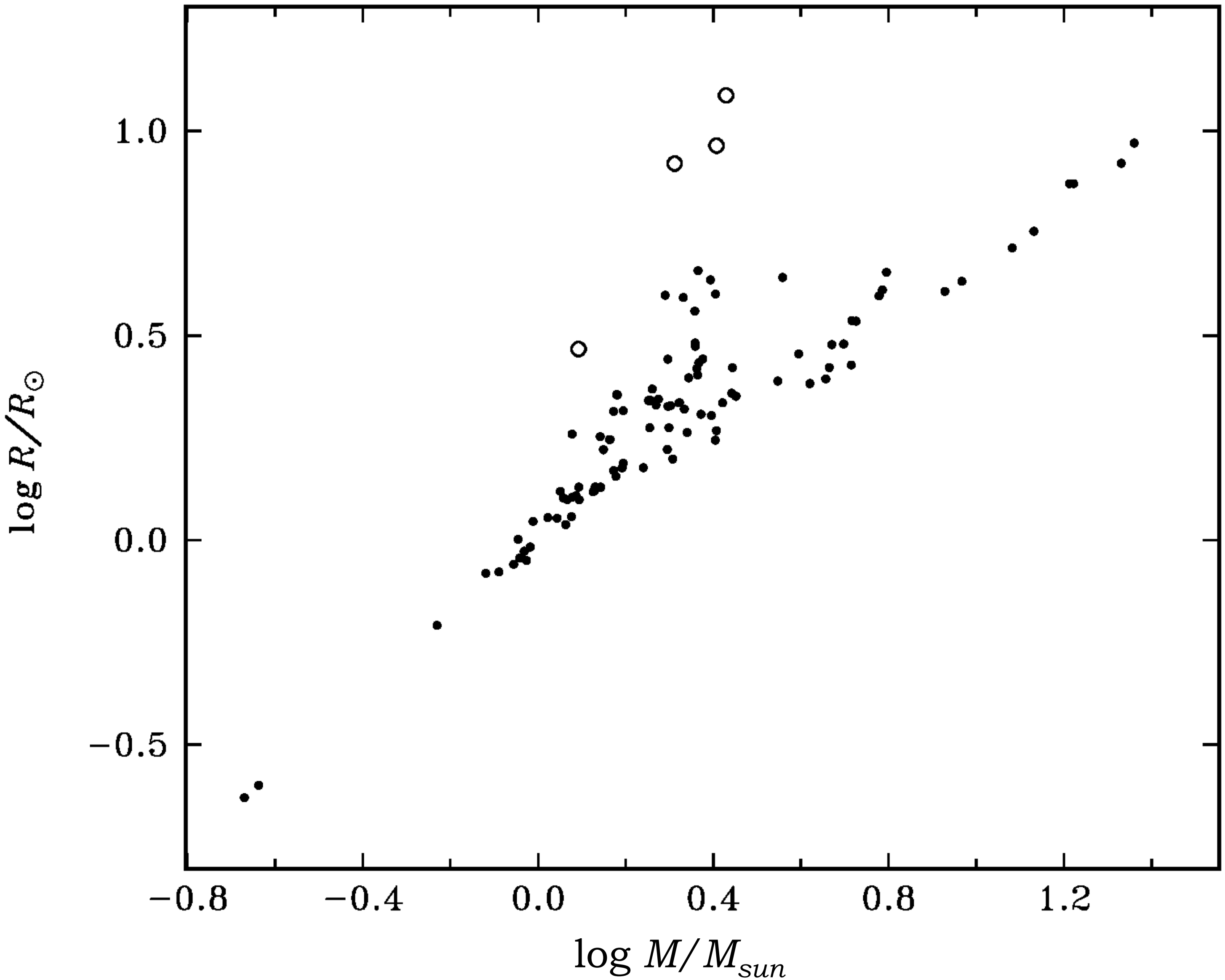

-

Low-mass stars and planets

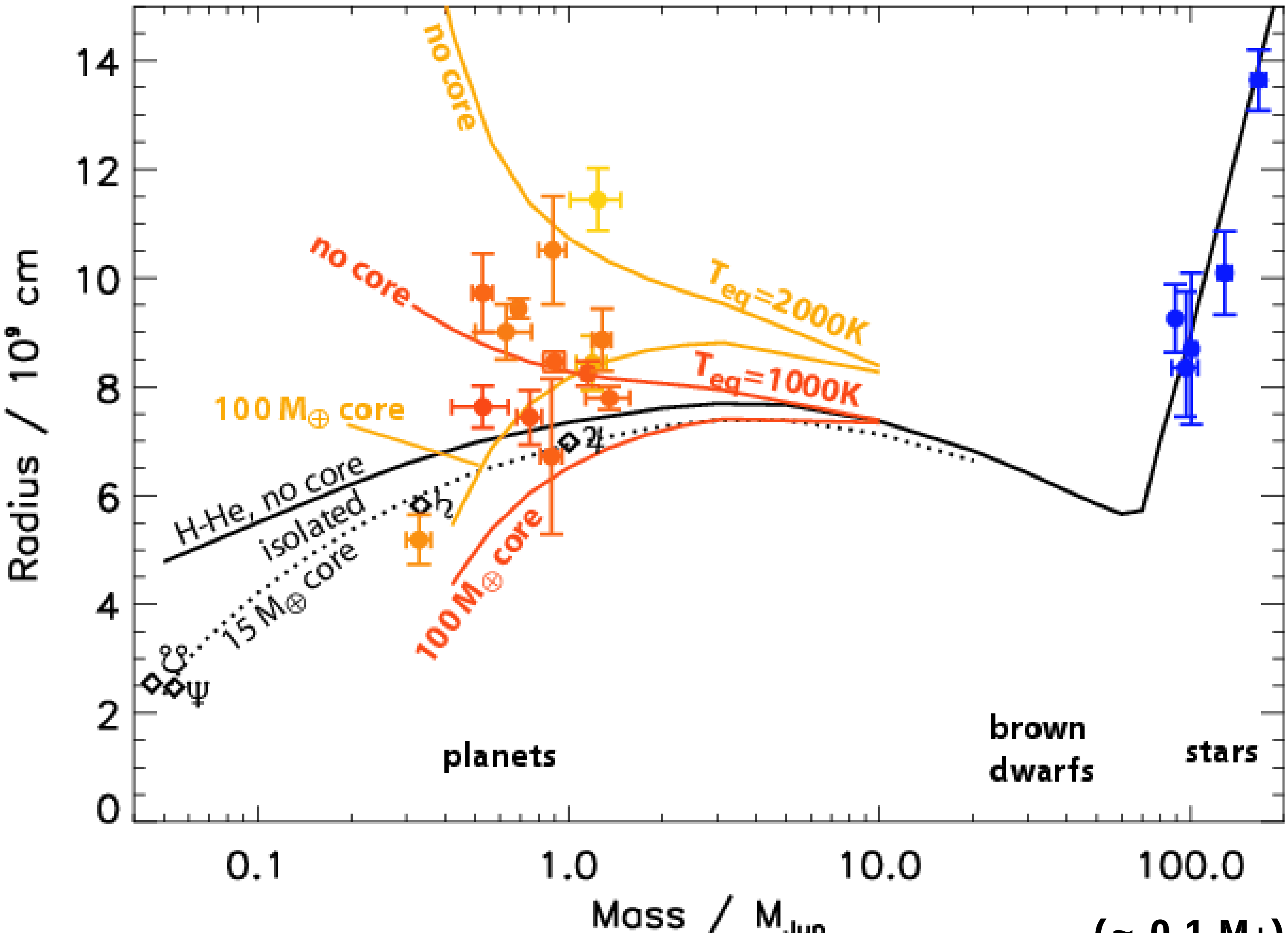

(~ 0.1 M_J)

pp-chains

$$^{1}\mathrm{H} + {}^{1}\mathrm{H} \rightarrow {}^{2}\mathrm{H} + e^{+} + \nu$$ 1.42 MeV (*2)

$$^{2}\mathrm{H} + {}^{1}\mathrm{H} \rightarrow {}^{3}\mathrm{He} + \gamma$$ 5.23 Mev (*2)

$$^{3}\mathrm{He} + {}^{3}\mathrm{He} \rightarrow {}^{4}\mathrm{He} + 2\,{}^{1}\mathrm{H}$$

12.86 MeV (*pp*1)

$$^{3}\mathrm{He} + {}^{4}\mathrm{He} \rightarrow {}^{7}\mathrm{Be} + \gamma$$

(18.62)

$$^{7}\mathrm{Be} + e^{-} \rightarrow {}^{7}\mathrm{Li} + \nu$$

$$^{7}\mathrm{Li} + {}^{1}\mathrm{H} \rightarrow {}^{4}\mathrm{He} + {}^{4}\mathrm{He}$$

(*pp*2)

$$^{7}\mathrm{Be} + {}^{1}\mathrm{H} \rightarrow {}^{8}\mathrm{B} + \gamma$$

$$^{8}\mathrm{B} \rightarrow {}^{8}\mathrm{Be} + e^{+} + \nu$$

$$^{8}\mathrm{Be} \rightarrow {}^{4}\mathrm{He} + {}^{4}\mathrm{He}$$

(*pp*3)

PPI: **Q ≈ 26.2 MeV**

CNO-cycles

$$^{12}C + {}^{1}H \rightarrow {}^{13}N + \gamma$$

$$^{13}N \rightarrow {}^{13}C + e^{+} + \nu$$

$$^{13}C + {}^{1}H \rightarrow {}^{14}N + \gamma$$

$$^{14}N + {}^{1}H \rightarrow {}^{15}O + \gamma$$

$$^{15}O \rightarrow {}^{15}N + e^{+} + \nu$$

$$^{15}N + {}^{1}H \rightarrow {}^{12}C + {}^{4}He$$

$$^{16}O + \gamma$$

$$^{16}O + {}^{1}H \rightarrow {}^{17}F + \gamma$$

$$^{17}F \rightarrow {}^{17}O + e^{+} + \nu$$

$$^{17}O + {}^{1}H \rightarrow {}^{14}N + {}^{4}He$$

CNO (main cycle): **Q ≈ 25.0 MeV**

CNO versus pp

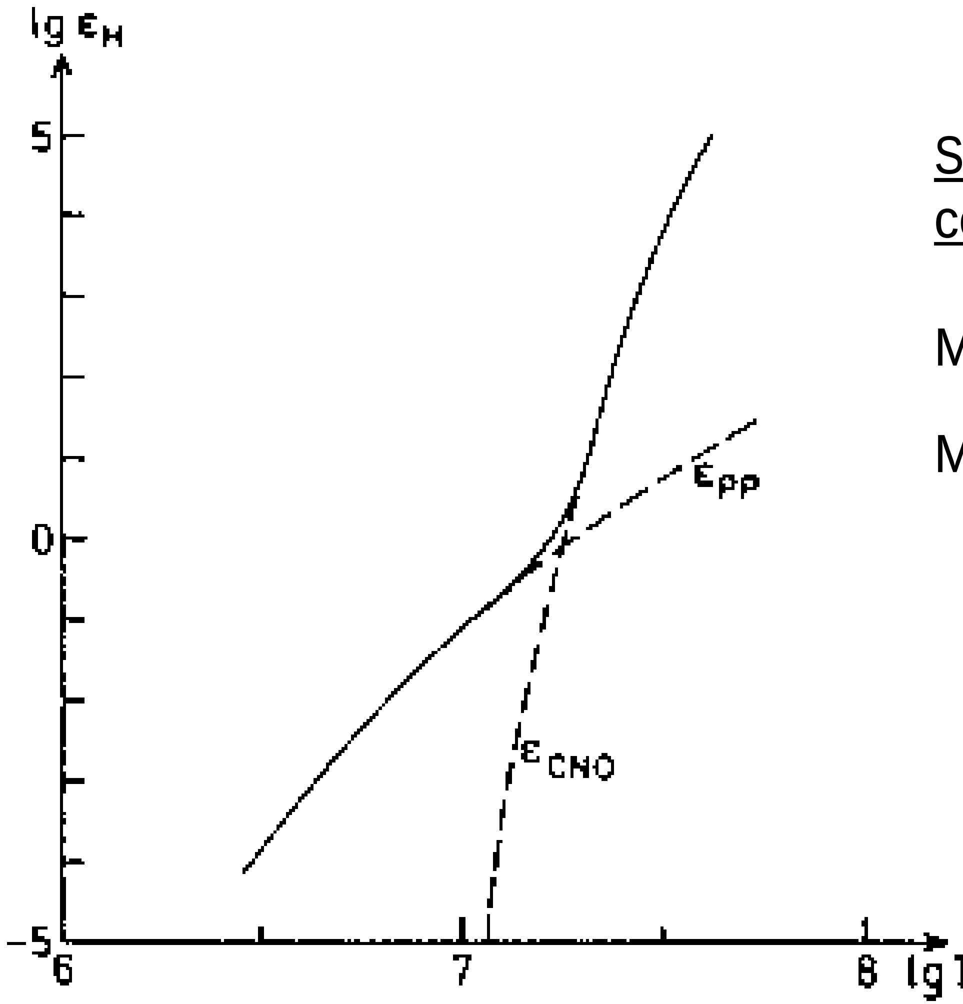

Solar composition:

M < 1.5 M_{sun}: pp

M > 1.5 M_{sun}: CNO

Structure of main sequence stars

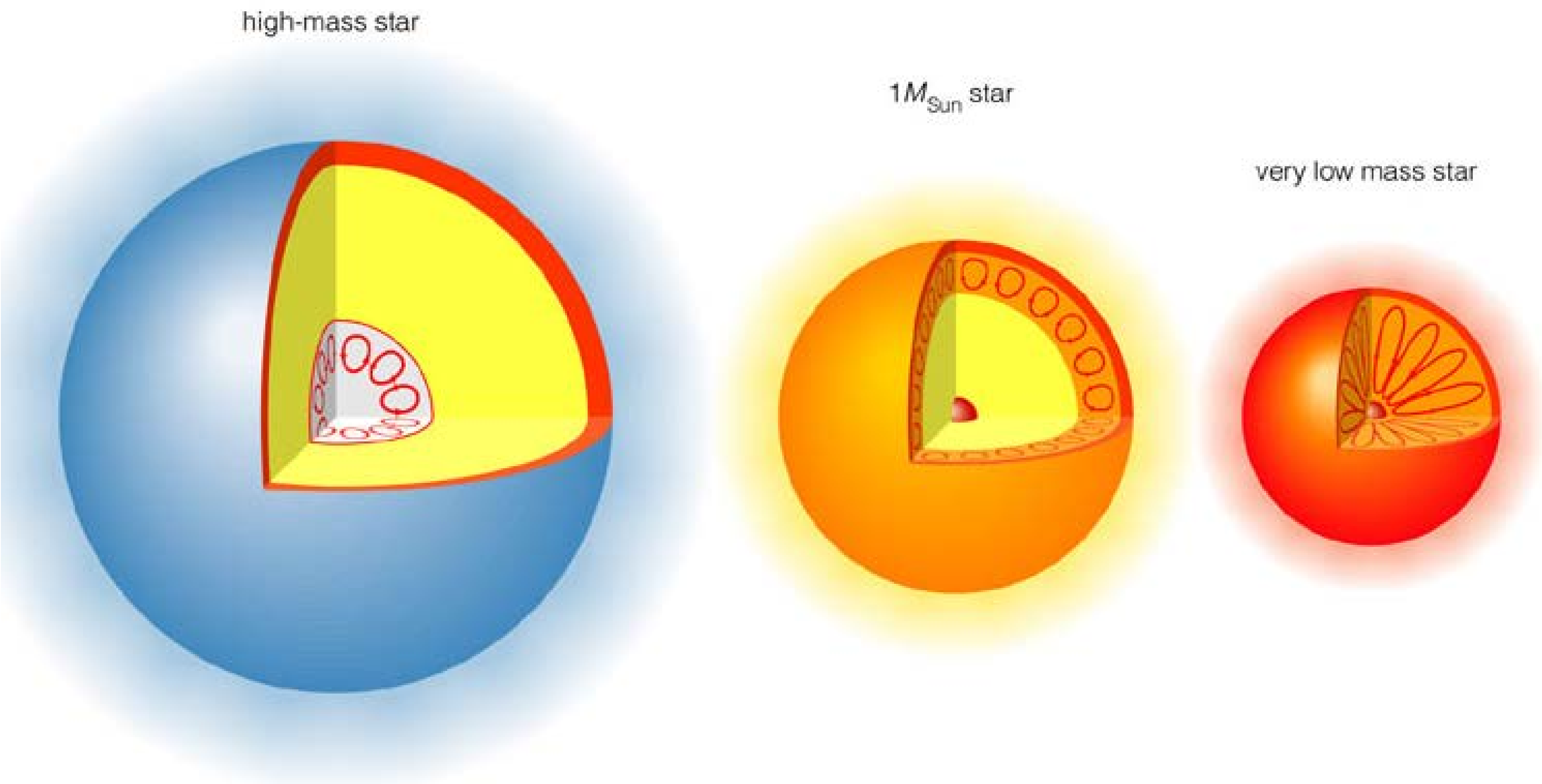

Structure of main sequence stars

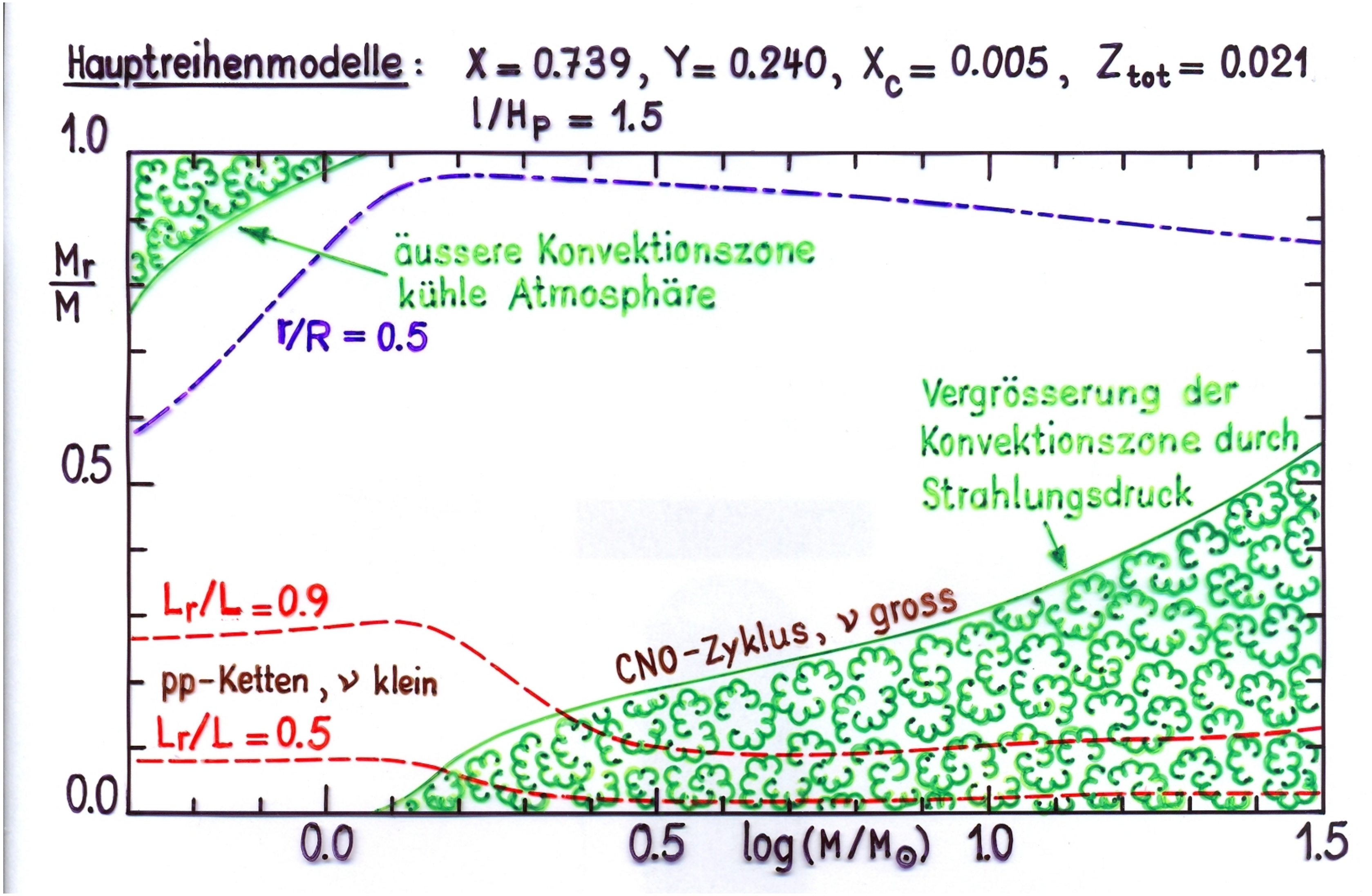

$(\varepsilon_{nuc} \sim T^{\nu})$

Structure of the sun

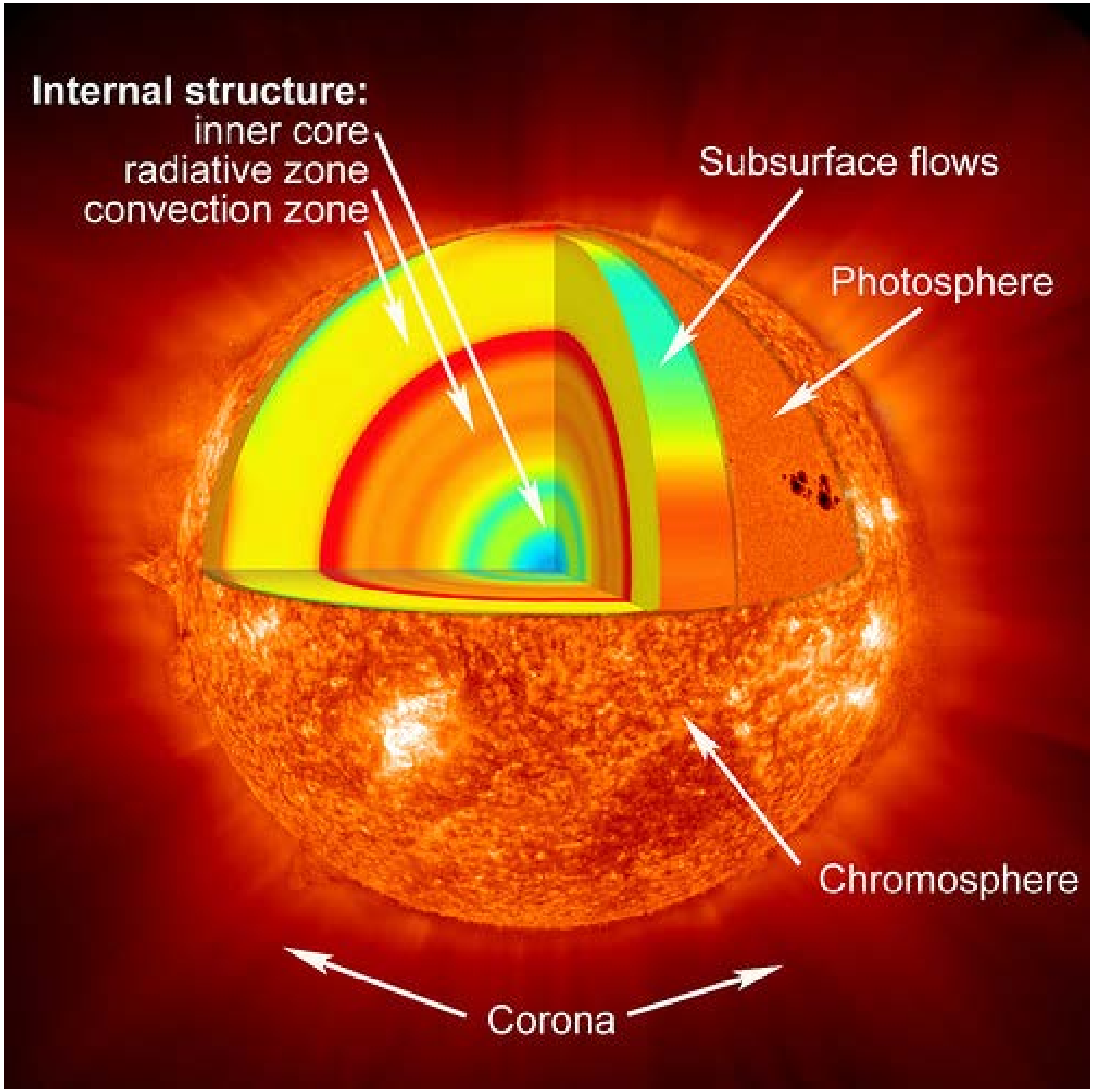

Evoltion of the sun

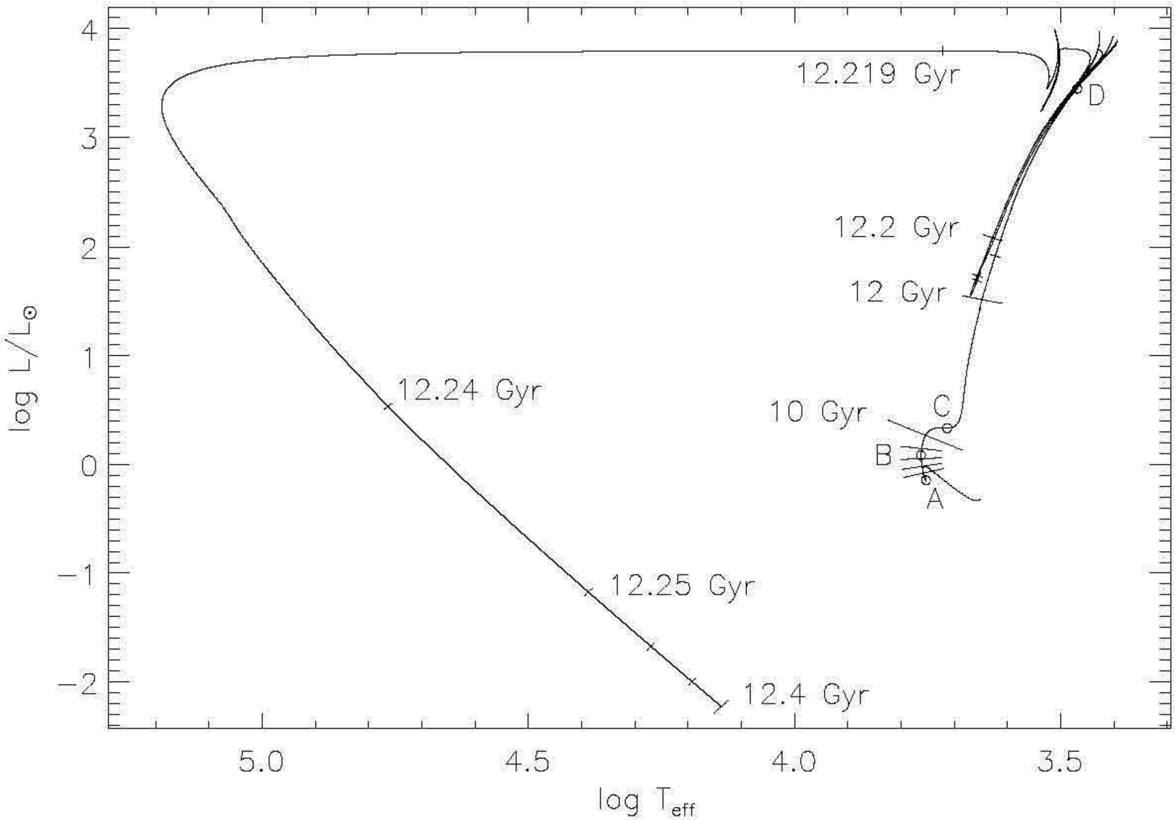

A: Middle of main sequene phase
B: Turn-off from the main sequence
C: End of core-H burning
D: He flash, formation of a planetary nebula

Main sequence evolution

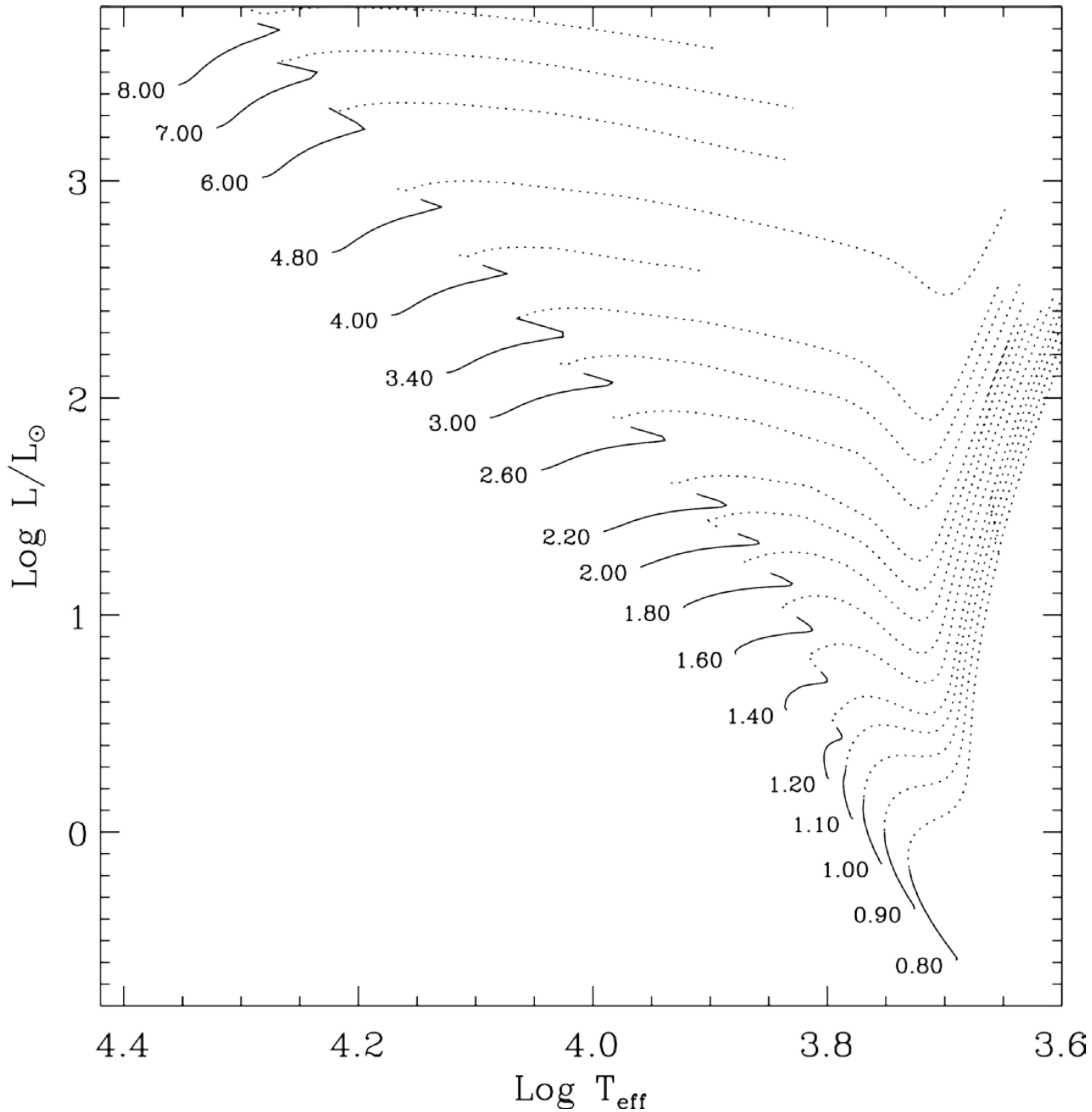

Main sequence evolution

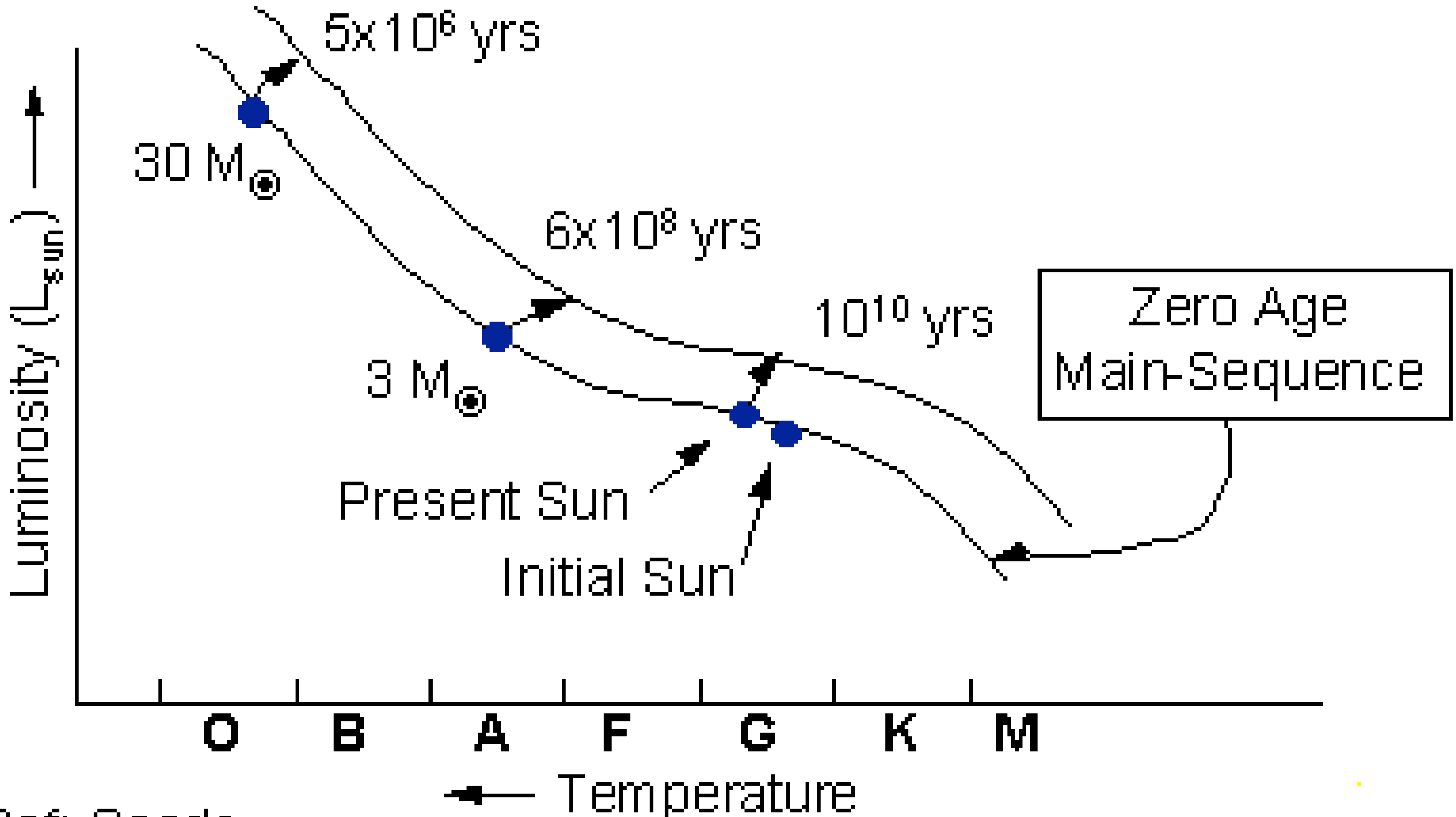

Ref: Seeds

Post-main sequence evolution

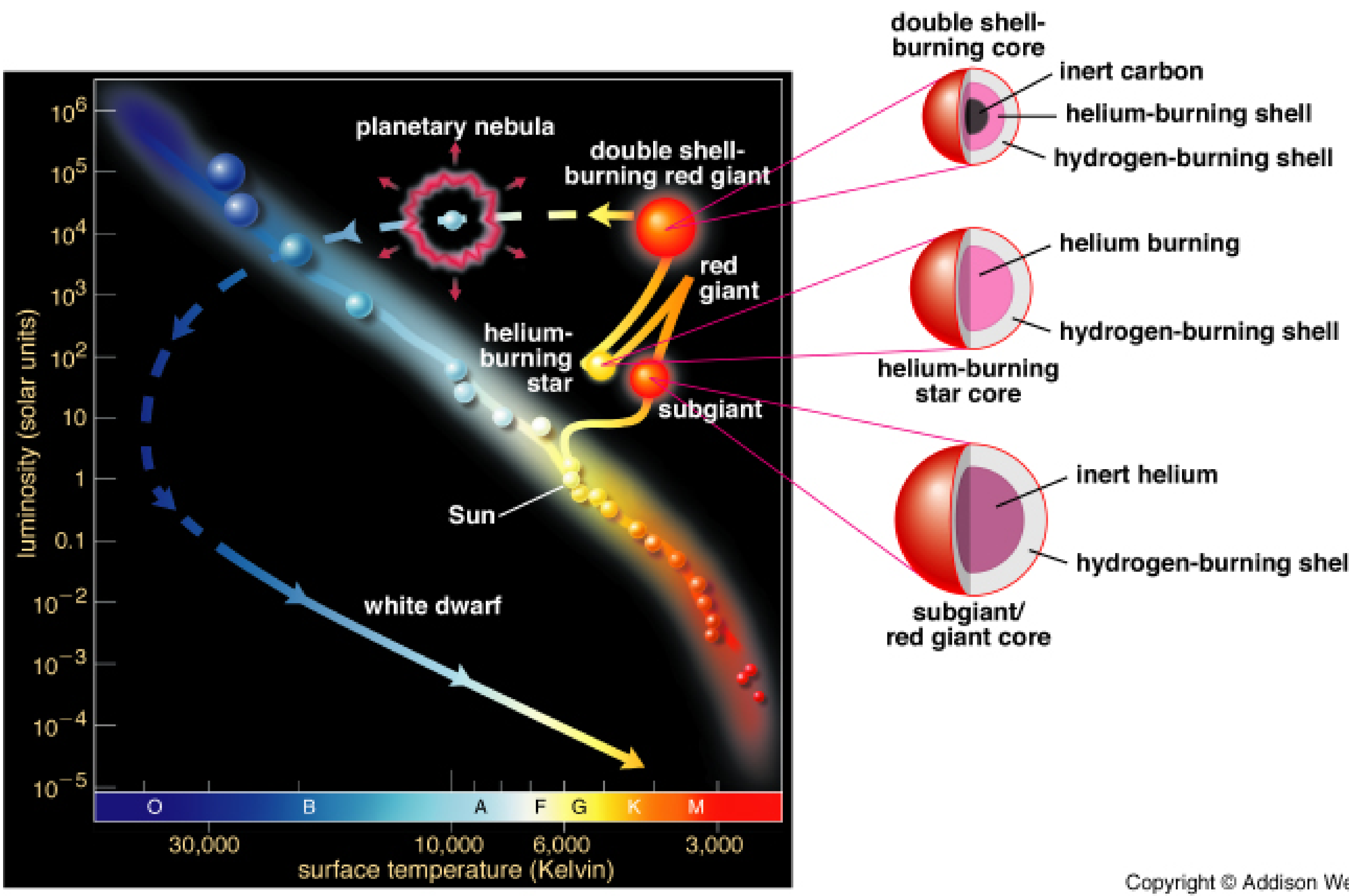

Post-main sequence evolution

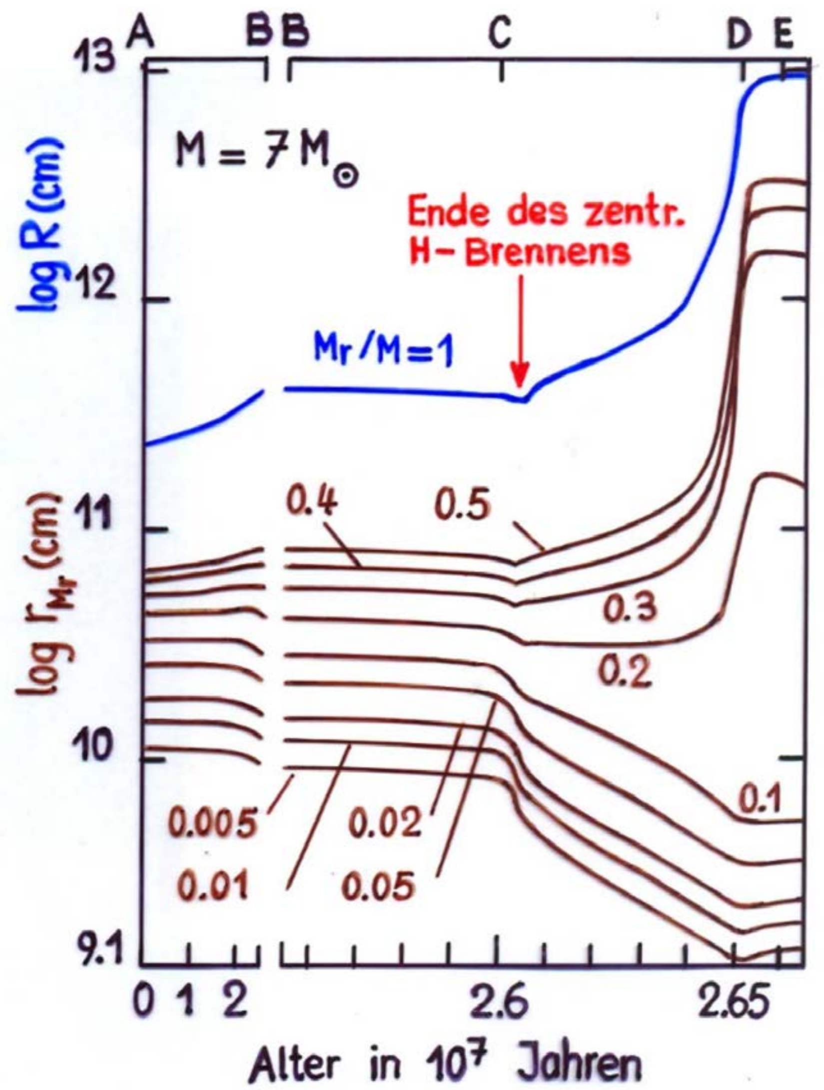

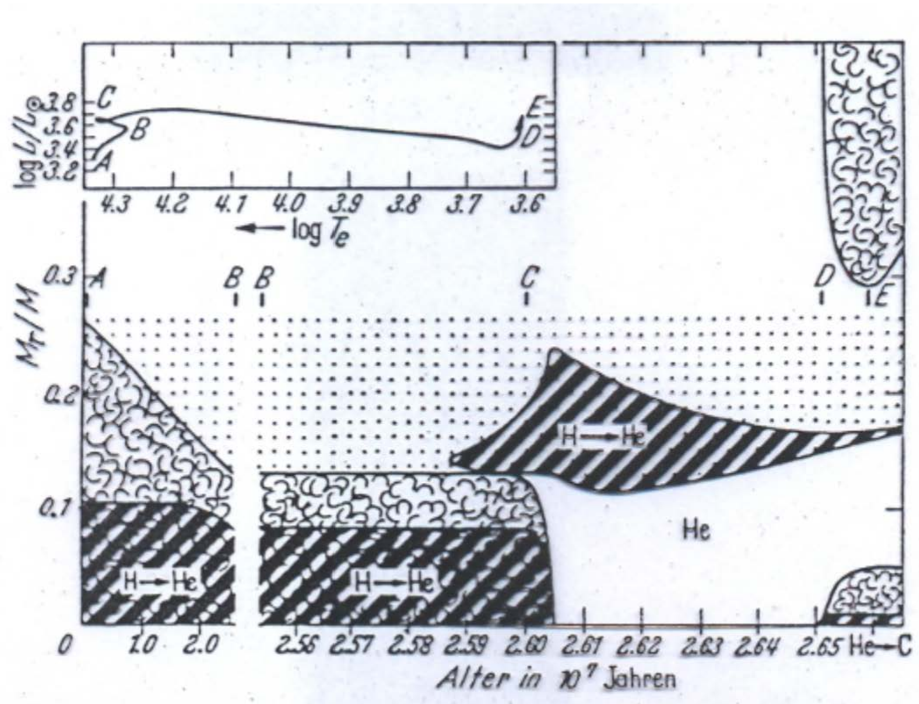

7 M_{sun} star

Post-main sequence evolution

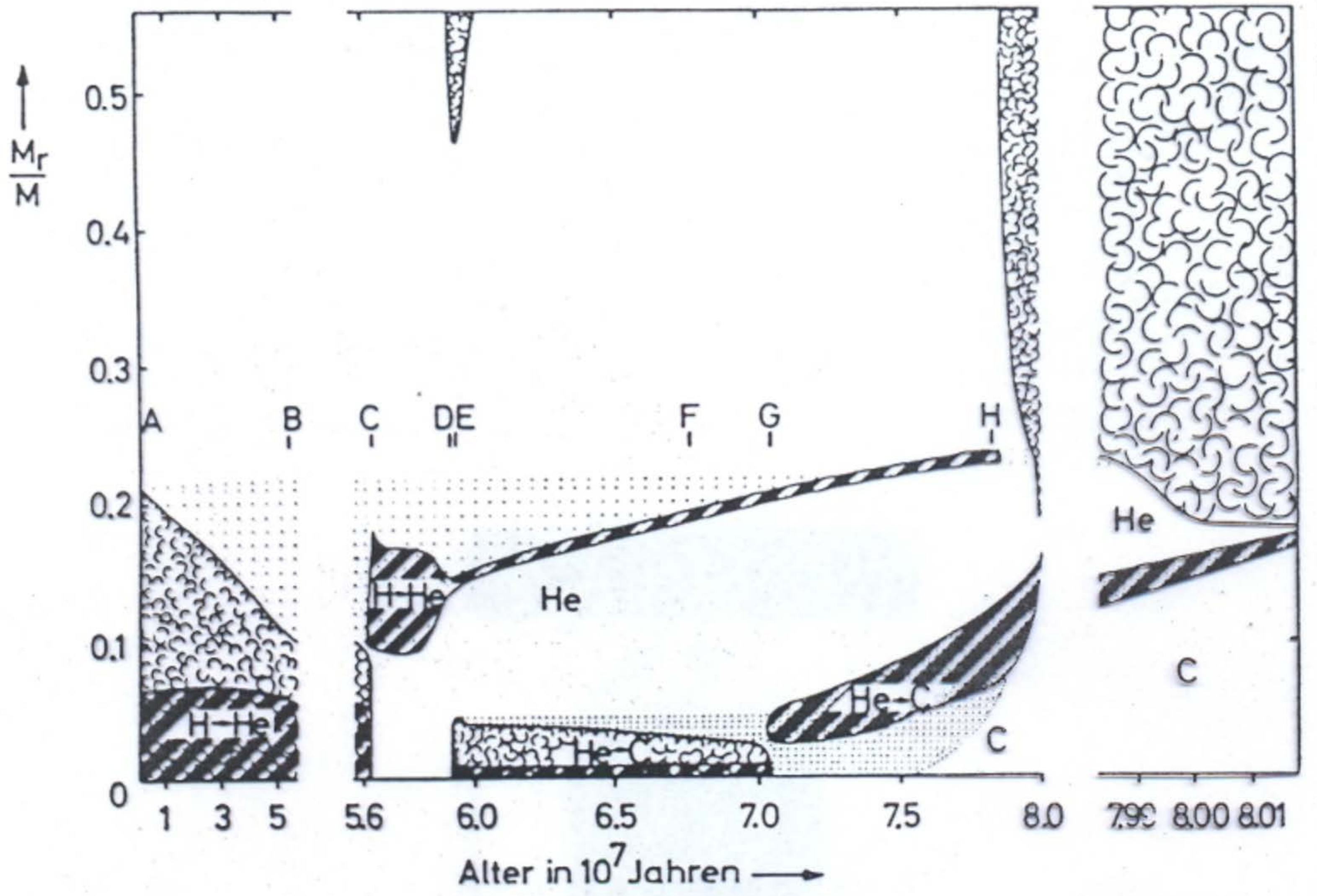

5 M_{sun} star

Red-giant branch star

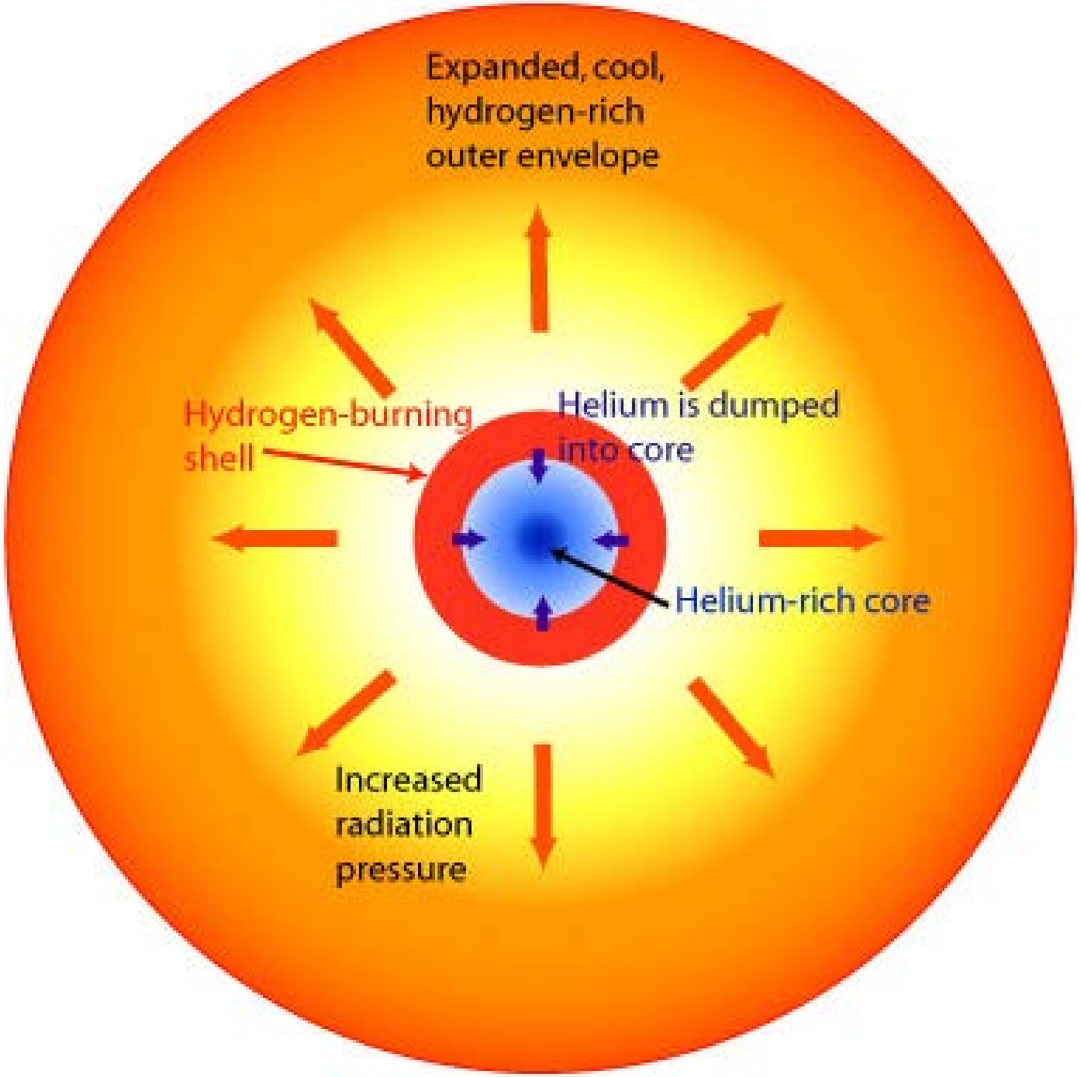

Hydrogen Shell Burning on the Red Giant Branch

Lifetimes of selected stars

Estimated Stellar Lifetimes(in units of 10^6 years)

MASS (solar masses)	SPECTRAL TYPE ON THE MAIN SEQUENCE	PERIOD OF CONTRACTION TO MAIN SEQUENCE (10^6 yrs)	ESTIMATED LIFETIME ON THE MAIN SEQUENCE (10^6 yrs)	PERIOD FOR MAIN SEQUENCE TO RED GIANT (10^6 yrs)	RED GIANT DURATION (10^6 yrs)
30	O5	0.02	4.9	0.55	0.3
15	B0	0.06	10	1.7	2
9	B2	0.2	22	0.2	5
5	B5	0.6	68	2	20
3	A0	3	240	9	80
1.5	F2	20	2,000	280	
1.0	G2	50	10,000	680	
0.5	M0	200	30,000		
0.1	M7	500	10^7		

Source: Fundamental Astronomy, edited by H. Karttunen et al., 1994

Post-main sequence evolution

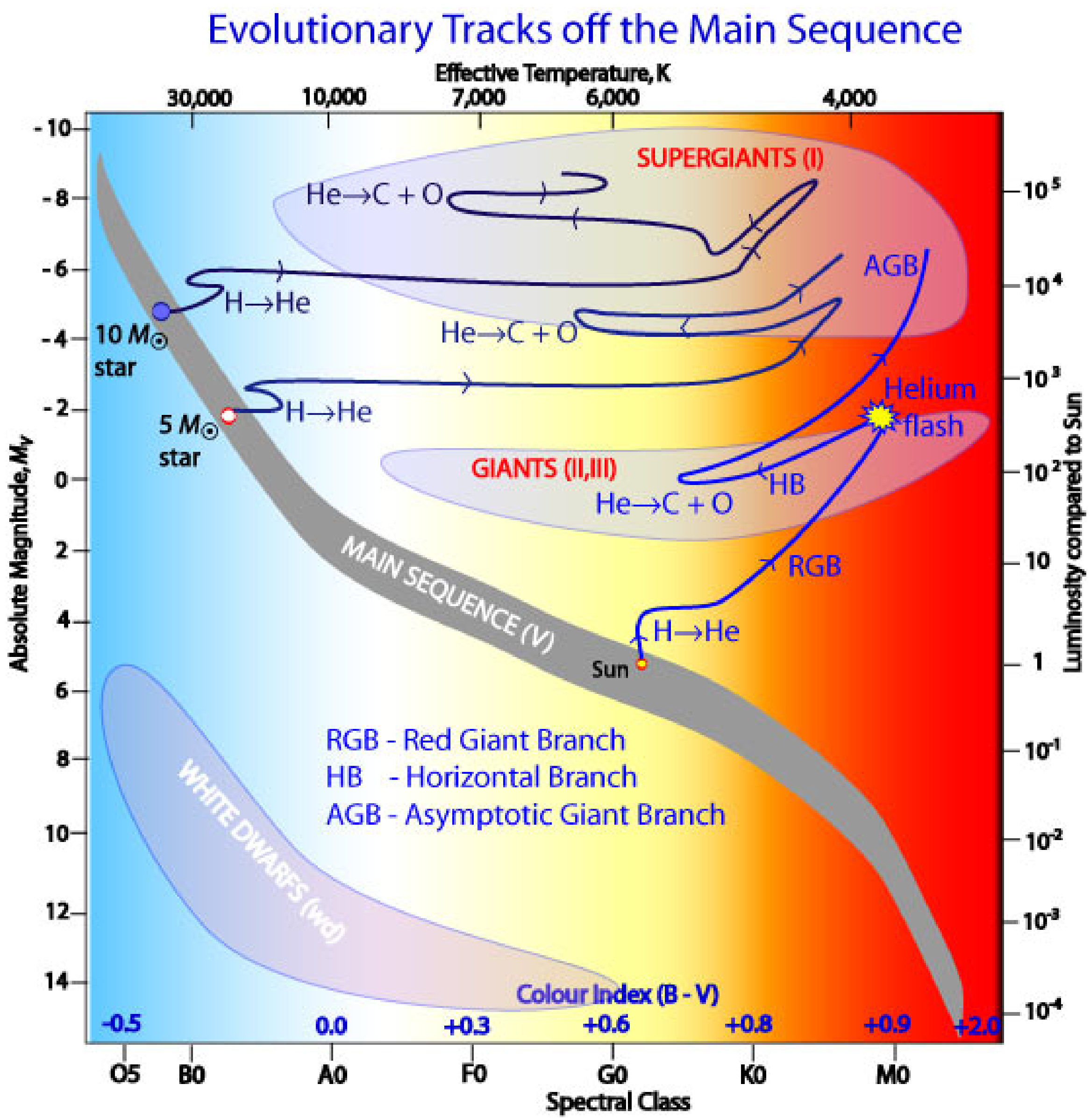

Post-main sequence evolution

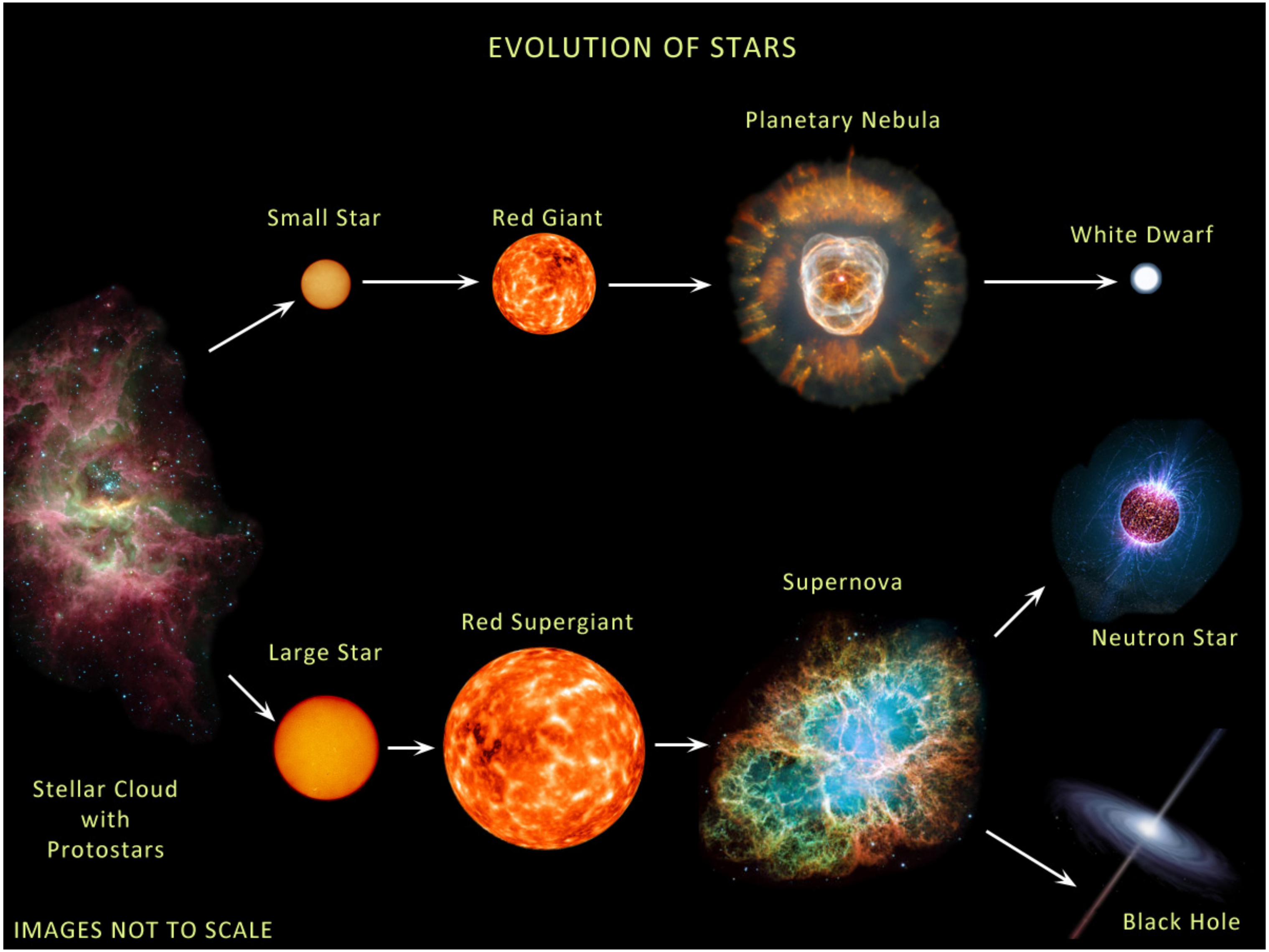

Core-He flash

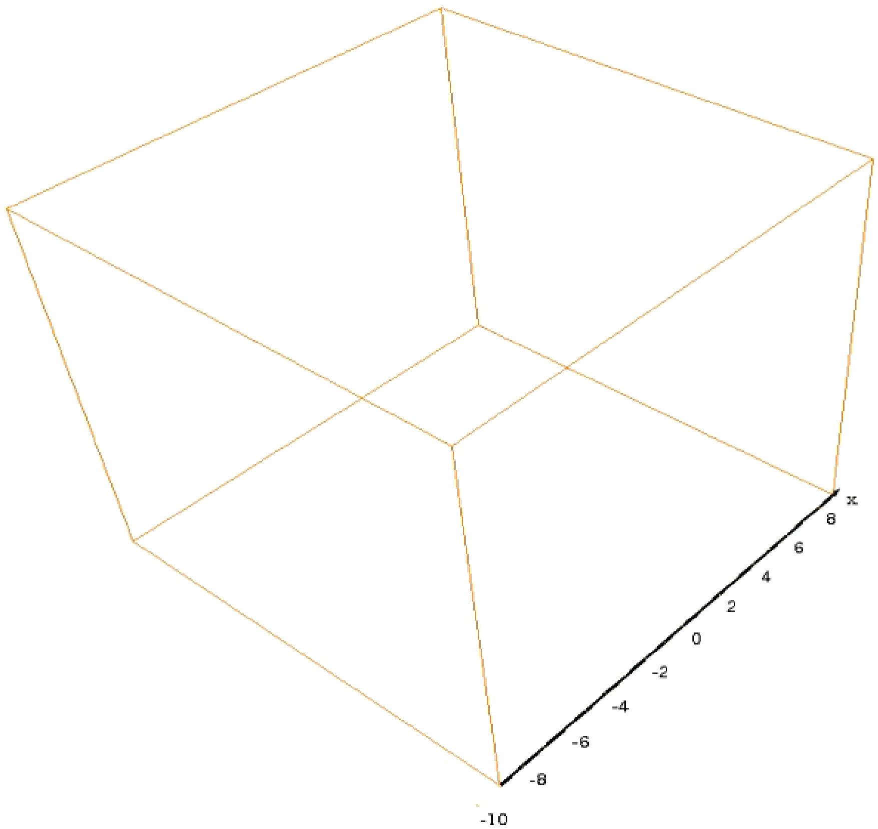

WD‘s & Planetary Nebulae

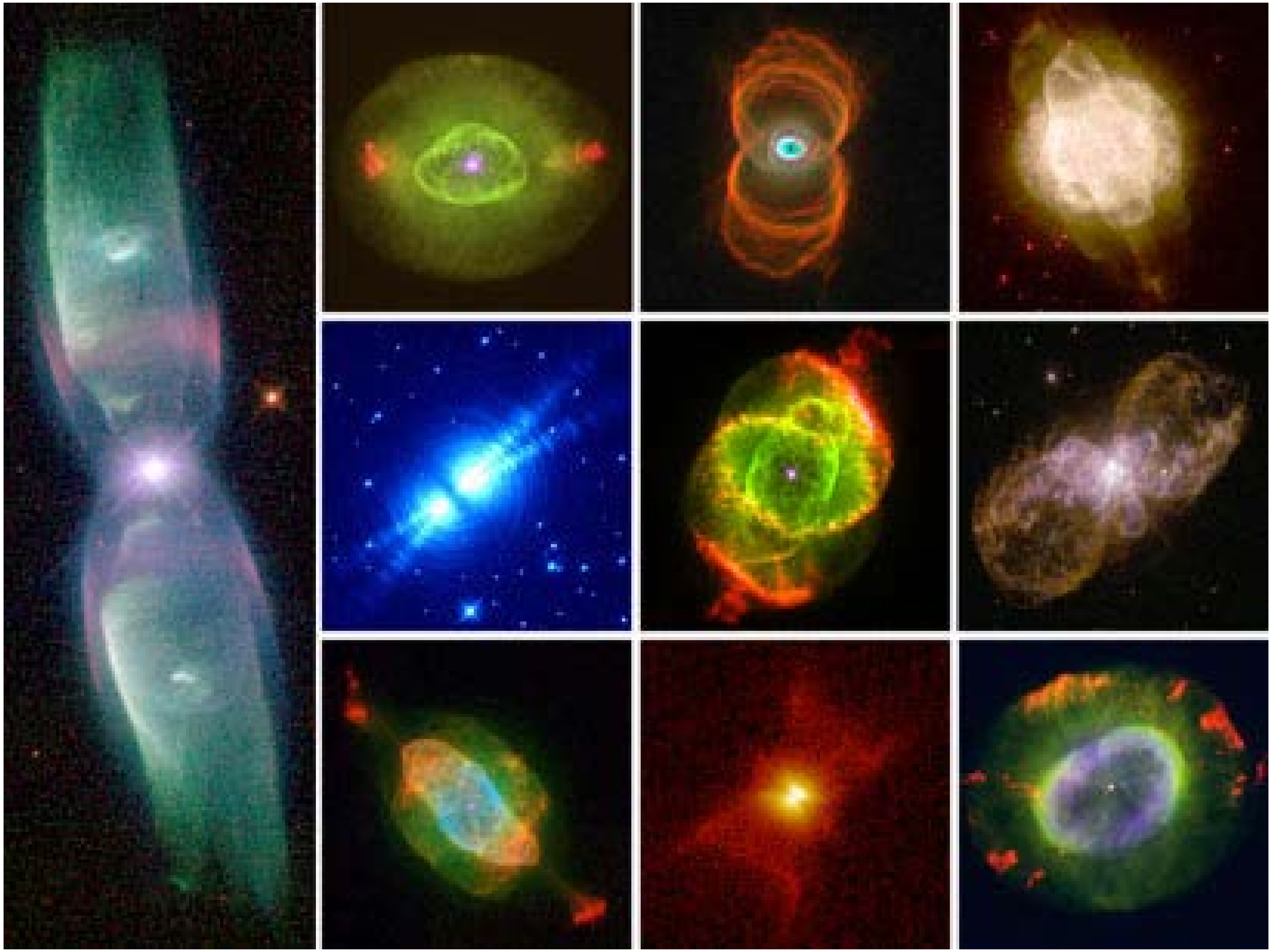

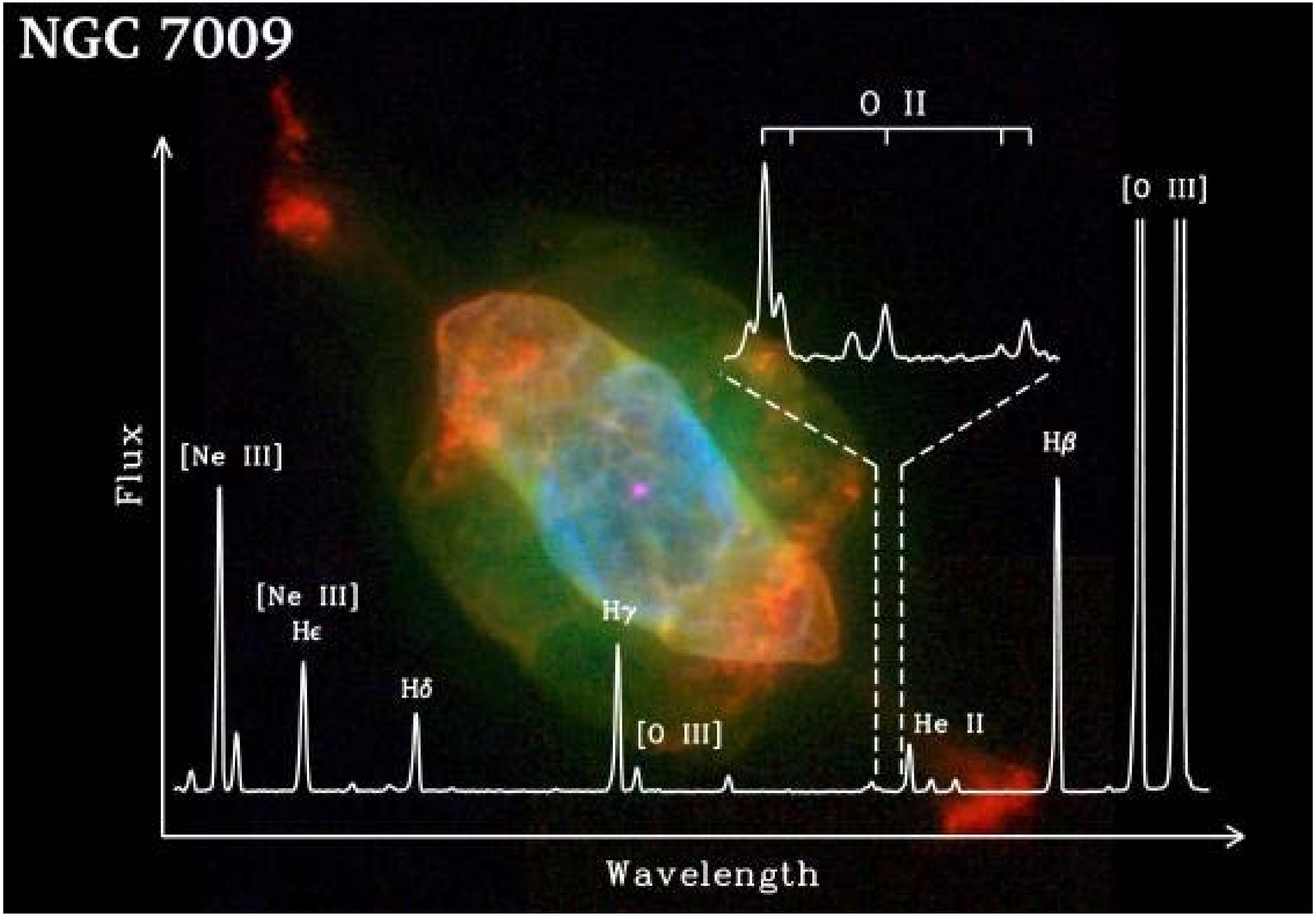
NGC 7009
O II
[O III]
Flux
[Ne III]
[Ne III]
Hϵ
Hδ
Hγ
[O III]
He II
Hβ
Wavelength

3-alpha Reaction

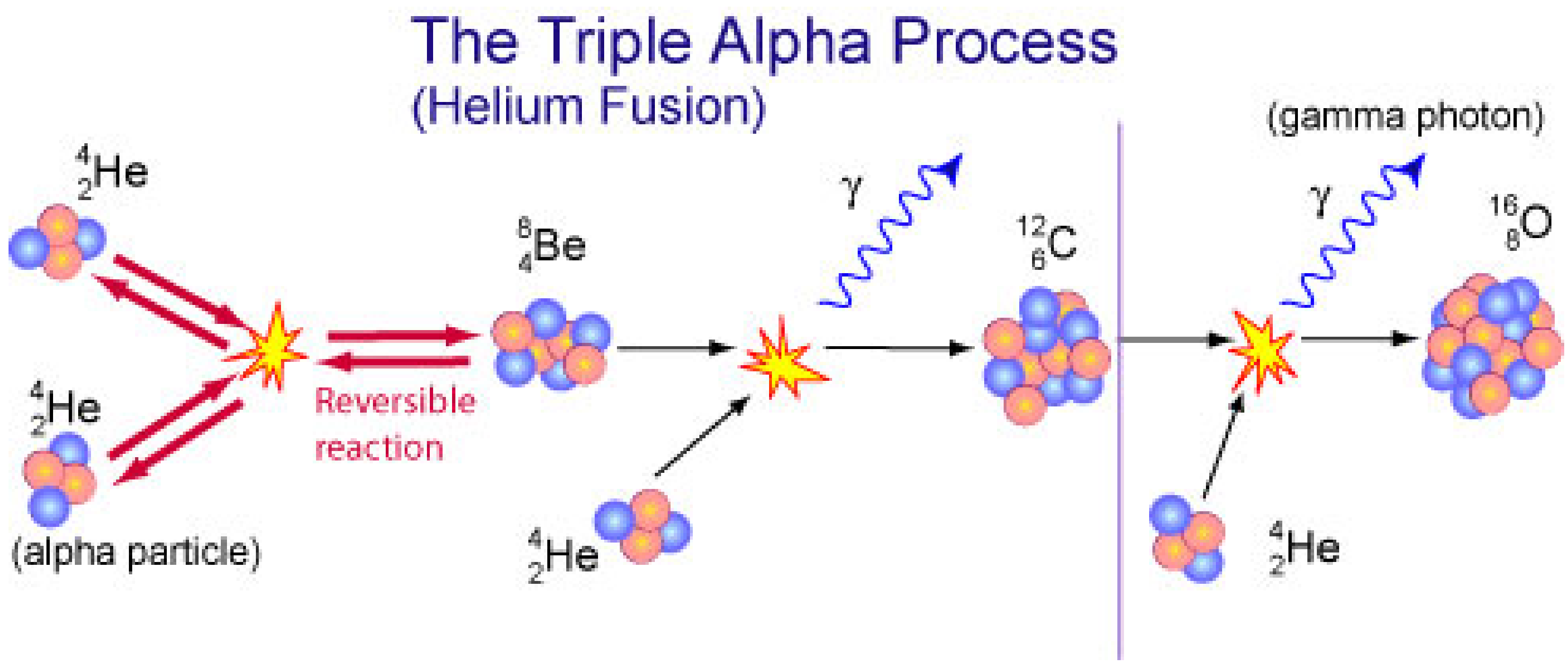

$$\epsilon_{3\alpha} = 5.3 \times 10^{21} \text{ ergs g}^{-1} \text{ s}^{-1} f \frac{\rho_5^2 Y^3}{T_8^3} \exp\left(\frac{-44}{T_8}\right)$$

(f = screening corrections; Y= He mass fraction)

3-alpha Reaction

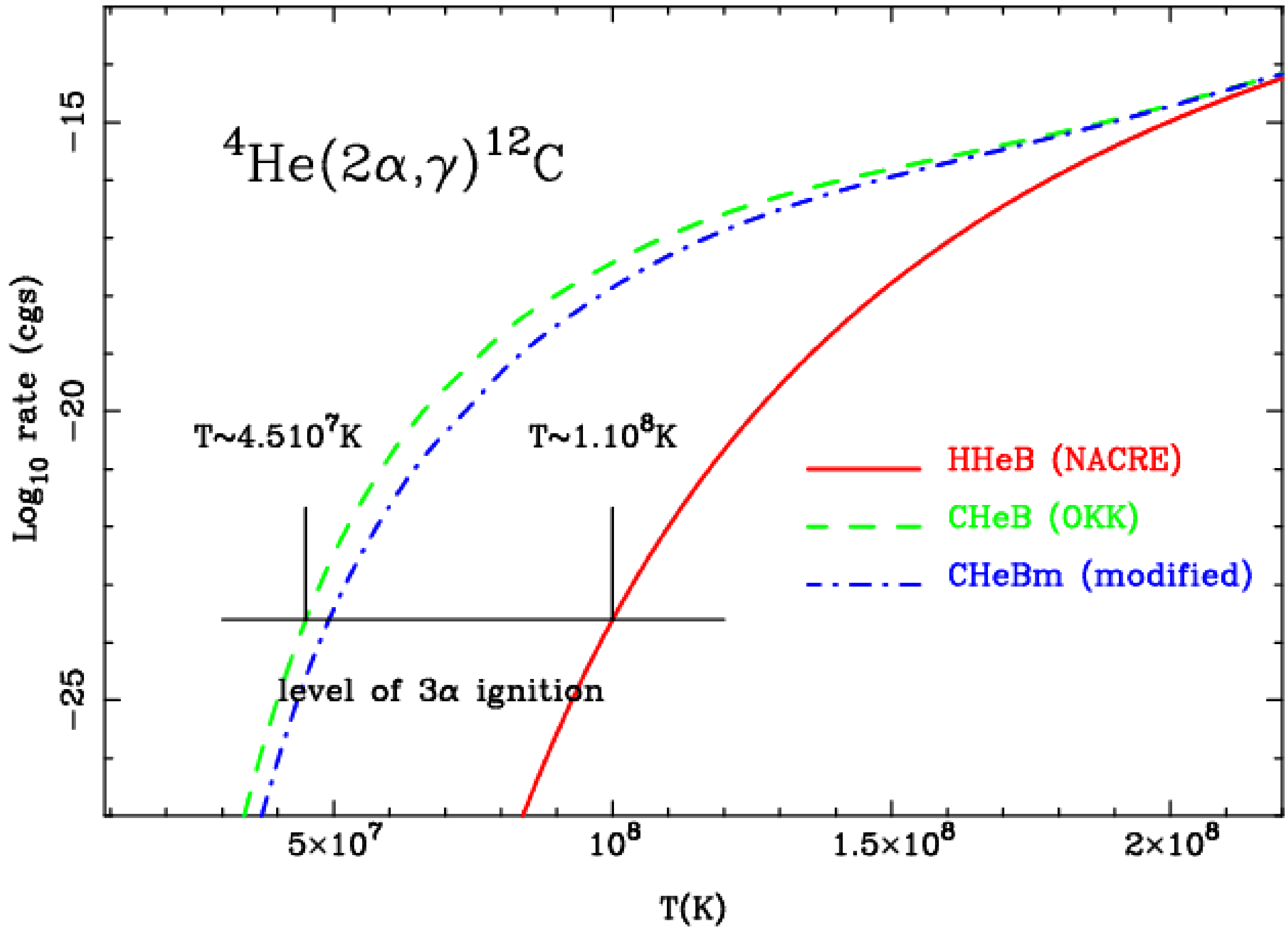

Morel et al. , A&A **520**, A41 (2010)

Detailed evolution: 5 M_{sun} star

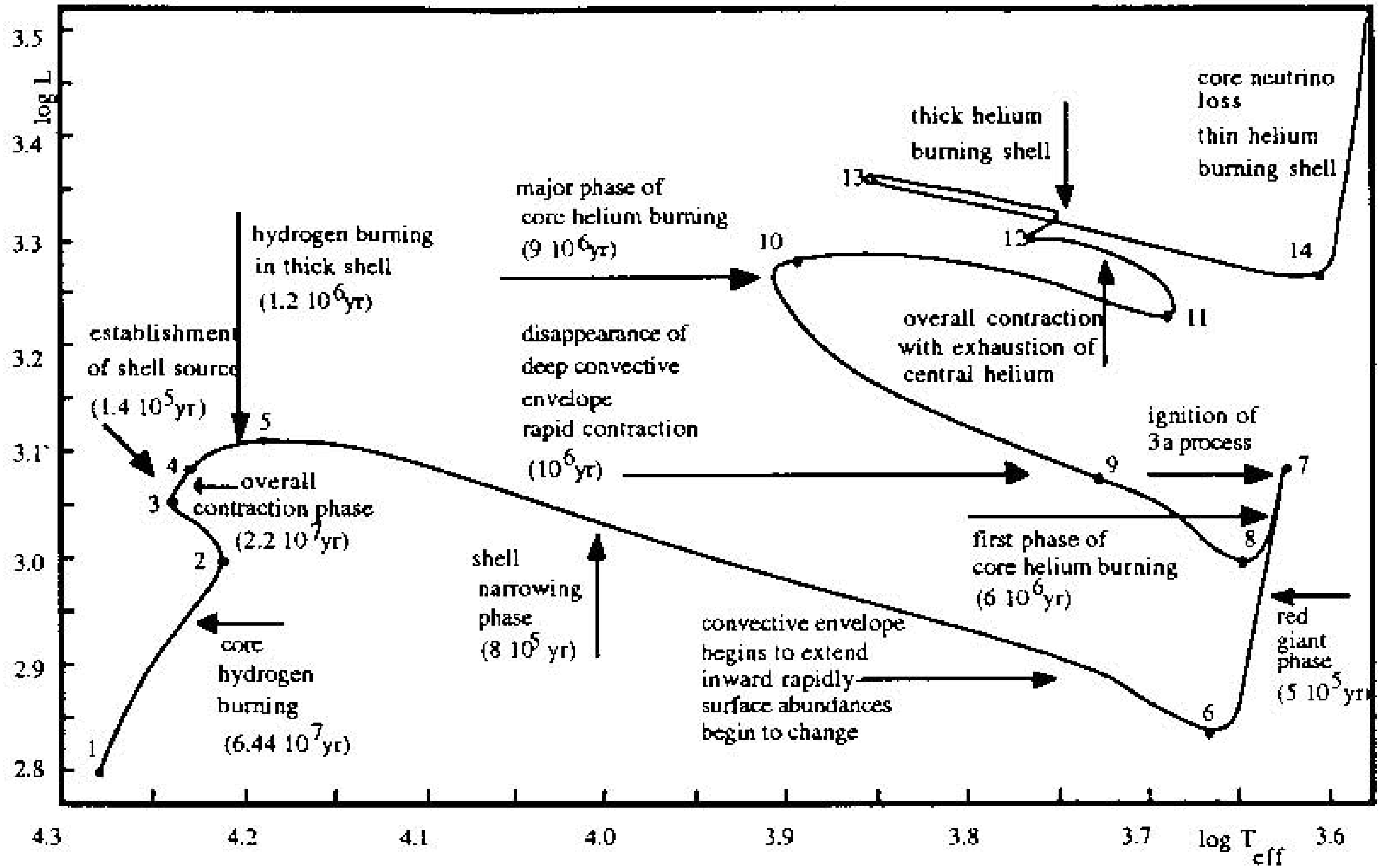

Core-He burning lifetimes

M / M_{sun}	$T_{c\text{-}He}$ (years)
3	$2.5 \cdot 10^7$
5	$6.0 \cdot 10^6$
9	$2.9 \cdot 10^6$
15	$1.4 \cdot 10^6$
25	$7.2 \cdot 10^5$

Homologous contraction & ignition masses

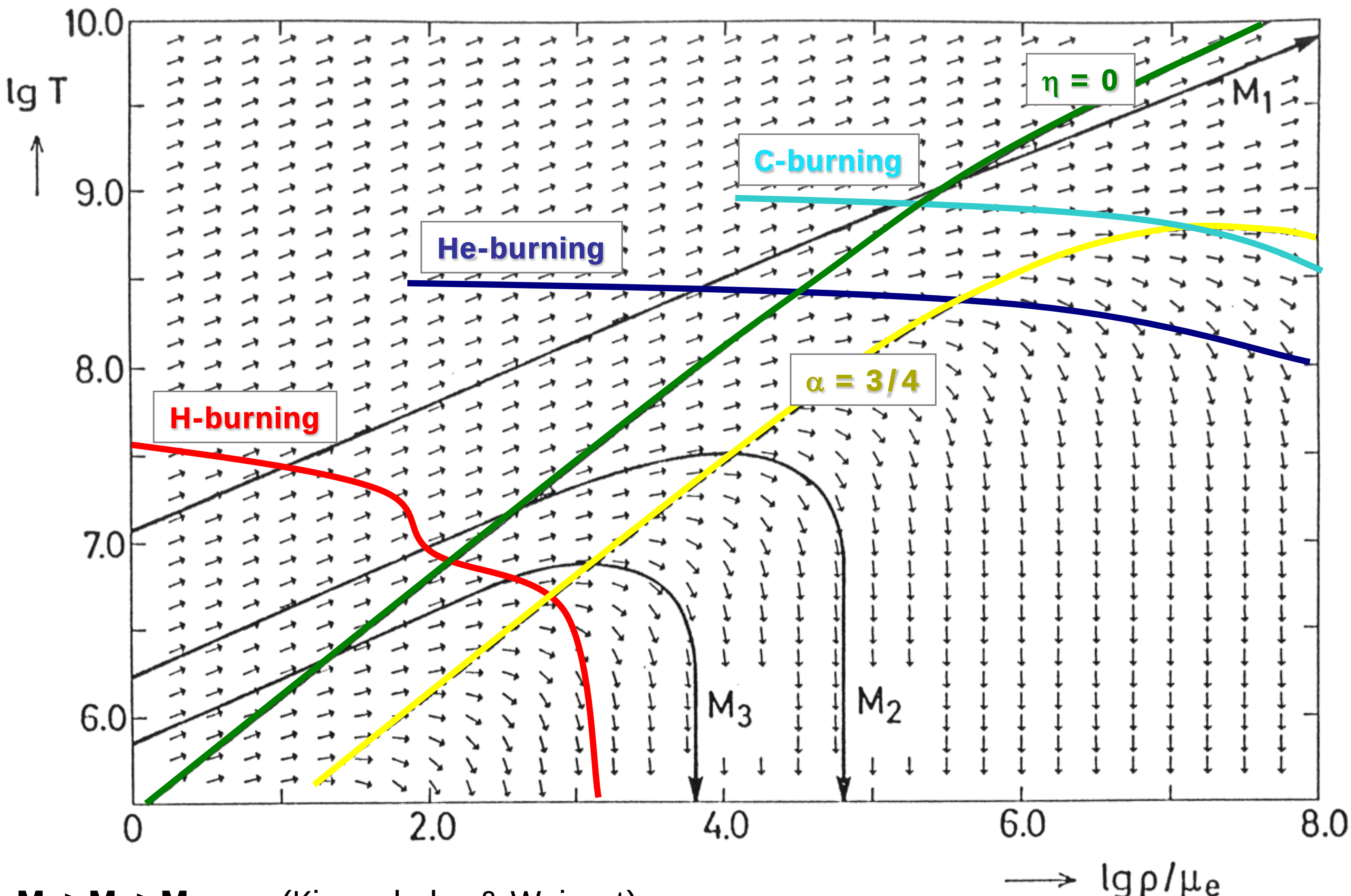

$M_1 > M_2 > M_3$ (Kippenhahn & Weigert)

Computed stellar evolution tracks

Iben (1991),

ApJ Suppl 76, 55

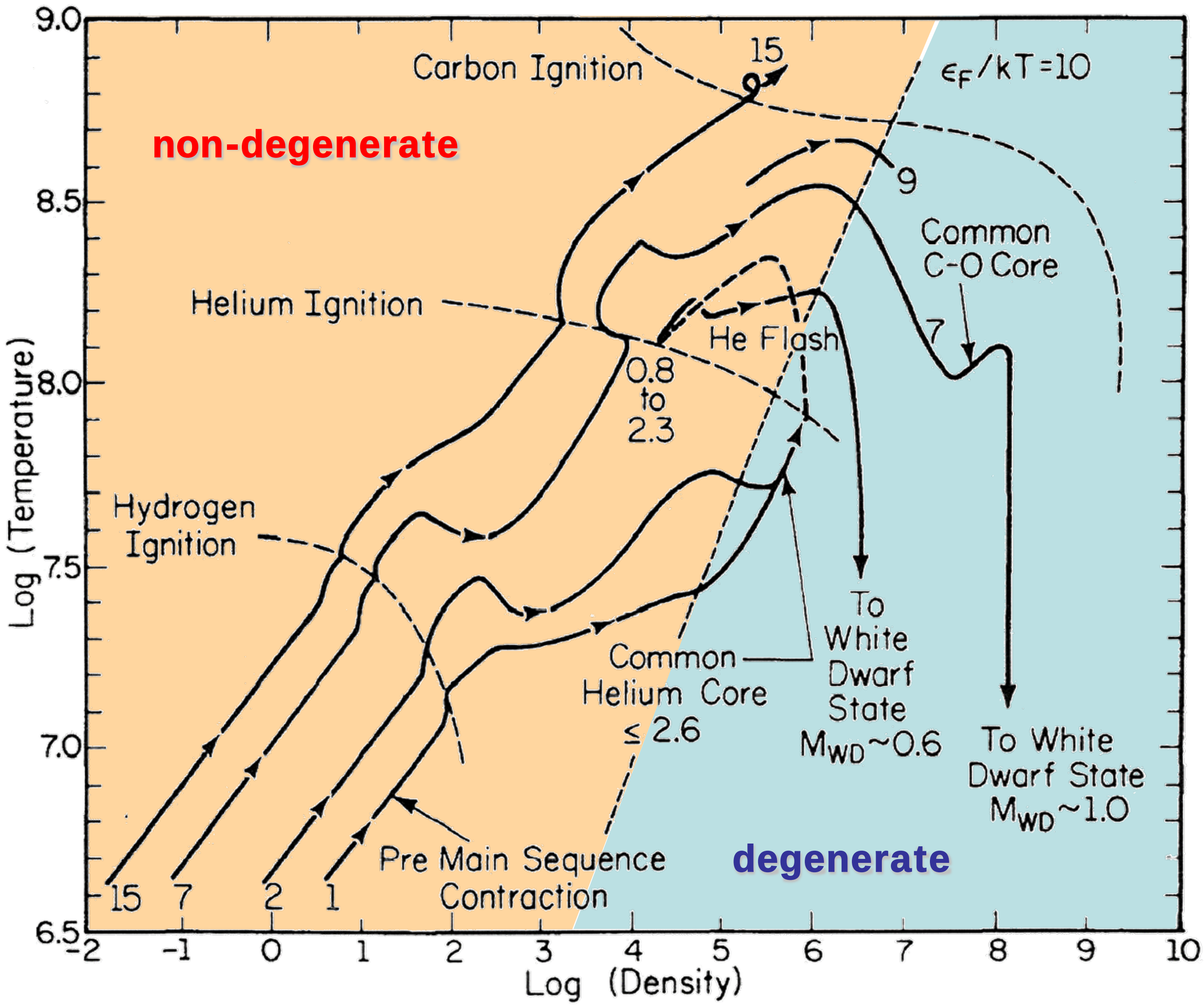

Asymptotic Giant Branch (AGB) stars

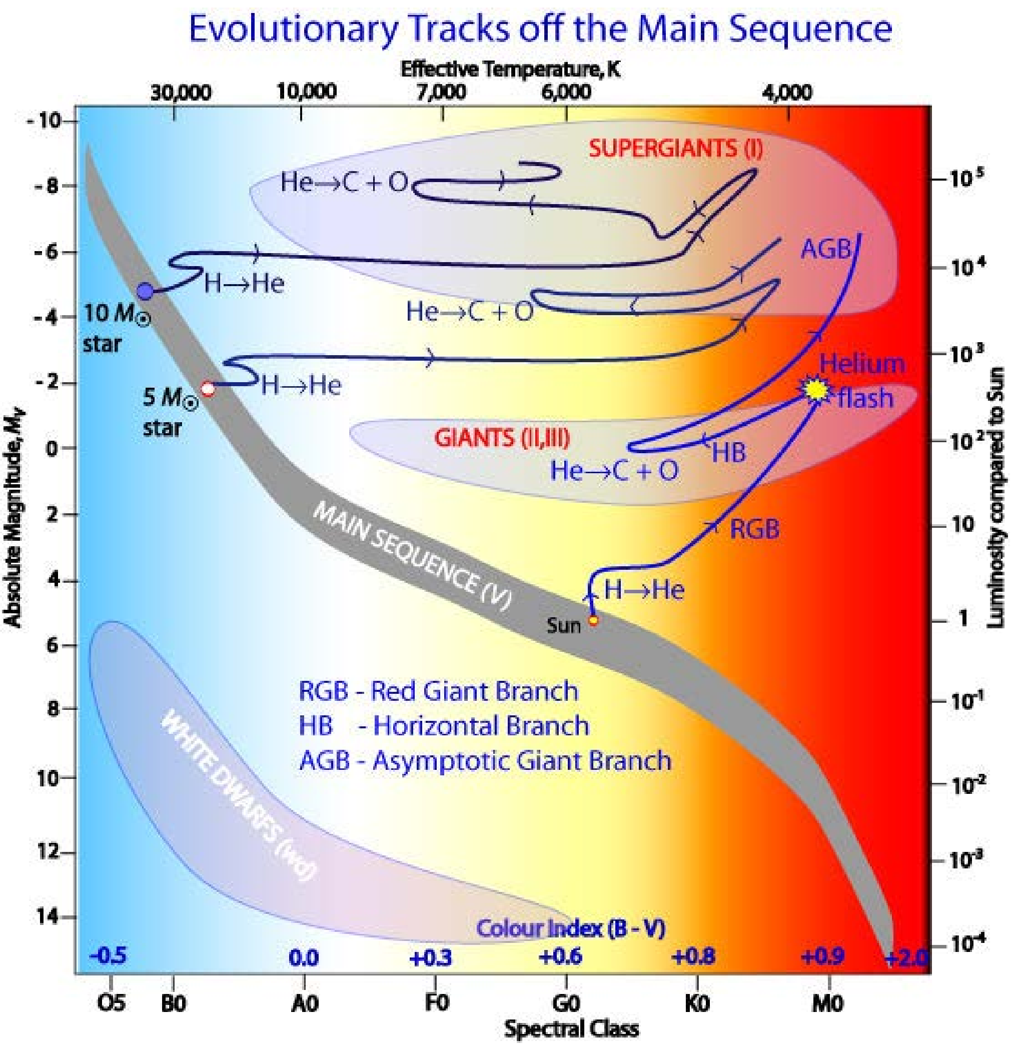

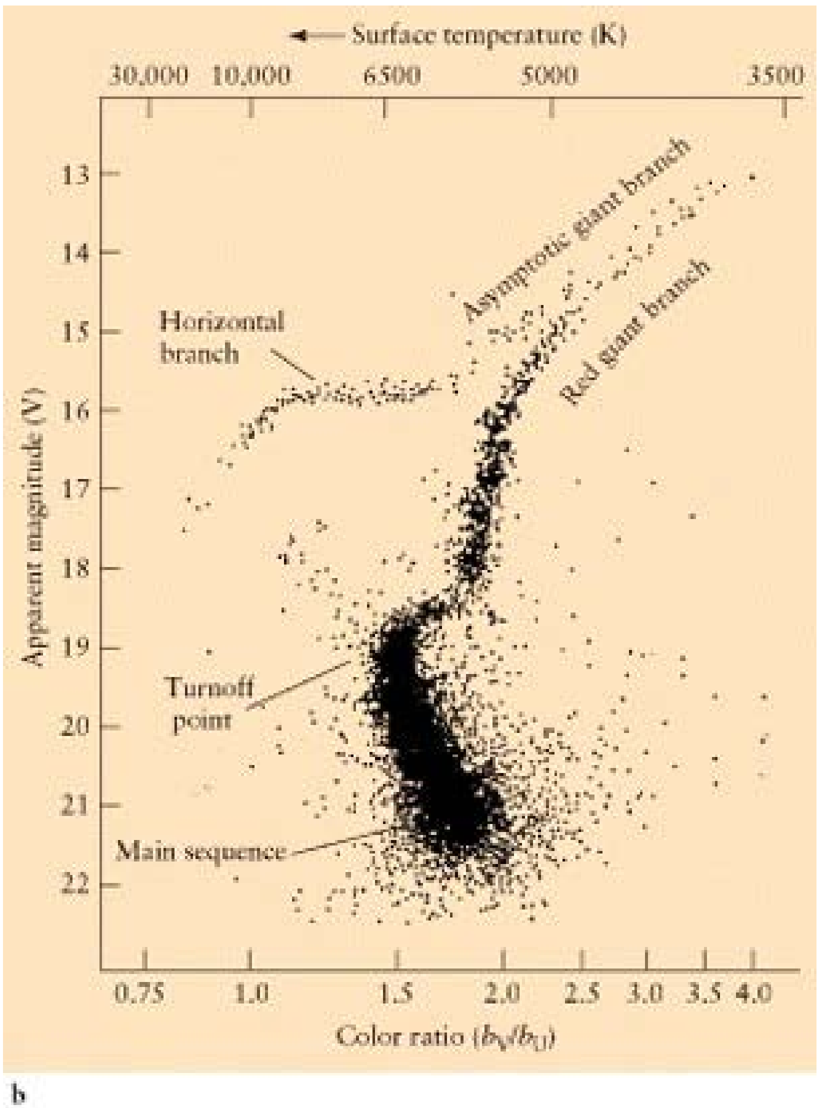

Asymptotic Giant Branch (AGB) stars

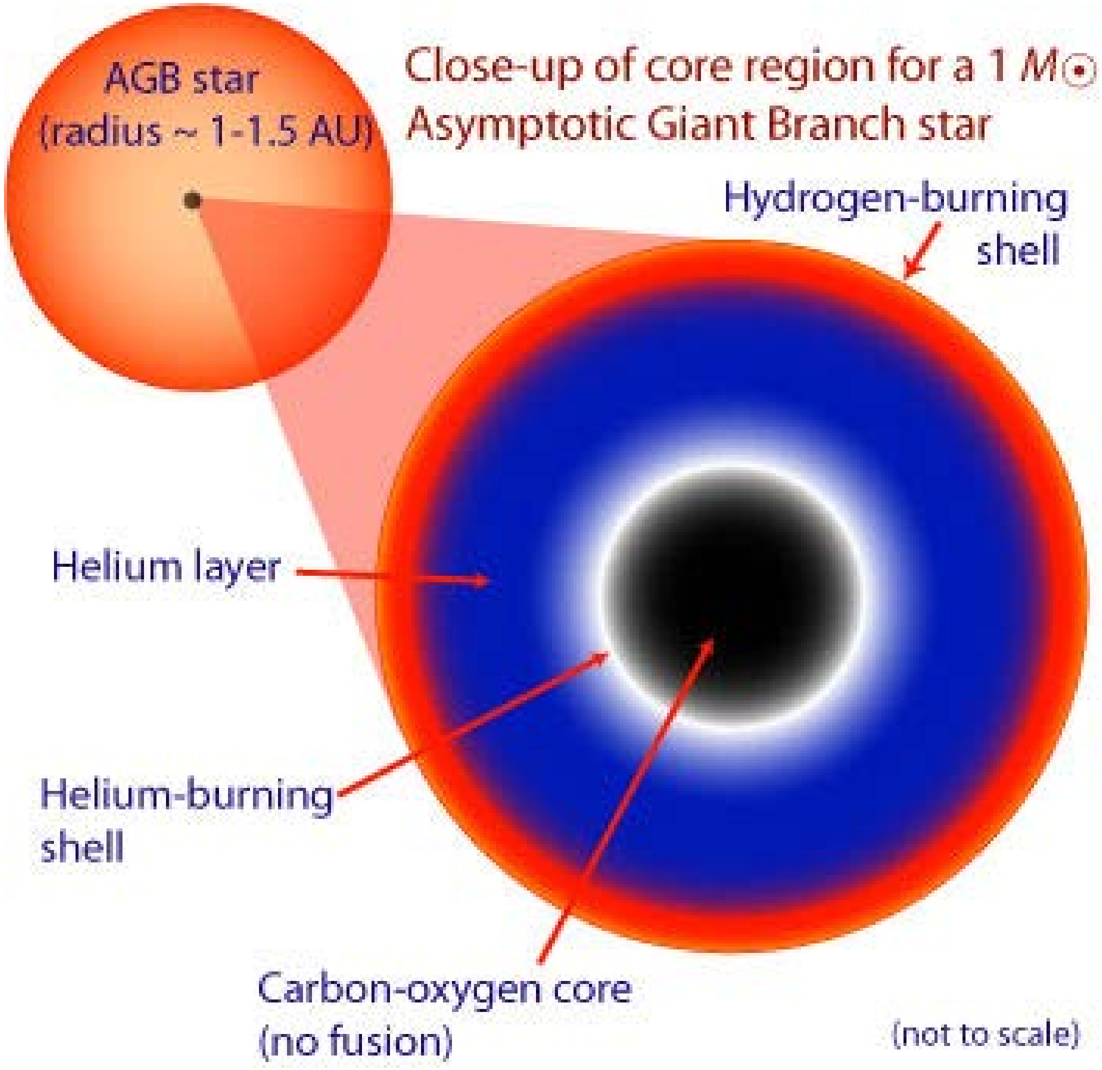

C-O core grows towards Chandrasekhar-mass (~1.4M_{sun})

⇒

Contraction, luminosity mostly from He shell

Thermal pulses of AGB stars

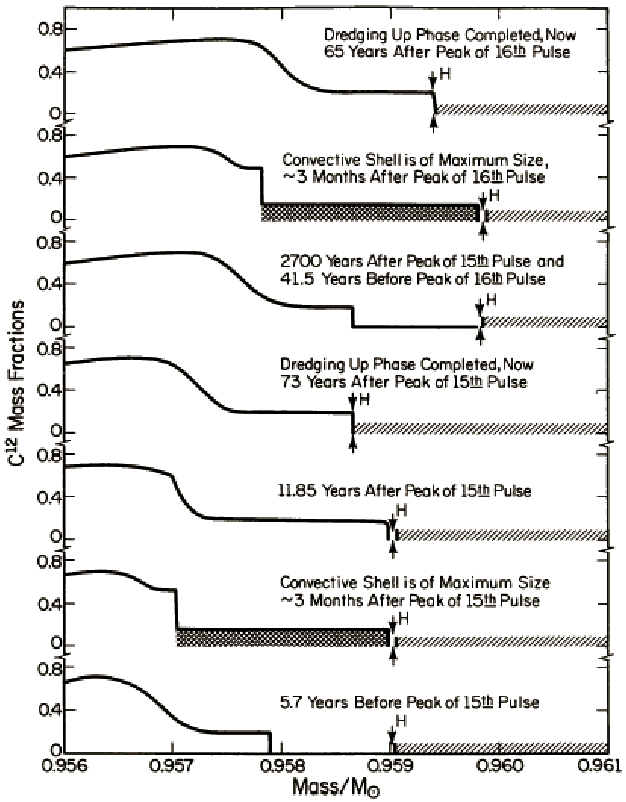

FIG. 13. Carbon-abundance profiles at selected times (time increasing upwards) during several pulse cycles of an asymptotic giant branch star of total mass 7 $M_\odot$ and core mass 0·95 $M_\odot$. Each panel gives the abundance by mass of ^{12}C as a function of mass outward from the centre. The cross-hatched regions mark the location of a helium-burning convective shell and the single hatched regions show how far envelope convection extends inward. During pulse peak, convection extends outward from the base of the burning shell almost, but not quite, to the point H beyond which hydrogen is found. After shell convection dies down, the base of the convective envelope moves inward into the region where freshly made carbon has been carried by shell convection during pulse peak. Fresh carbon is thereupon dredged to the stellar surface. Note that there is an 'overlap' between successive convective shells. That is, a portion of the matter that appears in any given convective shell also appears in succeeding convective shells. This has important consequences for the distribution of neutron-rich isotopes formed in each convective shell. From Iben, I. (Jr), 1976. *Astrophys. J.*, **208**, 165.

Mechanism:

He-shell source burns faster (outwards) than H-shell (nearly extinct)

Because of composition discontinuity at H-shell (He -> H) convection is blocked ("Ledoux criterion")

Heat accumulates: more He-burning <u>and</u> re-ignition of H-shell

$L^{max}_{He} \approx 10^6 - 10^7\ L_{sun}$ (pulse maximum)

$L^{max}_{H} \approx 10^4 - 10^5\ L_{sun}$ (in between pulses)

Energy generation -> expansion -> luminosity pulse

Expected: several $10^3 - 10^4$ pulses!

Thermal pulses of AGB stars

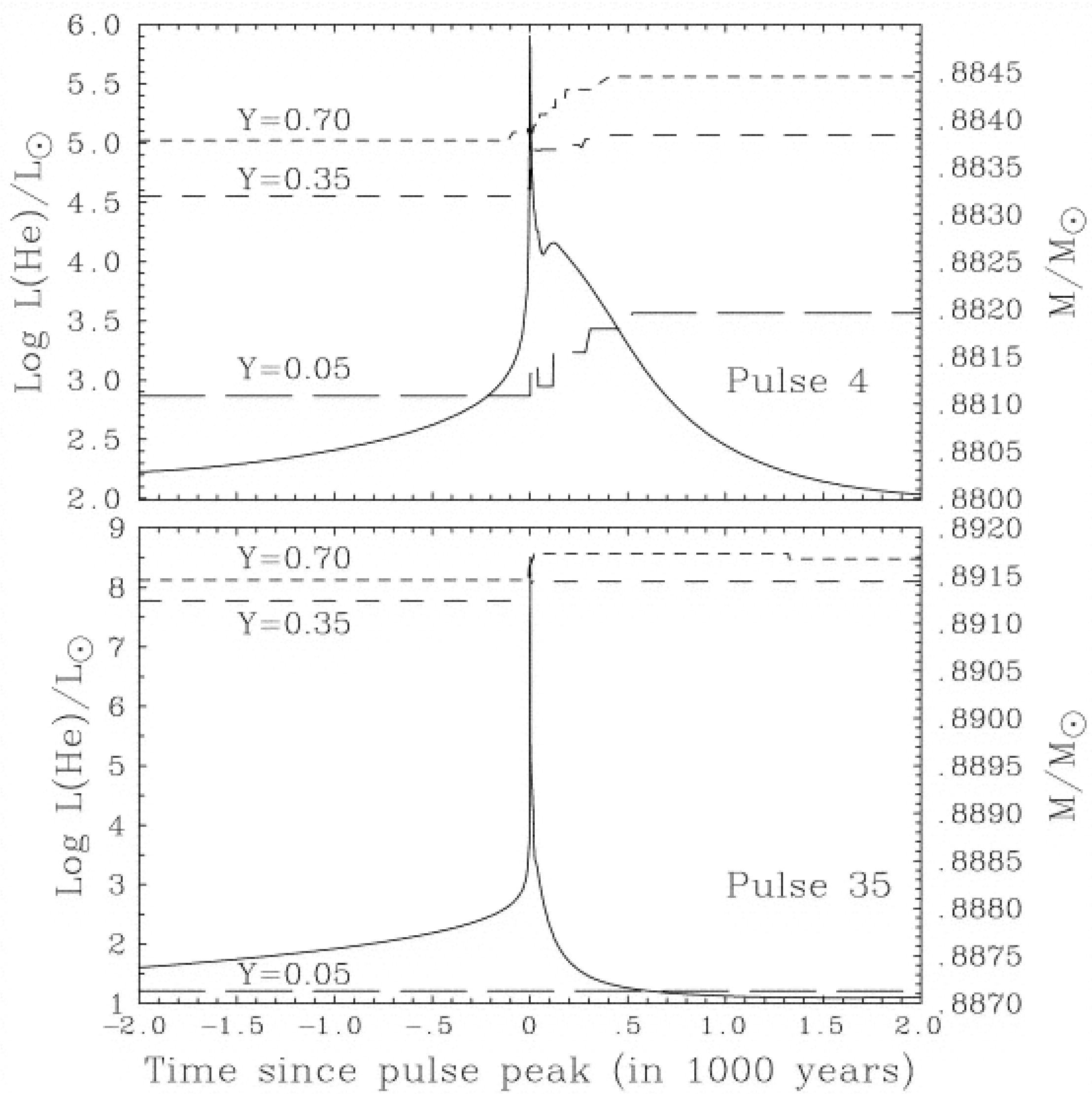

Thermal pulses of AGB stars

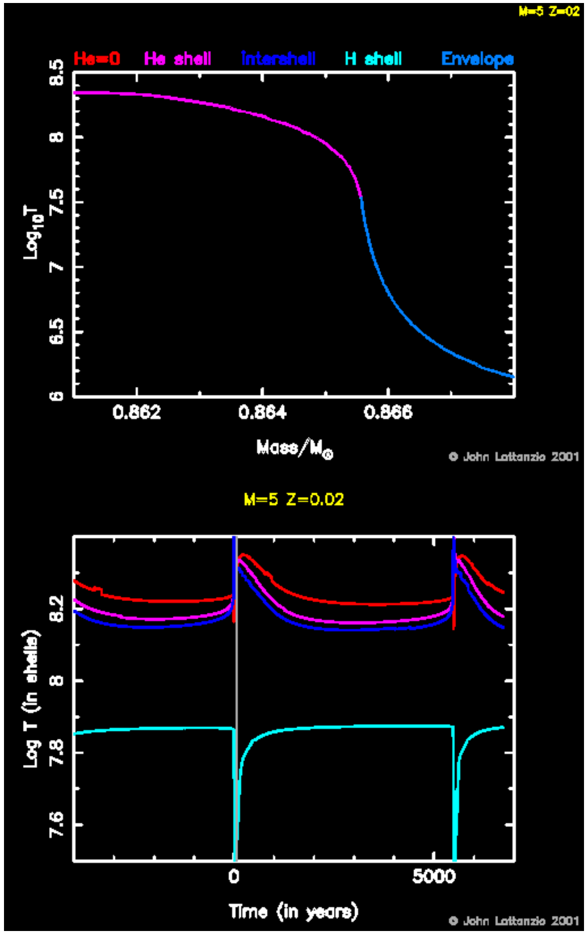

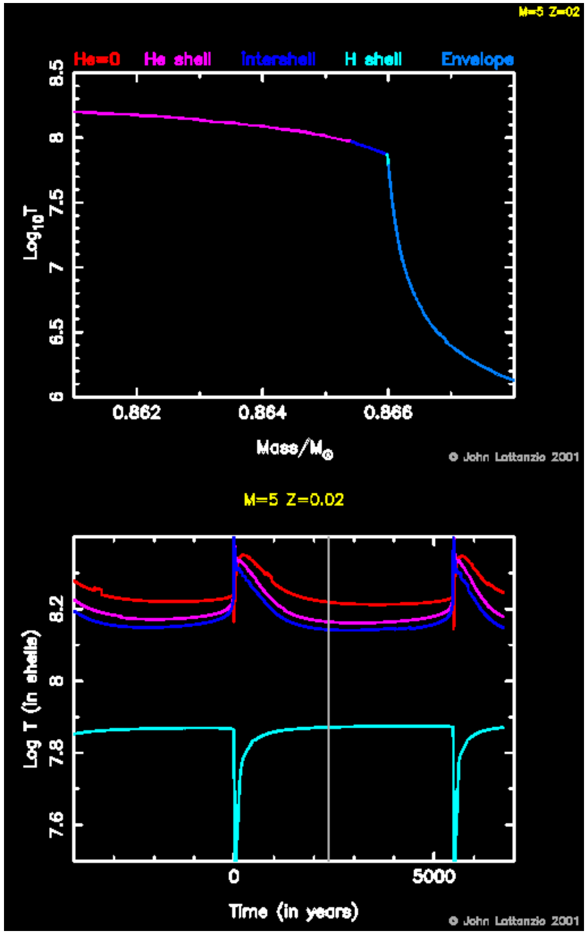

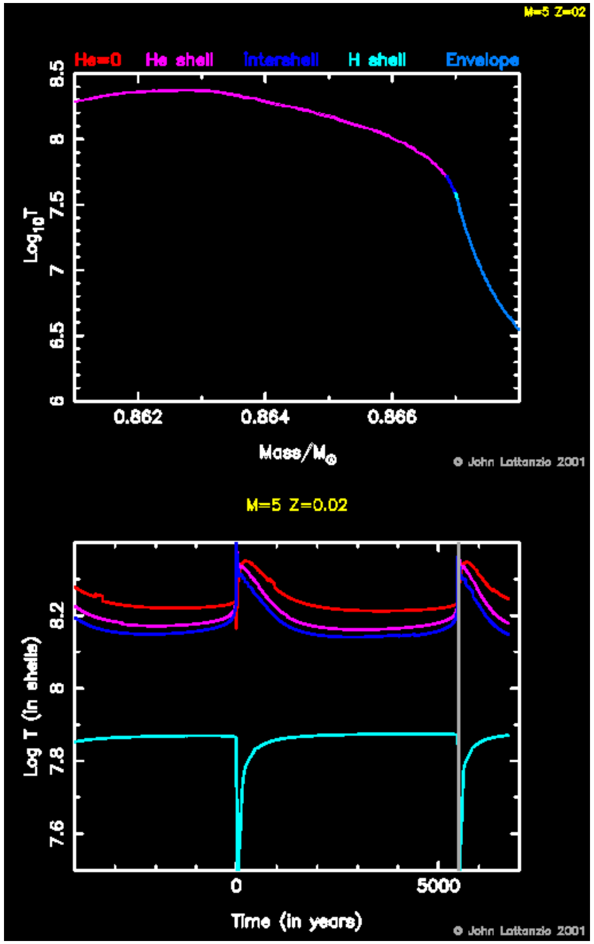

Thermal pulses of AGB stars

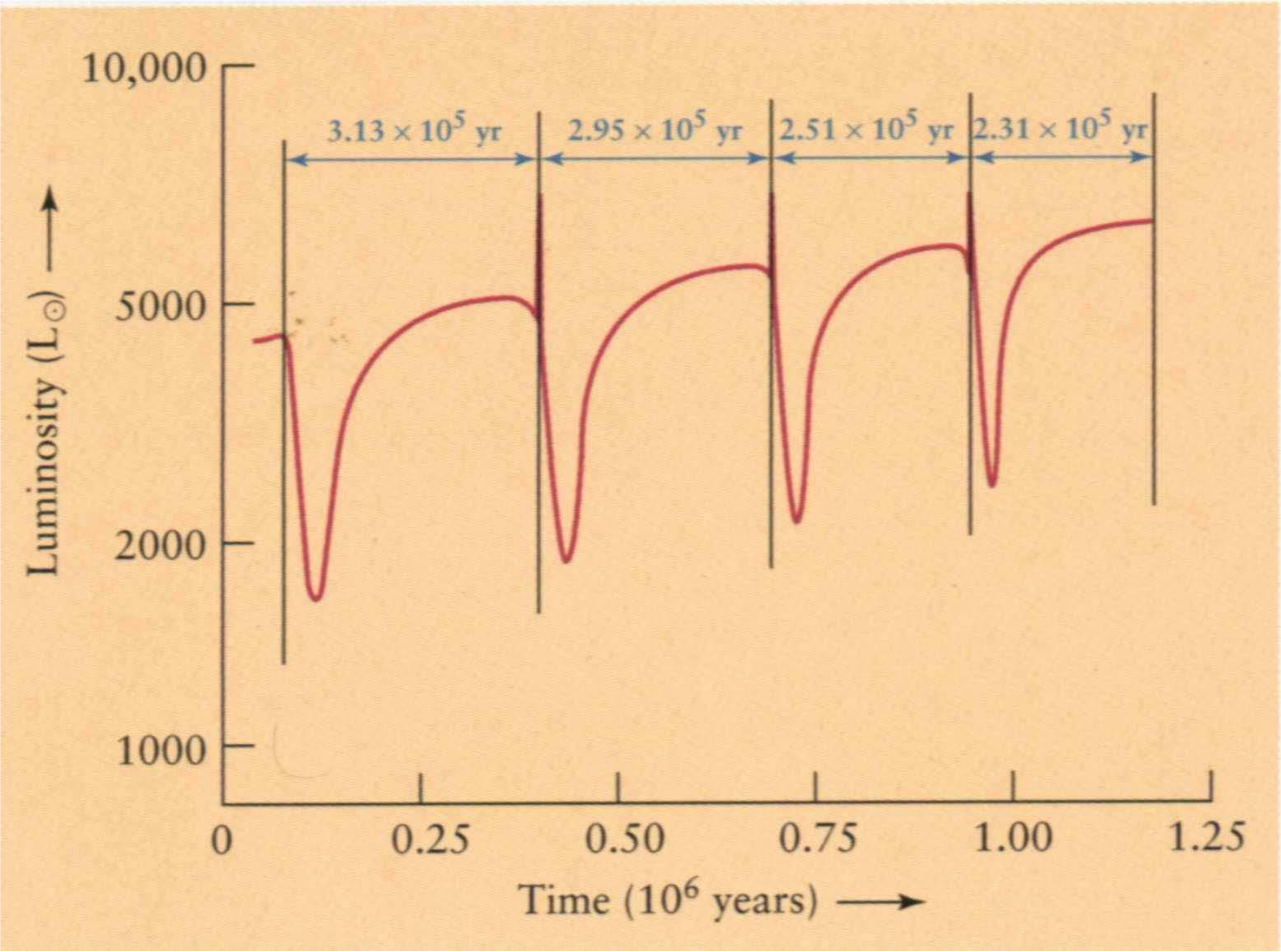

Thermal pulses of AGB stars

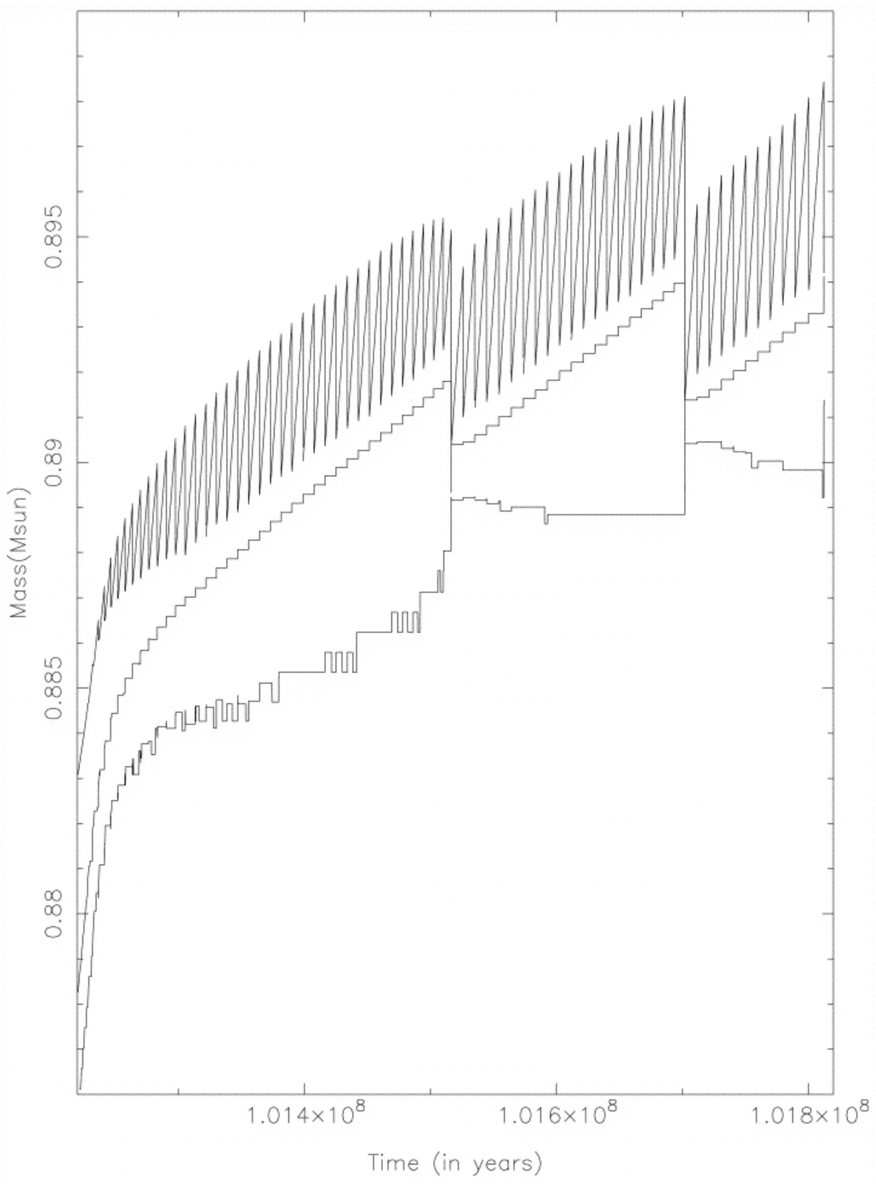

←**Hydrogen shell**

←**Center, He-shell**

←**Bottom, He-shell**

(Frost & Latanzzio 1998)


www.eso.org

www.eso.org

ESO

www.eso.org

www.eso.org

Post-AGB evolution

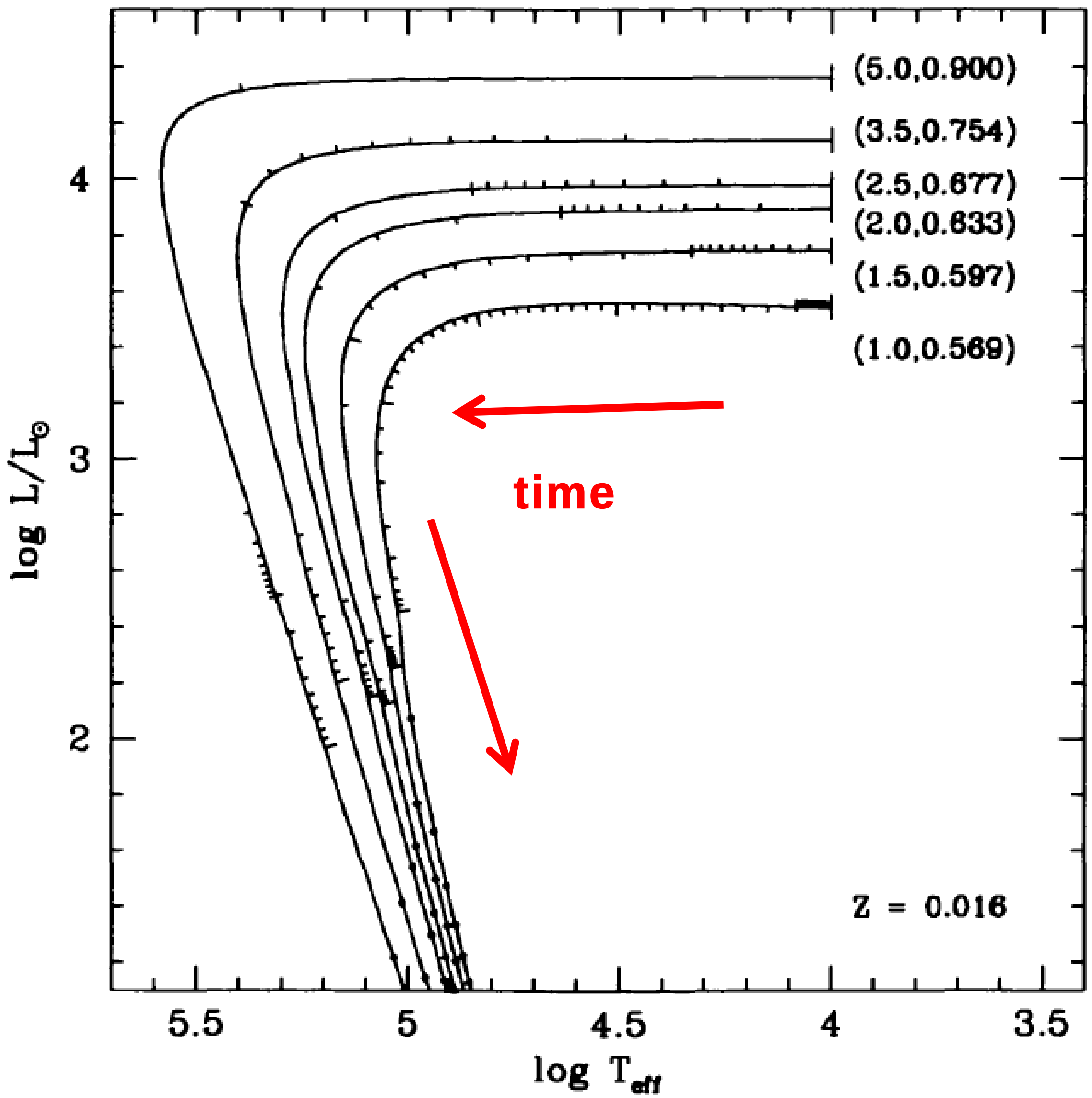

(MS mass, WD mass)

Planetary Nebulae and White Dwarfs

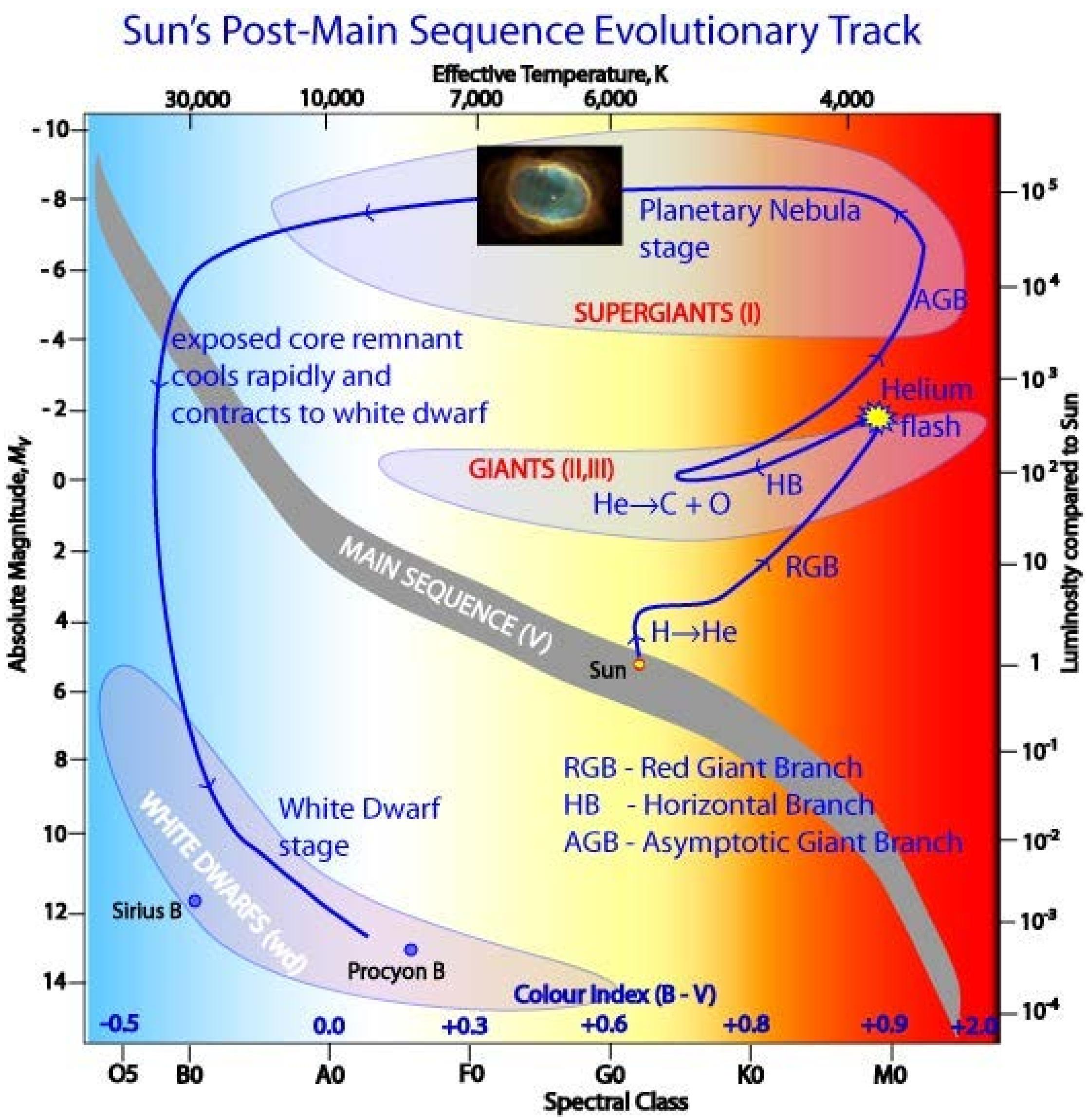

Initial-final mass relation

White-dwarf mass

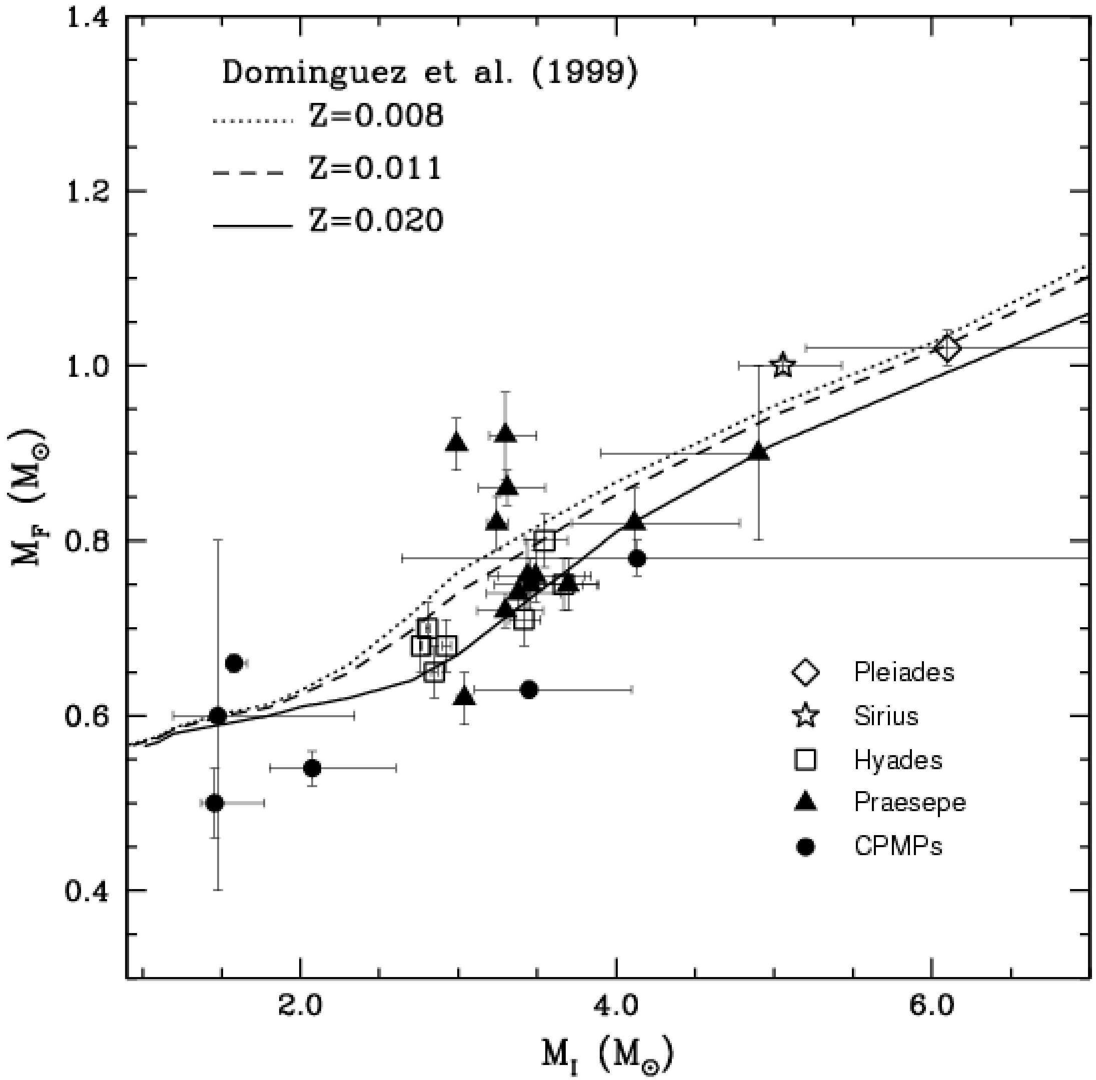

Main-sequence mass

Further evolution: massive stars

i) *Core-carbon burning*

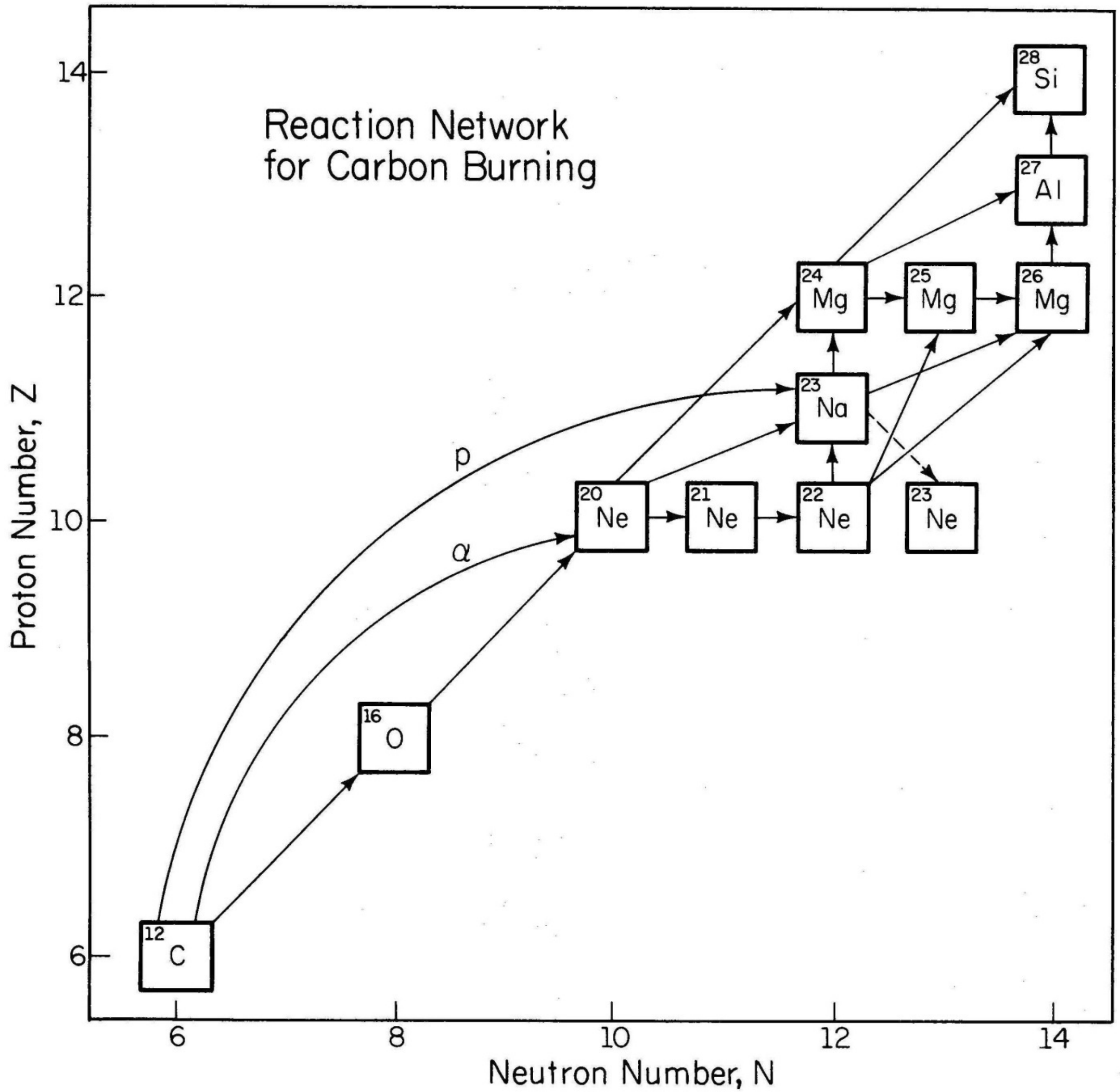

Carbon burning stars

At the onset of core-C burning:

$$T_{center} = \begin{Bmatrix} 7.5\ 10^8\ K\ (15\ Ms_{un}) \\ 7.8\ 10^8\ K\ (25\ M_{sun}) \end{Bmatrix}$$

$$\varrho_{center} = \begin{Bmatrix} 4.3\ 10^4\ gcm^{-3}\ (15\ M_{sun}) \\ 1.5\ 10^5\ gcm^{-3}\ (25\ M_{sun}) \end{Bmatrix}$$

During core-C burning:

$$T_{eff} = \begin{Bmatrix} 4.4\ 10^3 K\ (15 M_{sun}) \\ 4.0\ 10^3 K\ (25 M_{sun}) \end{Bmatrix}$$

$$R_{ph} = \begin{Bmatrix} 3.7\ 10^{13}\ cm\ (15\ M_{sun}) \\ 6.7\ 10^{13}\ cm\ (25\ M_{sun}) \end{Bmatrix}$$

"Red Supergiant"

Envelope does not change much: $\tau_C \leq \tau_{KH}$

He & onset of core-C burning

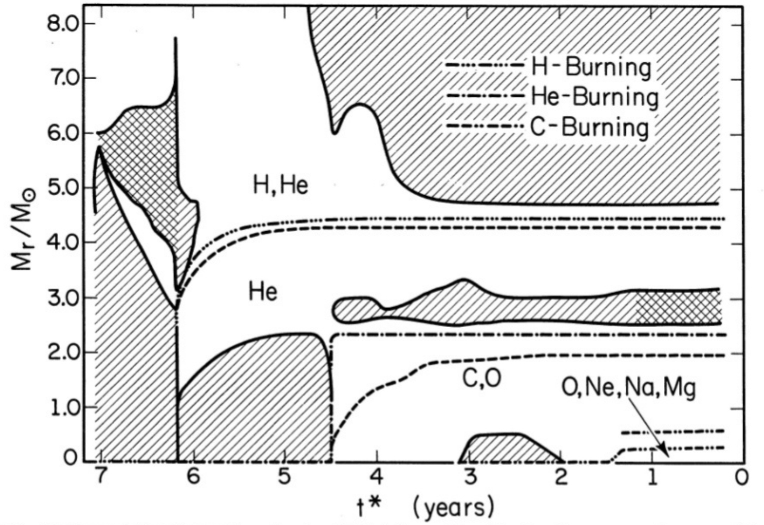

FIG. 2.—The time variation of convective regions in a 15 $M_\odot$ stellar model evolving from the zero-age main sequence into shell carbon burning. *Ordinate*, the Lagrangian mass coordinate measured in solar units; *abscissa*, the logarithm of the time measured backward from an evolutionary time slightly later than the last model calculated, that is, $t^* \equiv \log_{10}(t_f - t)$. *Cross-hatching*, convective regions; *Double cross-hatching*, regions only marginally unstable to convection. *Dashed lines*, discontinuities in the composition; *dash-dot lines*, regions of maximum energy generation.

15 $M_\odot$

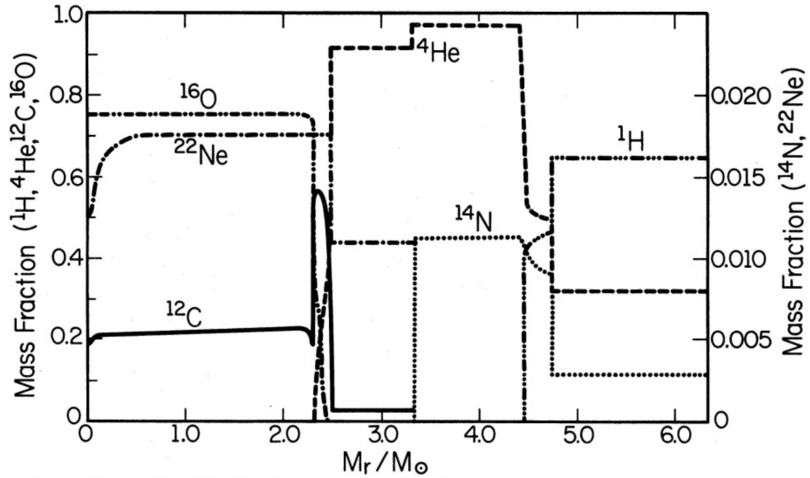

FIG. 9.—Composition profiles within the 15 $M_\odot$ star at a time just prior to carbon burning ($t^* \approx 3.11$). *Abscissa*, the Lagrangian mass coordinate; *ordinate*, the mass fraction. The scale for ^{14}N and ^{22}Ne is different from that for the other nuclei.

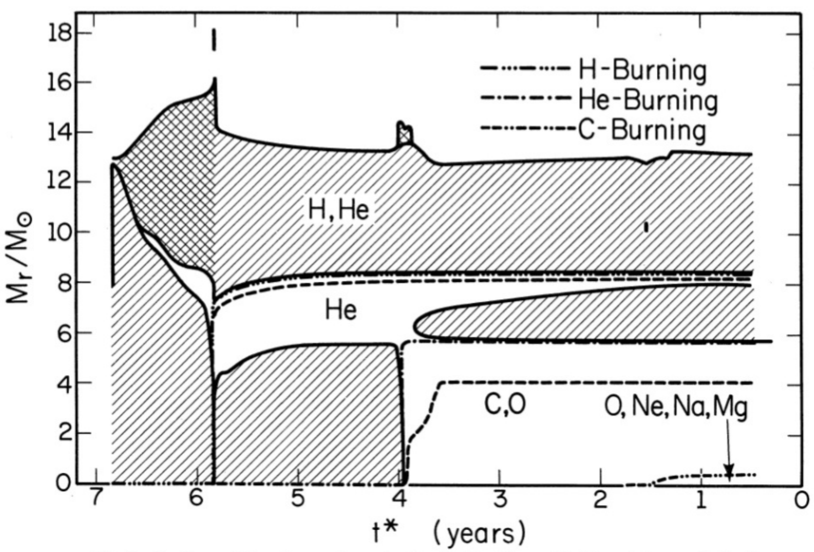

FIG. 3.—The time variation of convective regions in a 25 $M_\odot$ stellar model. All symbols are as in Fig. 2.

25 $M_\odot$

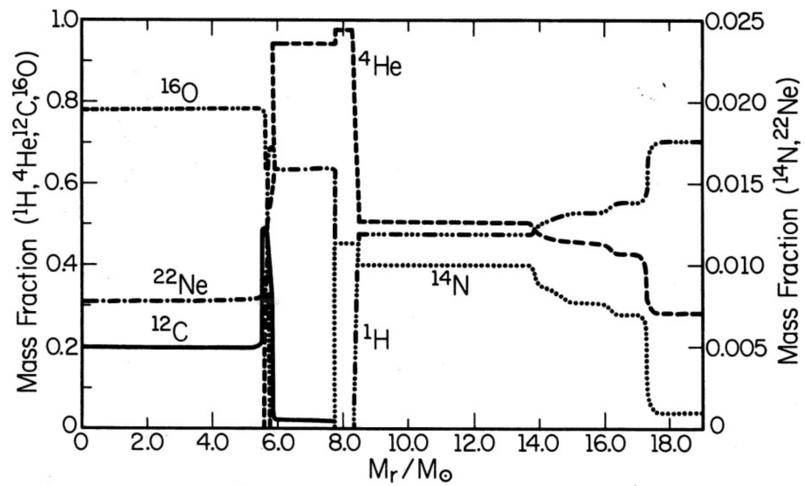

FIG. 10.—Composition profiles within the 25 $M_\odot$ star at a time just prior to carbon burning ($t^* \approx 2.28$)

Core-Carbon burning

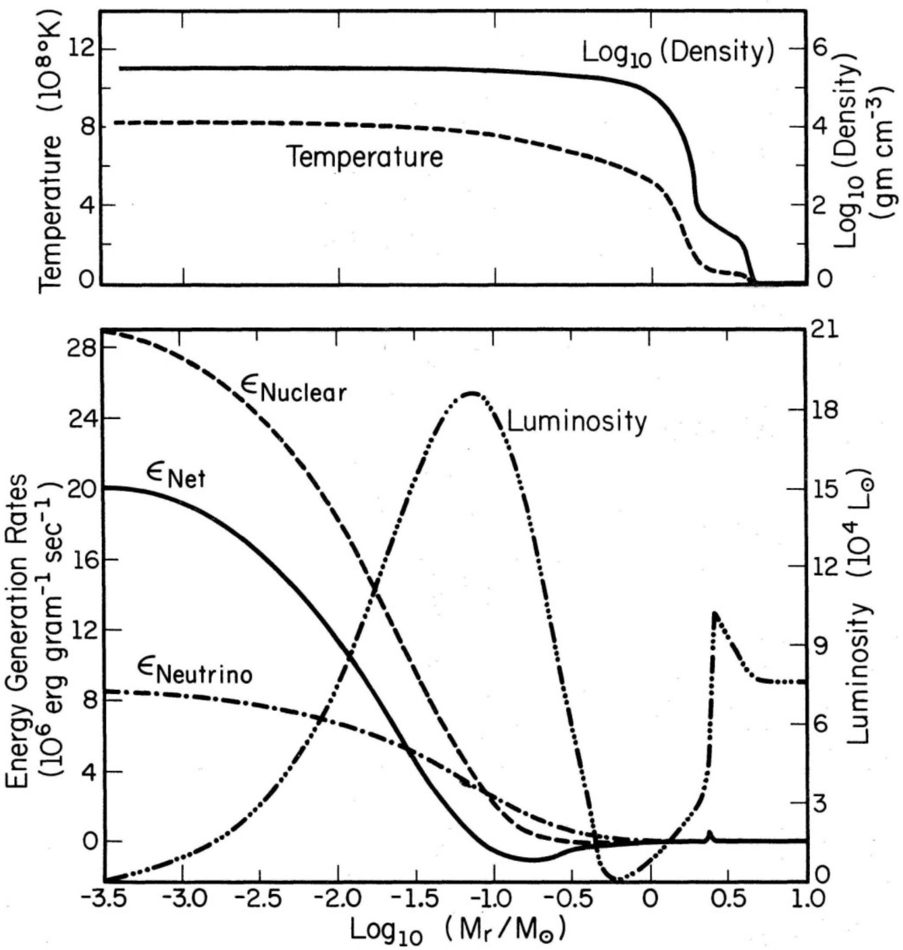

—The variation in energy generation rates, luminosity, temperature, and density through the core of the 15

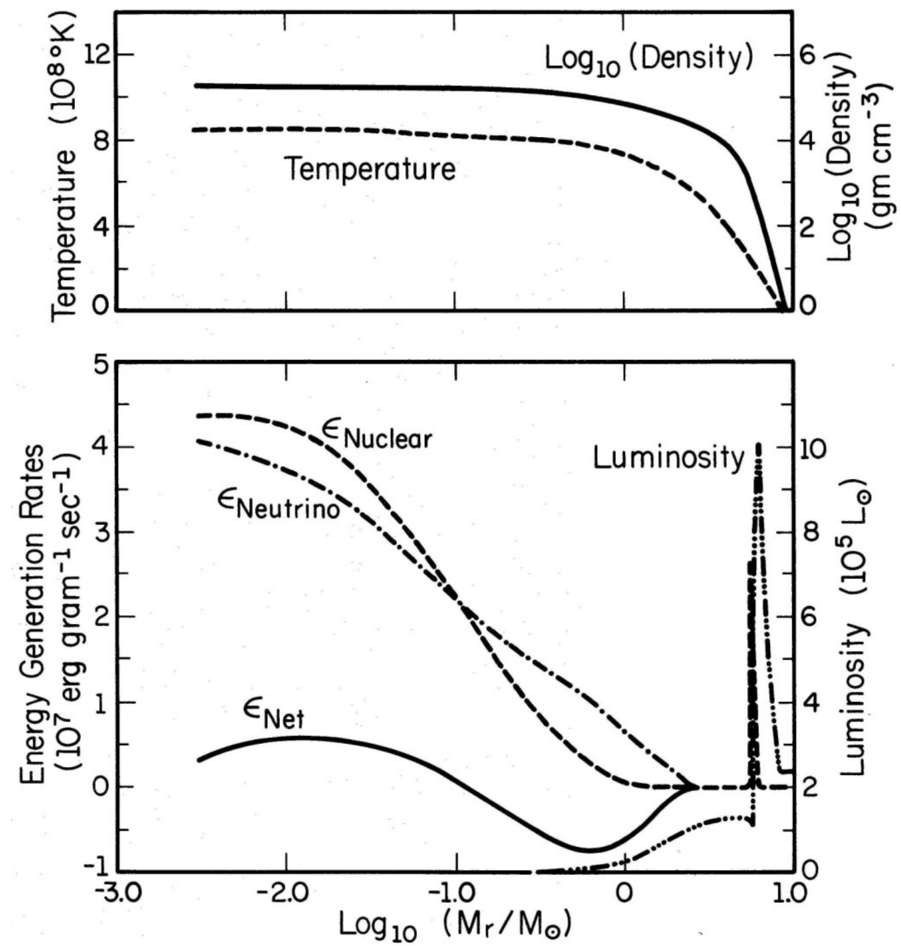

ariation in energy generation rates, luminosity, temperature, and density through the core of the 25 M

15 M_{sun}

25 M_{sun}

Massive stars: through core-C burning

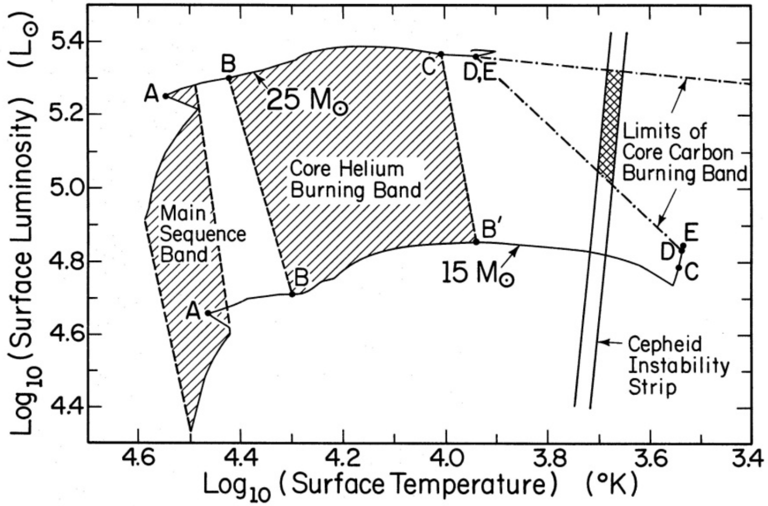

FIG. 7.—The paths of the 15 $M_\odot$ and 25 $M_\odot$ model stars in the H-R diagram. The path during the major core helium-burning phase is bounded by points B and C in the 25 $M_\odot$ case and by points B and B′ in the 15 $M_\odot$ case. Most observed blue supergiants should lie in the crosshatched region bounded by the lines BB and CB′. Core carbon burning occurs between points D and E along the evolutionary paths. The intersection of the Cepheid instability strip with the carbon-burning band defines the upper mass and period limits of observable Cepheids. Extreme possibilities for the outer boundaries of the carbon-burning band are shown by the dash-dot lines.

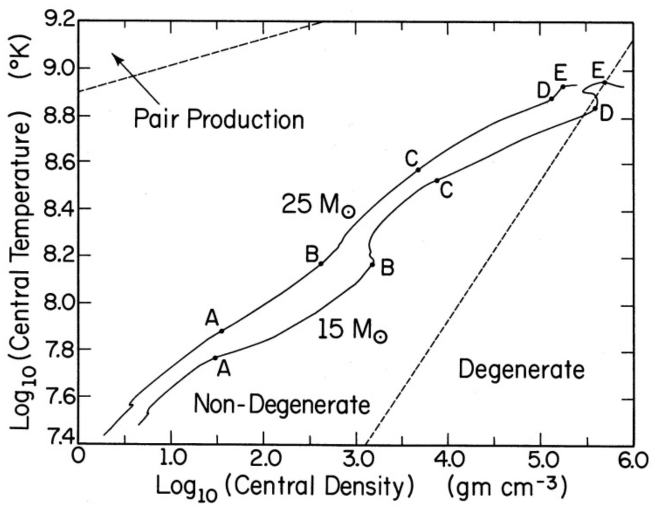

FIG. 8.—The variation of central density with central temperature from the zero-age main sequence into shell carbon burning. The demarcation line between degenerate and nondegenerate regimes ($\epsilon_F/kT \lesssim 1$) is indicated, as is the region where electron-positron pair production becomes important in the equation of state. The lettered points correspond to similarly lettered points in Fig. 7, and their significance is explained at the beginning of § III in the text.

Lamb et al. (1976)

Carbon burning stars

During core-C burning:

$$\varepsilon_C = \begin{Bmatrix} 2.8\ 10^7\ erg g^{-1} s^{-1}\ (15 M_{sun}) \\ 4.4\ 10^7 erg g^{-1}\ s^{-1}\ (25 M_{sun}) \end{Bmatrix}$$

Most of this energy is carried away by neutrinos!

$$L_\nu = \begin{Bmatrix} 3.4\ 10^{38}\ erg s^{-1}\ (15\ M_{sun}) \\ 1.0\ 10^{39}\ erg s^{-1}\ (25\ M_{sun}) \end{Bmatrix}$$

Processes:

$$\boldsymbol{\gamma} + \ \boldsymbol{e}^- \rightarrow \ \boldsymbol{e}^- + \boldsymbol{\nu}_e + \overline{\boldsymbol{\nu}}_e \quad (\text{"}photo\ neutrinos\text{"})$$

$$\boldsymbol{\gamma}_{plasmon} \rightarrow \ \boldsymbol{\nu}_e + \ \overline{\boldsymbol{\nu}}_e \qquad (\text{"plasmon neutrinos"})$$

Massive stars: after core-C burning

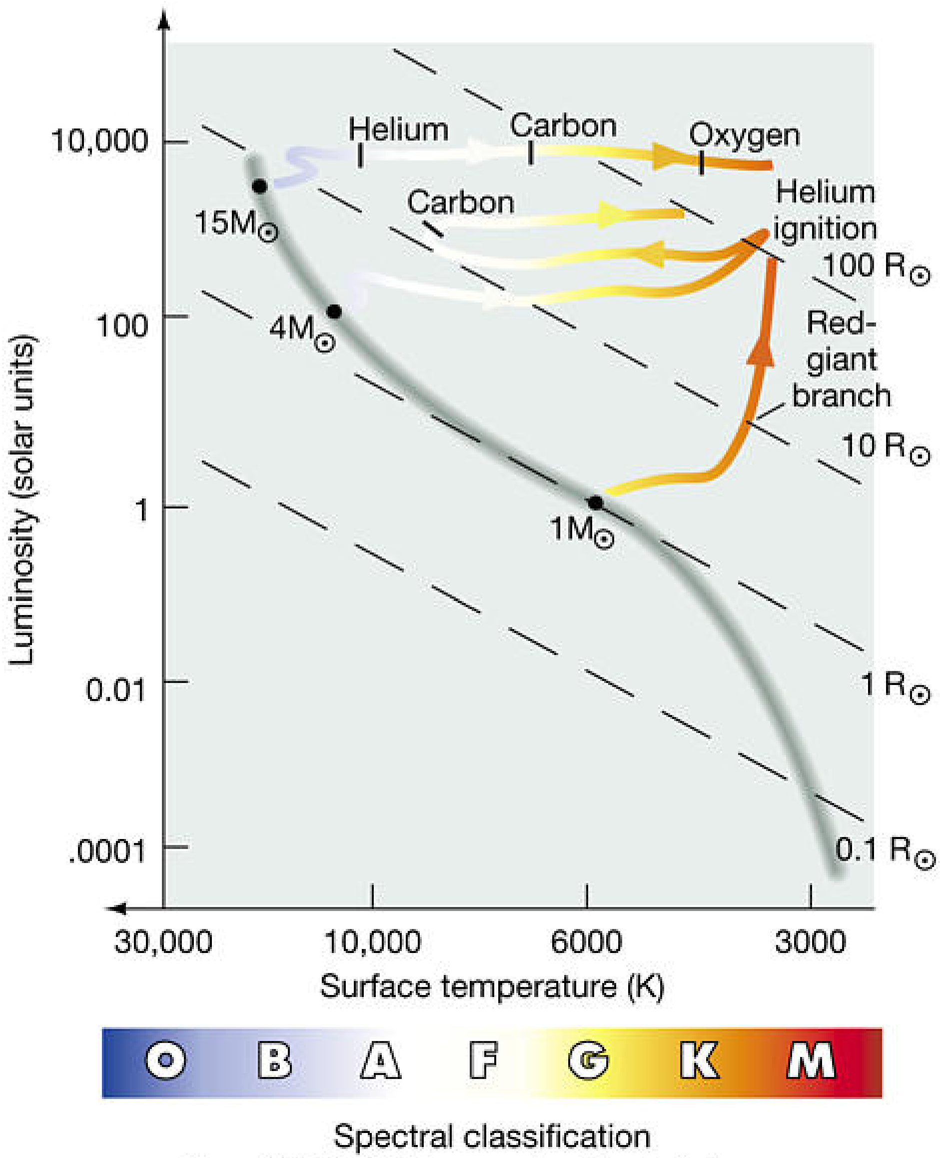

Without mass loss:
blue supergiant ->
yellow supergiant ->
red supergiant

Massive stars: O and Si burning

$$^{16}\mathrm{O} + {}^{16}\mathrm{O} \rightarrow {}^{24}\mathrm{Mg} + 2\,{}^{4}\mathrm{He}$$
$$\rightarrow {}^{28}\mathrm{Si} + {}^{4}\,\mathrm{He}$$
$$\rightarrow {}^{31}\mathrm{P} + p^{+}$$
$$\rightarrow {}^{31}\mathrm{S} + n$$
$$\rightarrow {}^{32}\mathrm{S} + \gamma$$

$$^{28}_{14}Si + {}^{4}_{2}He \longrightarrow {}^{32}_{16}S + \gamma$$
$$^{32}_{16}S + {}^{4}_{2}He \longrightarrow {}^{36}_{18}Ar + \gamma$$

.

.

$$^{52}_{24}Cr + {}^{4}_{2}He \longrightarrow {}^{56}_{26}Fe + \gamma$$

α- particles from
$$^{28}Si + \gamma \rightarrow {}^{24}Mg + \alpha$$

Massive stars: O and Si burning

Oxygen burning (~middle):

	$15\ M_{sun}$	$25\ M_{sun}$
T_C (K)	$1.9\ 10^9$	$1.8\ 10^9$
ρ_c (g cm^{-3})	$5.4\ 10^6$	$1.7\ 10^6$
L_ν (erg s^{-1})	$7.9\ 10^{42}$	$2.3\ 10^{43}$
τ (s)	$5.7\ 10^7$	$1.2\ 10^7$

Massive stars: O and Si burning

Silicon burning (beginning):

	$15\ M_{sun}$	$25\ M_{sun}$
T_C (10^9 K)	3.1	3.4
ρ_c (10^7 g cm^{-3})	2.3	1.1
L_ν (10^{44} erg s^{-1})	3.4	38
τ (10^5 s)	5.2	1.2

Massive stars: after core-Si burning

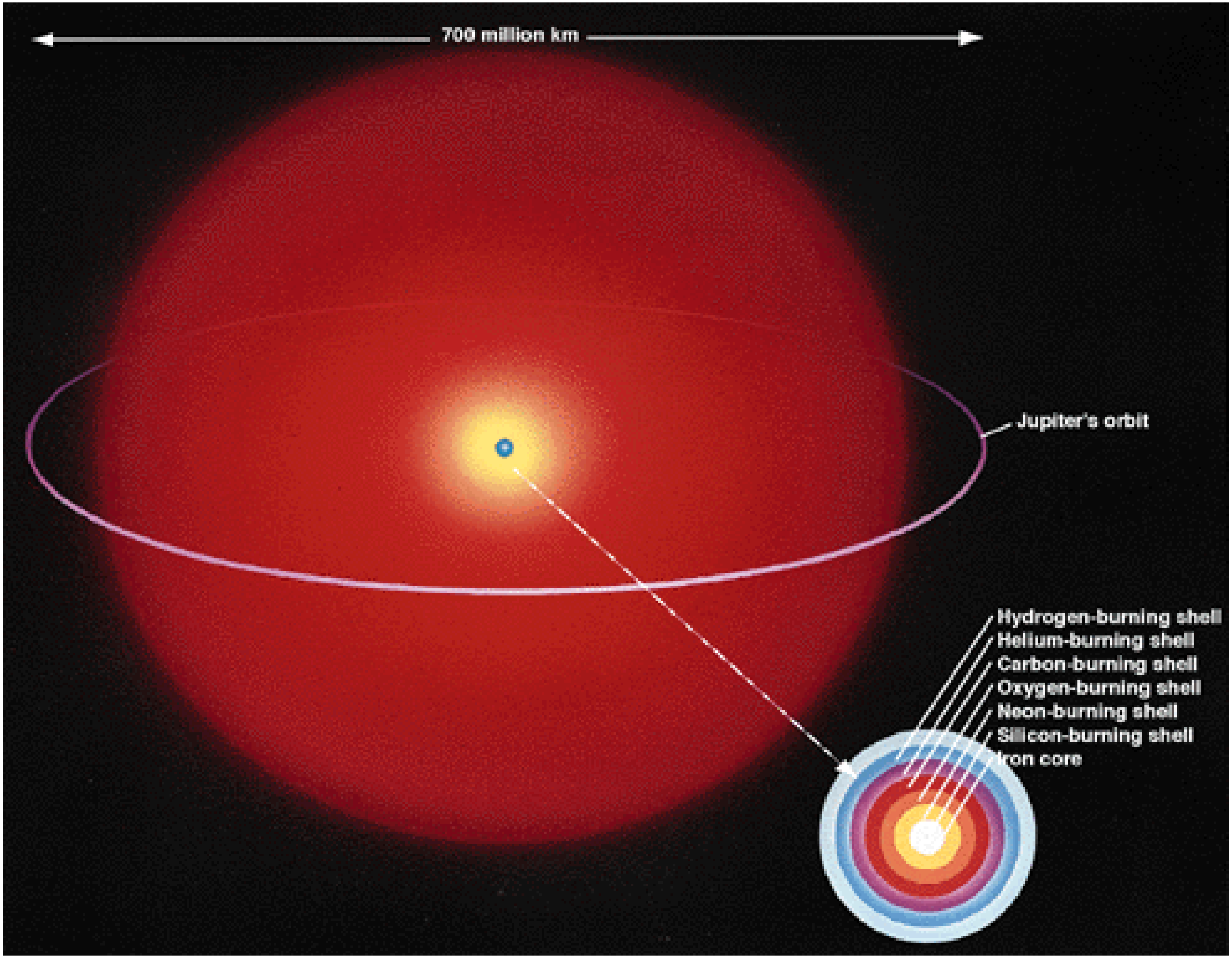

Massive stars: after core-Si burning

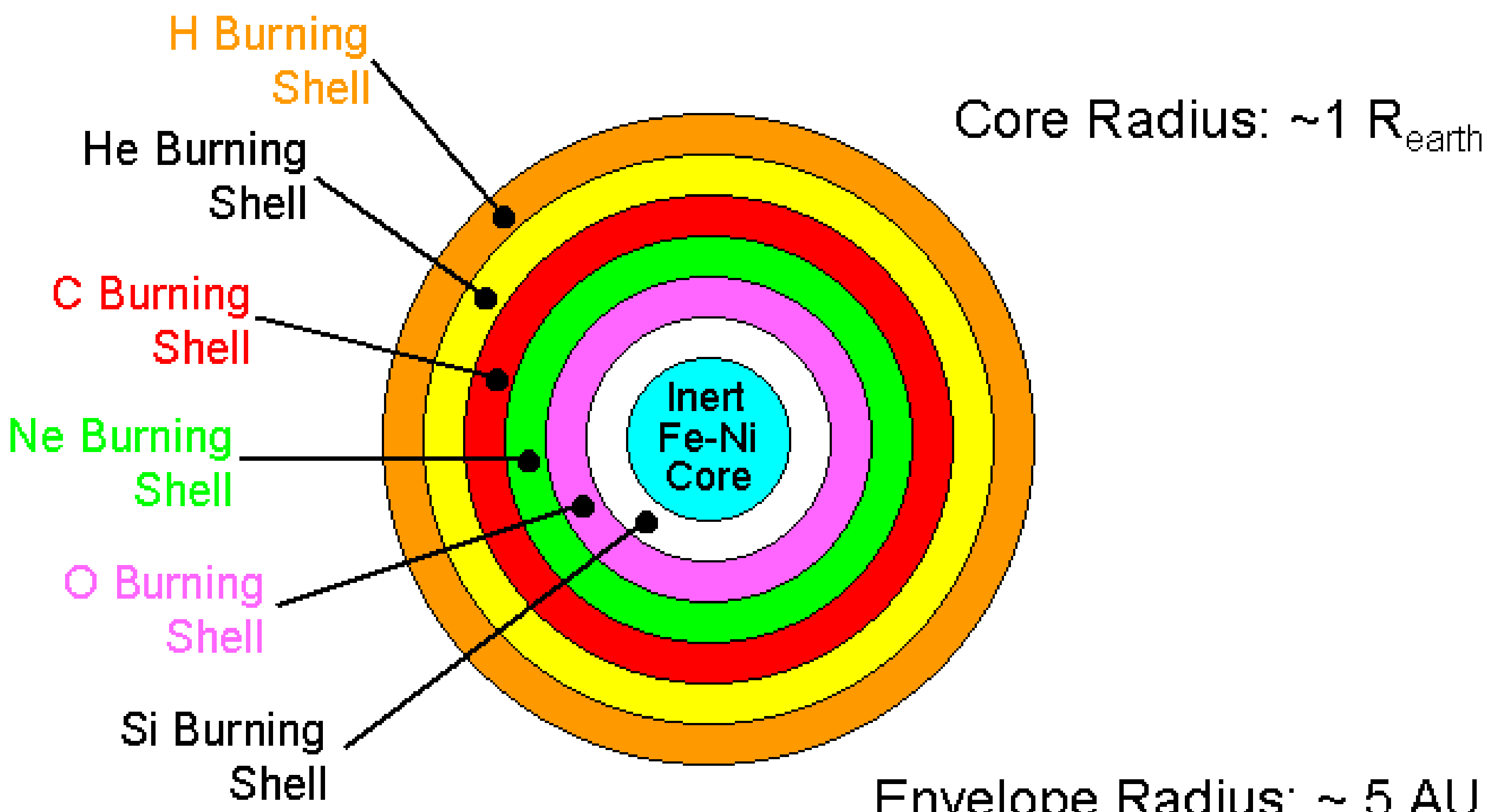

Massive stars: end of Si burning

- All stars more massive than 8-9 M_{sun} evolve a central core of Fe-group elaments of about 1.5 M_{sun} ($\geq M_{Chandrasehar}$)
- This core contracts and heats up (Virial theorem!)
- Photo-dissociation of “Fe”, $\gamma<4/3$: collapse to neutron star or black hole (+ supernova)
- All massive stars (with solar metallicity) should be *red* supergiants when the explode
- *But: The progenitor of SN 1987A was a blue supergiant!*

SN 1987 A in the LMC

- Progenitor: Sanduleak -69º 202
- Blue supergiant (B3Ia)
- $L_{bol} \sim 10^5 L_{sun}$
- $T_{eff} \sim 15\,000$ K
- $M_{MS} \sim (20 \pm 2) M_{sun}$ (stellar models)
- $M_{He} \sim (6 \pm 1) M_{sun}$ (stellar models)
- M_H(ejected) $\sim (10 \pm 1) M_{sun}$ ⟹ mass loss before explos.!
- "Rings": Star was "red" ~40 000 years before the explosion!

SN 1987 A in the LMC

SN 1987 A in the LMC

Supernova 1987A in the LMC

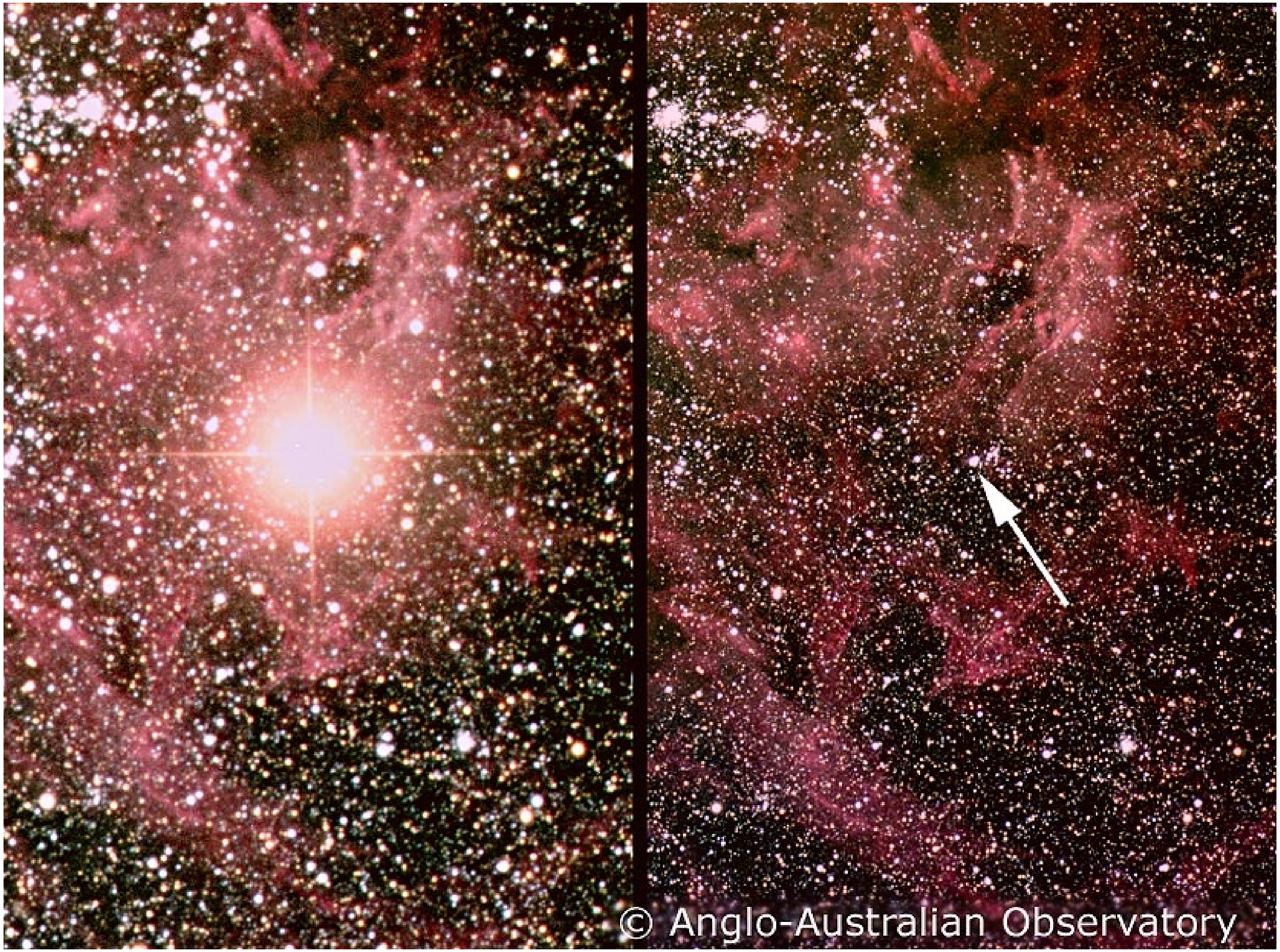

Supernova 1987A
7:35 UT 23.2.1987

Blue Supergiant
Sanduleak 69.202

SN 1987 A

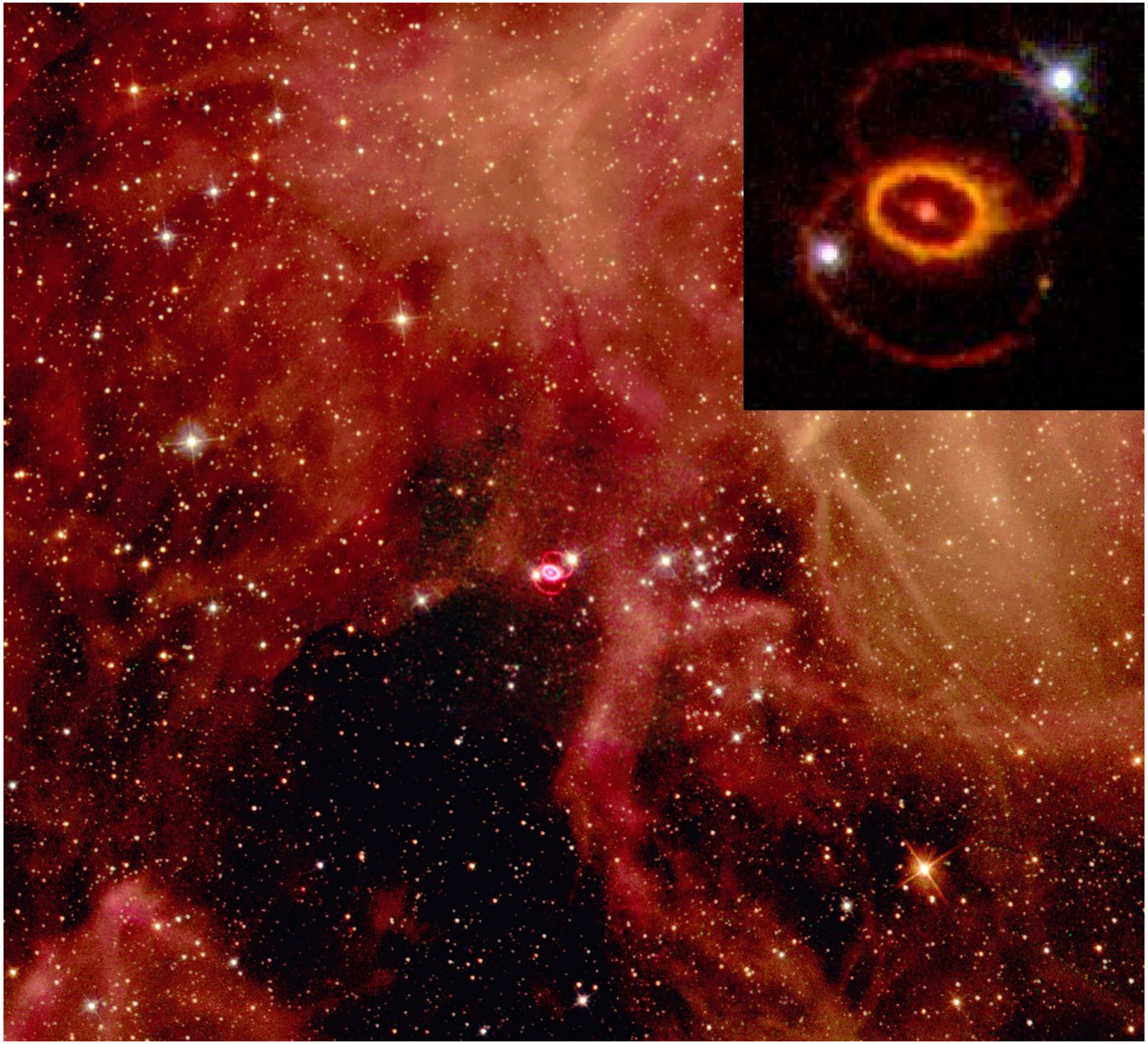

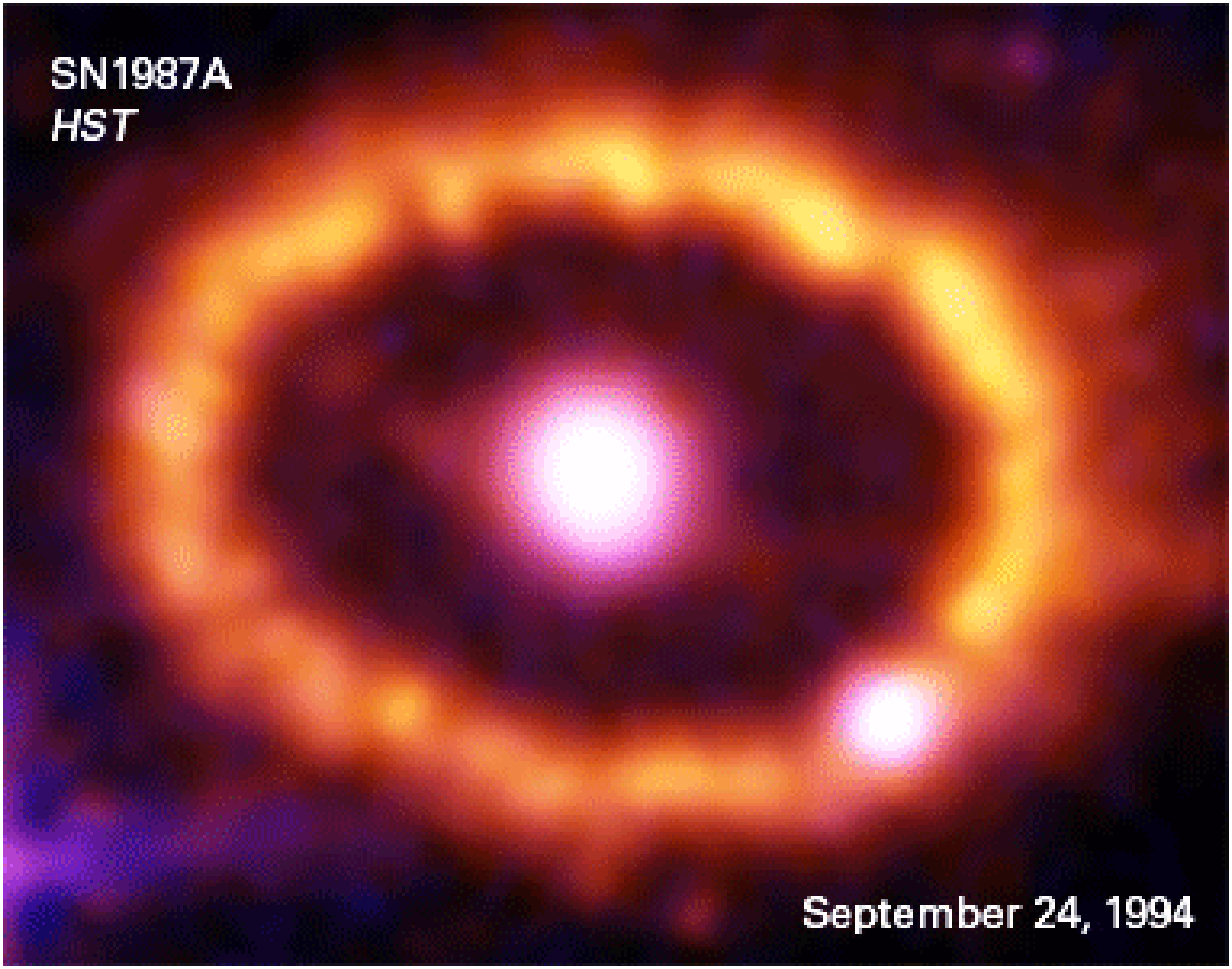
SN1987A
HST
September 24, 1994

SN 1987 A

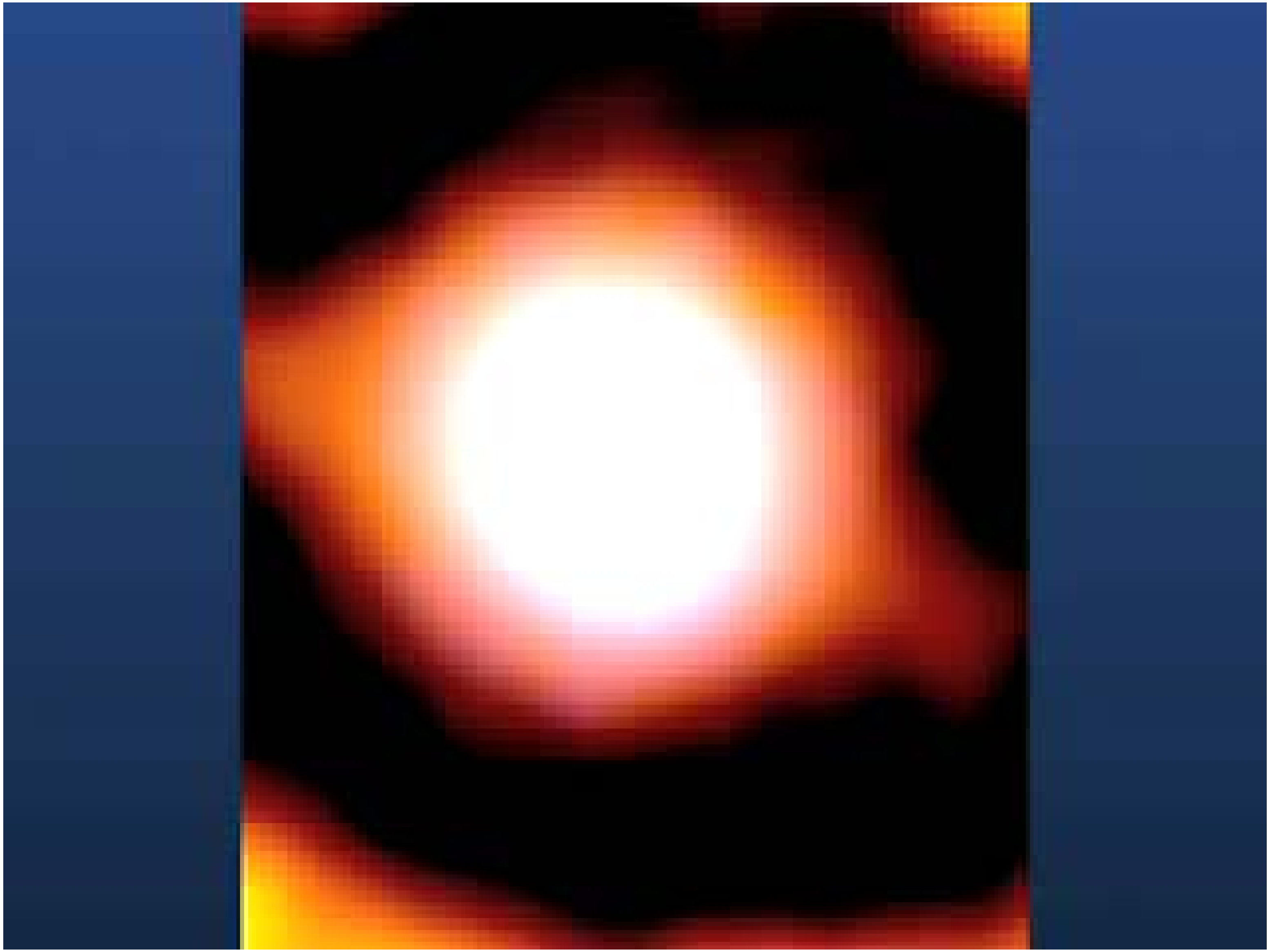

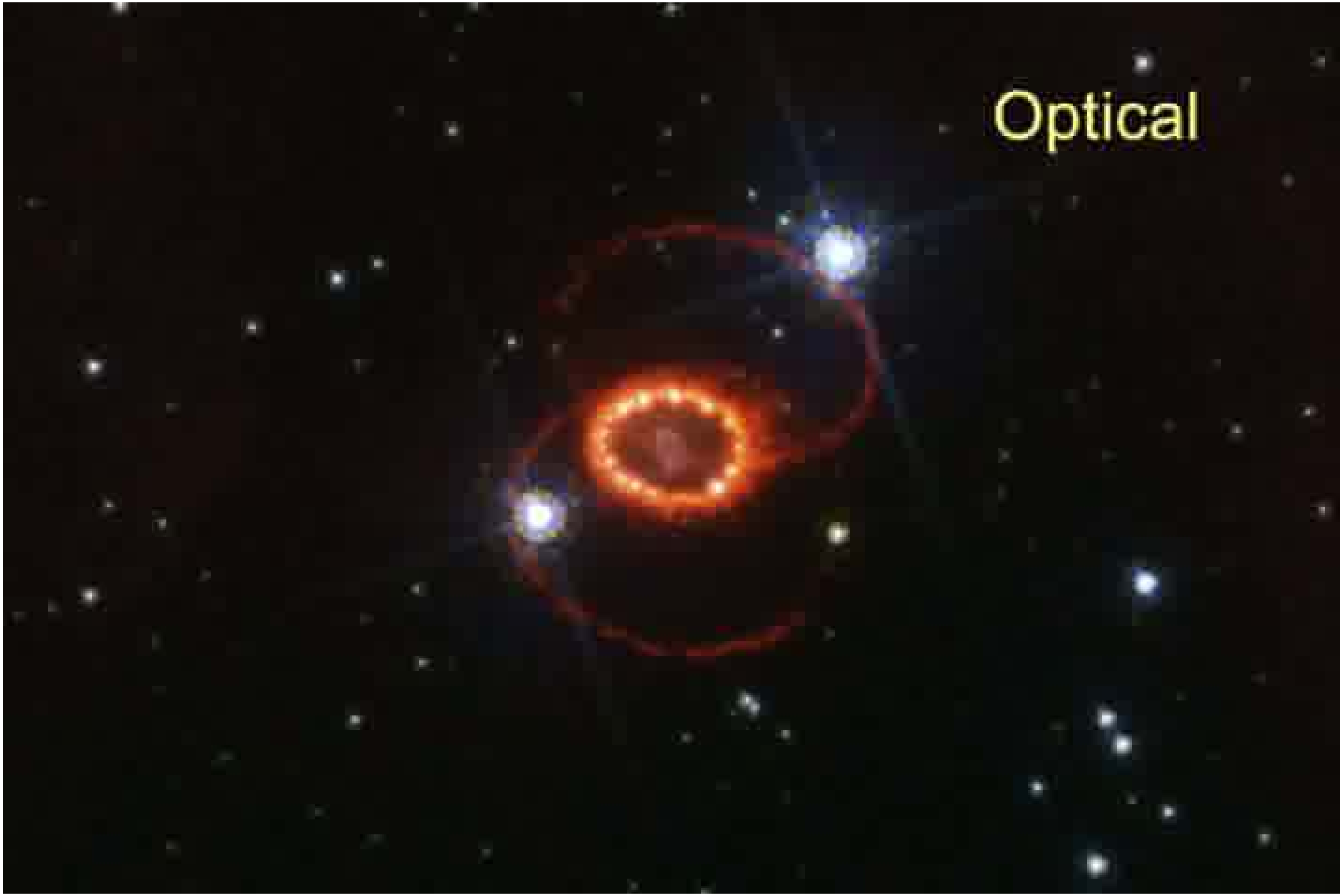
Optical

SN 1987A progenitor evolution

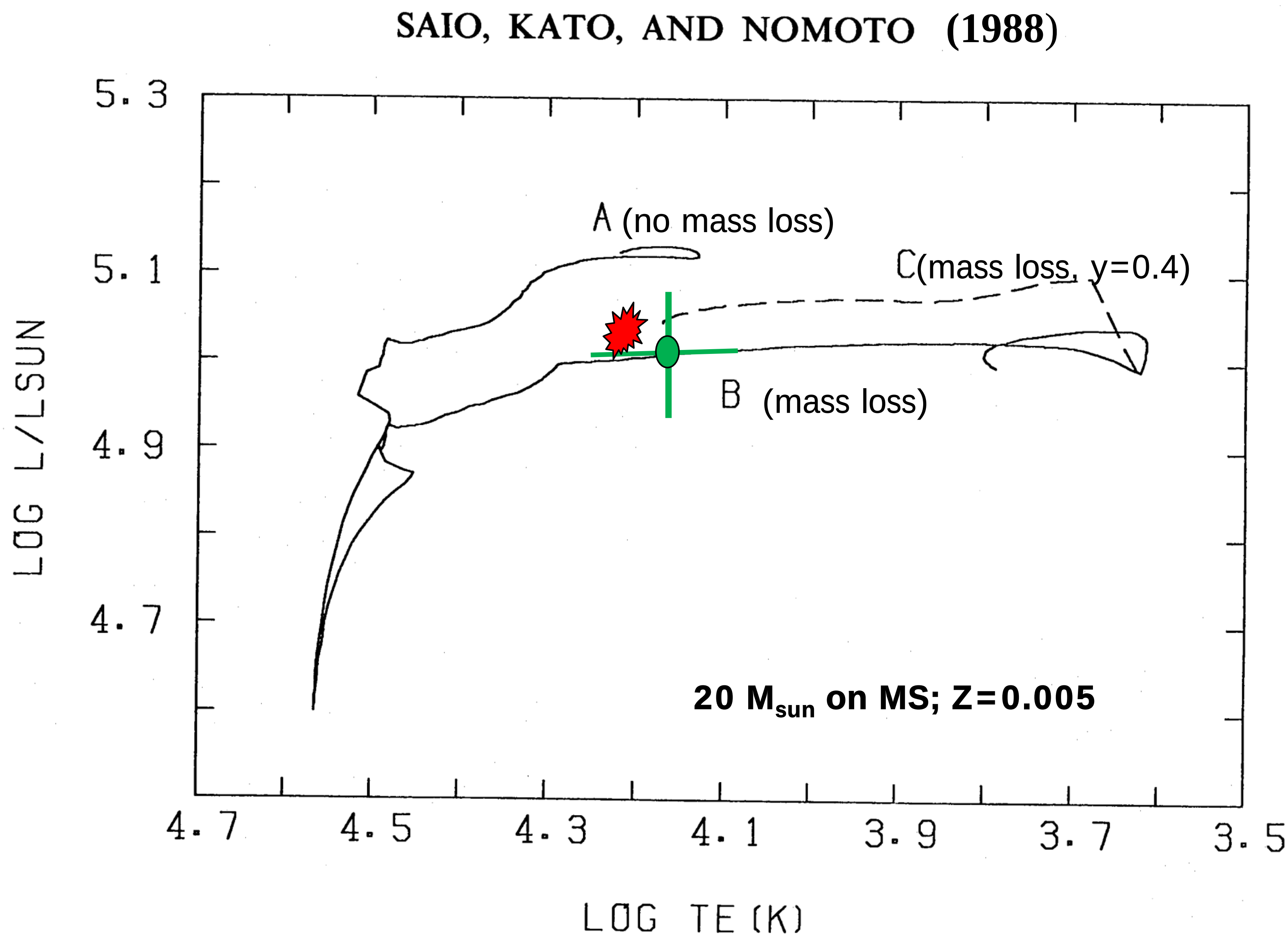

WDs: initial-final mass relation

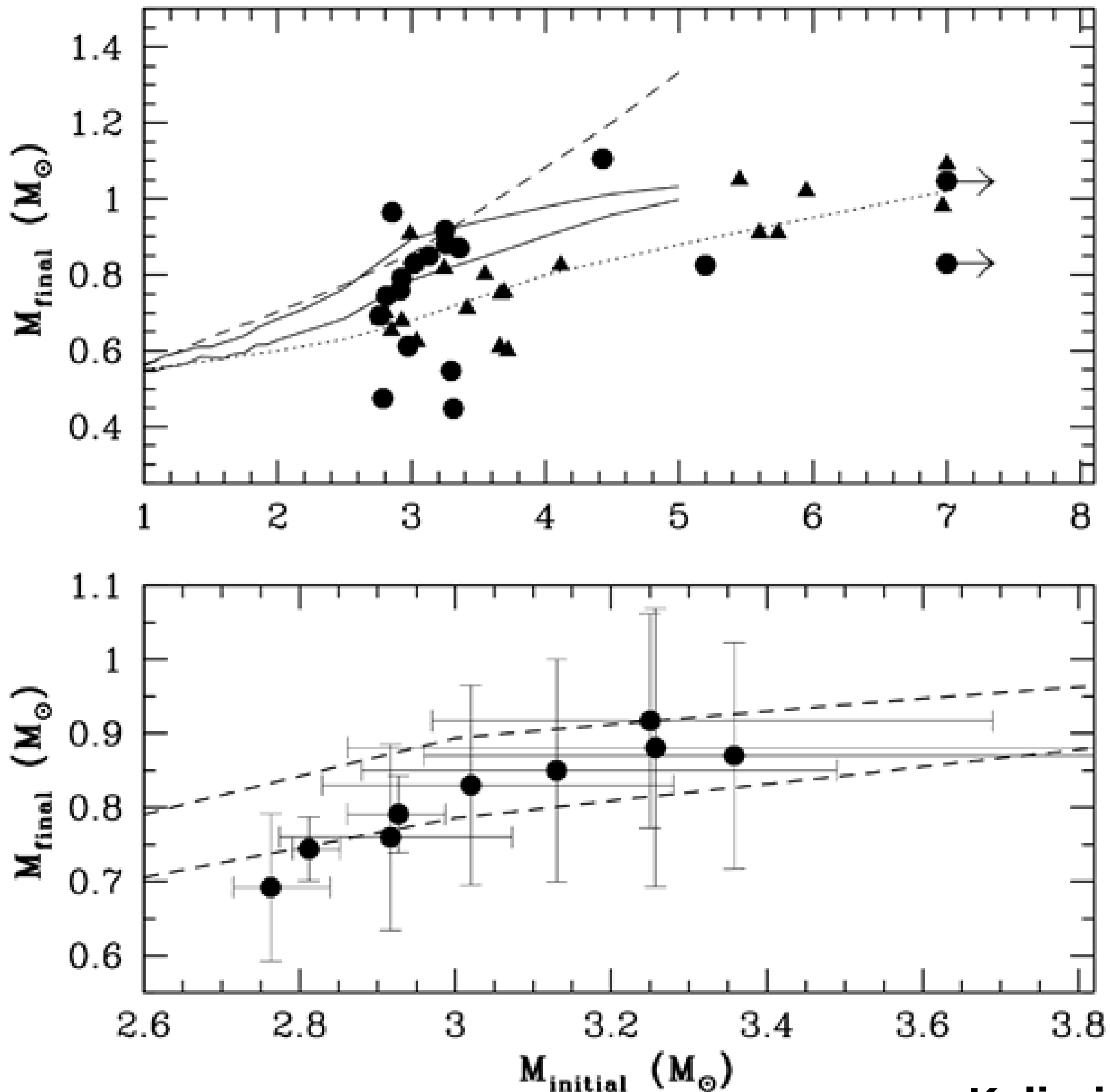

Kalirai et al. (2005)

WDs: mass distribution

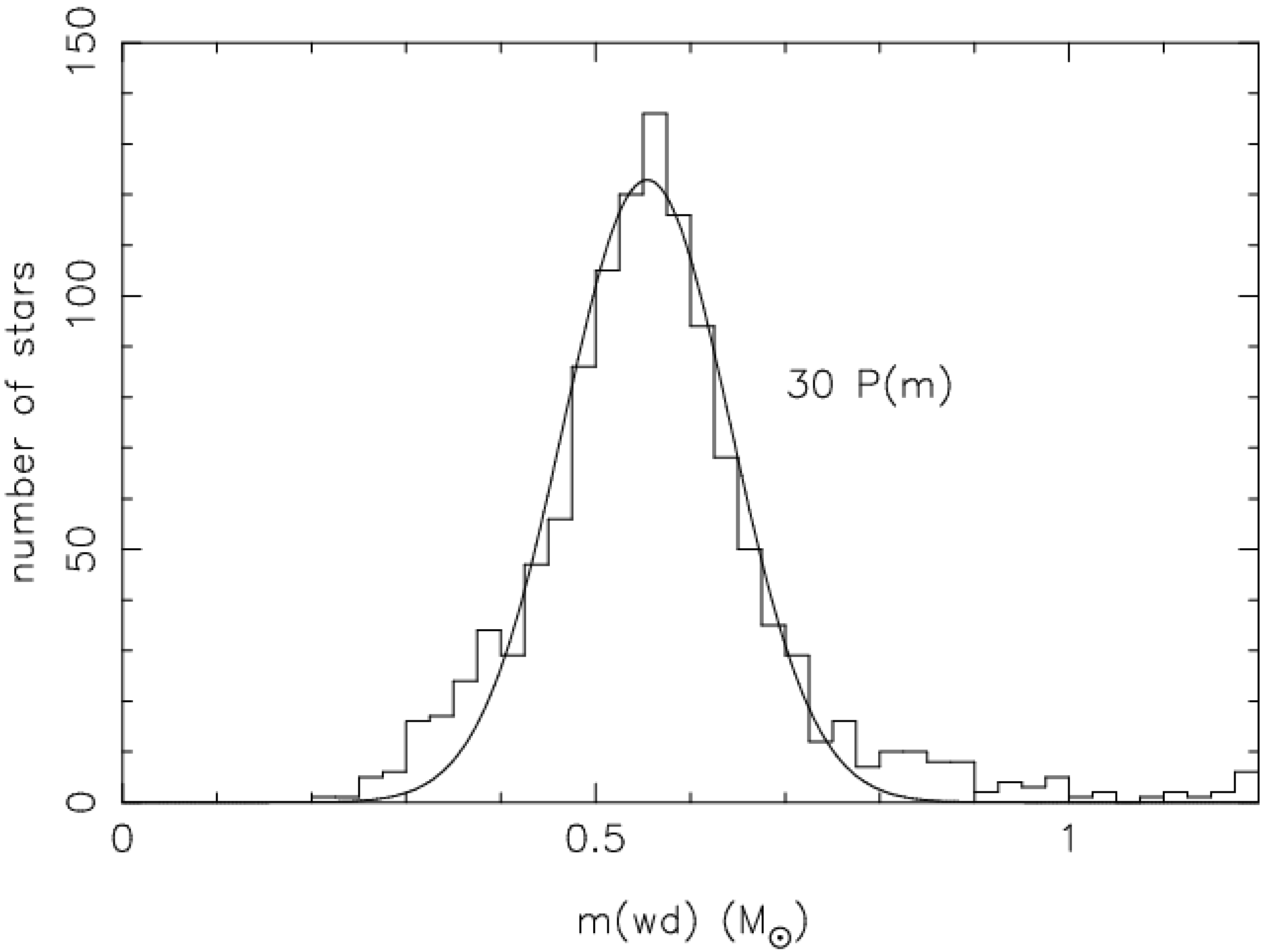

Central stars of PNe; Maciel et al. (2010)

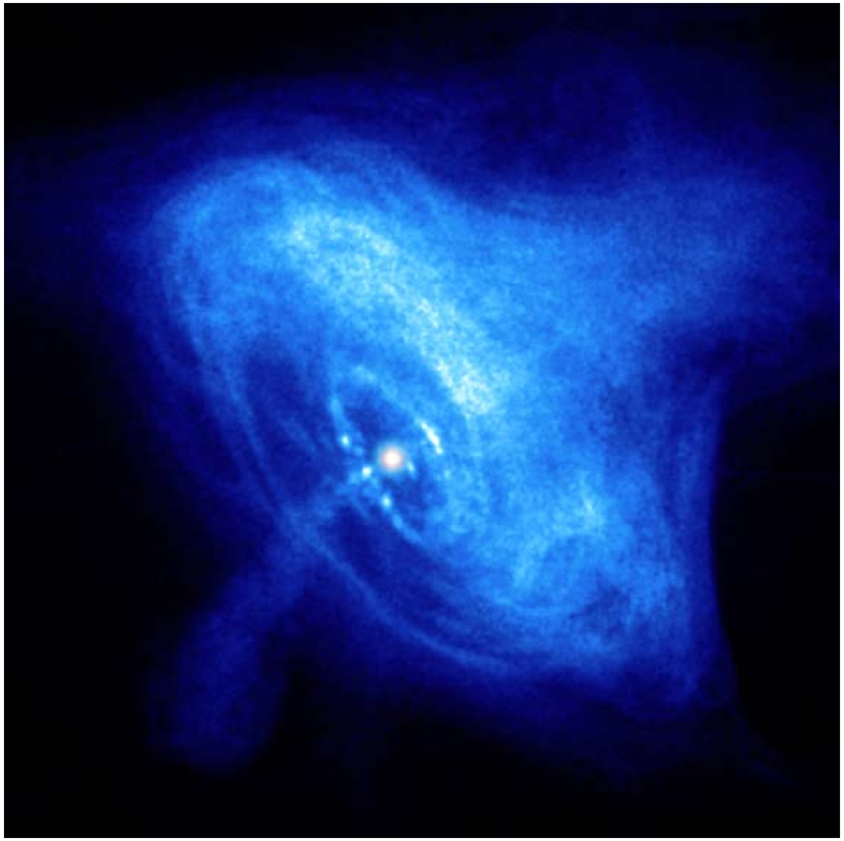

Neutron stars: the Crab pulsar

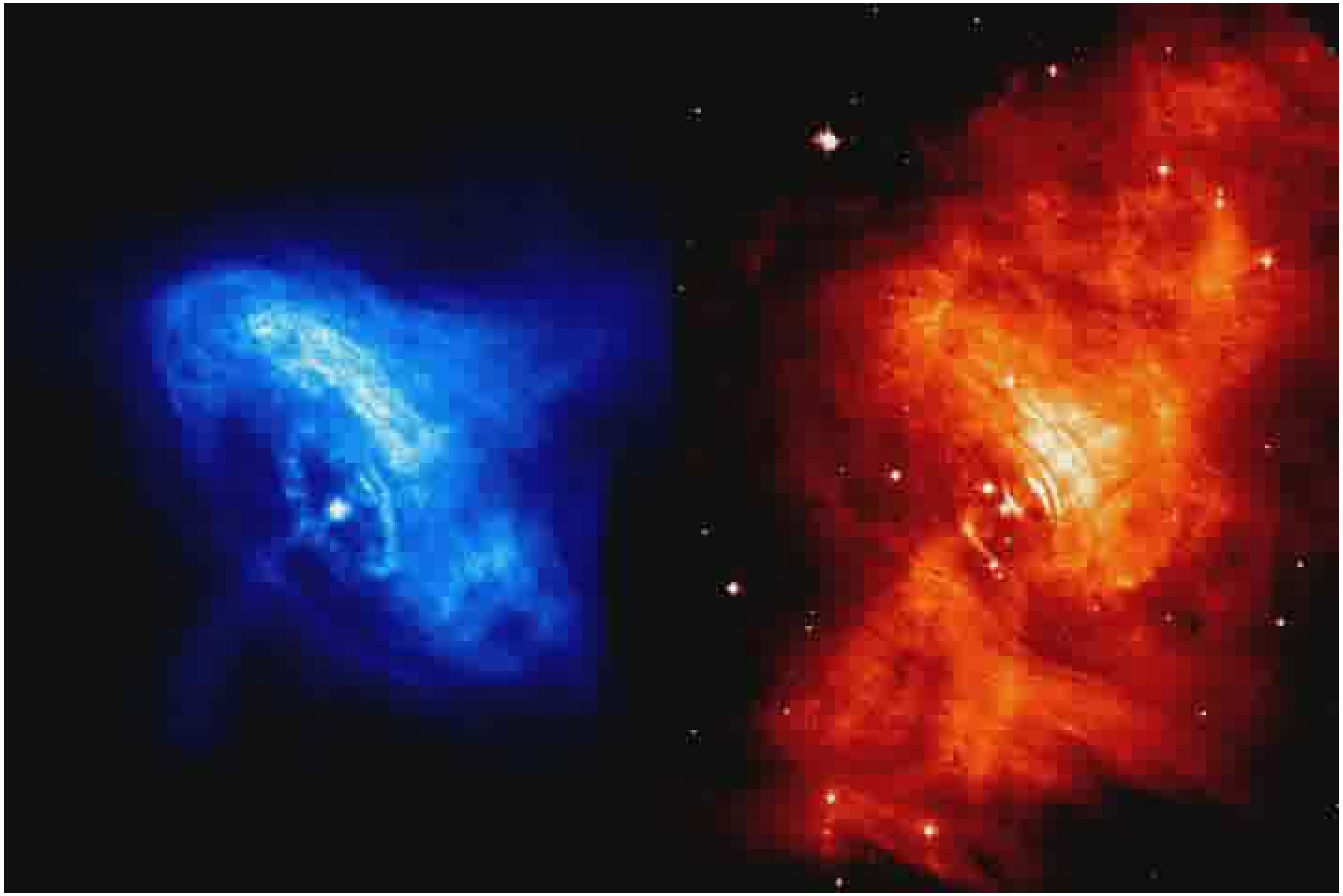

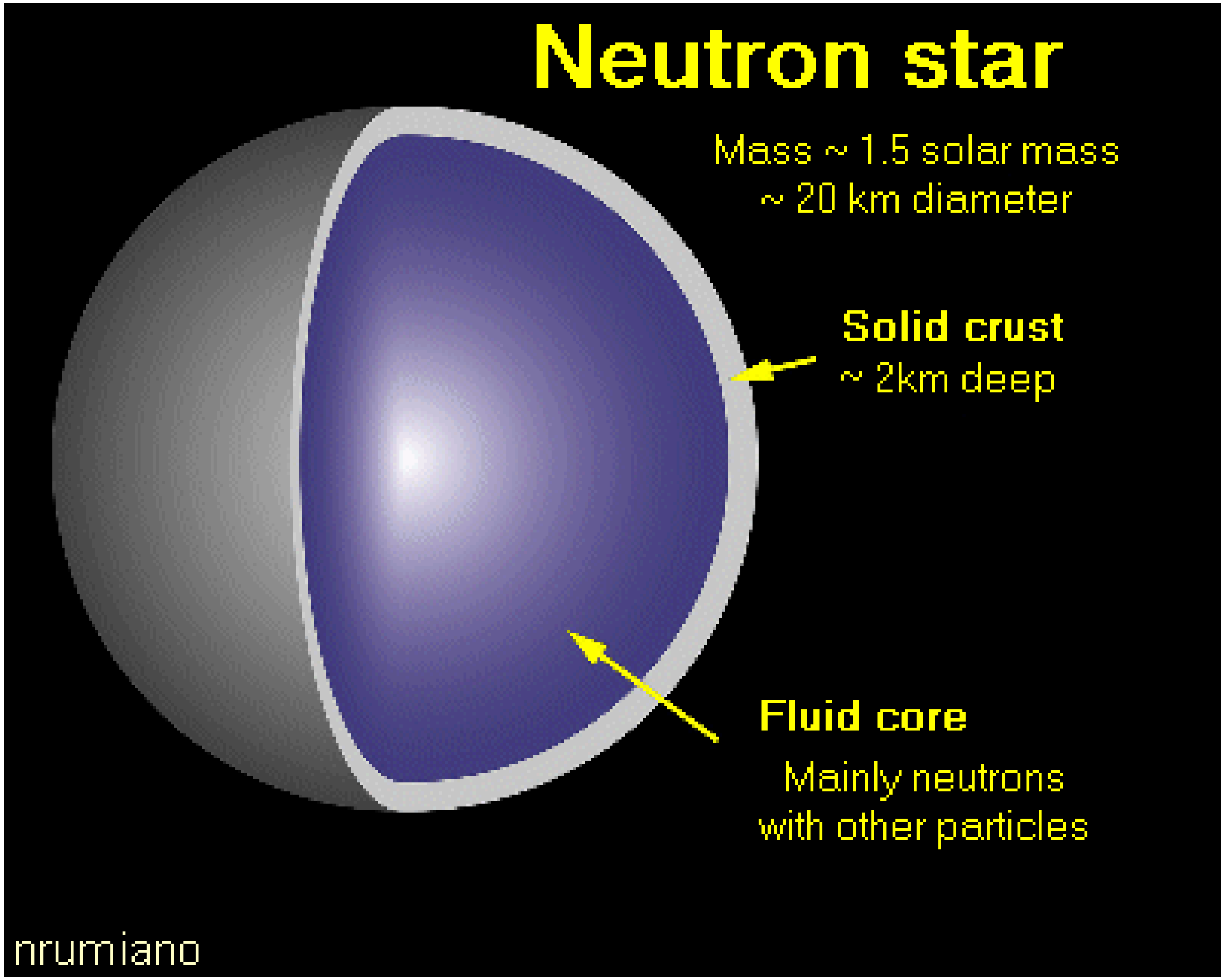
Neutron star
Mass ~ 1.5 solar mass
~ 20 km diameter
Solid crust
~ 2km deep
Fluid core
Mainly neutrons
with other particles
nrumiano

Neutron star interiors

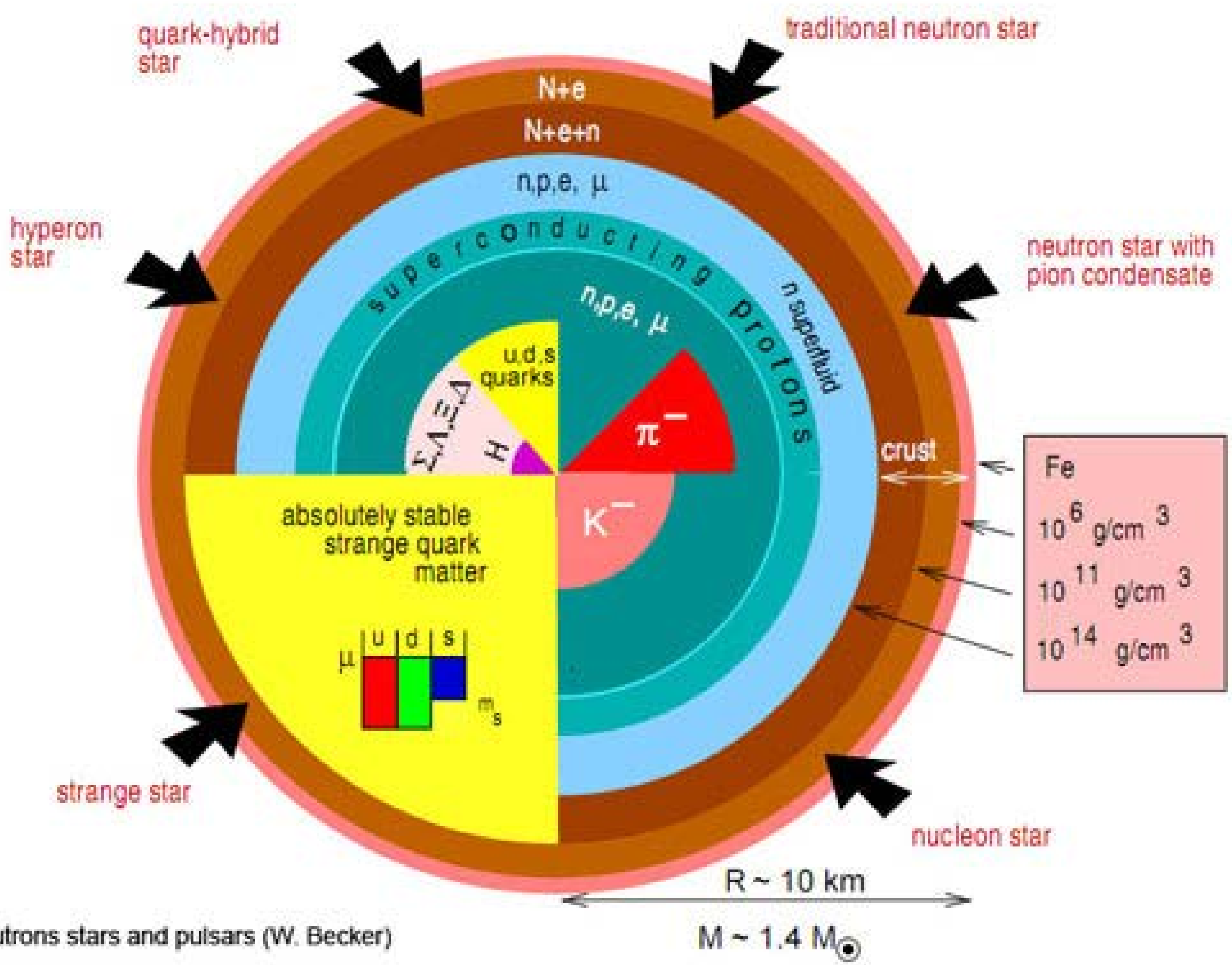

Source : Neutrons stars and pulsars (W. Becker)

Neutron star masses

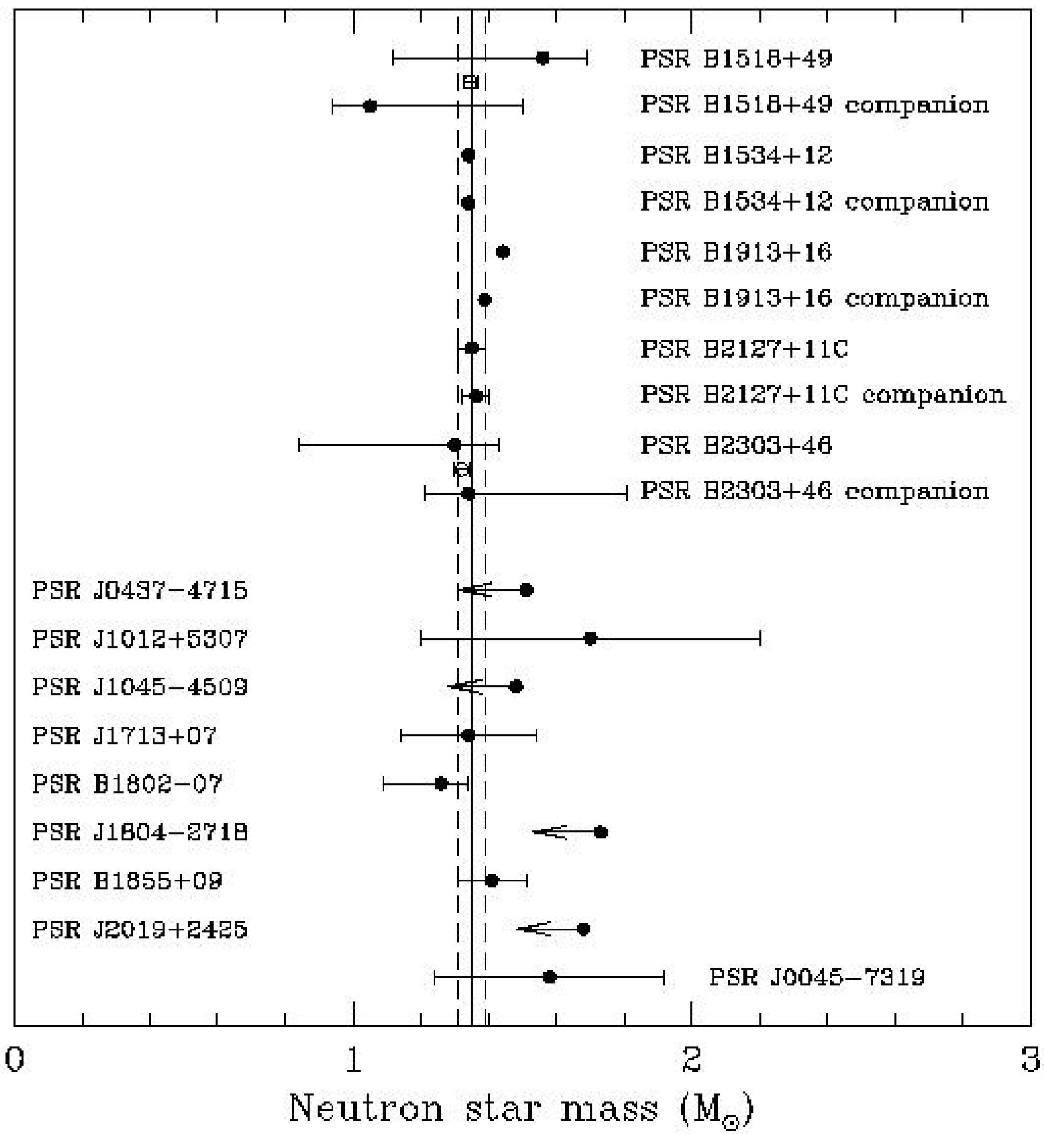

Binary pulsar: orbit

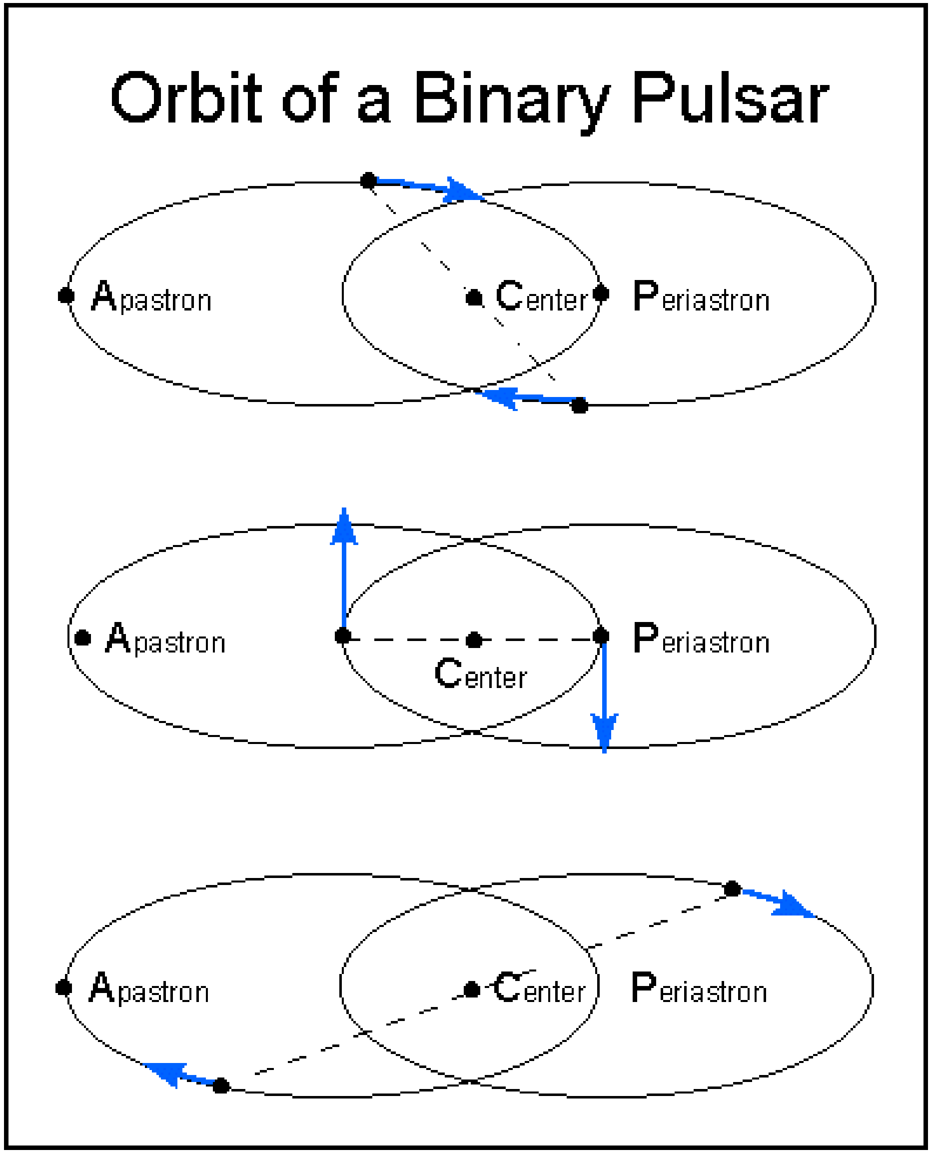

Binary pulsar: orbit

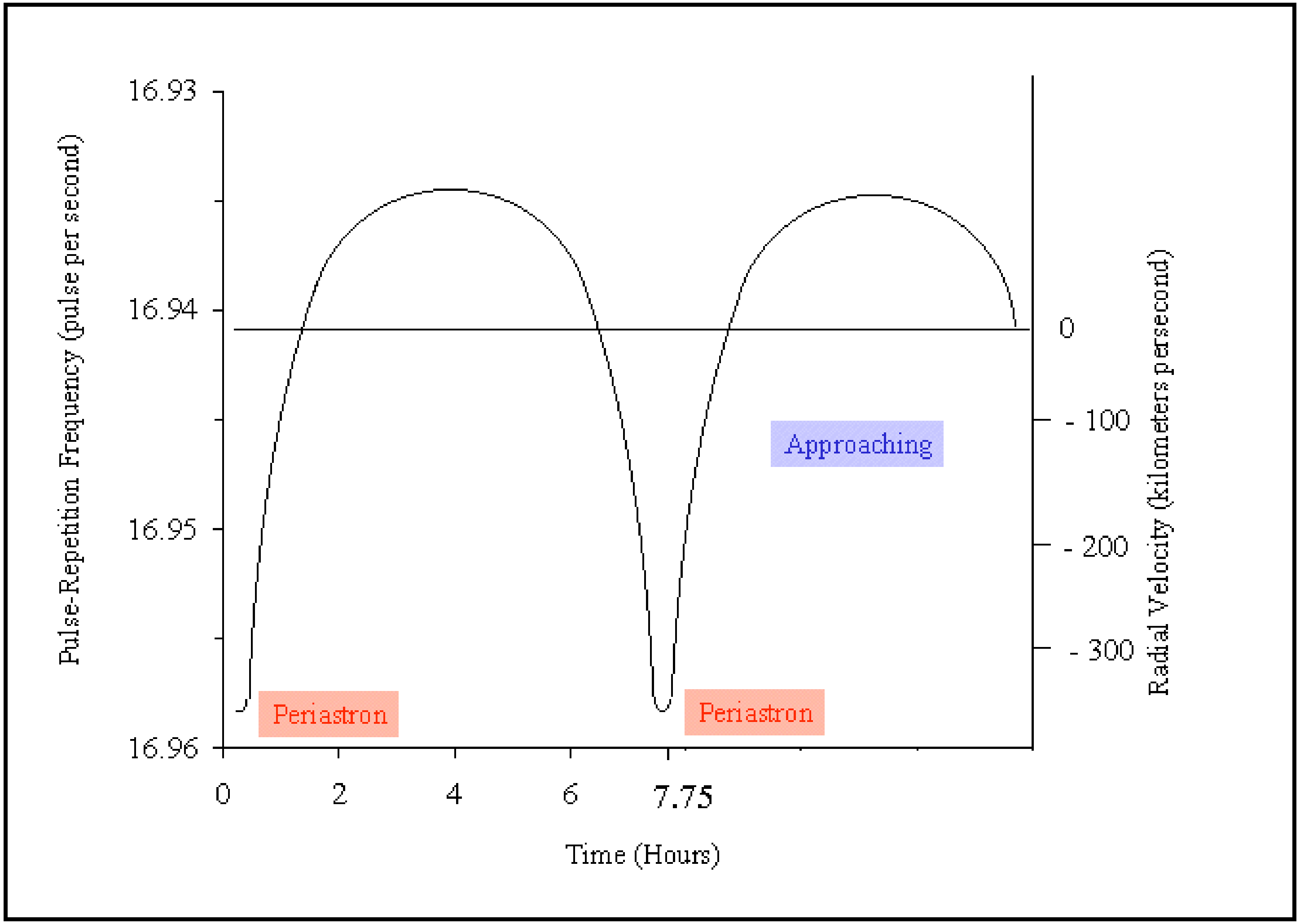

Binary pulsar: gravitational waves

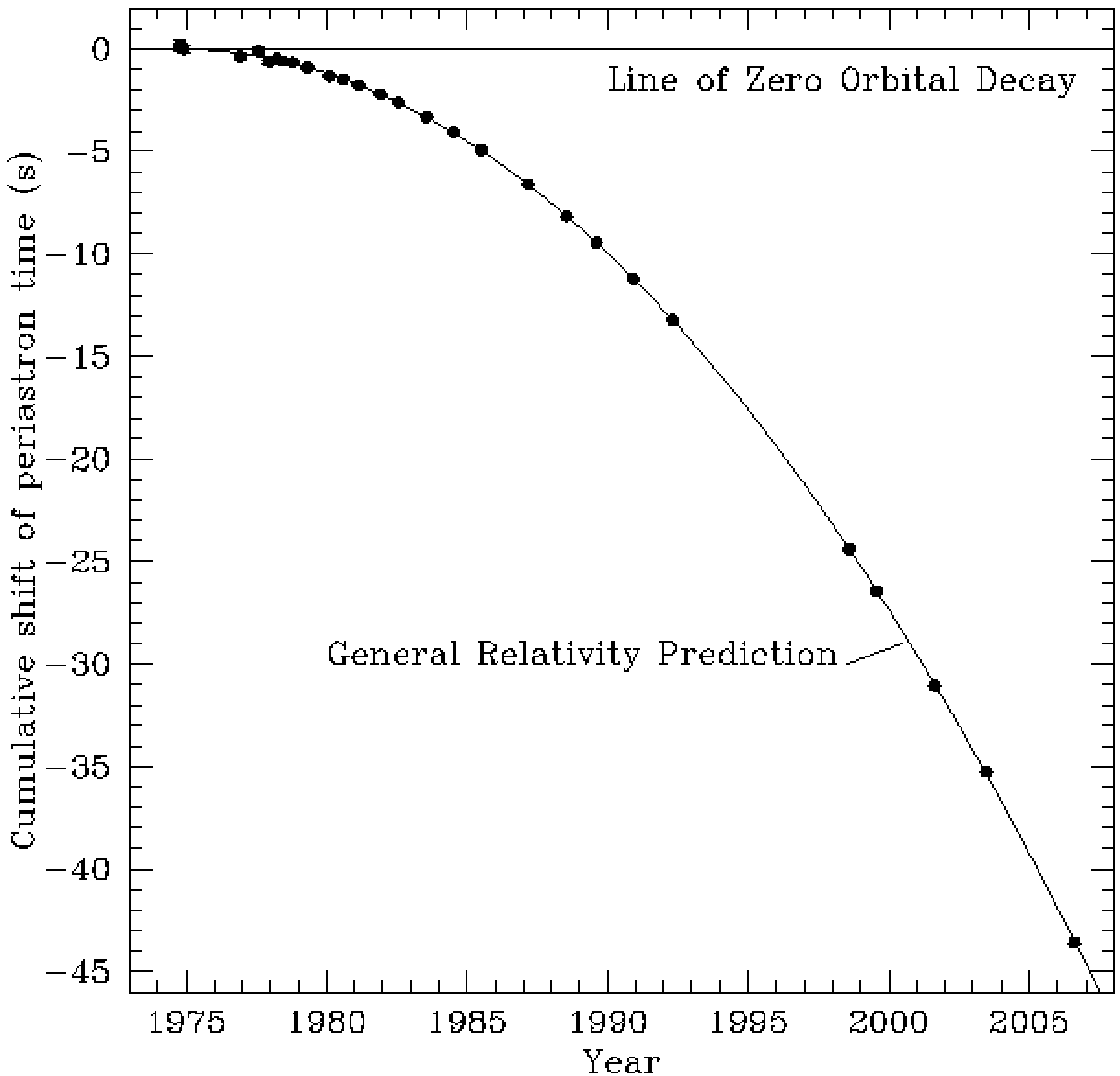

J. Weisberg

Black hole masses

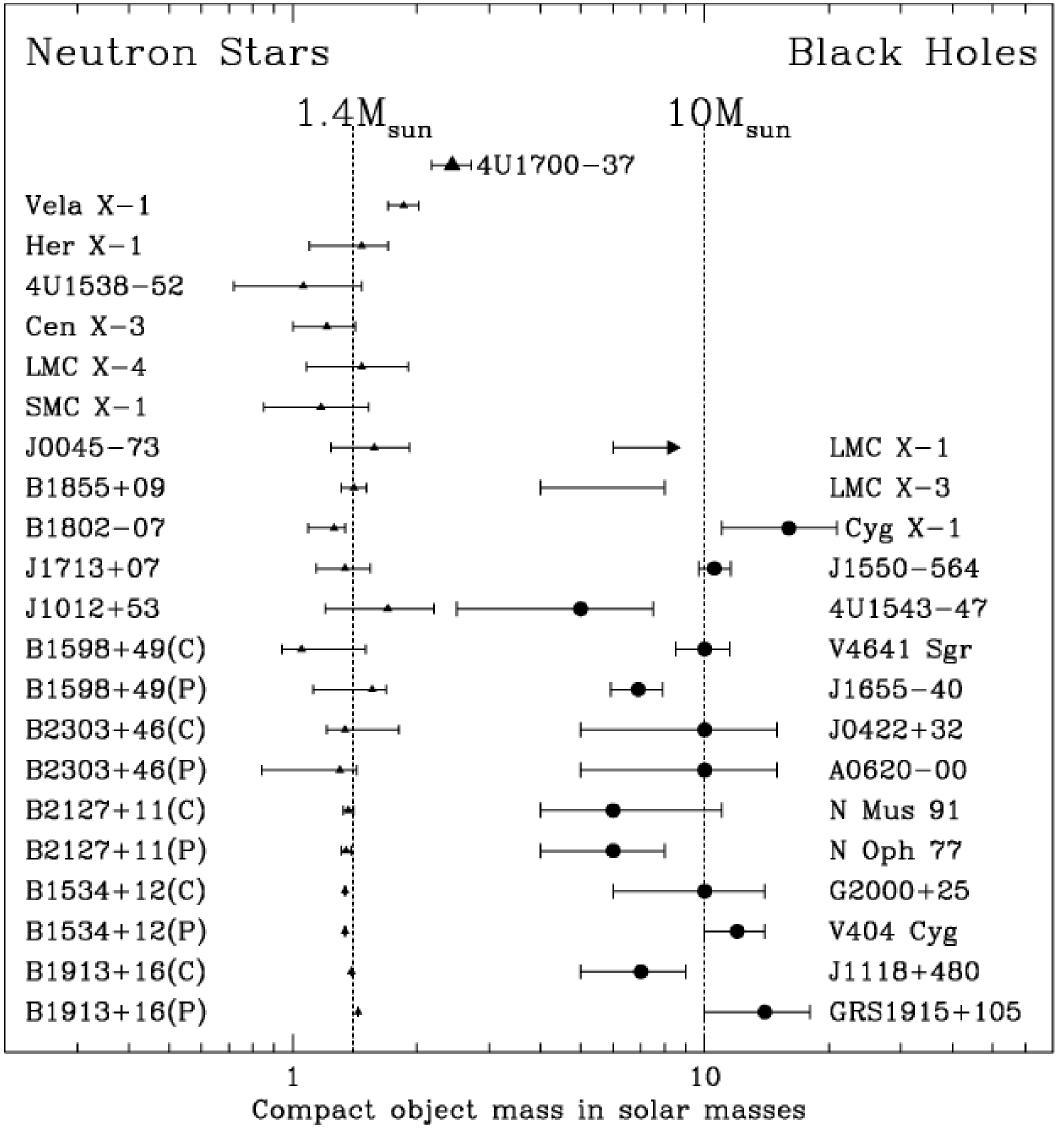

Final fate of single (non-rotating) stars

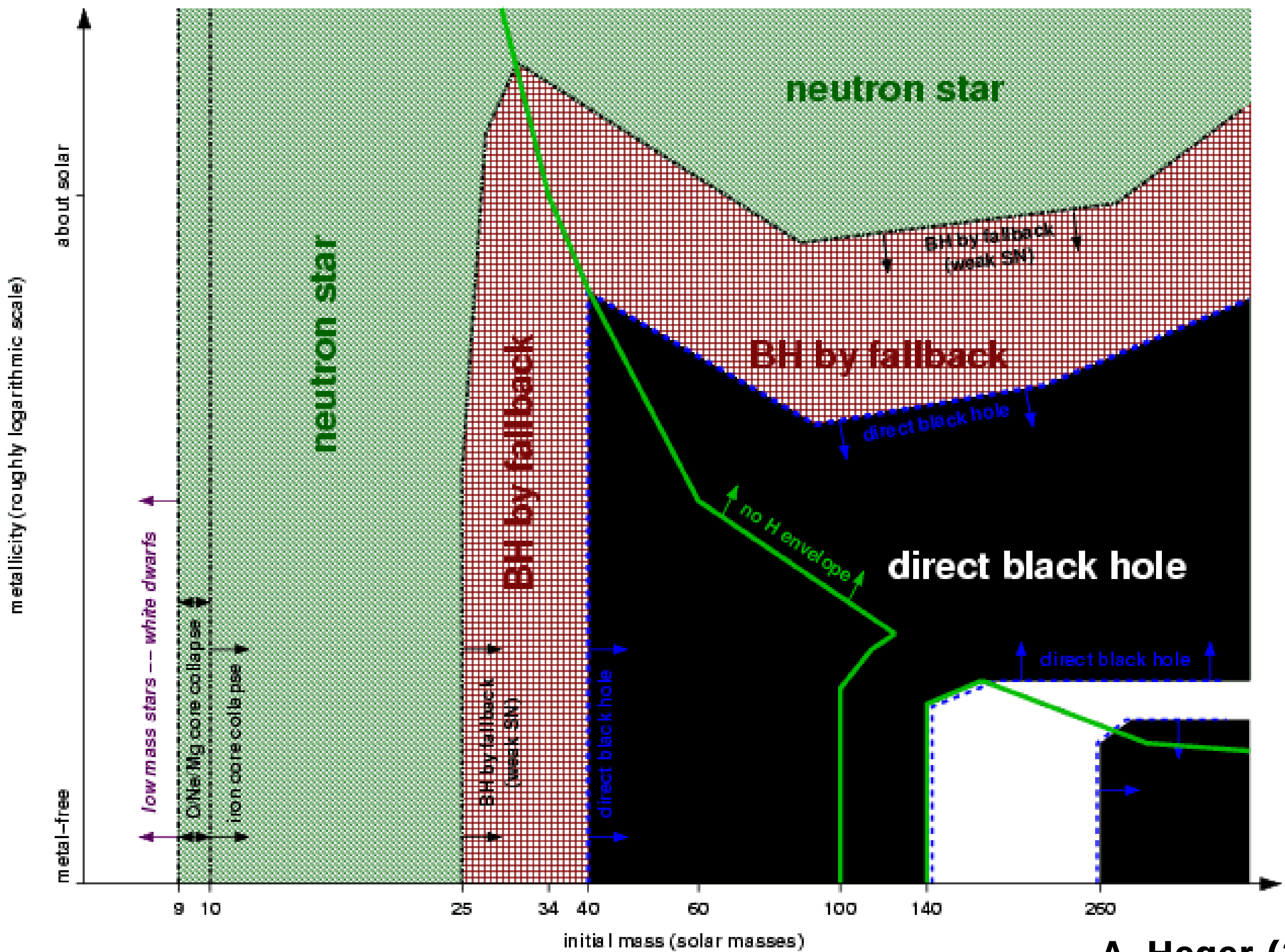

A. Heger (2003)

Roche model: coordinates

$M_1 > M_2$; $M_1\, a = M_2\, b$ (CoM)

$M := M_1 + M_2$

$M_2 =: f\, M$

$a + b = R$

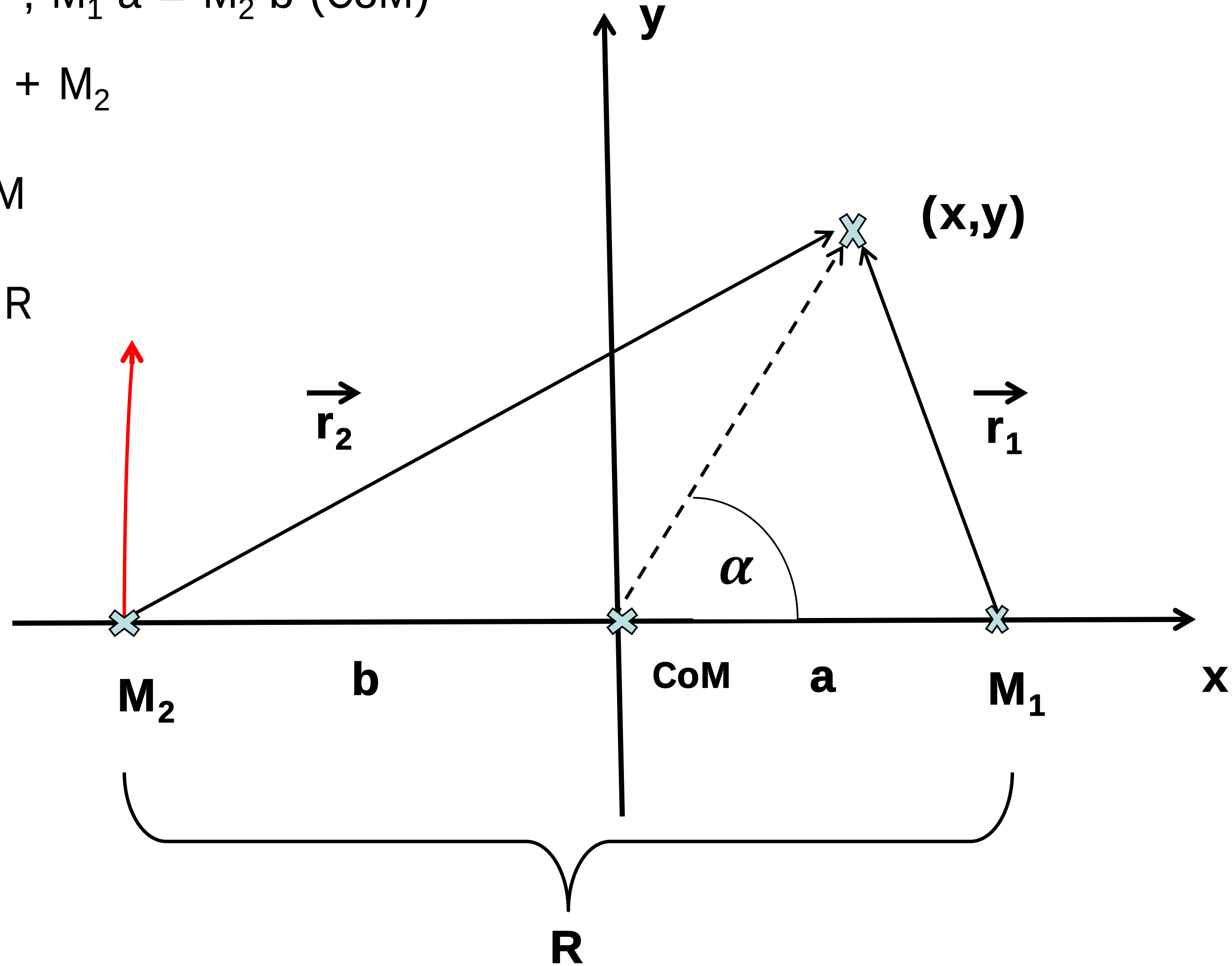

Roche model: potential at (x,y)

$$-\Phi \equiv \Omega(x,y) = \frac{GM_1}{r_1} + \frac{GM_2}{r_2} + \frac{1}{2}(x^2+y^2)\omega^2$$

$$\omega = \frac{\sqrt{GM}}{R^{3/2}} \ (3rd\ Kepler's\ law)$$

$$\Longrightarrow\ \Omega = GM\left(\frac{1-f}{r_1} + \frac{f}{r_2} + \frac{x^2+y^2}{2GM}\omega^2\right)$$

$$Equipotential\ surfaces: \frac{\Omega}{GM} = const$$

$${r_1}^2 = (x^2+y^2) + a^2 - 2\sqrt{x^2+y^2}\, a \cos\alpha$$

$${r_2}^2 = (x^2+y^2) + b^2 - 2\sqrt{x^2+y^2}\, b \cos\alpha$$

Roche model: equipotential surfaces

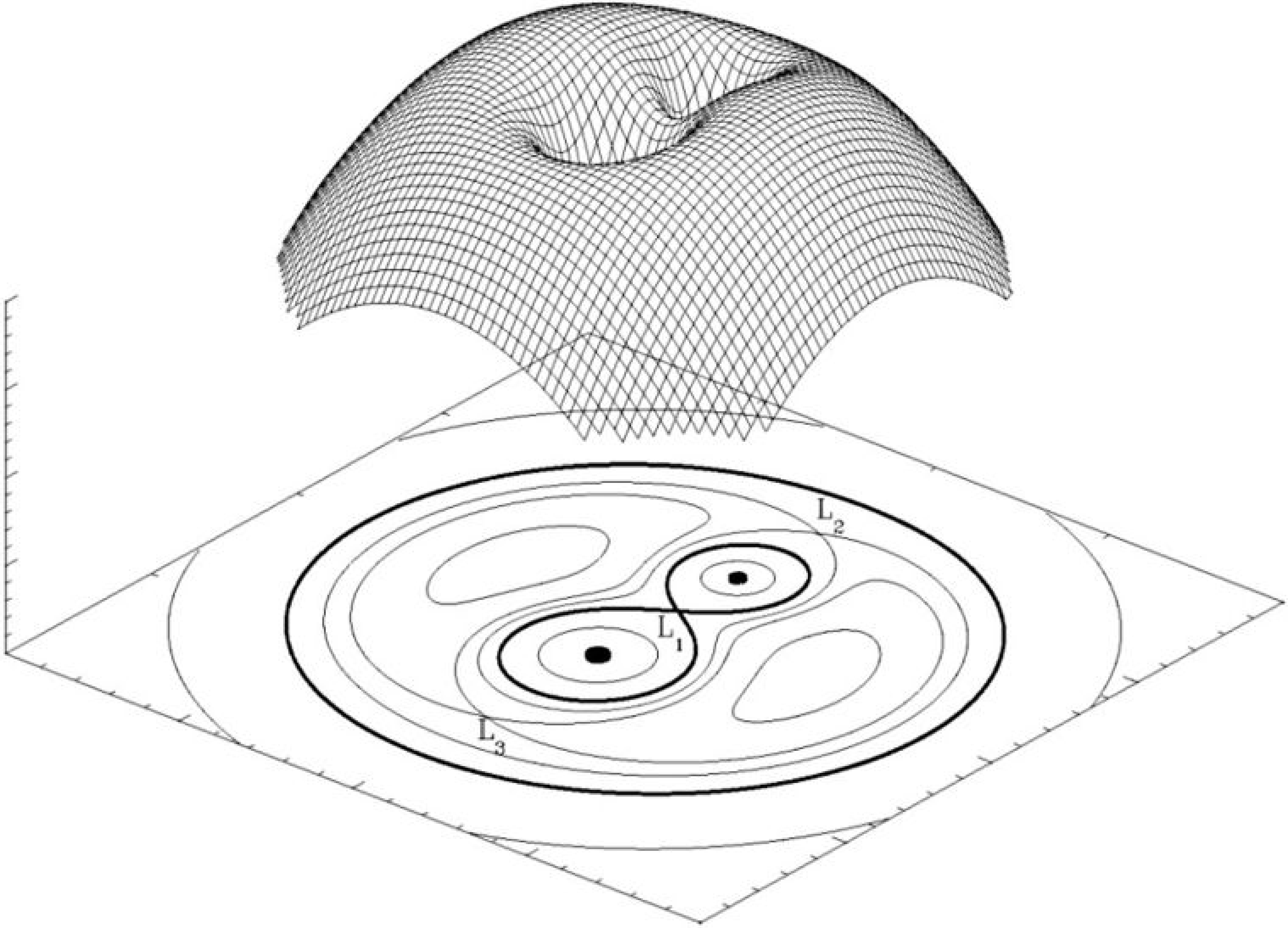

Roche lobes

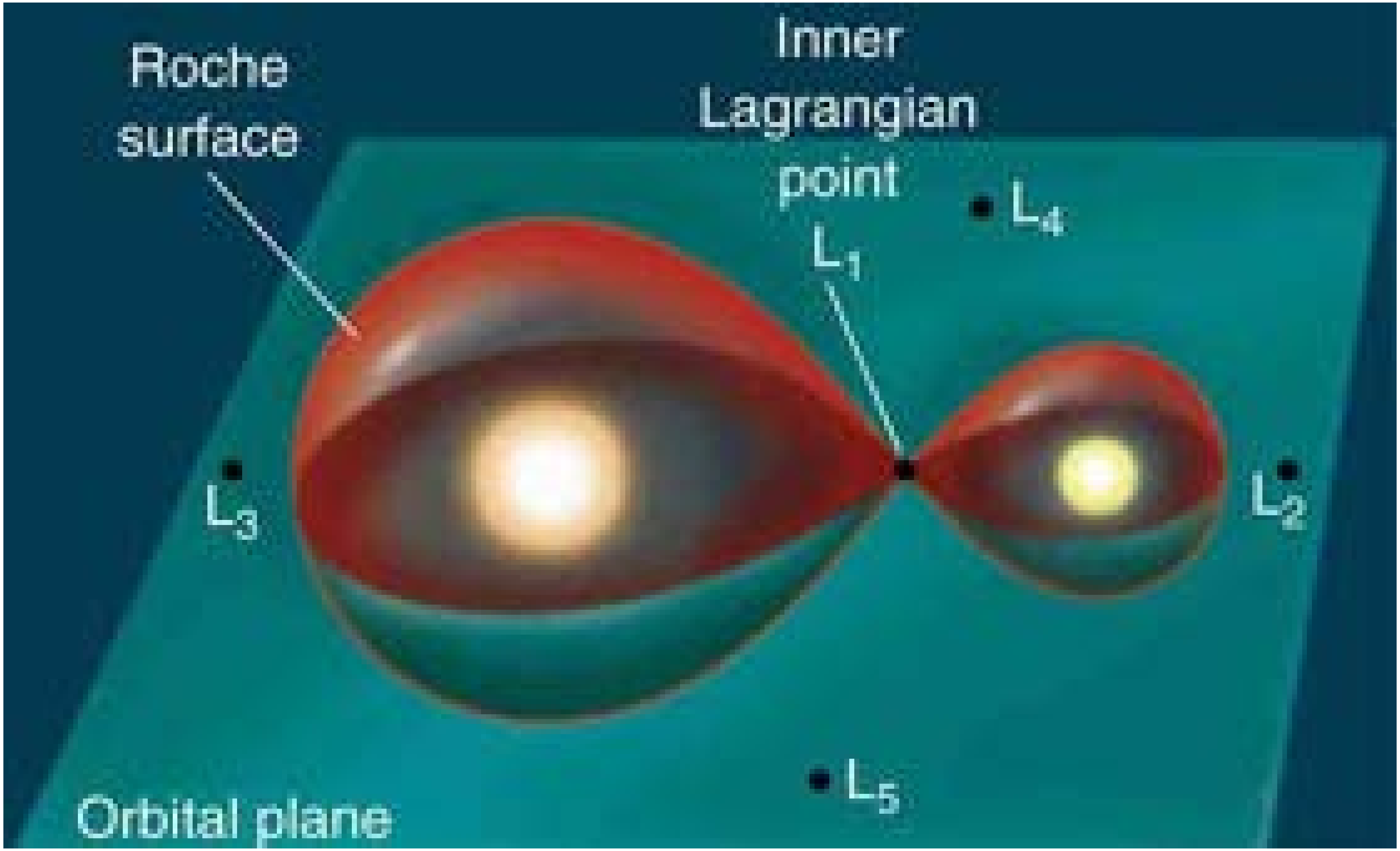

Roche surface
Inner Lagrangian point L_1
L_4
L_3
L_2
L_5
Orbital plane

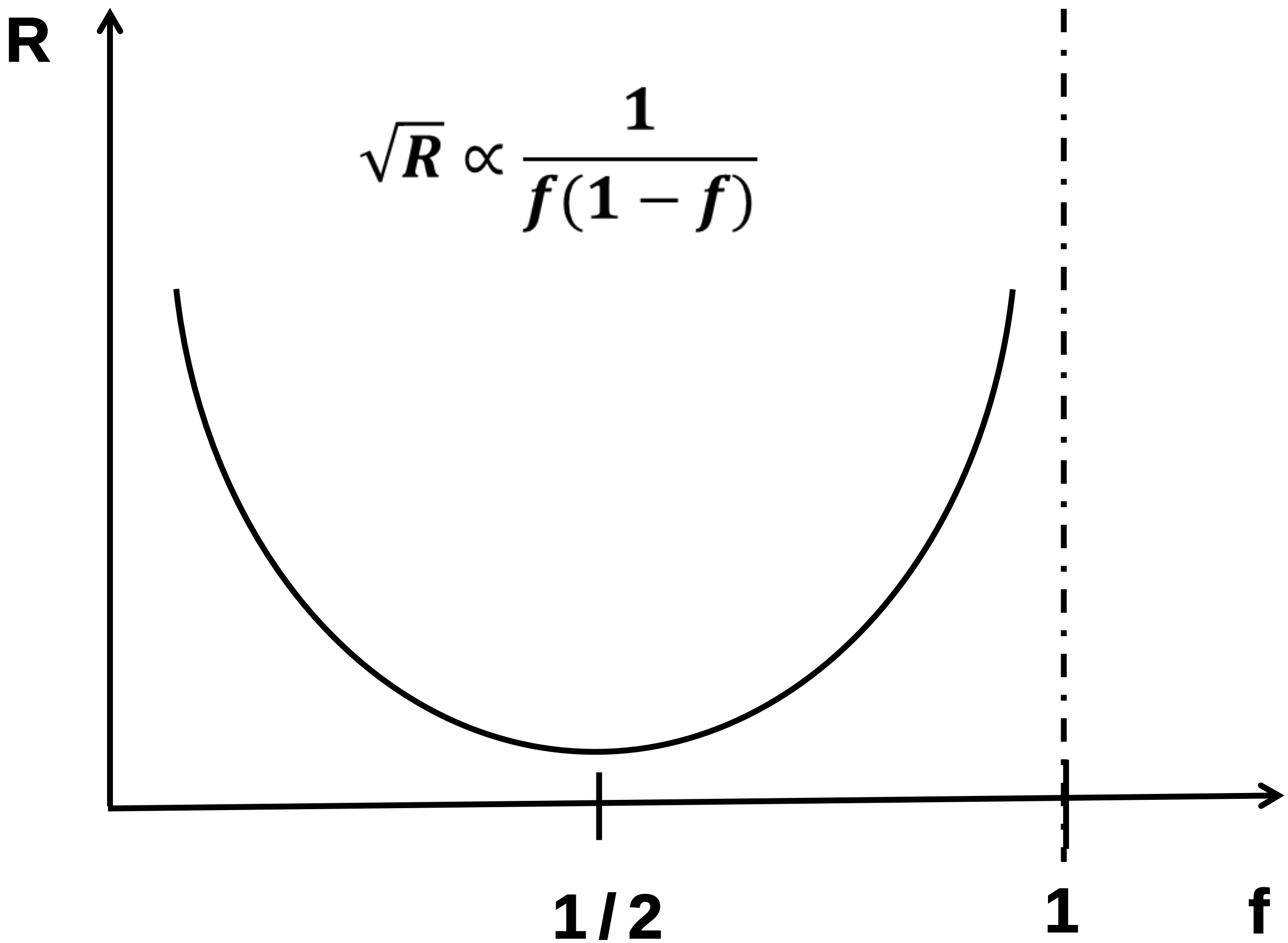
R
$\sqrt{R} \propto \frac{1}{f(1-f)}$
1/2
1
f

Close-binary types

semi-
detached

semi-
detached
with disk

contact

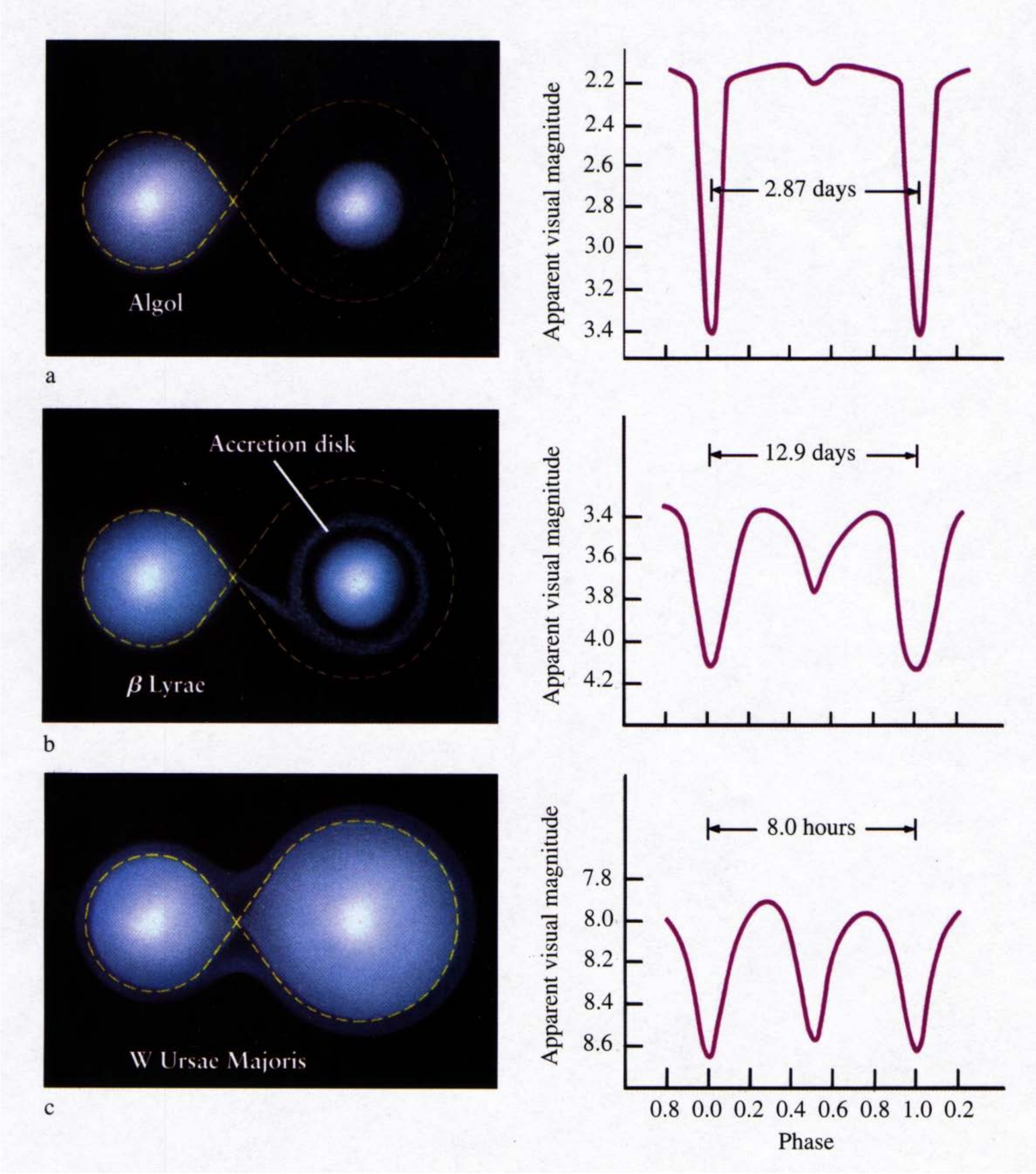

Binary stars: Algol

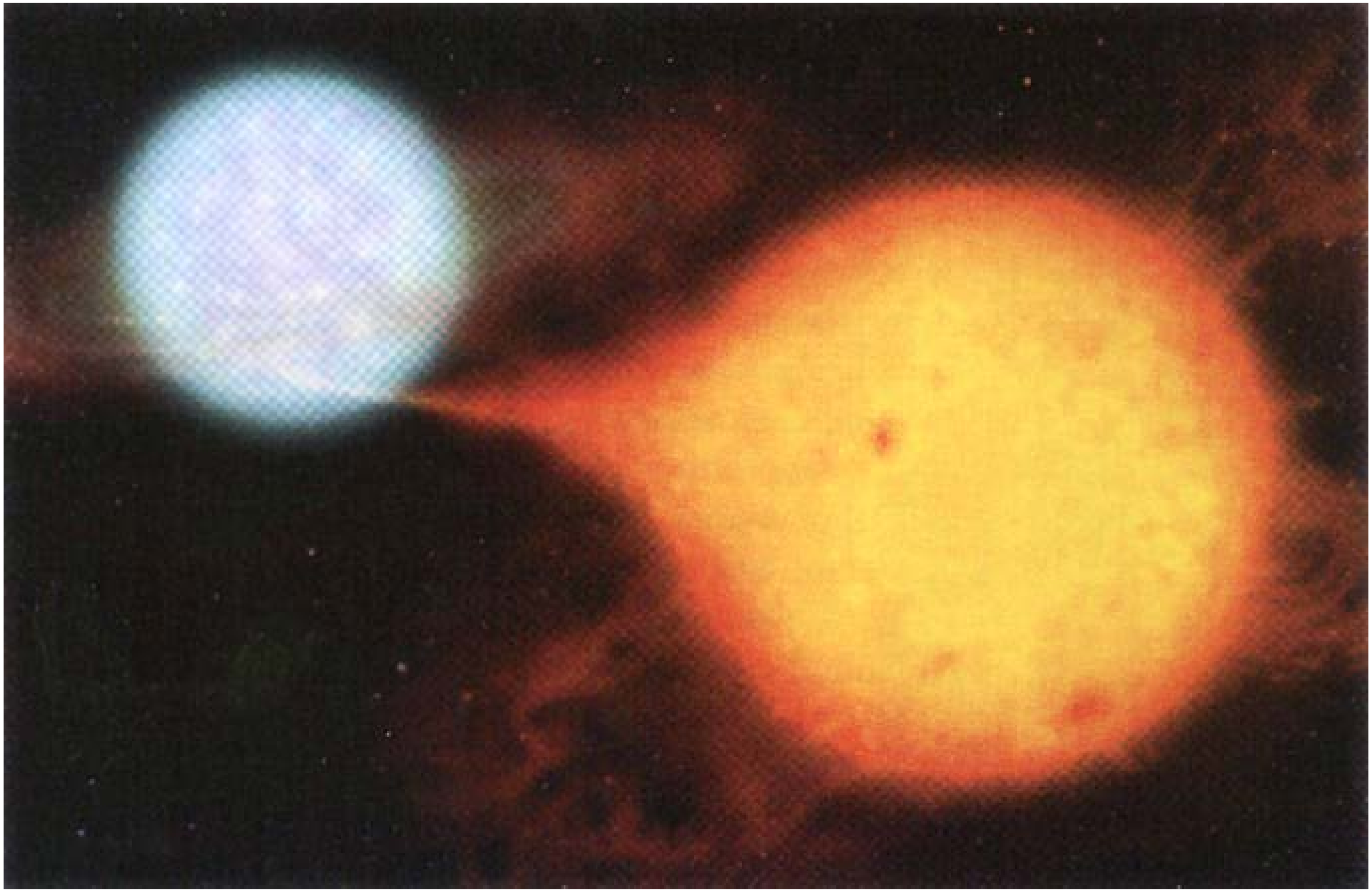

Binary stars: Algol's lightcurve

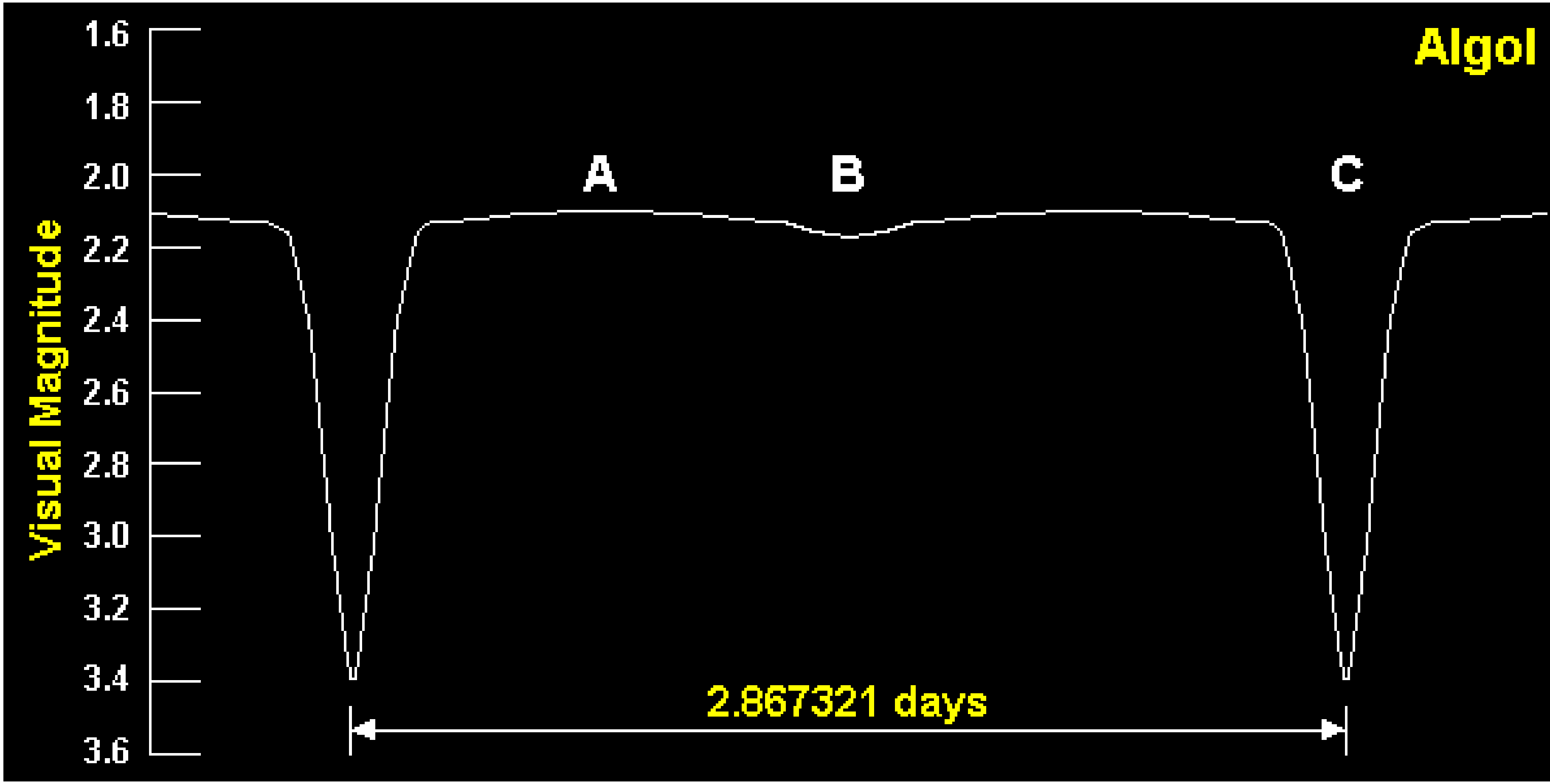

Examples for detached systems

Main sequence star + White Dwarf

	Period (days)	M_{WZ}/M_{sun}	M_{MS}/M_{sun}
V471 Tau	0.5212	0.71	0.73
UU Sag	0.4651	1.05	0.60
LSS 2018	0.3571	0.70	0.31

Binary stars: „Case A“ evolution

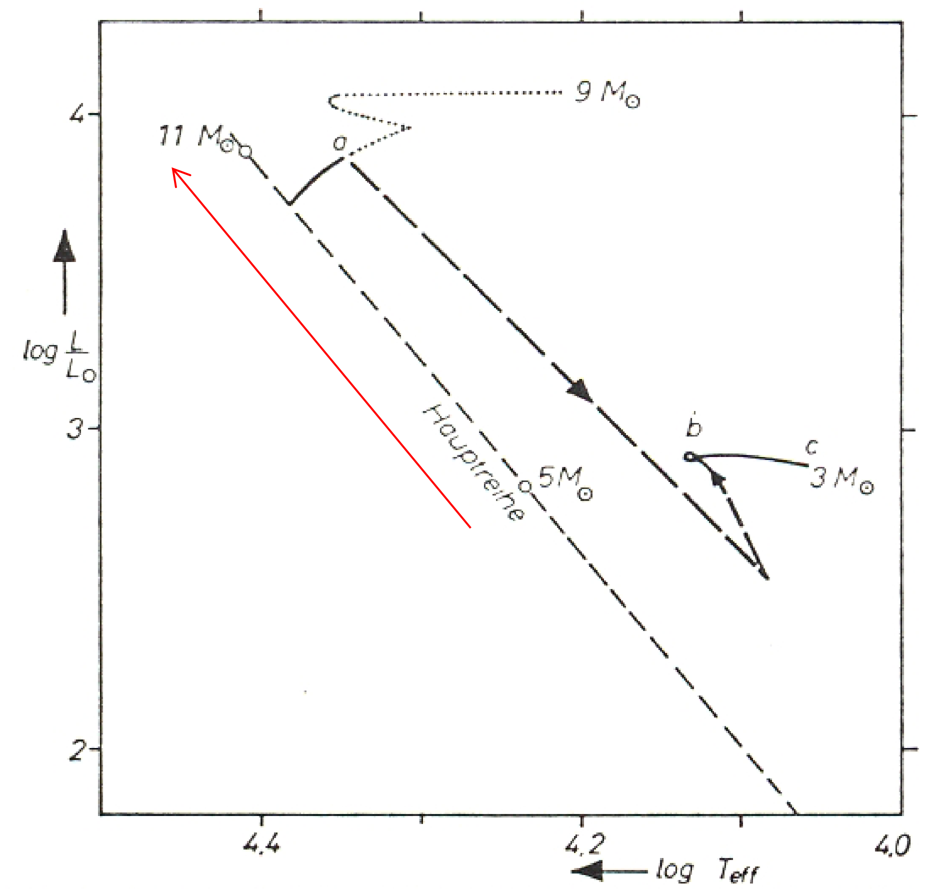

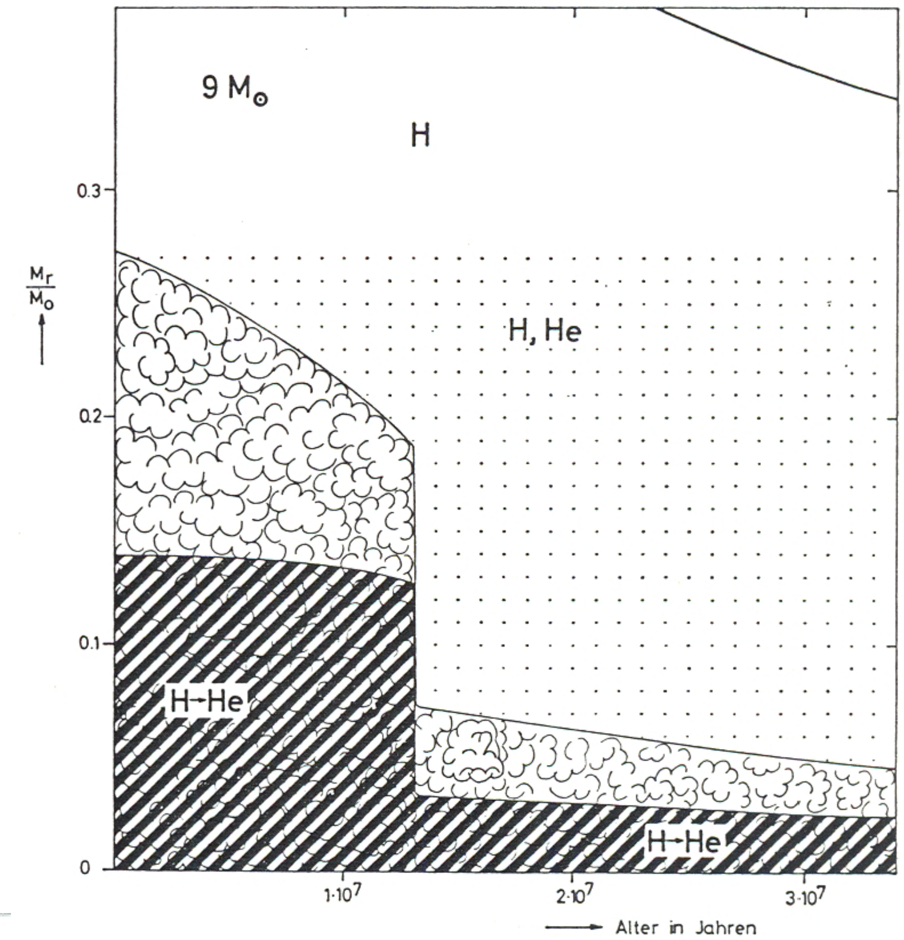

M_1=9M_{sun} , M_2=5M_{sun} , R=10^{12}cm, R_{c1}=4 10^{11}cm, reached 1.25 107 years after onset of core-H burning

Binary stars: „Case B“ evolution

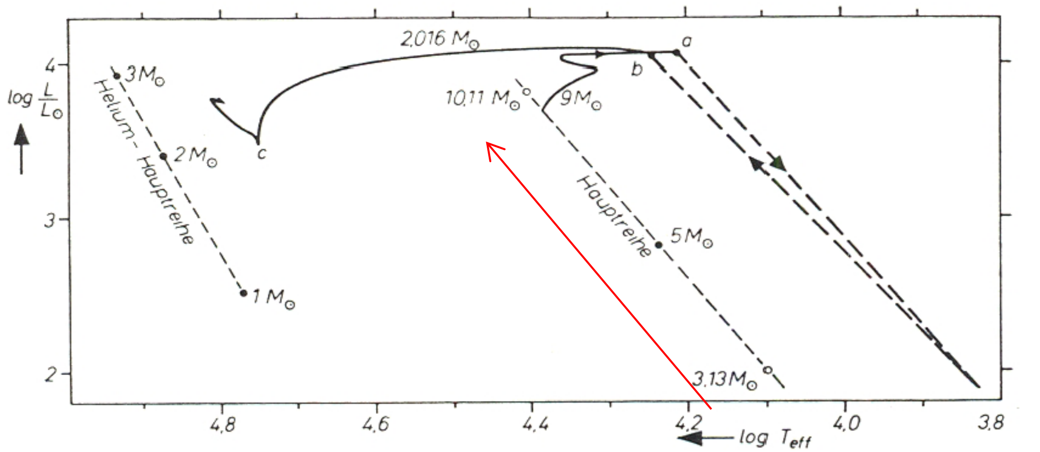

Abb. 4. Der Entwicklungsweg im Fall B. Der Massenverlust beginnt bei (*a*) und endet bei (*b*). Bei (*c*) ist eine Phase ruhigen Heliumbrennens mit anschließendem Erschöpfen des zentralen Heliums. Der zweite Stern bewegt sich während des Massenverlustes längs der Hauptreihe von 3.13 M☉ zum Punkt von 10.11 M☉

Abb. 5. Zeitliche Veränderungen im Sterninnern bei Fall B. Die Symbole sind die gleichen wie in Abb. 3. Die Darstellung beginnt links nicht auf der Hauptreihe, sondern wenn sich bereits eine Schalenquelle gebildet hat und der konvektive Kern abstirbt. Die Sternoberfläche kommt nahezu senkrecht von oben herab, was zeigt, daß der Massenverlust sehr rasch erfolgt. Erst gegen Ende wird er langsamer. Nach dem Ende des Massenverlustes, das mit dem Zünden des Heliums im Zentrum zeitlich zusammenfällt, ist die Oberfläche eine horizontale Gerade. Die Materie, welche jetzt die Oberflächenschicht bildet, war vorher bereits einige Zeit dem Wasserstoffbrennen ausgesetzt

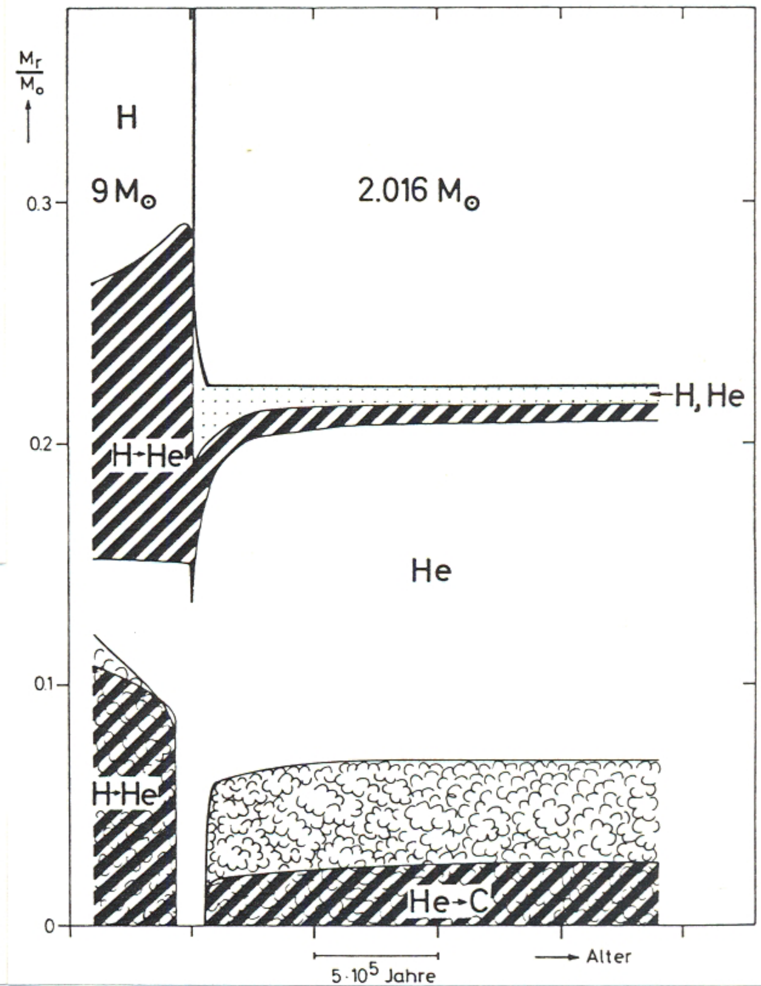

$M_1=9M_{sun}$, $M_2=3.13M_{sun}$, $R=2\ 10^{12}$cm, $R_{c1}=10^{12}$cm, reached during shell-H burning, $R_1{}^*{}_{max}$(core-H)=5 10^{11}cm

Binary stars: Classical Novae

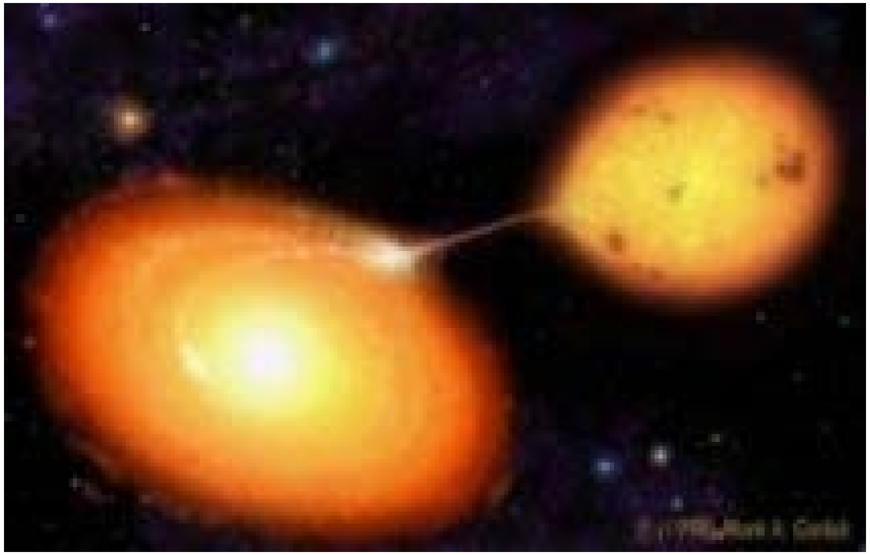

Nova Cygni 1992
Hubble Space Telescope
Faint Object Camera

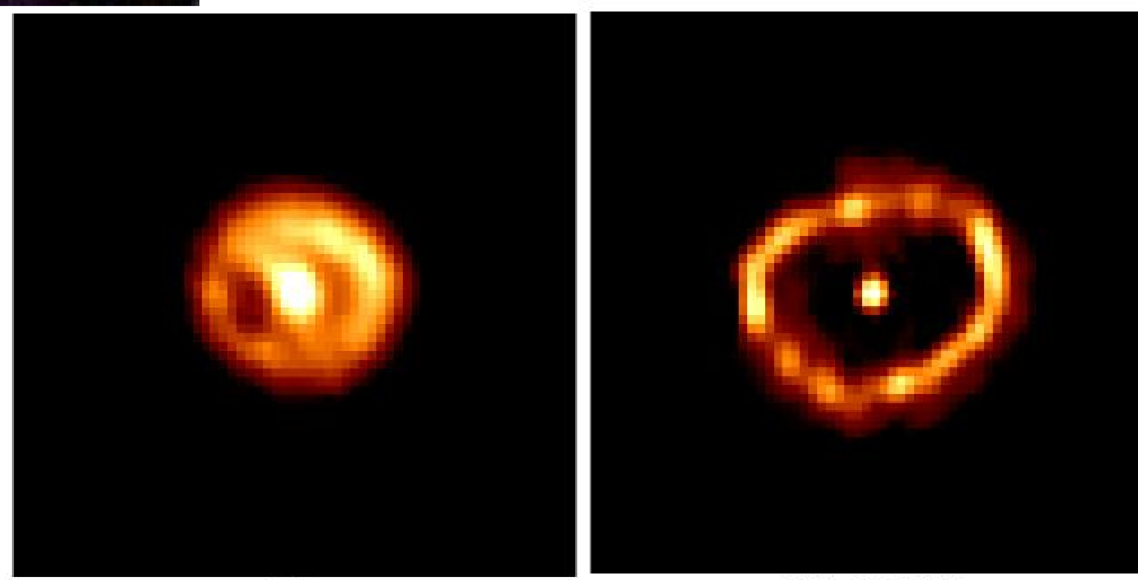

Pre-COSTAR Raw Image | With COSTAR Raw Image

Binary stars: Classical Novae

Nova
GK Per

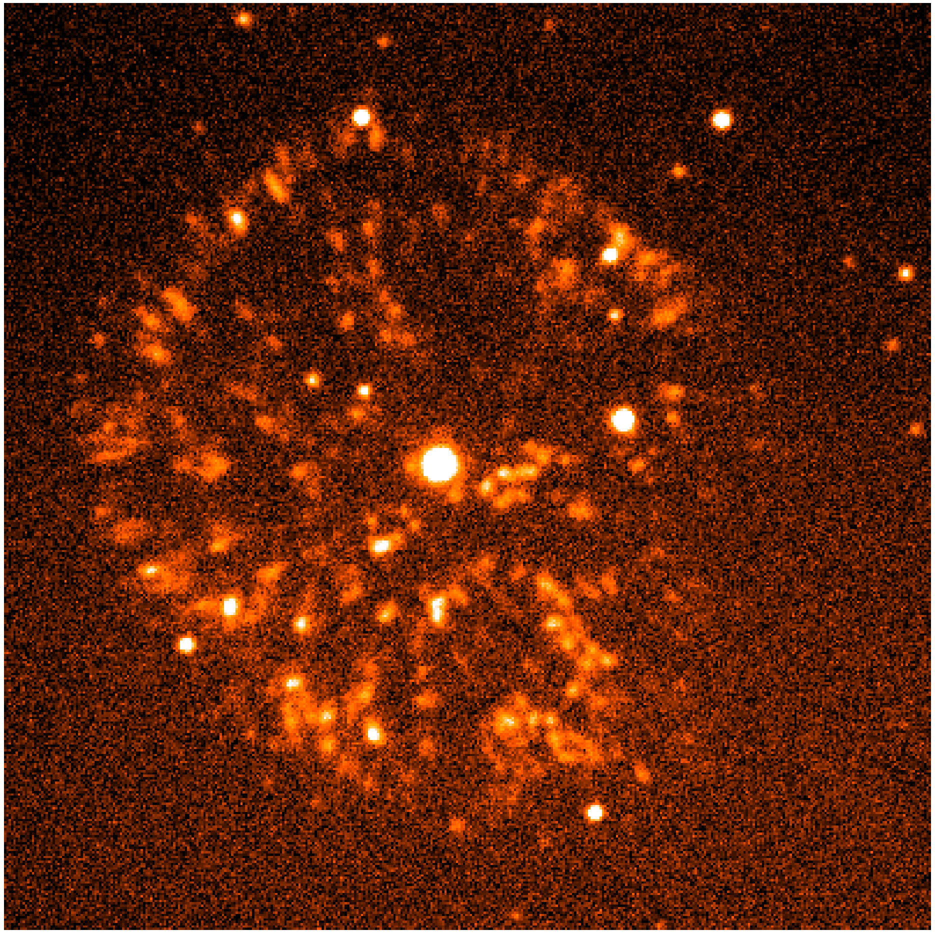

Classical Novae: Lightcurves

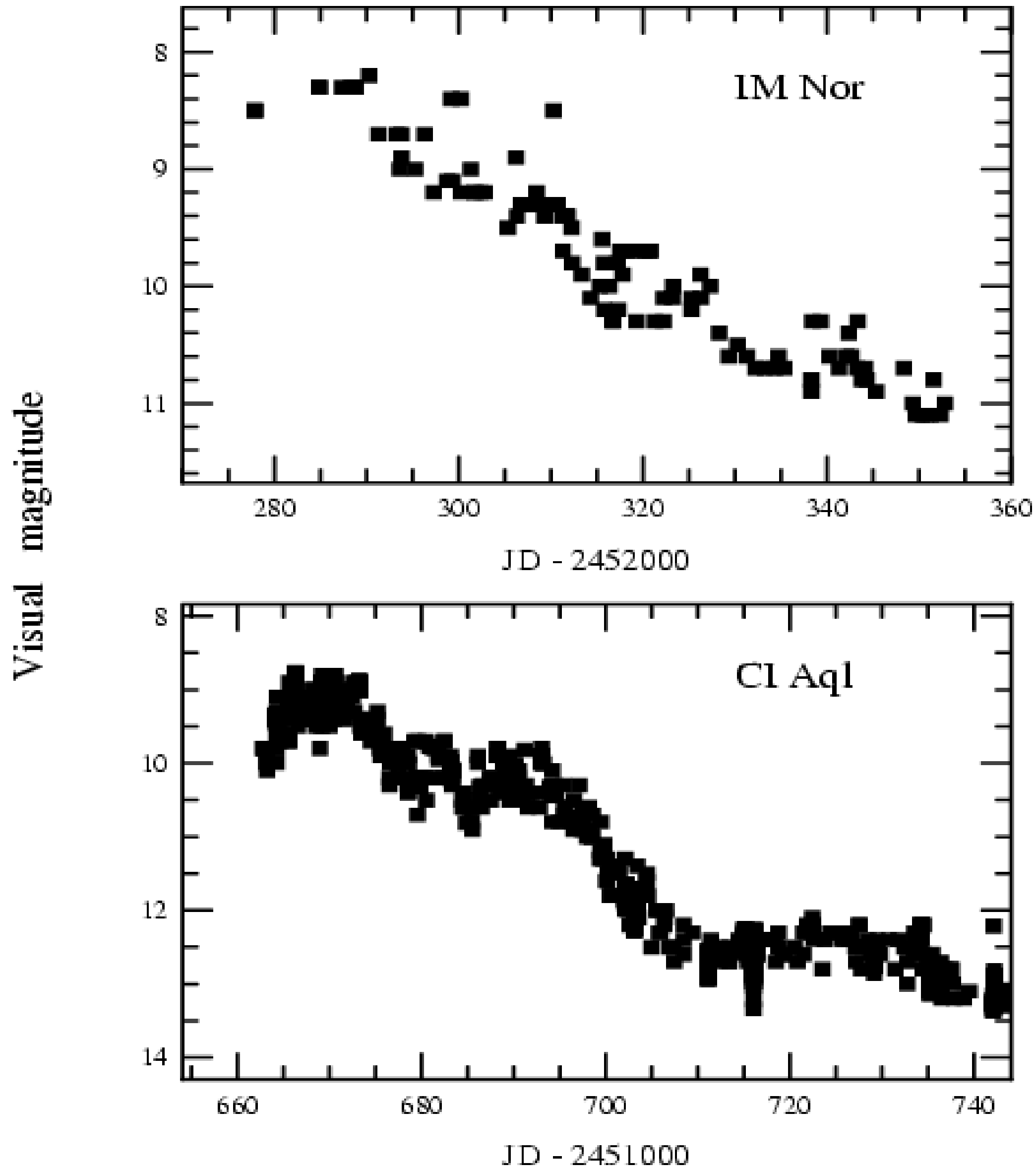

Kato et al. (2002)

Classical Novae: Lightcurves

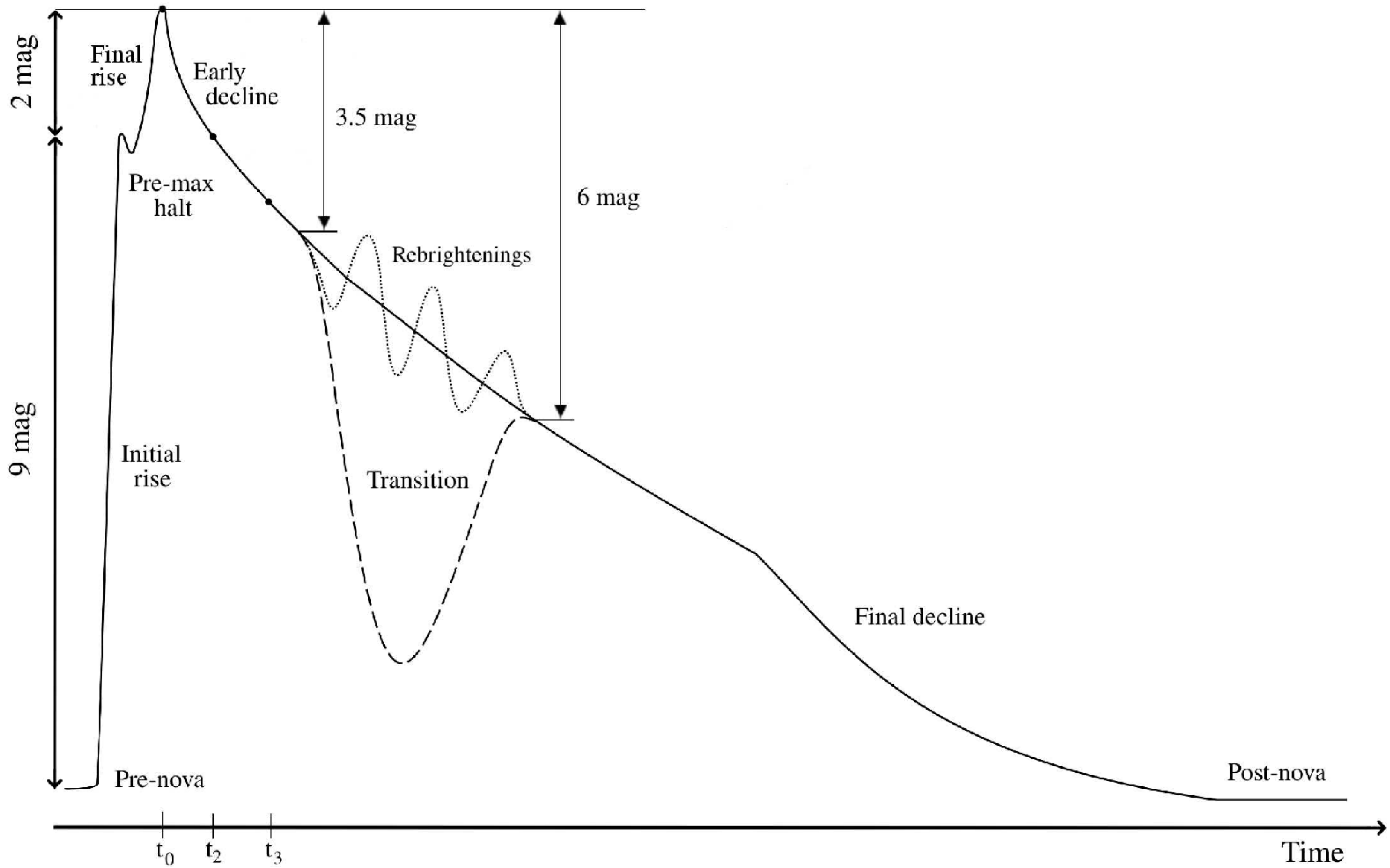

Bode & Evans (1989)

Supernova classification

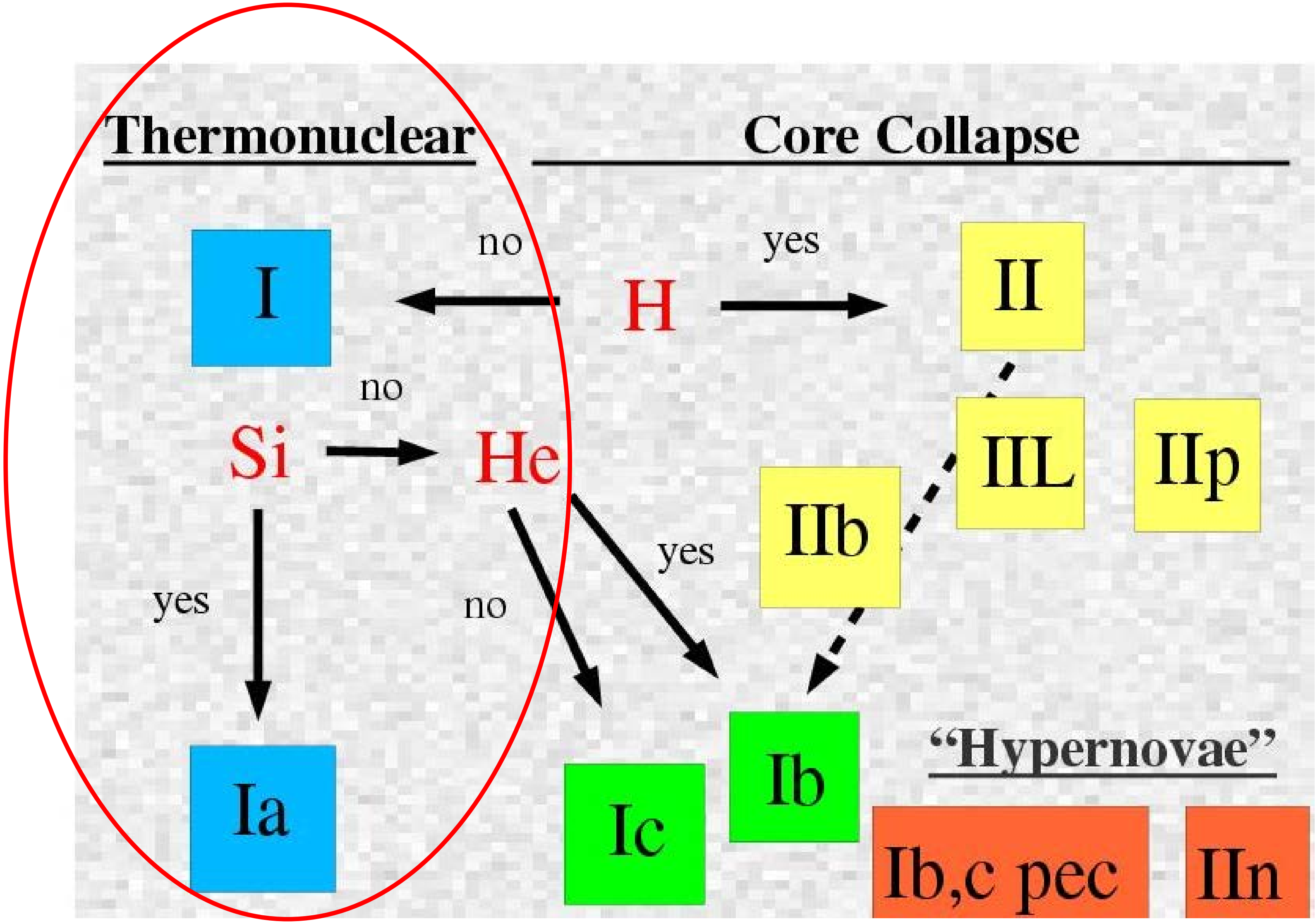

Supernova light curves (schematically)

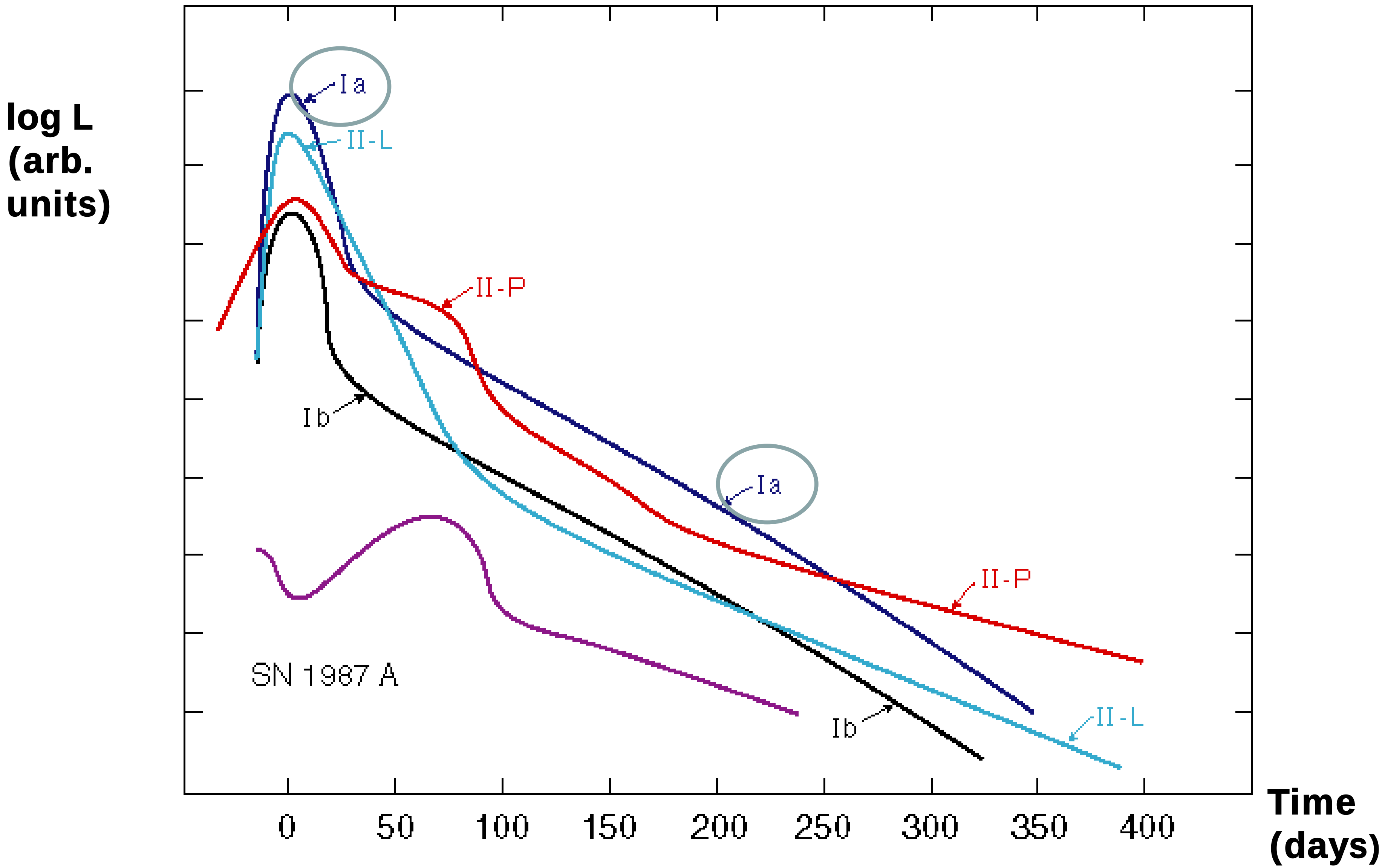

Supernova spectra (schematically)

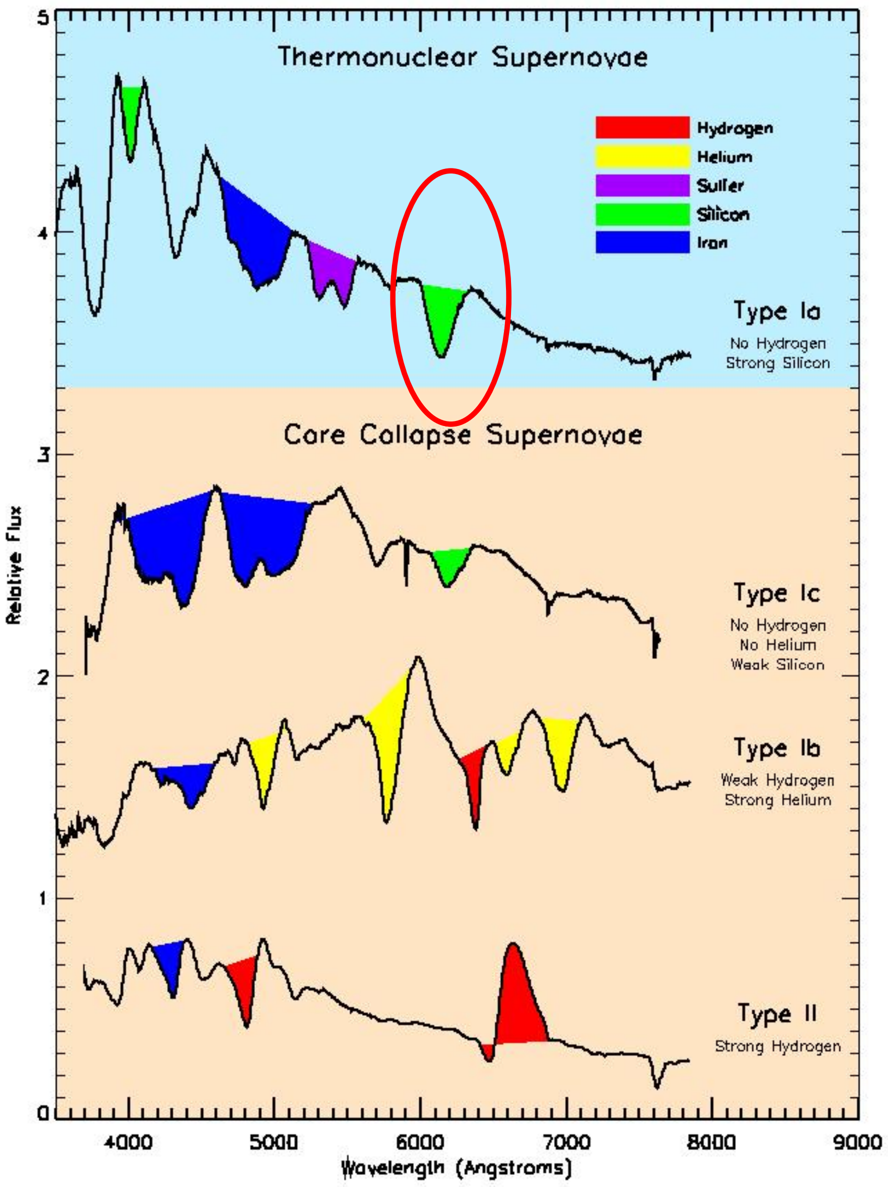

Type Ia supernovae

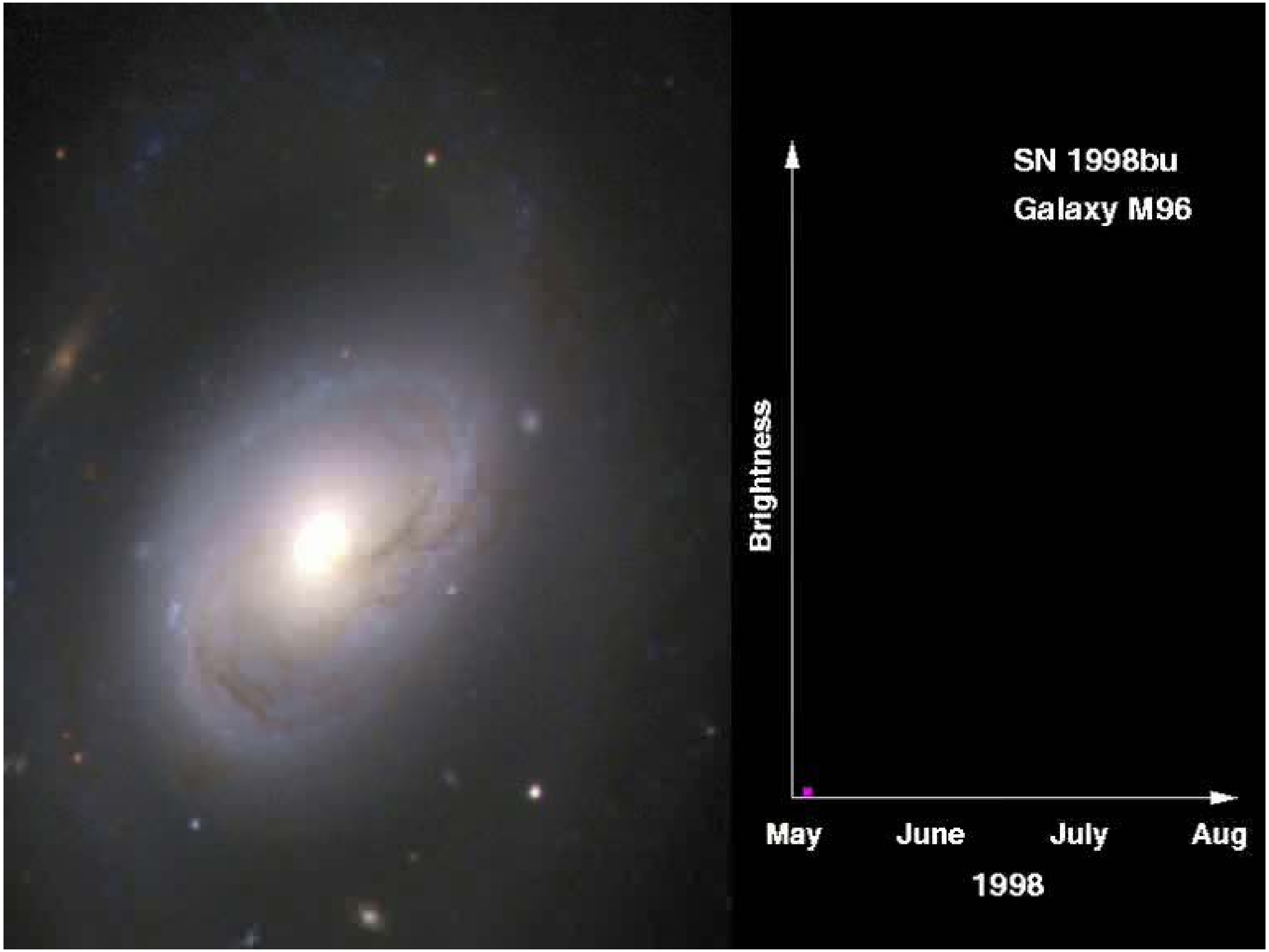

© P. Challis

The ‘zoo’ of thermonuclear explosions

- ***‘Single degenerates’***
  - **Chandrasekhar mass**
    - **Pure deflagration**
    - **‘delayed’ detonation**
  - **sub-Chandrasekhar mass**

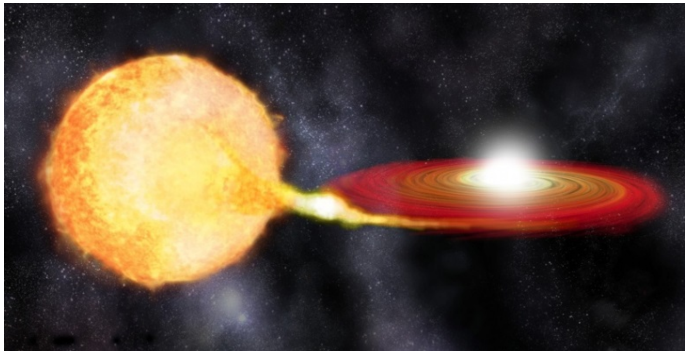

- ***‘Double degenerates’***
  - **C/O + C/O**
  - **C/O + He**

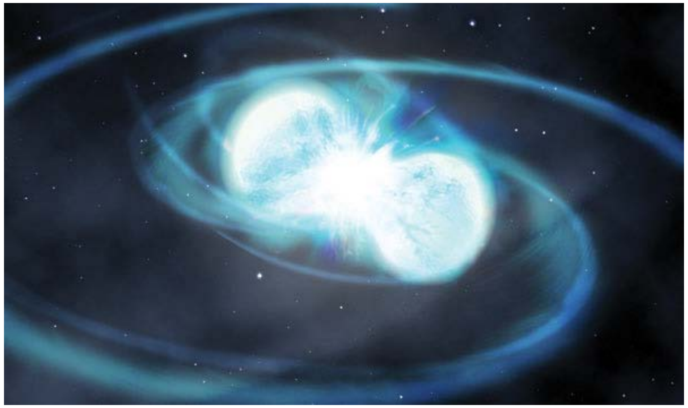

Which of them are realized in Nature? All of them?

Type Ia supernovae

© NASA

The standard 'single-degenerate' model

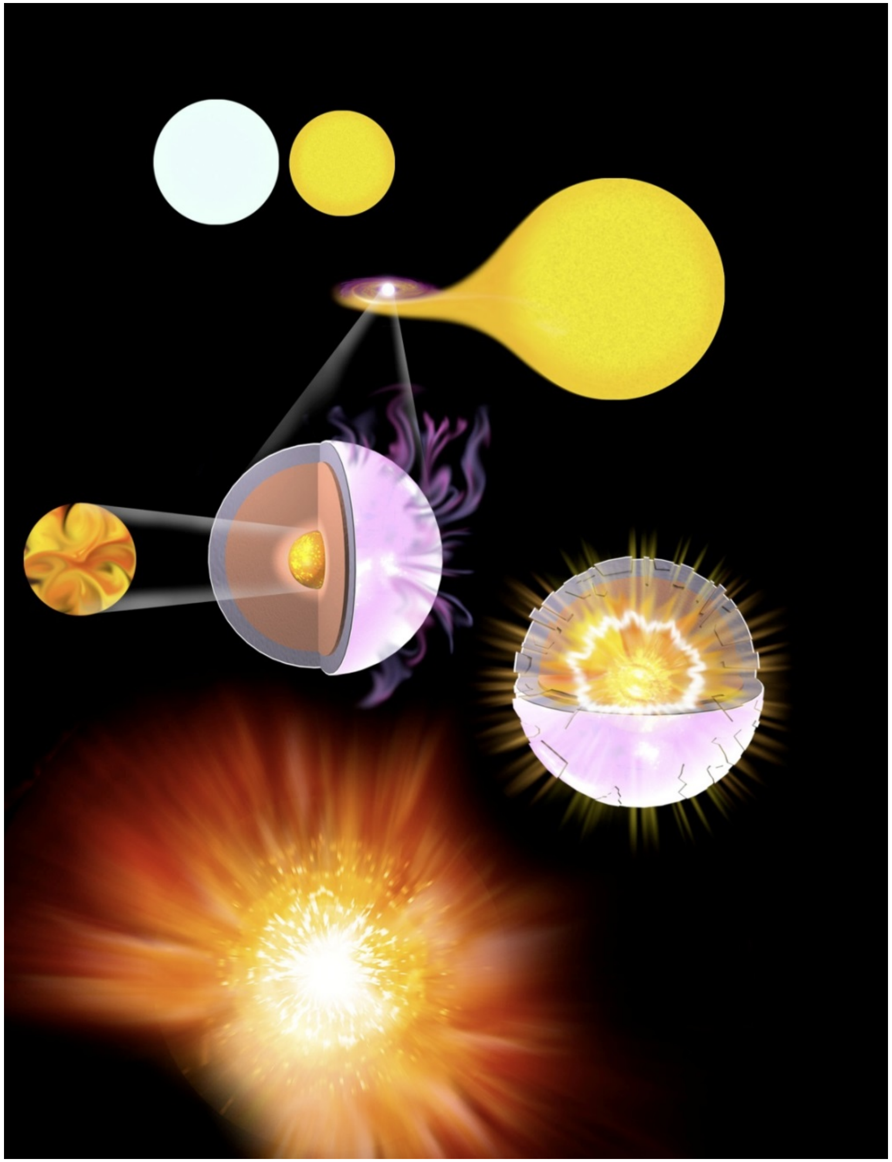

- **White dwarf star in a binary system with MS or (R)G star**
- **Growing to the critical mass ($M_{chan} \approx 1.4\ M_{\odot}$) by mass transfer**
- **Disrupted by a thermo-nuclear explosion (fusion of C and O to iron-group elements)**
- **Light comes from radioactive decay :** **$^{56}Ni \rightarrow {}^{56}Co \rightarrow {}^{56}Fe$**

The standard ‘single-degenerate’ model

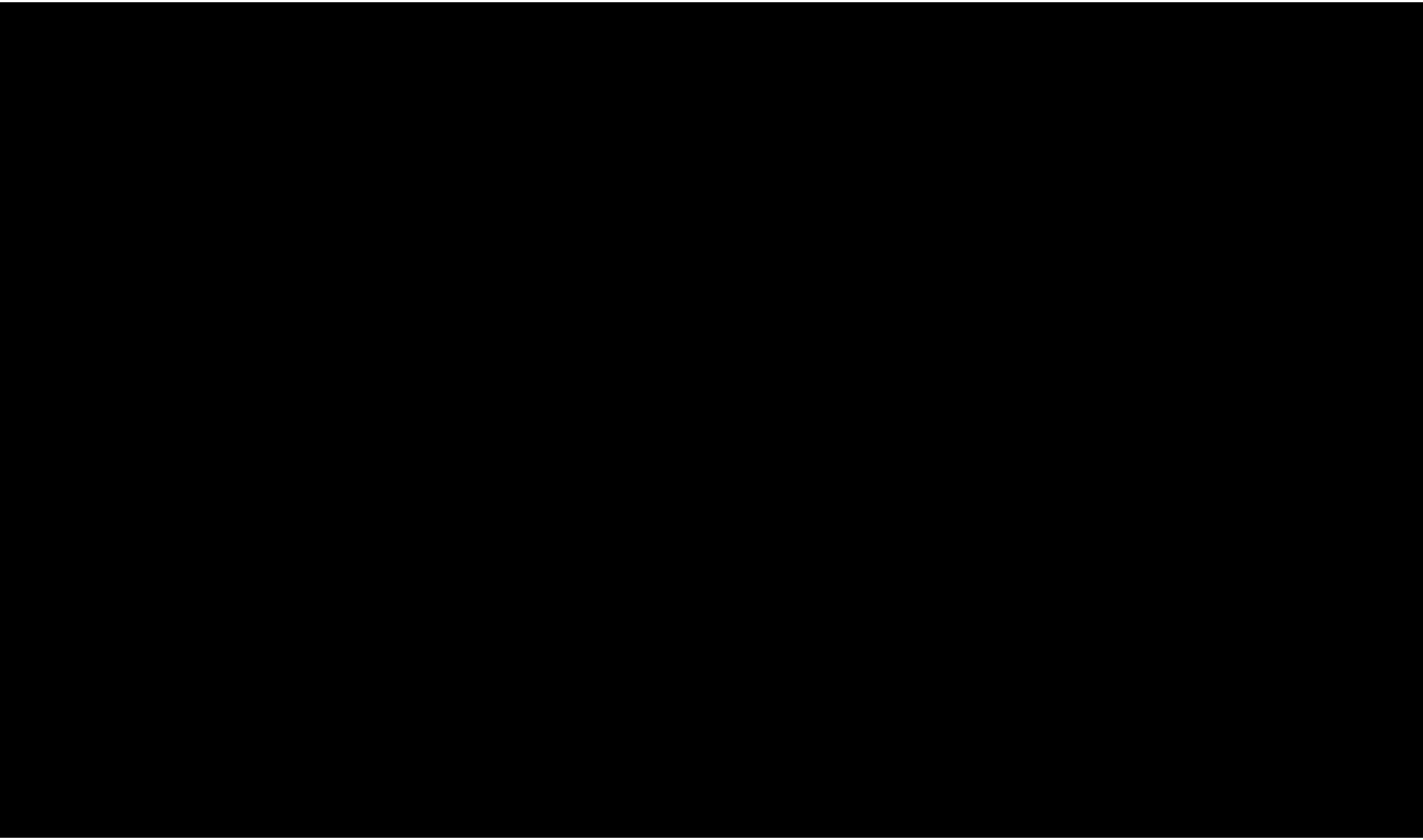

‘sub-Chandra double-detonation’

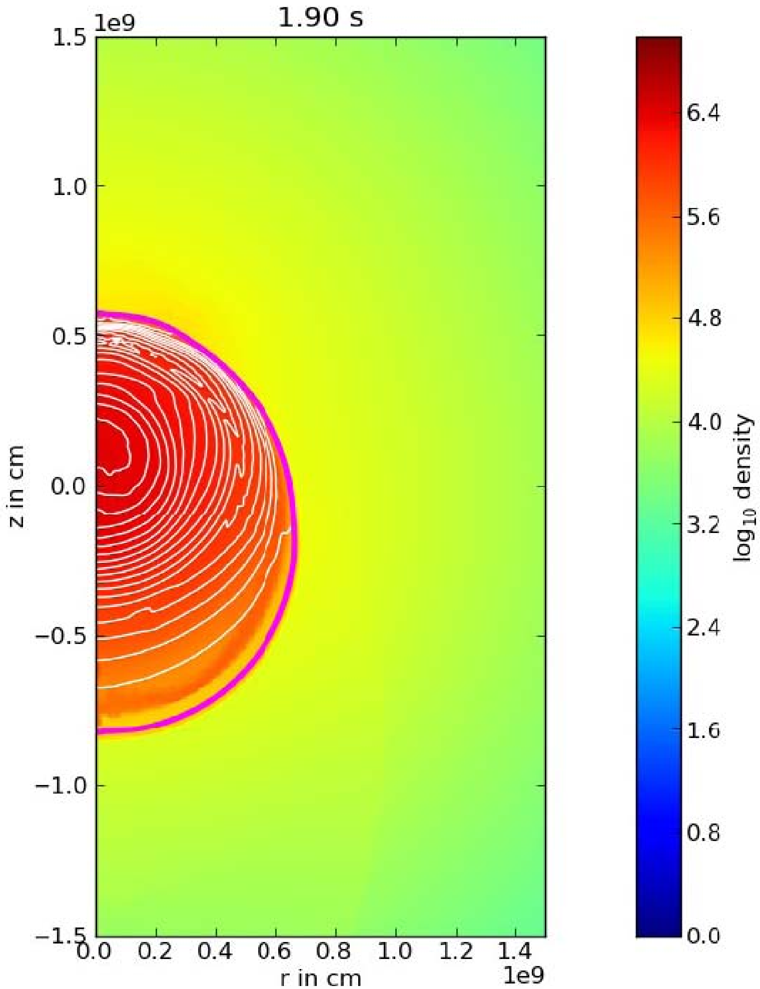

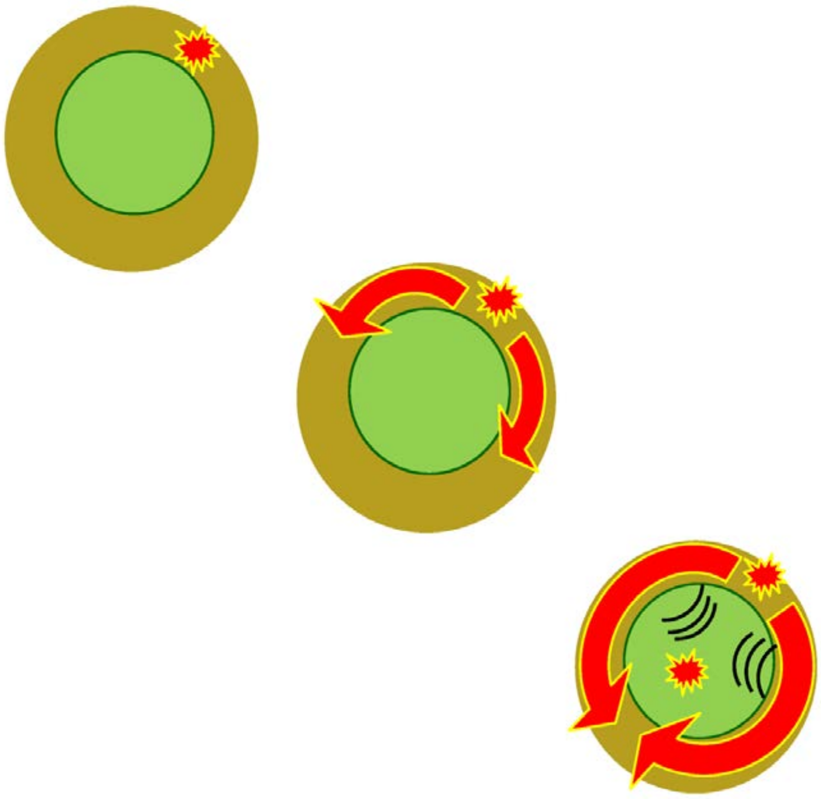

Fink et al. (2010)

Type Ia supernovae: merger

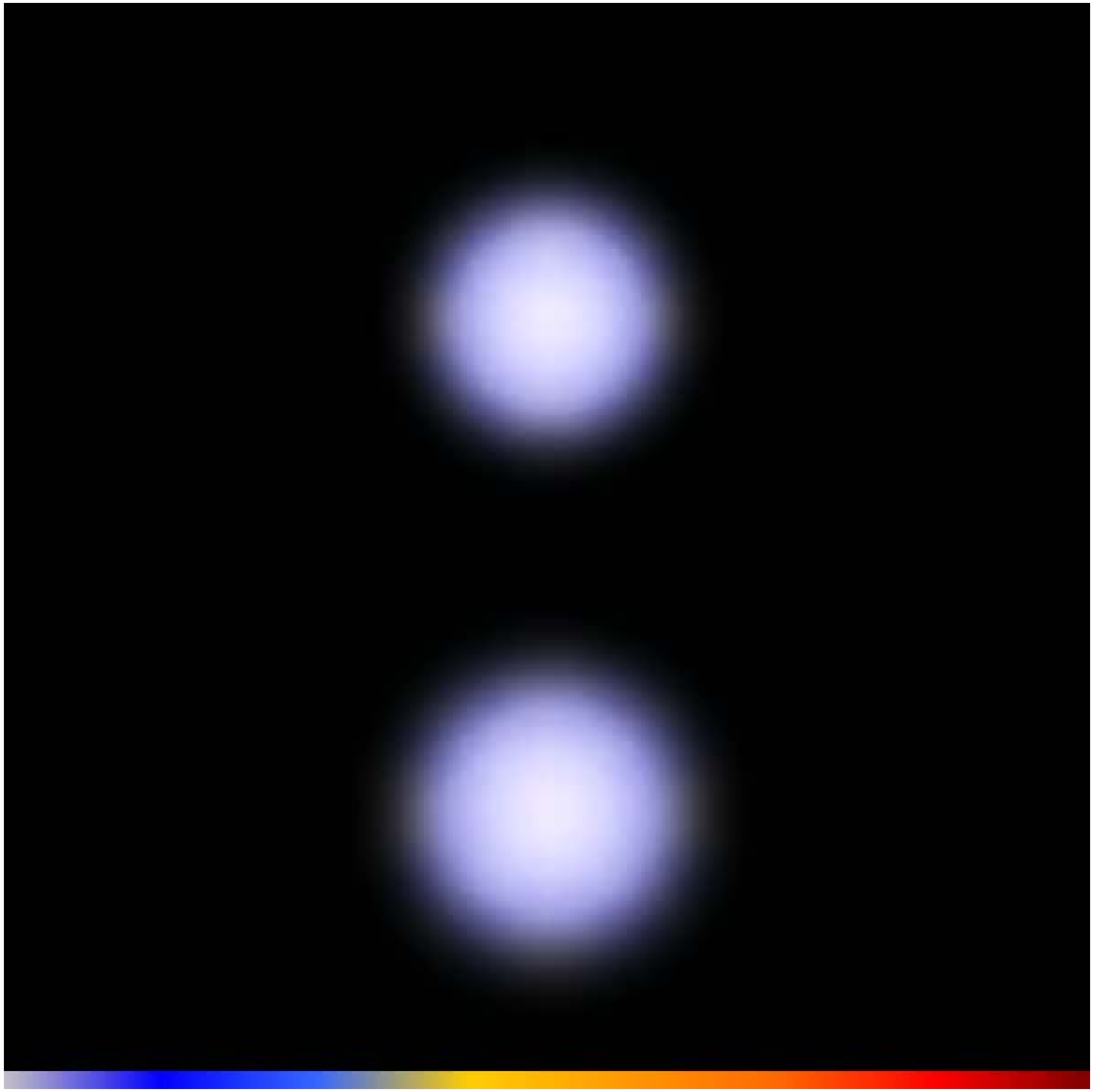

© R. Pakmor

Double-degenerate merger

(with a He layer on top of the secondary C+O WD)

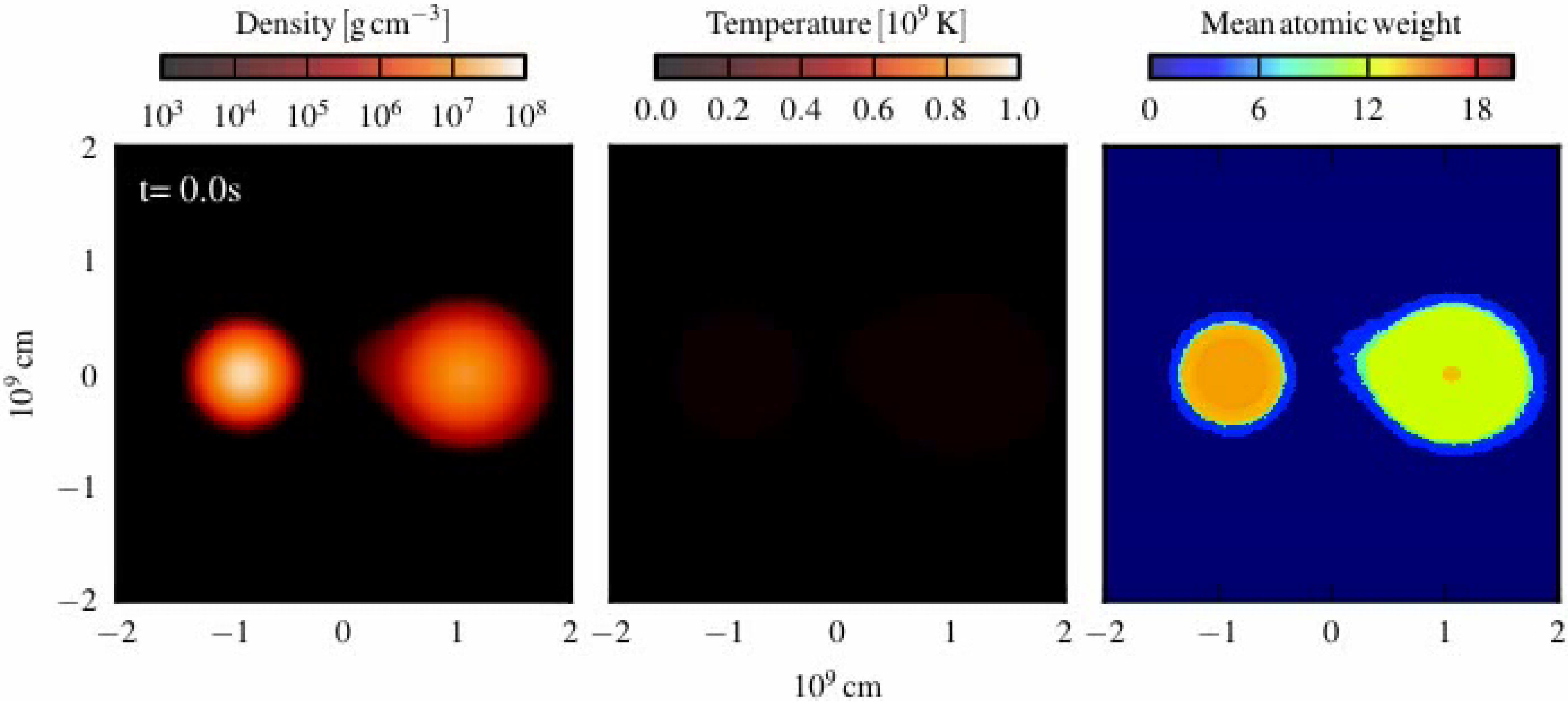

Pakmor et al. (2013)

Einstein's quadropole formula

$$h = \frac{\delta l}{l}$$

$$h = \frac{2G}{c^4}\frac{1}{r}\frac{\partial^2 Q}{\partial t^2}$$

$2G/c^4 \sim 10^{-44}$
(SI units)

Binary pulsar

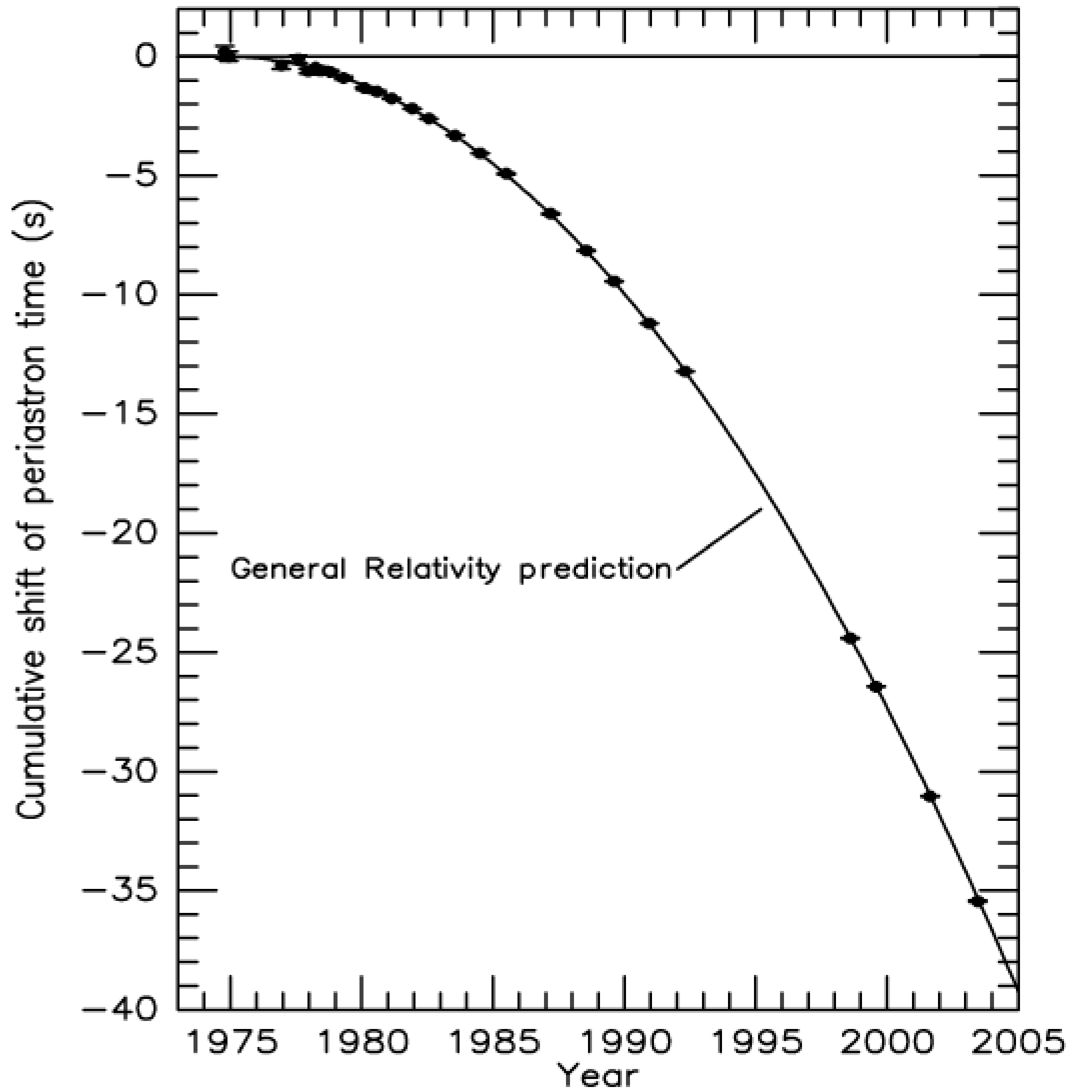

GW frequencies (BH mergers)

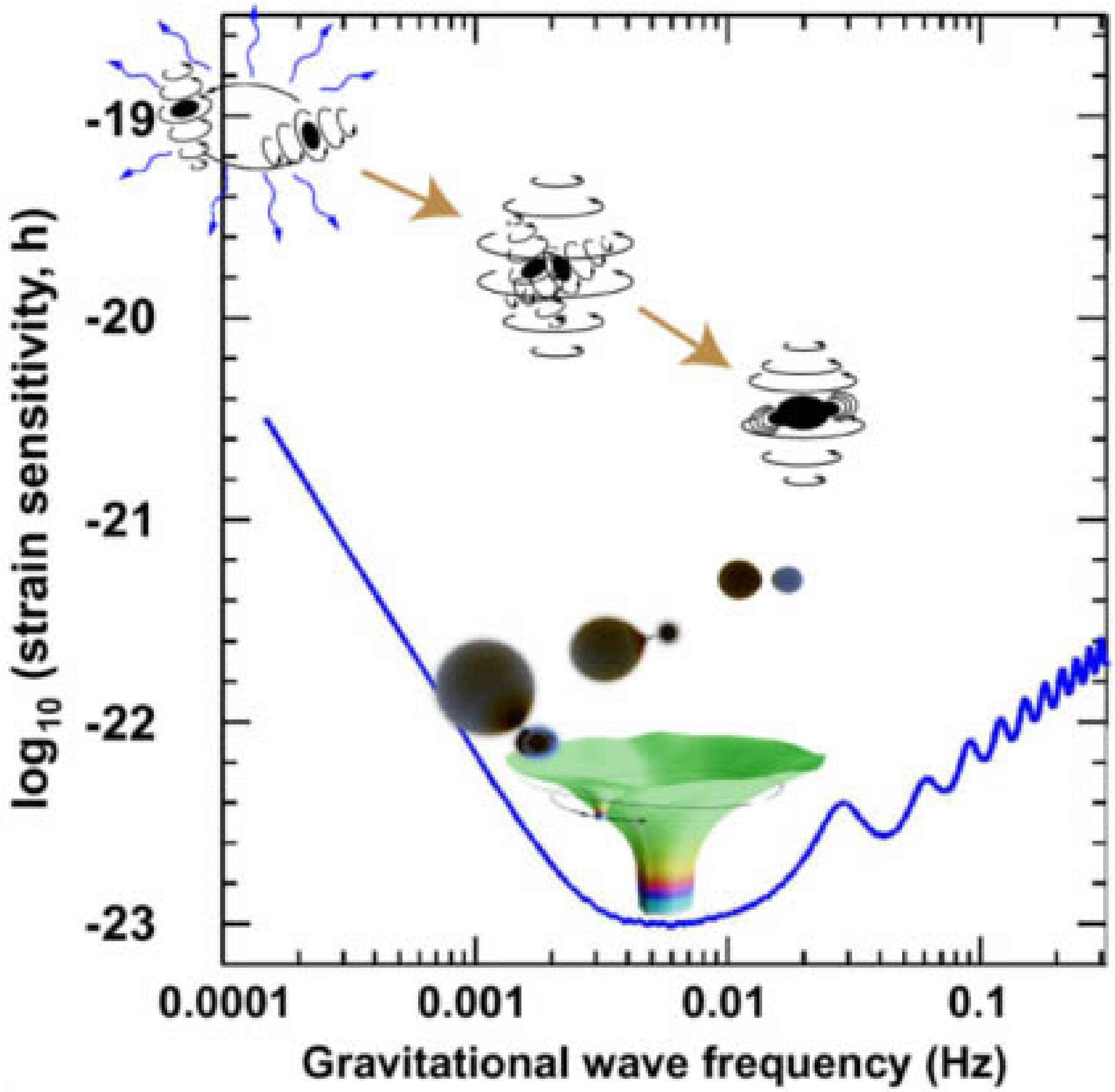

GW detectors (e.g. LIGO)

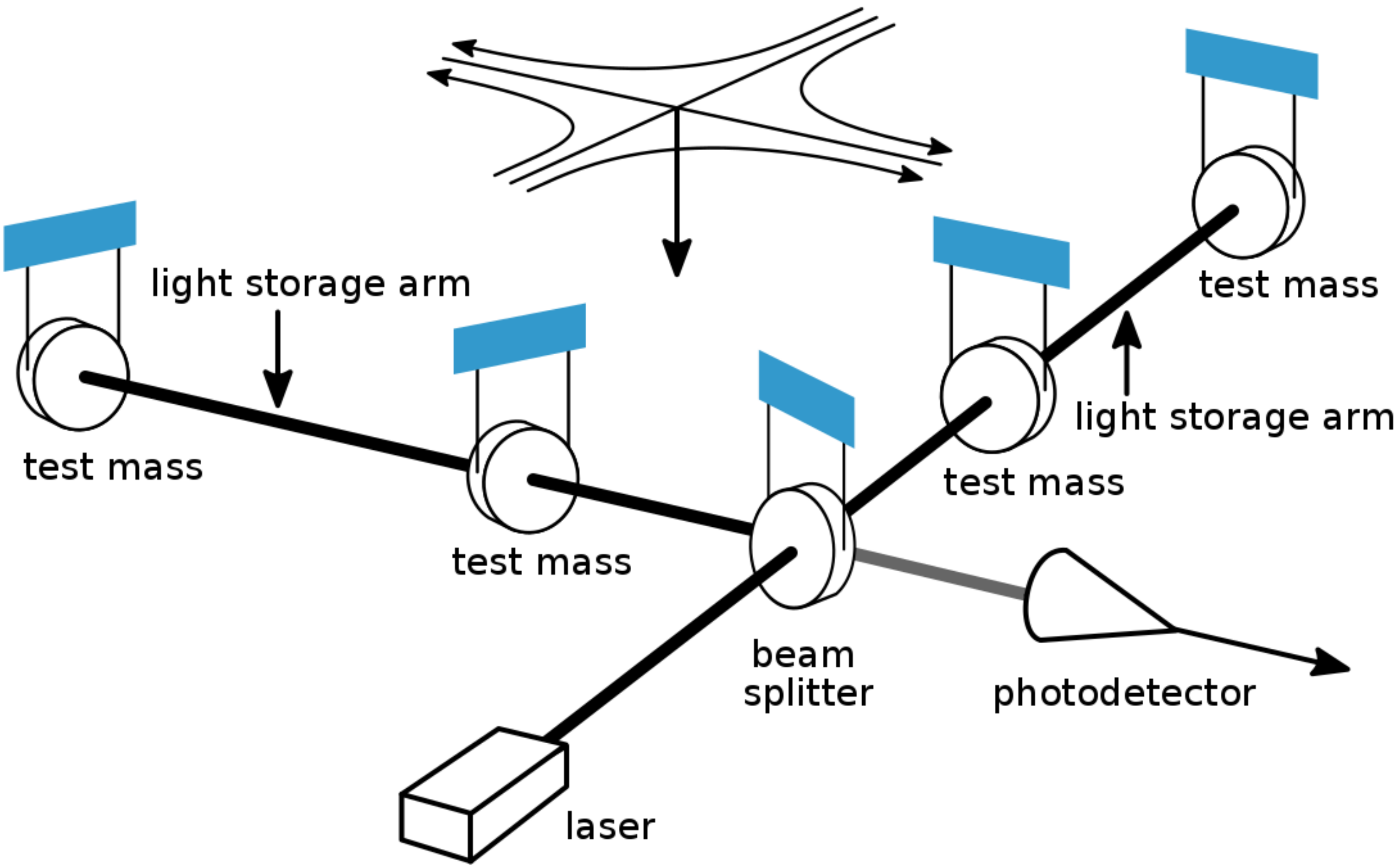

GW detectors (e.g. LIGO)

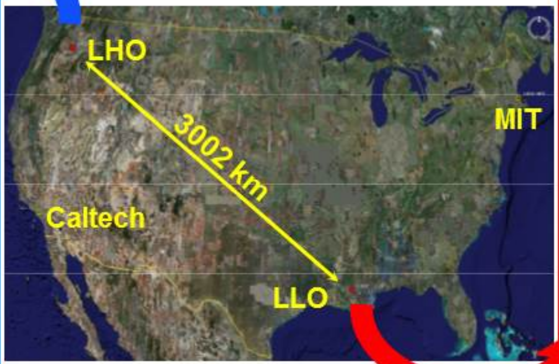

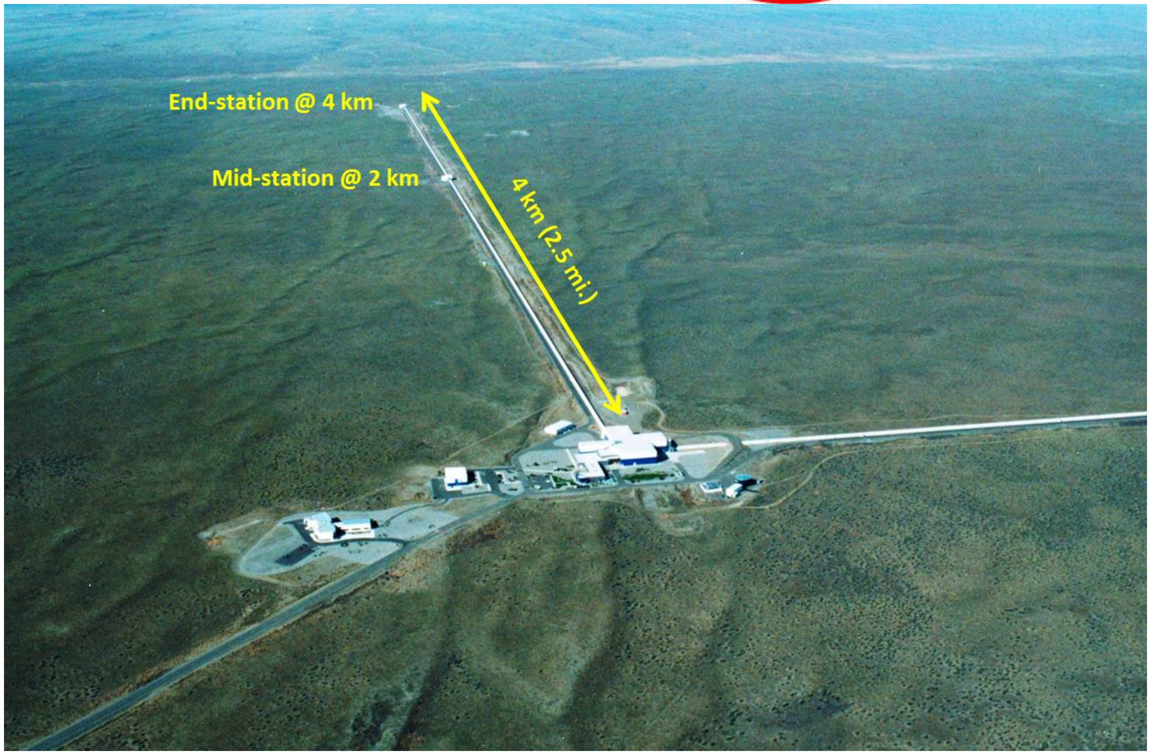

GW detectors: a bit of history

MPA, 1970

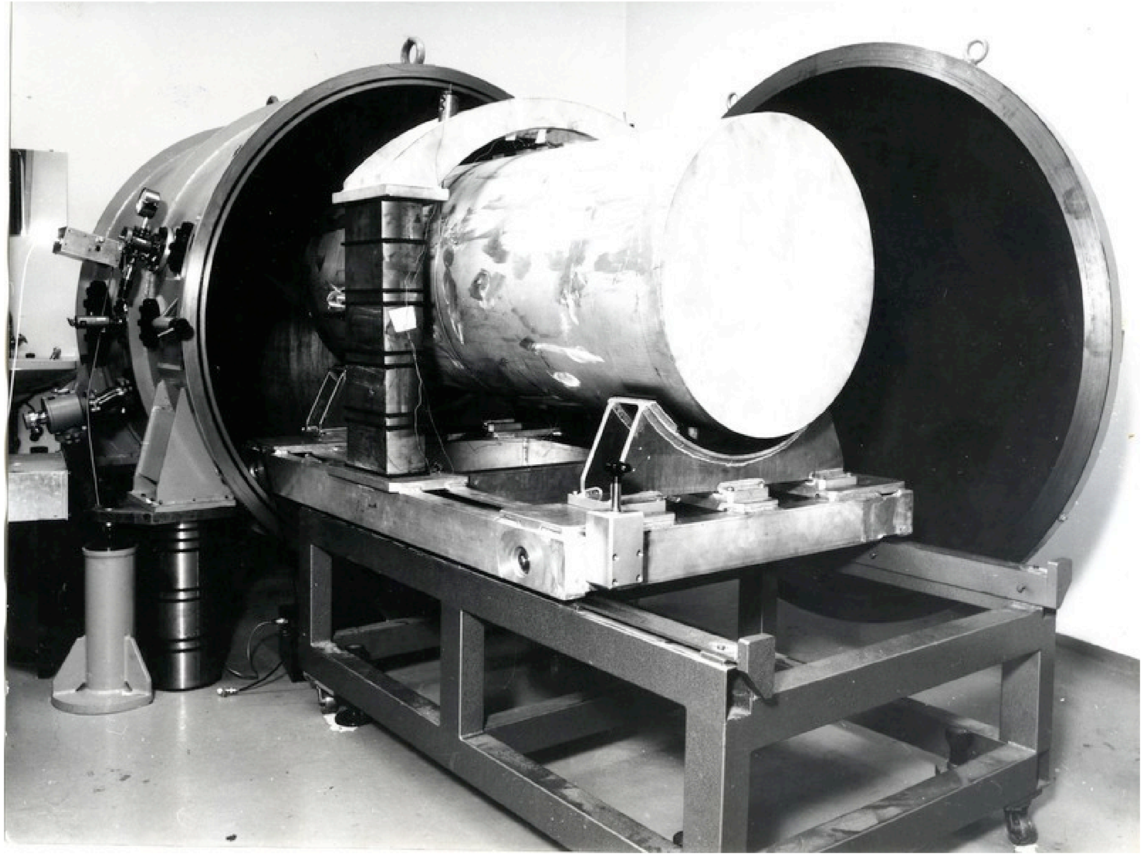

GW detectors: a bit of history

MPA, 1975

GW detectors: a bit of history

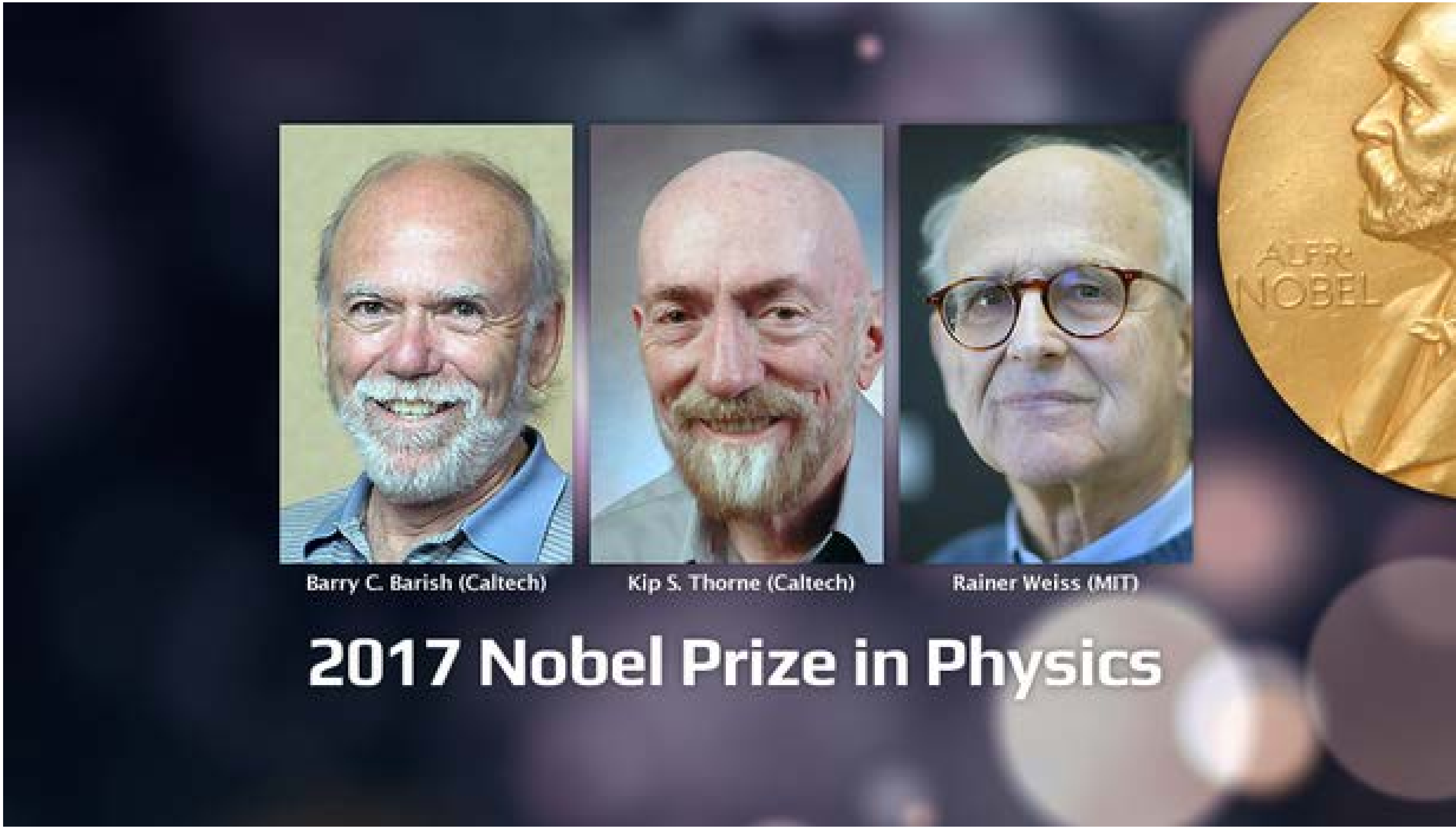

Merging Black Hole Binaries & GWs

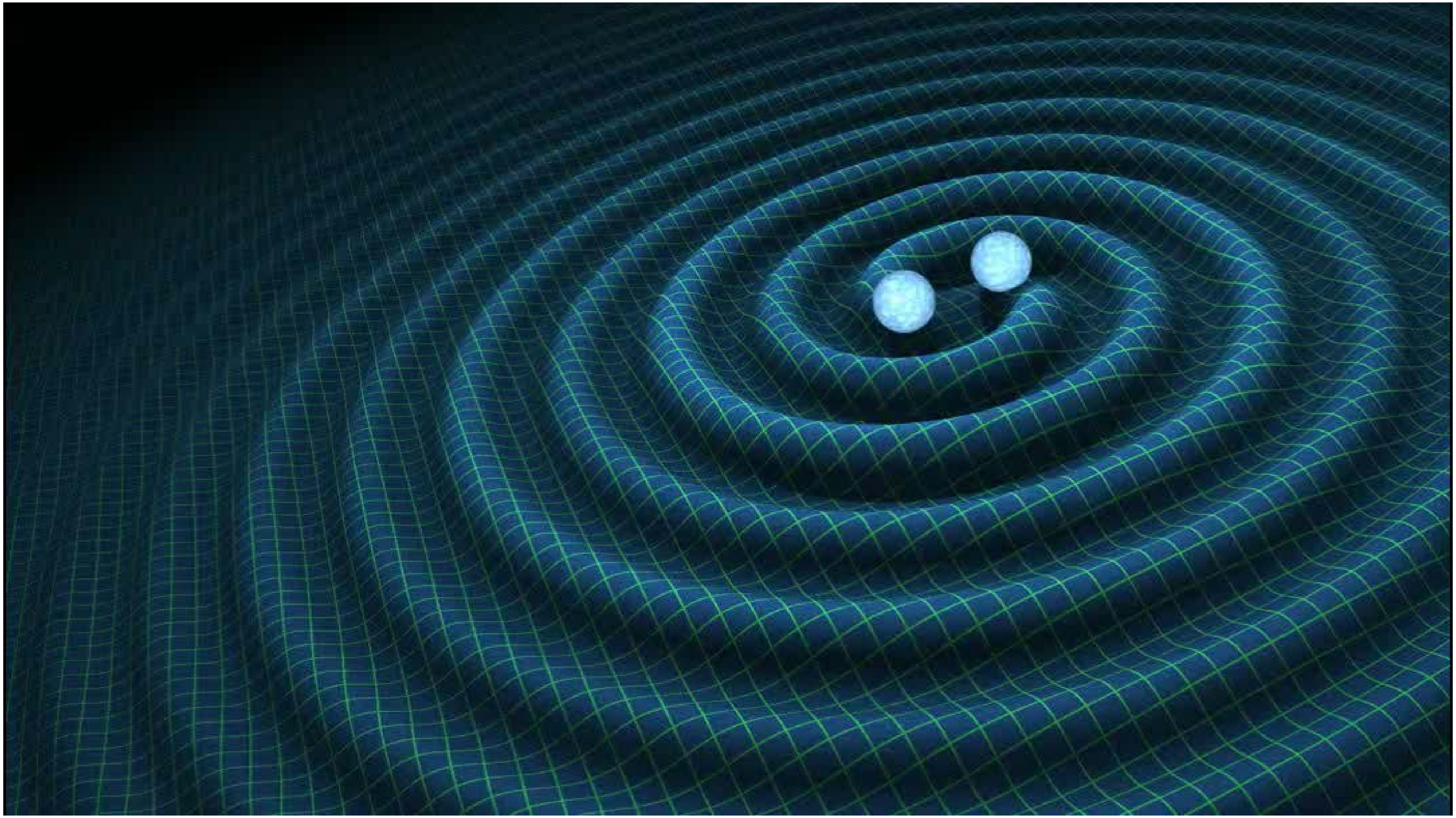

Merging Black Hole Binaries & GWs

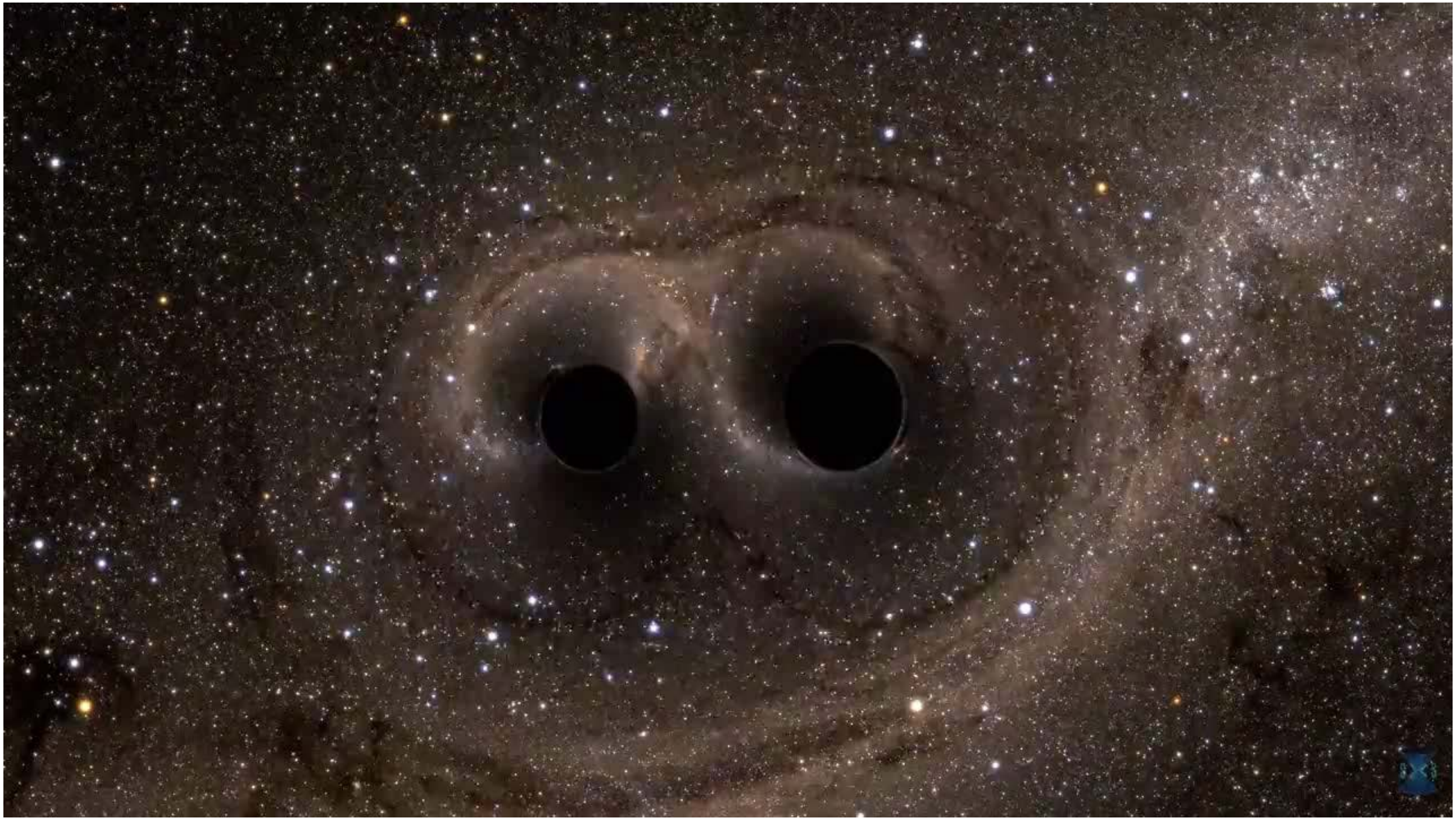

GW150914 © Caltech Ligo Lab

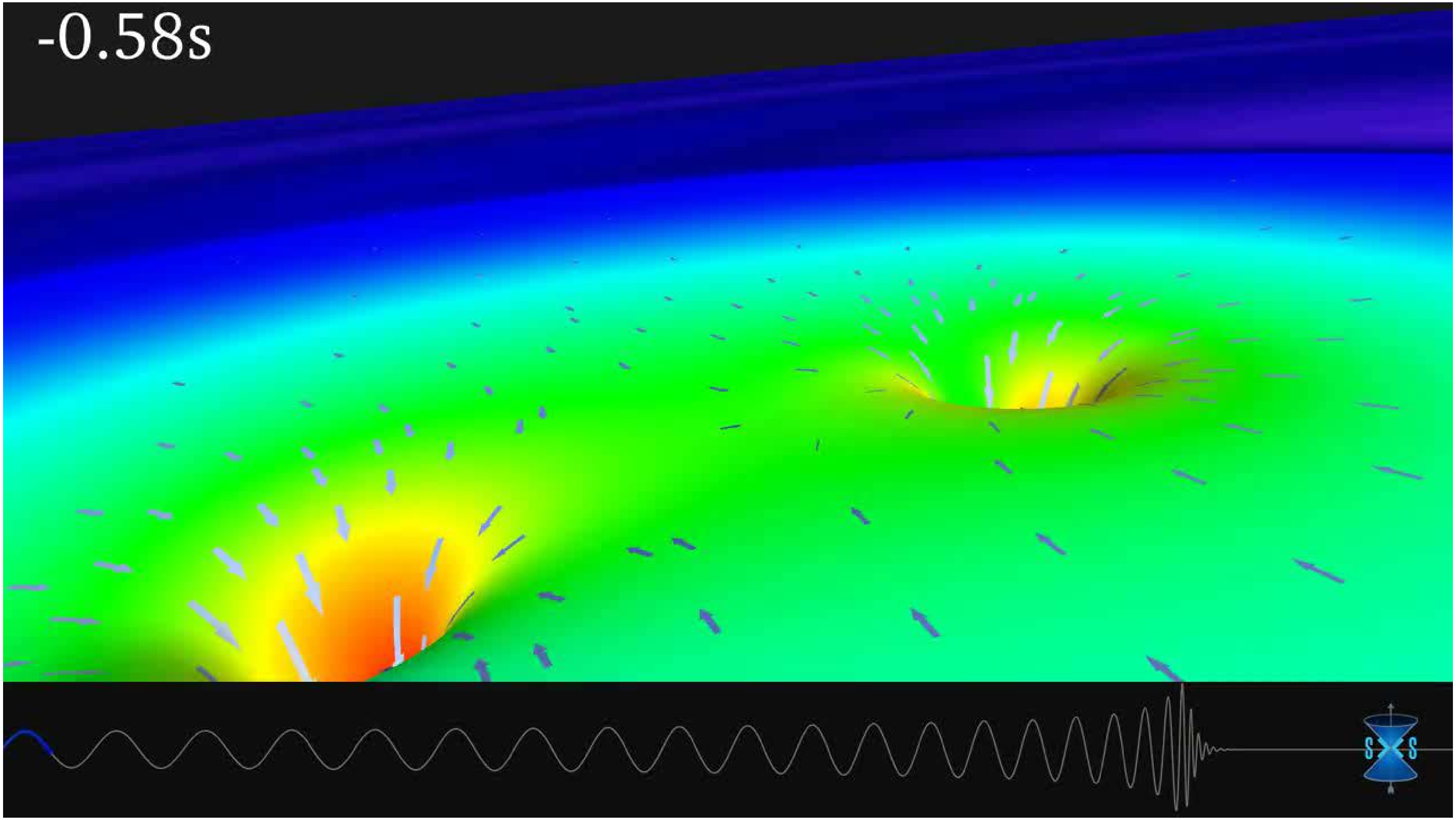

GW150914

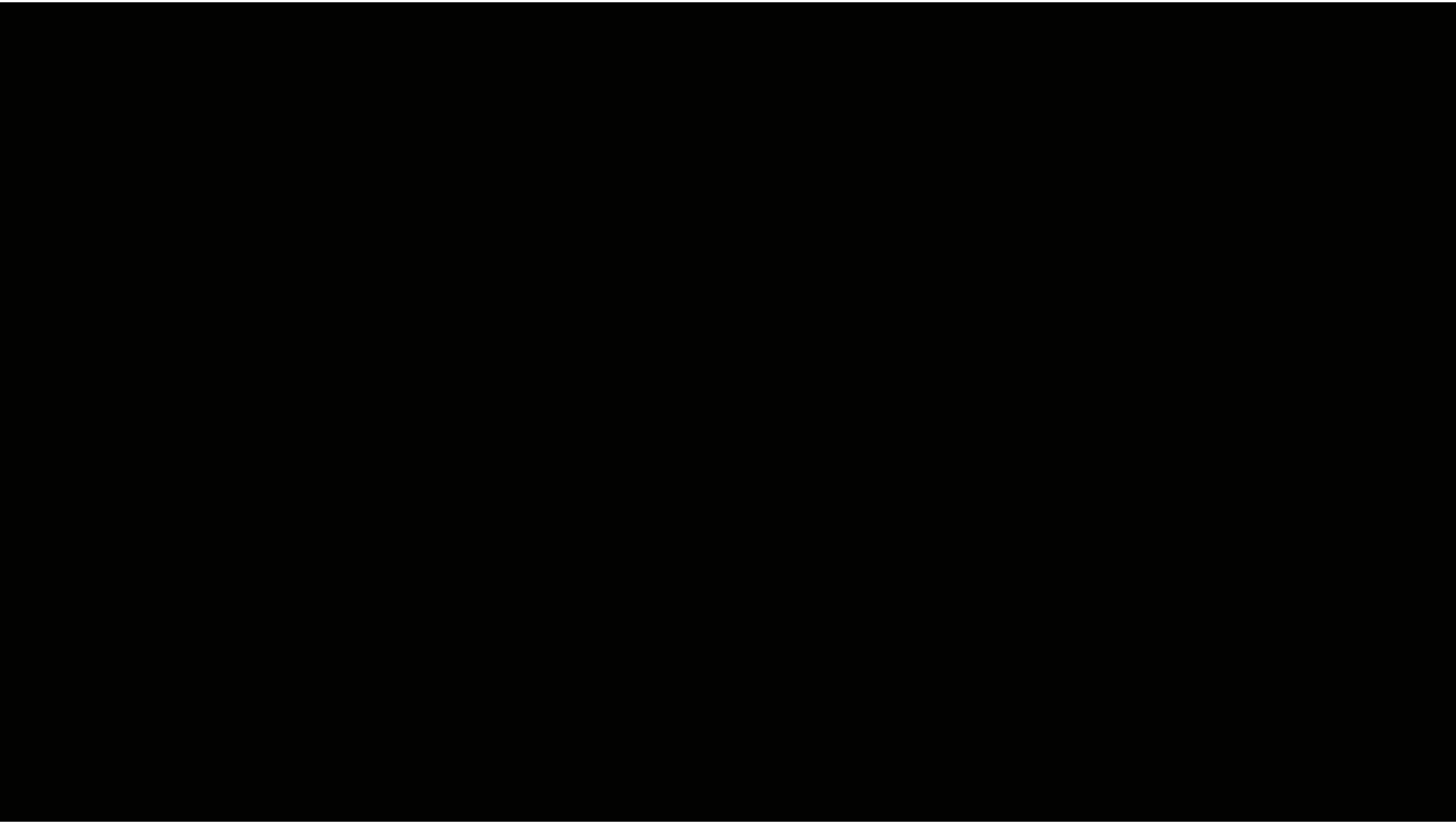

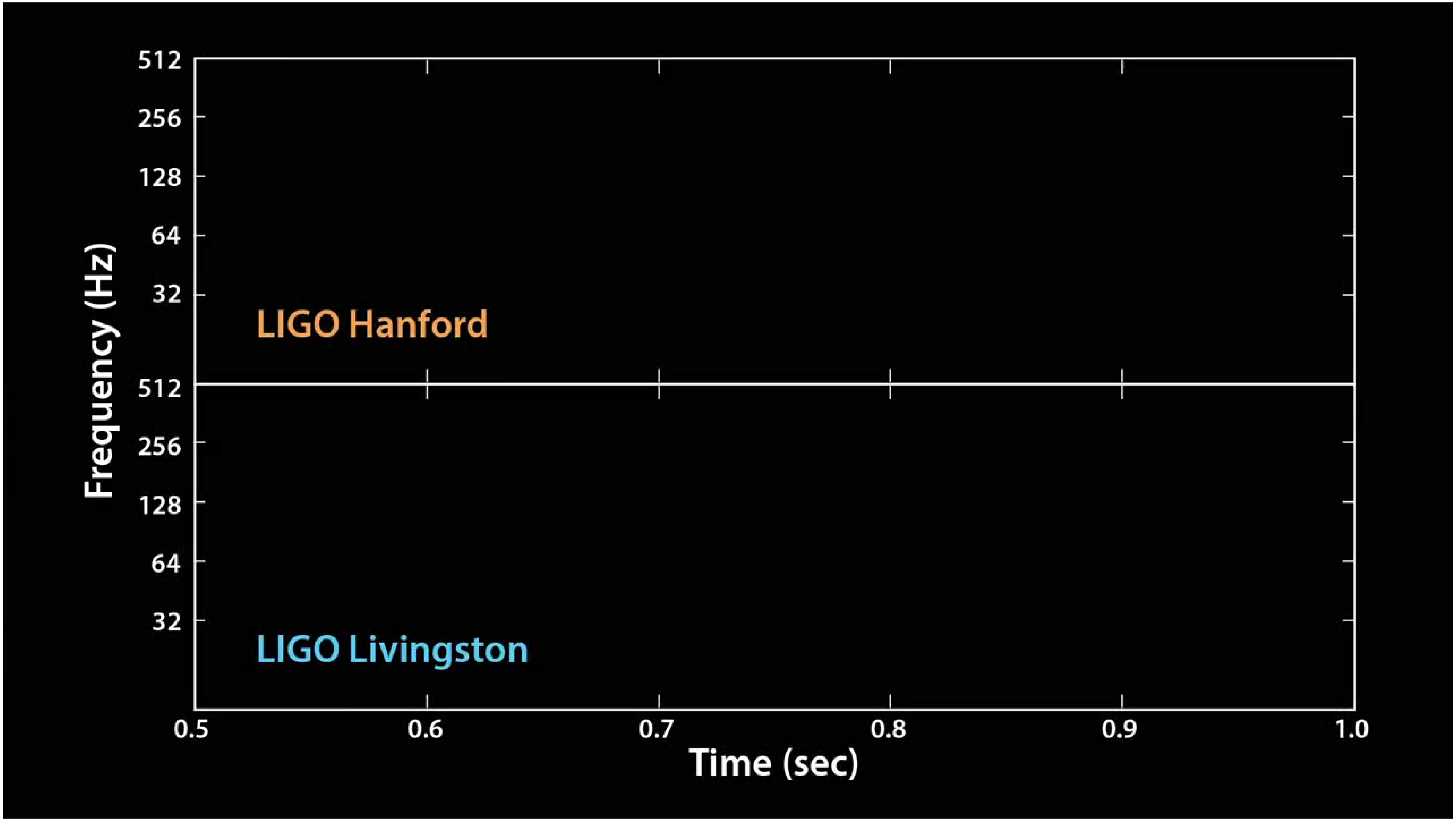
512
256
128
64
32
LIGO Hanford
512
256
128
64
32
LIGO Livingston
Frequency (Hz)
0.5
0.6
0.7
0.8
0.9
1.0
Time (sec)

Merging Black Hole Binaries & GWs

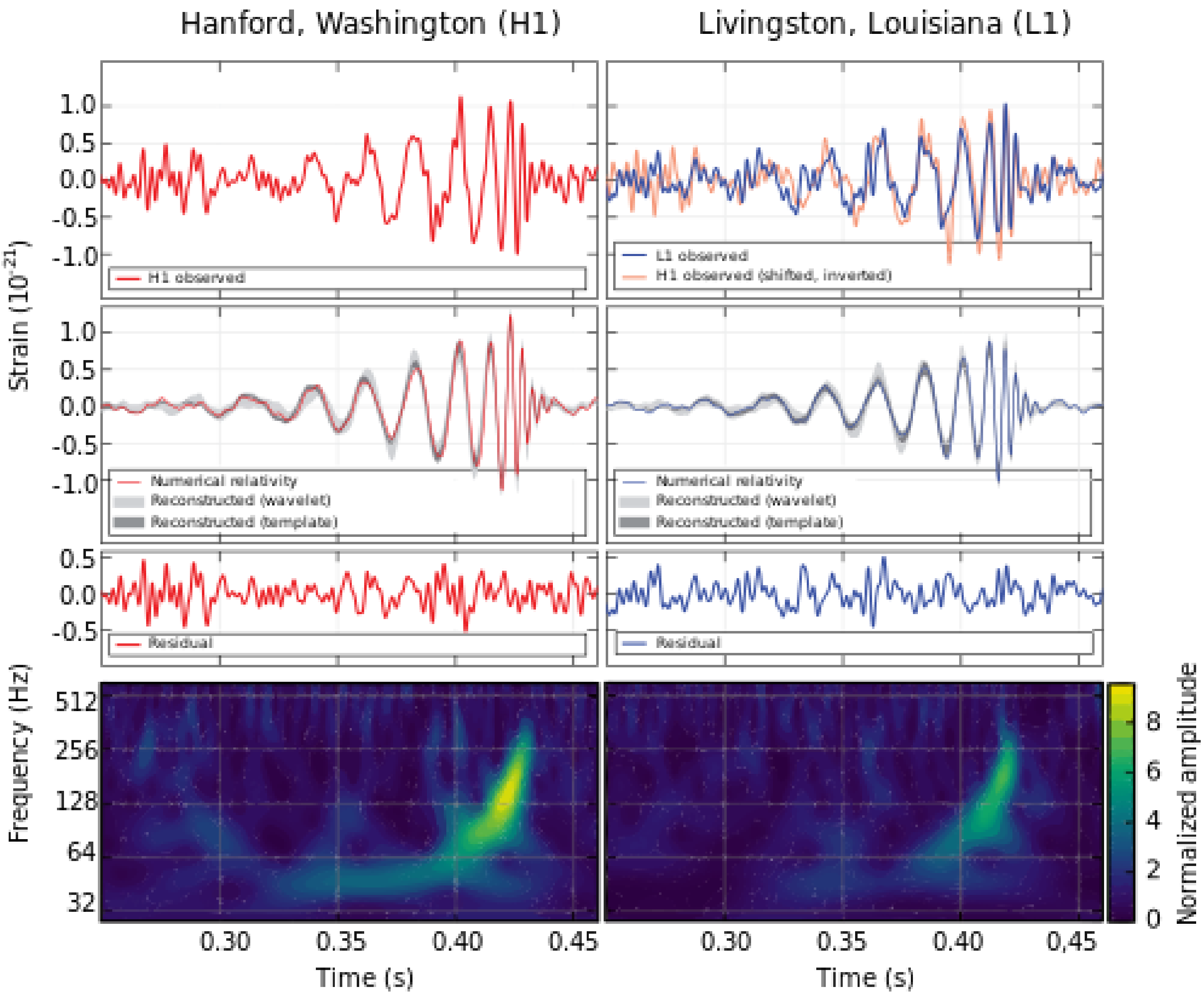

Masses of Black Hole Binaries

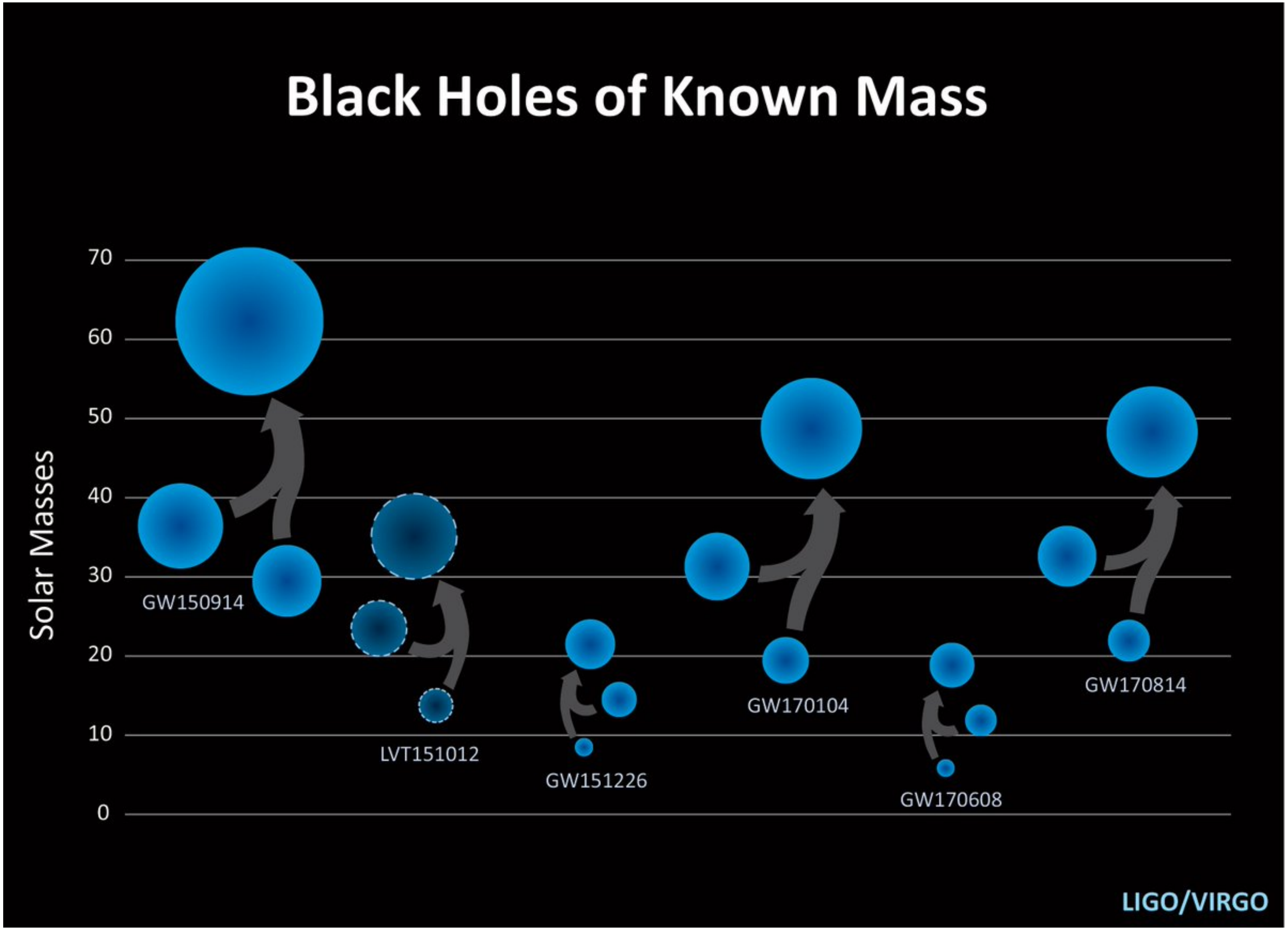

Possible formation channels:

I. Dynamical formation in dense clusters

- in dense clusters: dynamical interactions $\rightarrow$ close BH+BH binaries

II. Non-dynamical formation

- common-envelope scenarios: conversion of wide binary to close binary
- homogeneous evolution scenarios: close binary from the beginning

(References:
P. Podsiadlowski, http://www-astro.physics.ox.ac.uk/~podsi/grav_waves.pdf
S.Stevenson et al. (2017): *Nature communications **8**)*

Dynamical Formation

- in dense clusters, BHs segregate quickly and can form sub-clusters of BHs (Spitzer instability)
- three-body encounters $\rightarrow$ BH+BH binaries
- most are ejected, but some harden sufficiently to ultimately merge
- aLIGO detection rates (e.g. Banerjee 2016): $10 - 300\,\mathrm{yr}^{-1}$

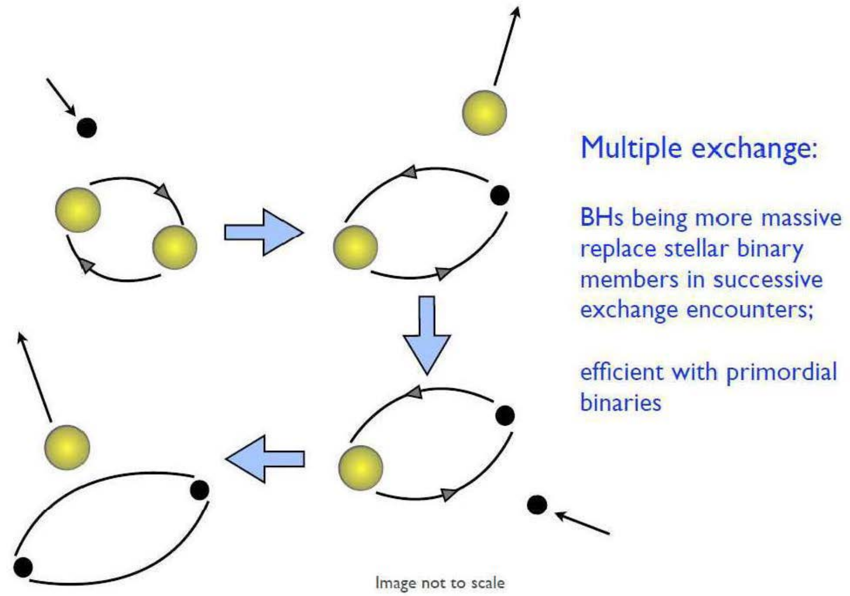

(Credit: Banerjee 2016)

Dynamical Formation

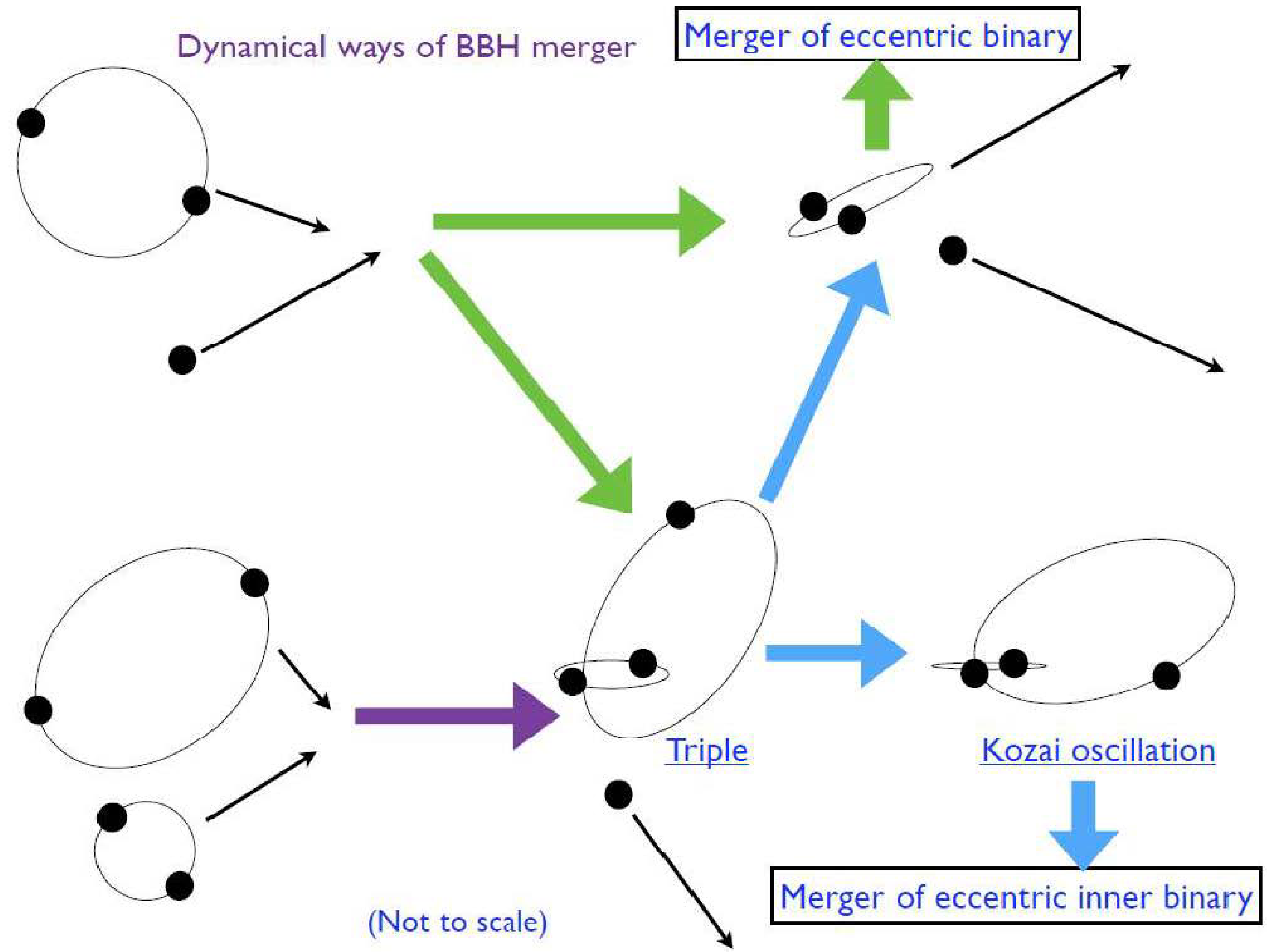

(Credit: Banerjee 2016)

Non-Dynamical Formation

- the progenitors of black holes are big stars
- need to get them into a close orbit to merge
- possible solution: common-envelope evolution
- standard scenario to produce compact NS+NS binaries (Hulse-Taylor pulsar, PSR J0737-3039)
- problem with black holes:
  - ▷ difficult to form two black holes (requires late mass transfer)
  - ▷ but possible with some fine-tuning
  - ▷ rates highly uncertain (Belczynski et al. [2016] vs. Kruckow, et al. [2016])

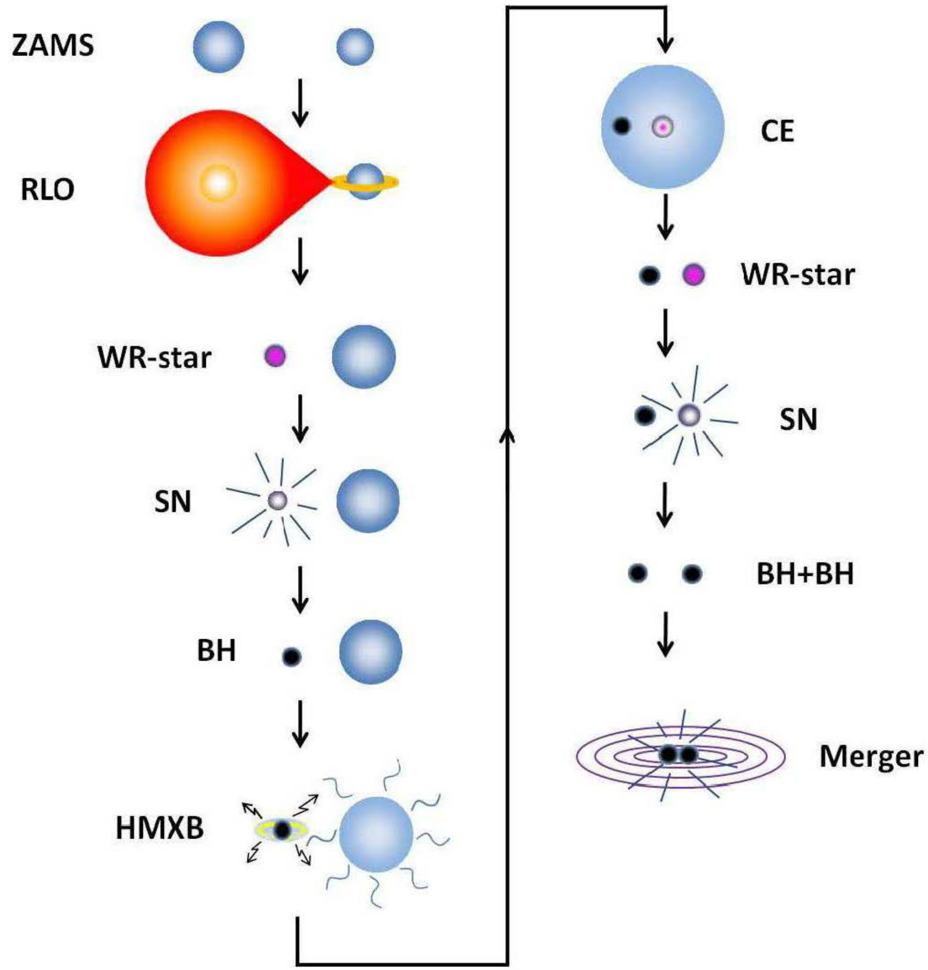

Non-Dynamical Formation

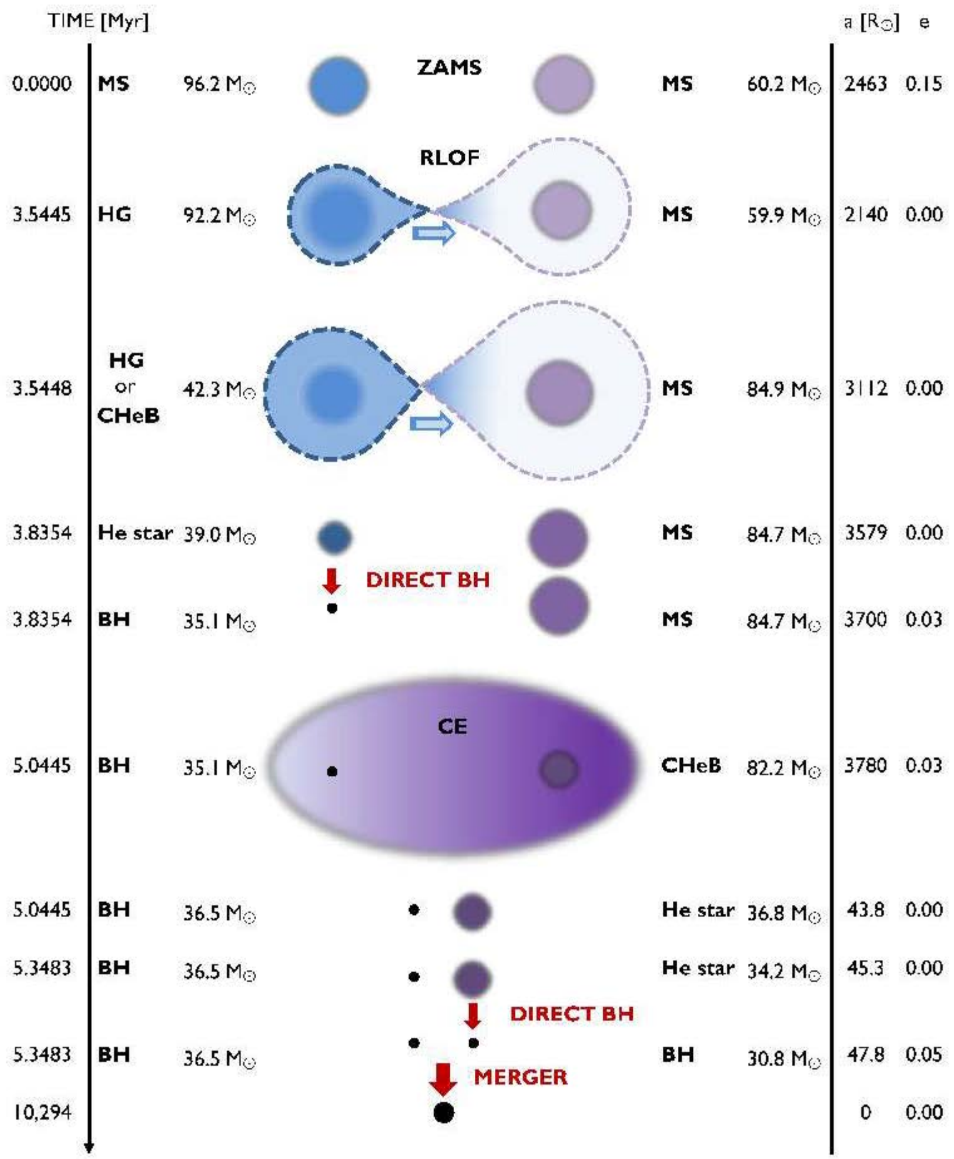

Non-Dynamical Formation

The Massive Overcontact Binary (MOB) Model

(Marchant et al. 2016; also de Mink & Mandel 2016a,b)

- initial homogeneous evolution is enforced by tidal locking in a very close massive binary (de Mink et al. 2009)
- needs to avoid binary widening by stellar wind mass loss

→ requires low metallicity

- most systems pass through contact phase on main sequence

→ evolution drives systems towards mass ratio of 1

Model Description

- uses latest MESA code (Paxton et al. 2015)
- with binary evolution fully implemented (Marchant)
- mass loss:
  - ▷ Vink (2001) ×1/3 (H-rich), Hamann (1995) (no H)
  - ▷ $\dot{M} \propto Z^{0.85}$

Non-Dynamical Formation

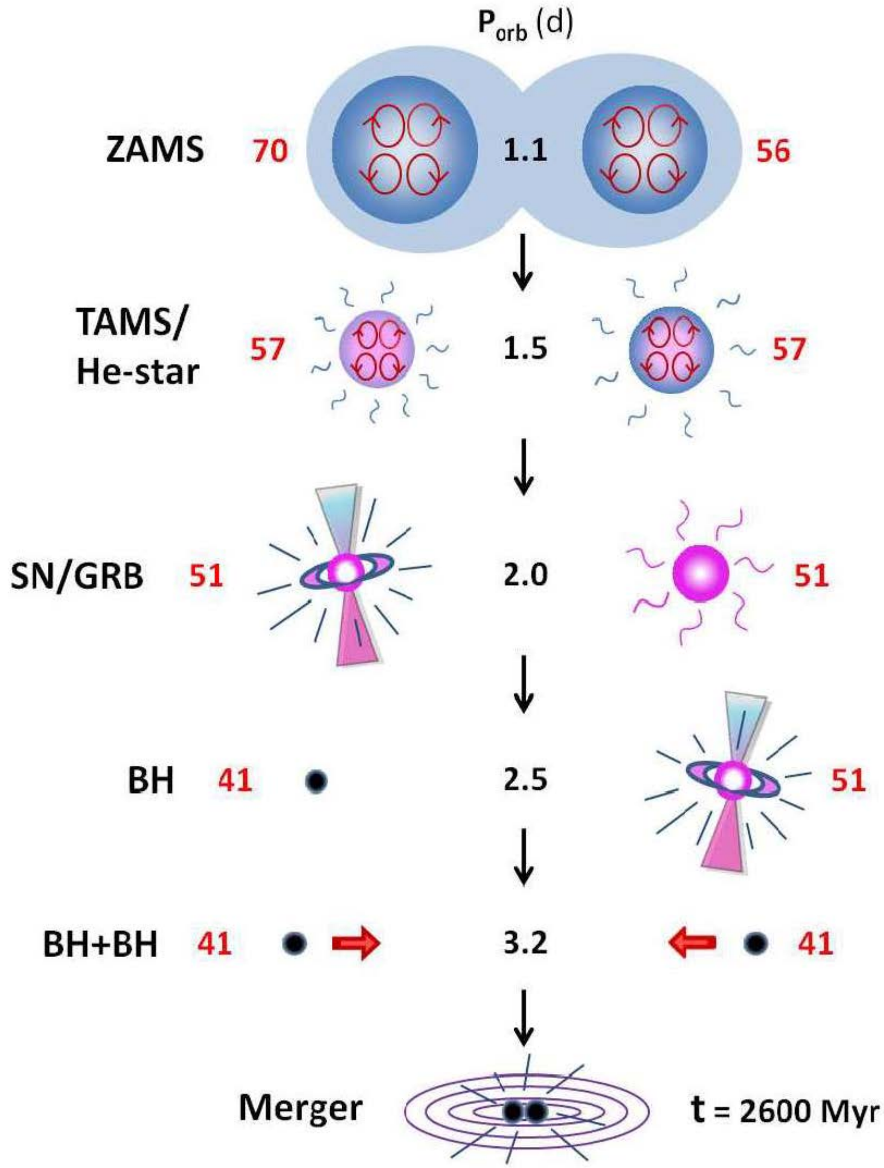

Non-Dynamical Formation

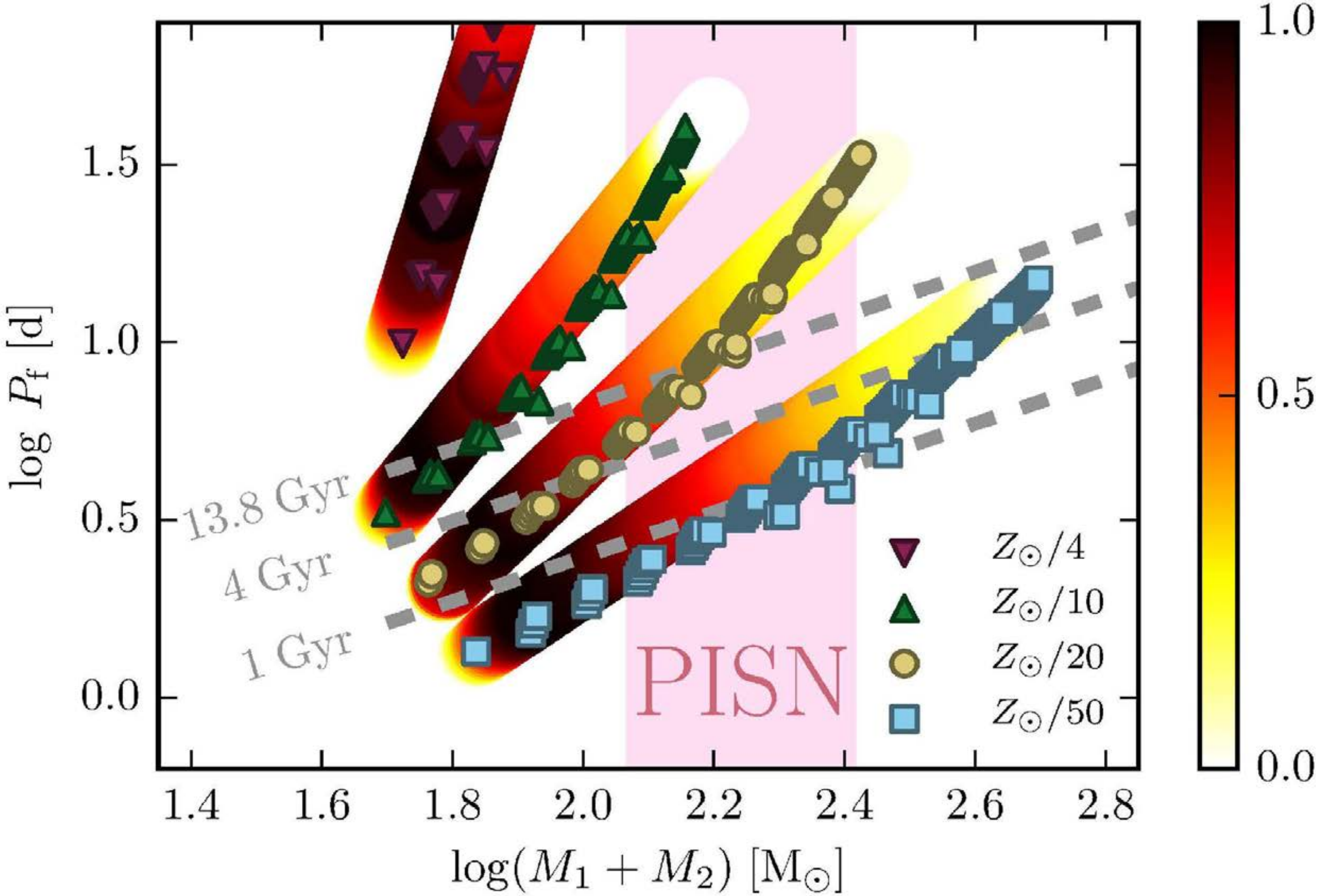

Non-Dynamical Formation

But: *Very massive stars are active ('LBVs'), show eruptions, …. (example: Eta Carinae)*

Very idealized models!

The Cosmic Distance Scale H_0

- H_0 measures the present expansion rate of the Universe
- It enters as a scale factor into most other cosmological parameters
- Different methods to measure it claim uncertainties below 3%
- However, on this level they are inconsistent
- What is the reason?
  Systematic errors? 'New physics?

The Cosmic Distance Scale H_0

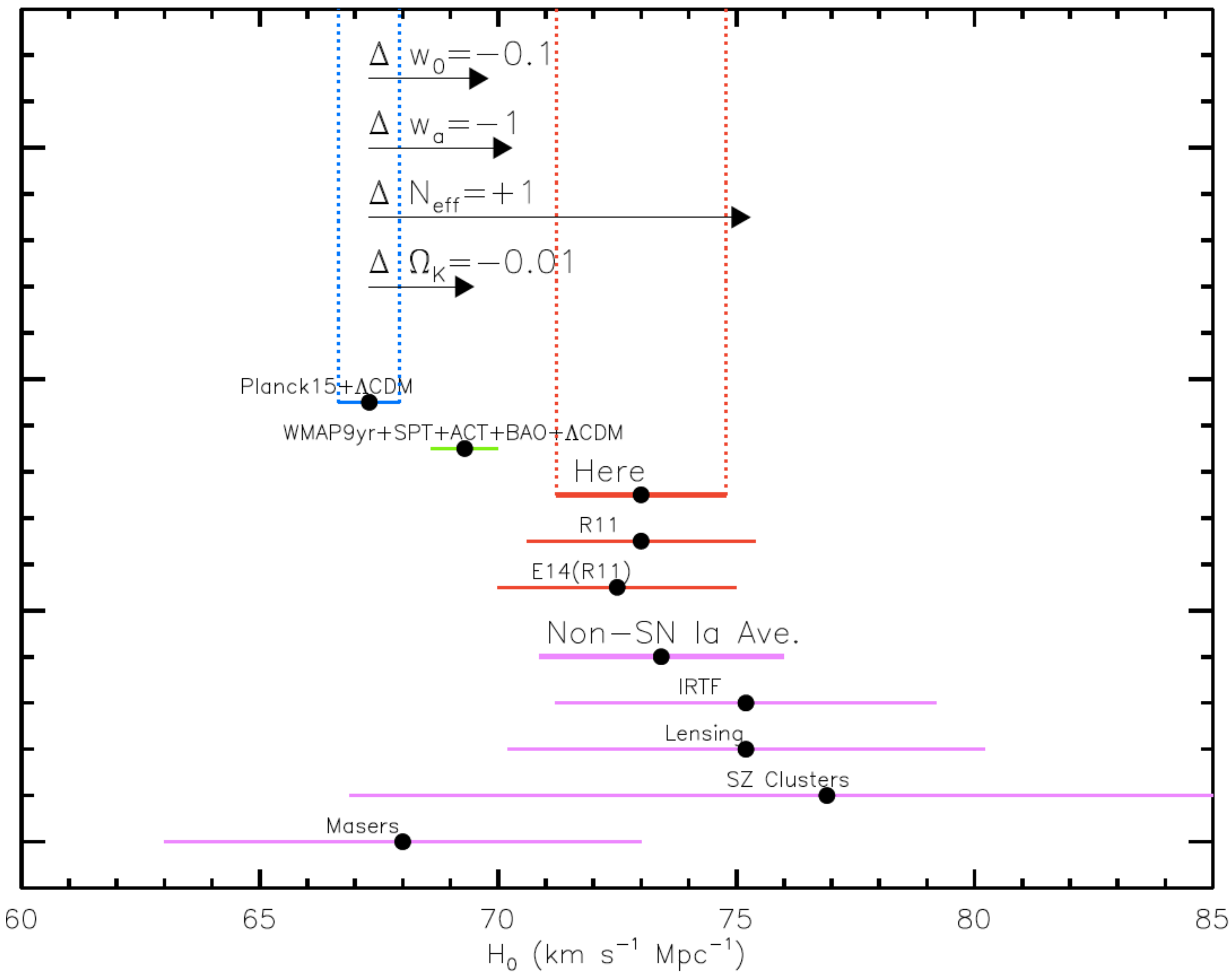

Riess et al., ApJ (2016)

Direct Measurements: Measuring the physical distance to an object directly

Standard Rulers: Size = Distance x q(angle on sky)
Need to know the real size of the object

Standard Candles: $L_{apparent} = L_{absolute} / D^2$
Need to know the true luminosity of an object

The “distance ladder”

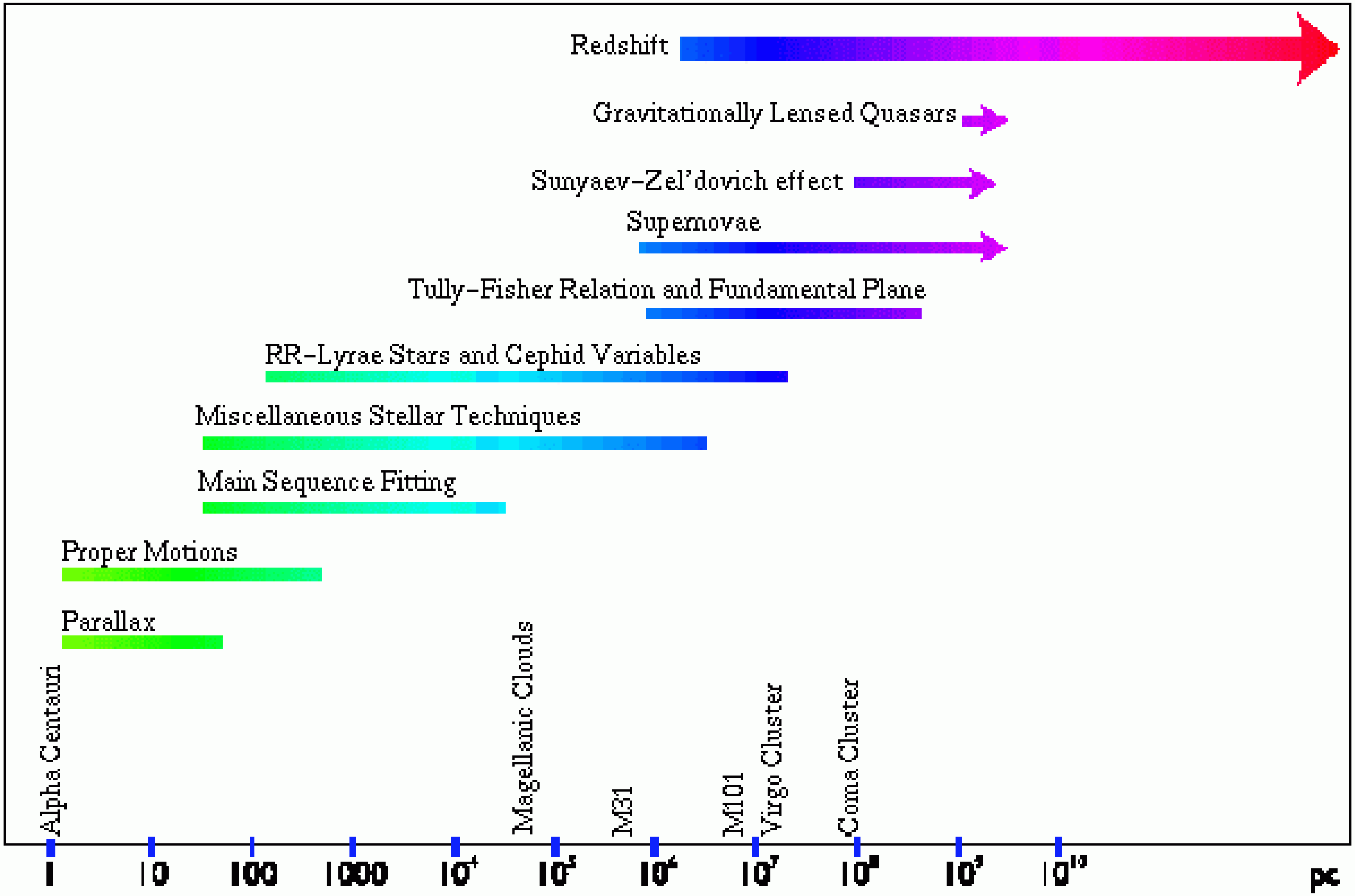

Figure 3.2: *The different distance estimators. This seemingly simple plot shows a grand overview of our efforts to measure distances in the Universe. Adapted from [Rowan-Robinson, 1985] and [Roth and Primack, 1996].*

Parallaxes

- Measure the position of an object with respect to its background
- Nearby objects show a larger “motion” than objects far away do
- The parallax angle θ, the distance of the object D and the diameter of the Earth’s orbit d are connected by simple geometrical relations. For small angles, it is

$$d = D \times \theta \quad \text{[units !!!! } \theta \text{ measured in rad !]}$$

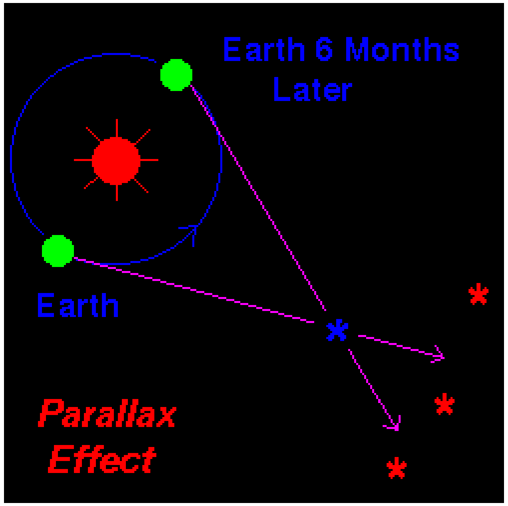

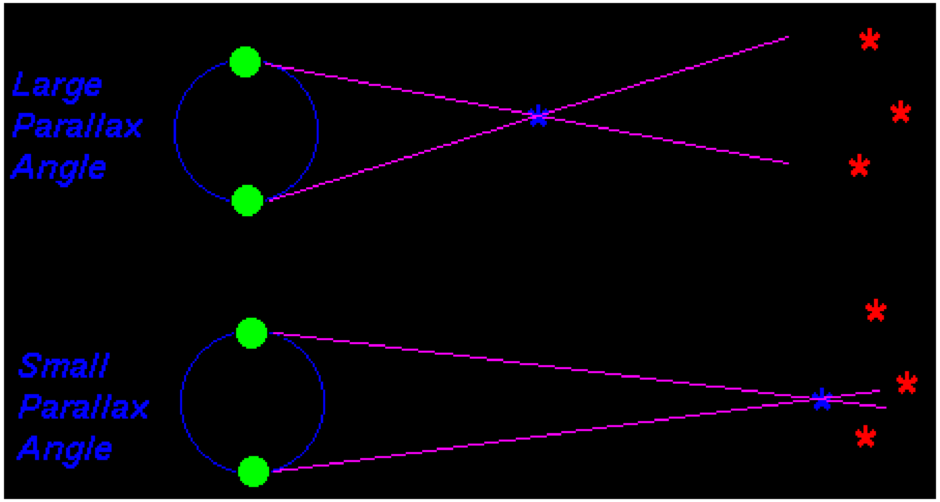

Parallaxes

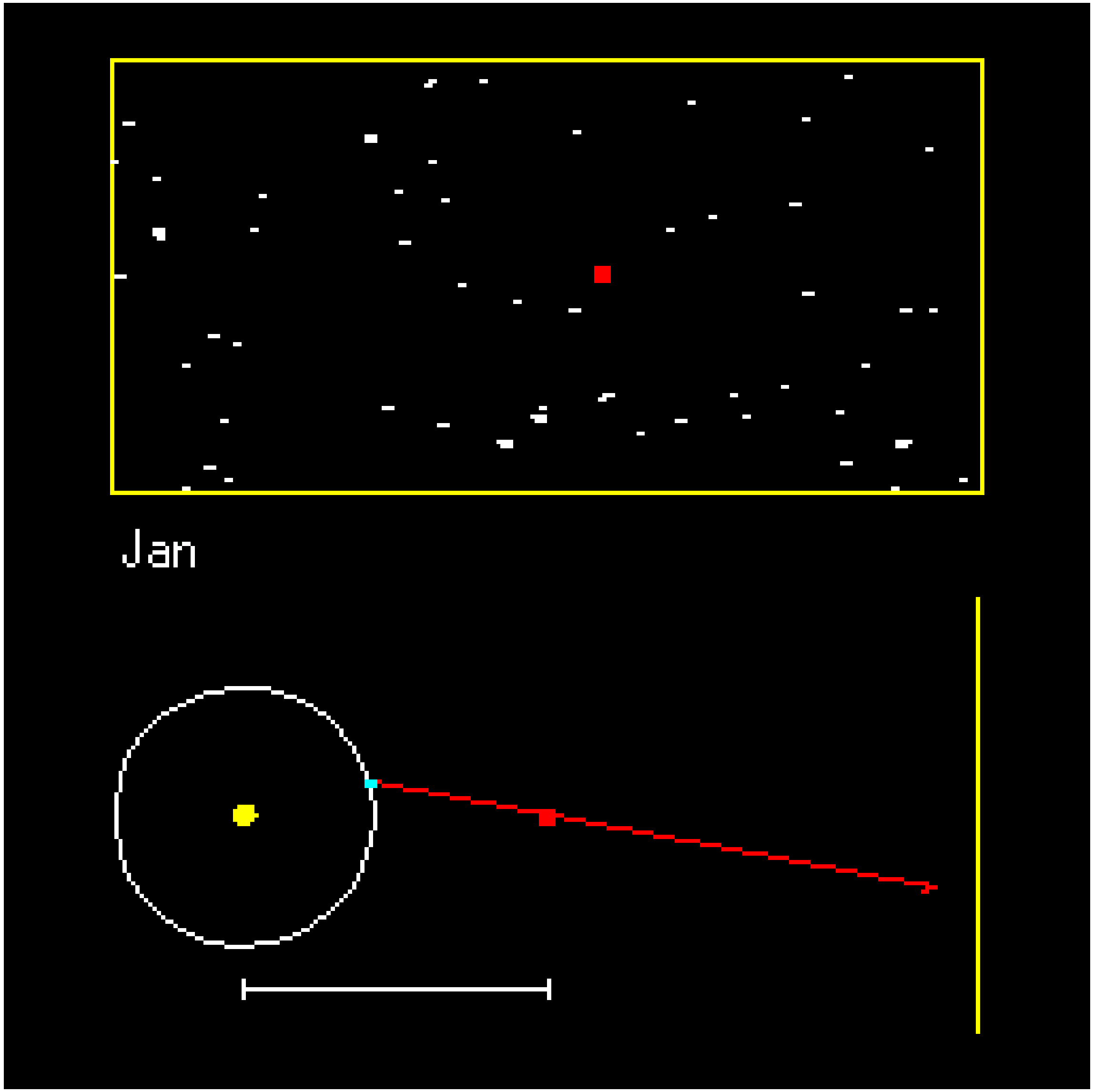

Parallaxes

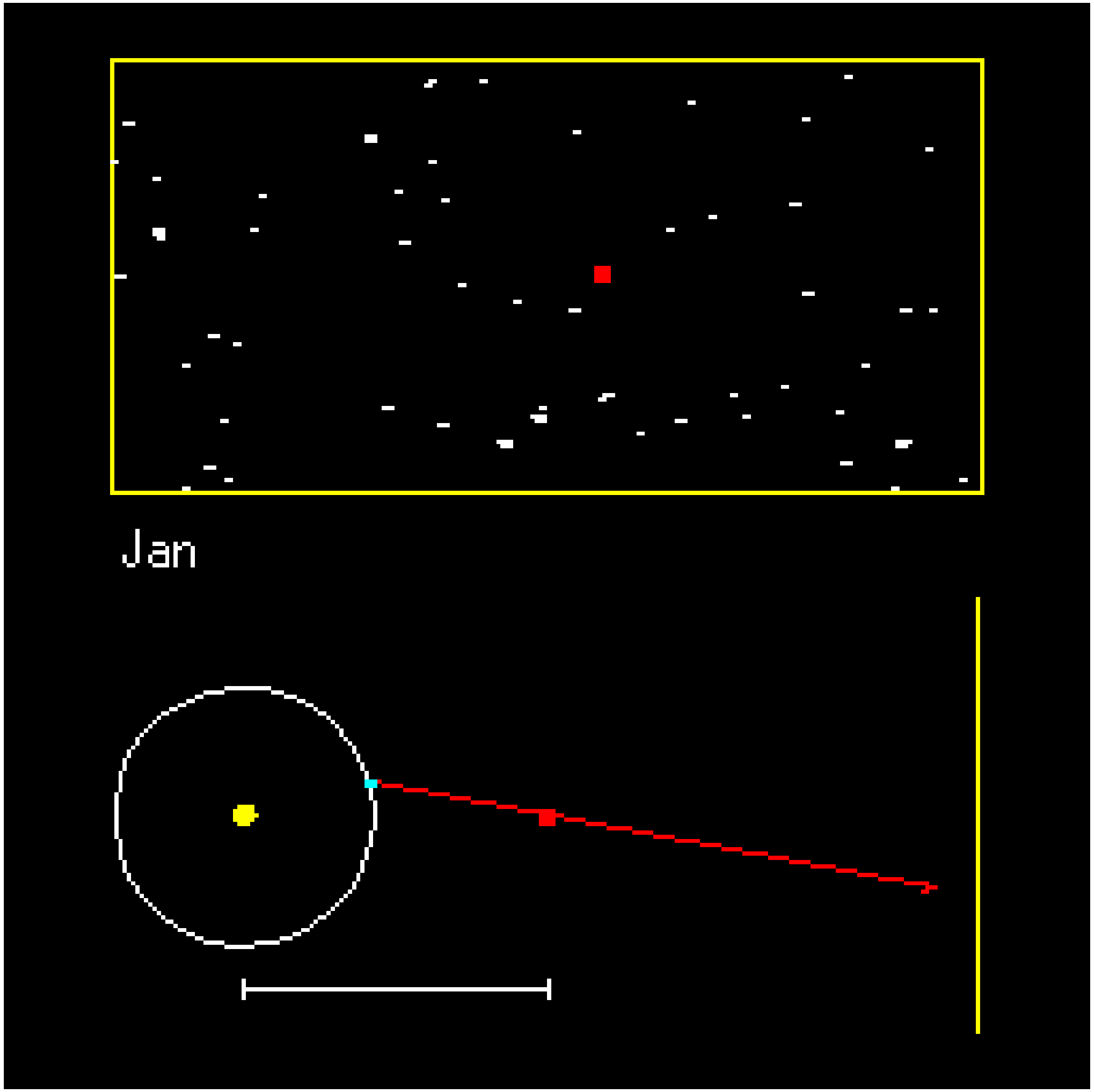

The “distance ladder”

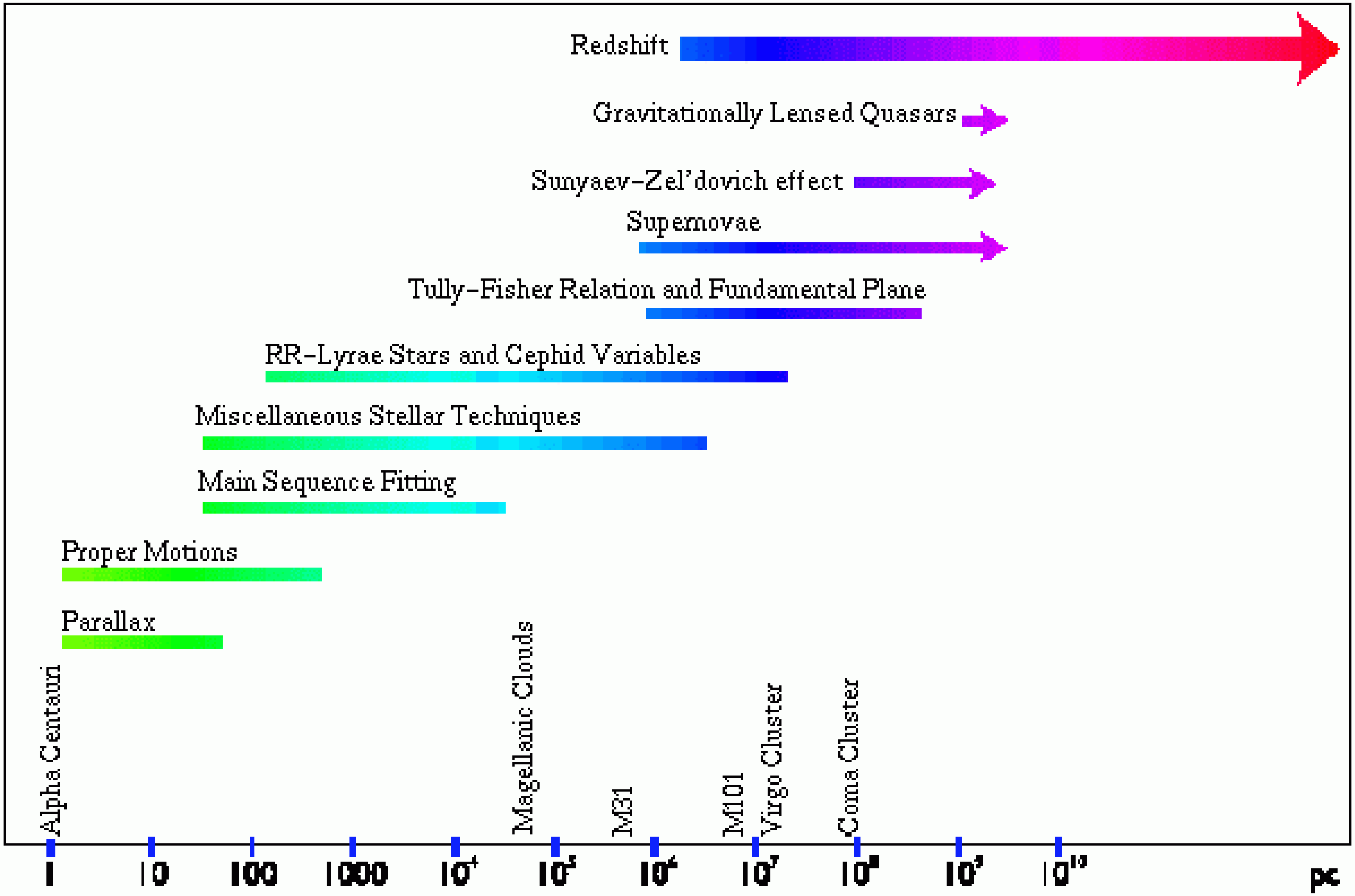

Figure 3.2: *The different distance estimators. This seemingly simple plot shows a grand overview of our efforts to measure distances in the Universe. Adapted from [Rowan-Robinson, 1985] and [Roth and Primack, 1996].*

(Stellar) Standard Candles

- Main Sequence fitting: Calibrate the luminosity of main sequence stars in nearby clusters with parallax distances and fit clusters farther out. Good to 10-100 kpc.

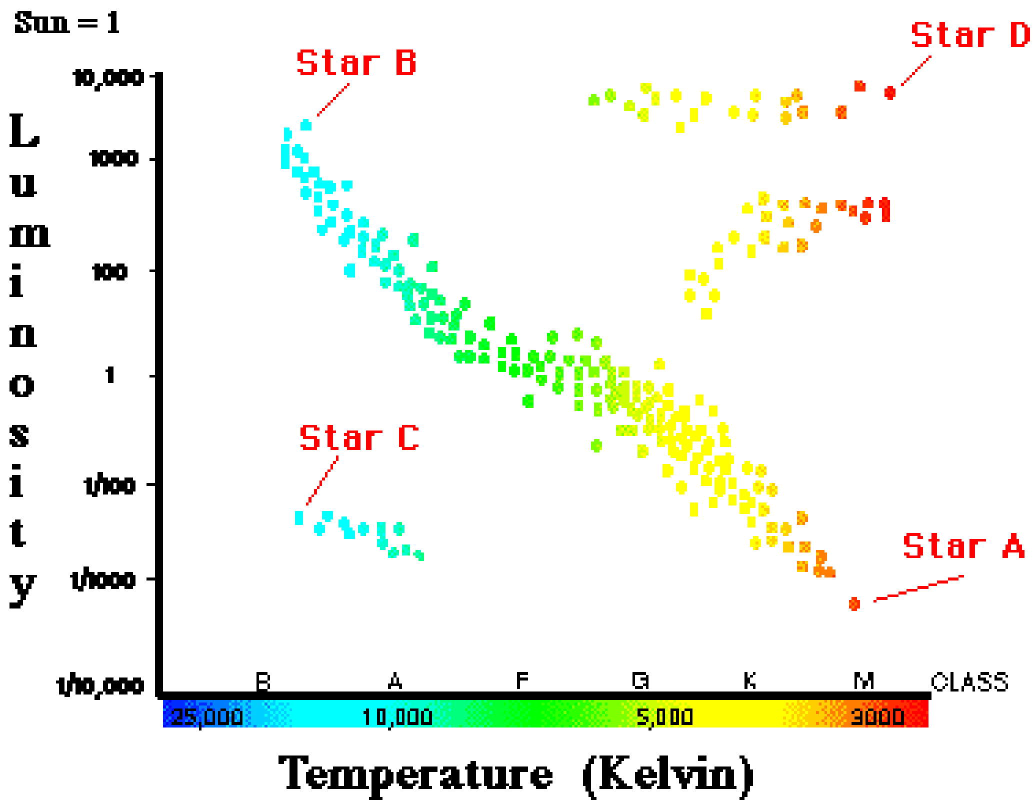

The “distance ladder”

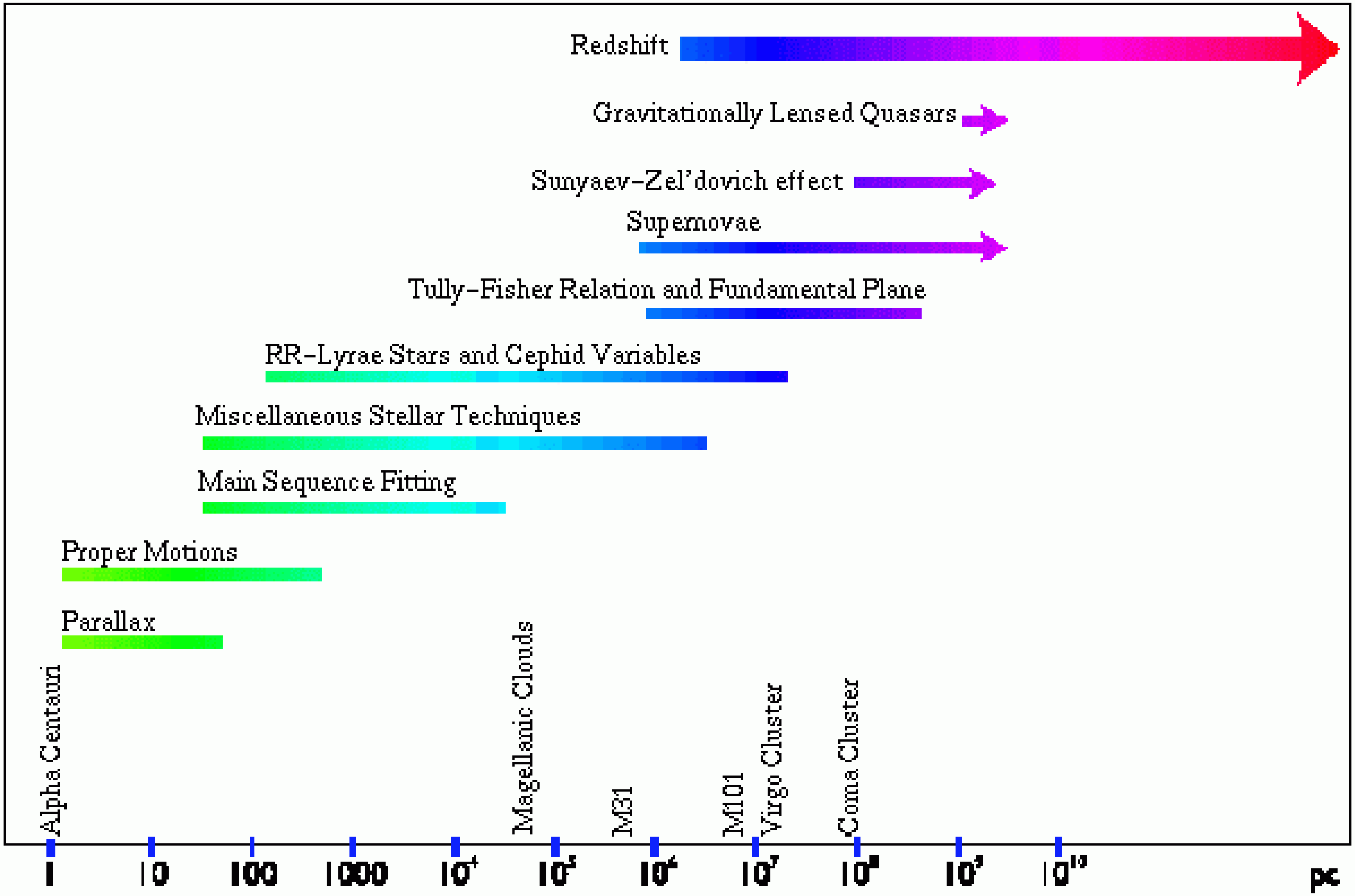

Figure 3.2: *The different distance estimators. This seemingly simple plot shows a grand overview of our efforts to measure distances in the Universe. Adapted from [Rowan-Robinson, 1985] and [Roth and Primack, 1996].*

(Stellar) Standard Candles

- Luminosity functions
  - Choose a type of object with a characteristic distribution of absolute luminosities
  - Measure distribution of apparent luminosities in a distant galaxy
  - Scale to match true luminosities, get distance
  - Globular clusters and planetary nebulae good to ~50-100 Mpc

(Stellar) Standard Candles

- Surface brightness fluctuations (SBF)
  - Distant objects appear smaller
  - More stars per pixel in a galaxy far, far away
  - Smoother light distribution, less variation from pixel to pixel
  - Amplitude of fluctuations proportional to distance
  - Good to ~100 Mpc, z~0.01

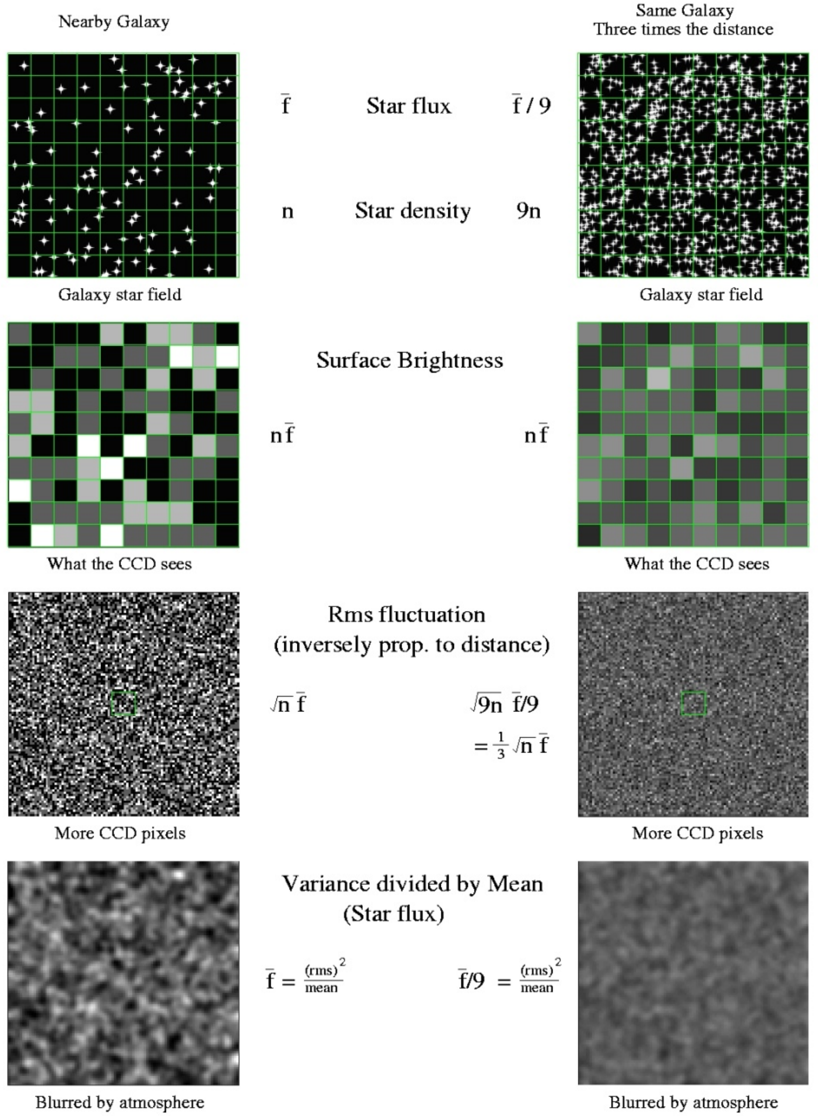
Nearby Galaxy
Same Galaxy
Three times the distance
$\bar{f}$ Star flux $\bar{f}/9$
n Star density 9n
Galaxy star field
Galaxy star field
Surface Brightness
$n\bar{f}$
$n\bar{f}$
What the CCD sees
What the CCD sees
Rms fluctuation
(inversely prop. to distance)
$\sqrt{n}\,\bar{f}$
$\sqrt{9n}\,\bar{f}/9$
$= \frac{1}{3}\sqrt{n}\,\bar{f}$
More CCD pixels
More CCD pixels
Variance divided by Mean
(Star flux)
$\bar{f} = \frac{(\mathrm{rms})^2}{\mathrm{mean}}$
$\bar{f}/9 = \frac{(\mathrm{rms})^2}{\mathrm{mean}}$
Blurred by atmosphere
Blurred by atmosphere

(Stellar) Standard Candles

- Cepheid and RR Lyrae variables
  - Pulsating stars which change in brightness with a characteristic period
  - Period is proportional to absolute luminosity
  - Common and bright (esp. Cepheids), thus visible in nearby galaxies
  - Good to ~20 Mpc

The "distance ladder"

- Different techniques useful at different distances: use nearby standards to calibrate more distant ones where they overlap
- *Cepheids are a key step:* many in the Milky Way and LMC, so distances are directly measurable by parallax, yet bright enough to overlap many secondary distance indicators
- Cepheids $\Rightarrow$ luminosity functions, SBF ($\longrightarrow$ galaxy kinematics, SNe Ia)

Edwin Hubble (1888 – 1953)

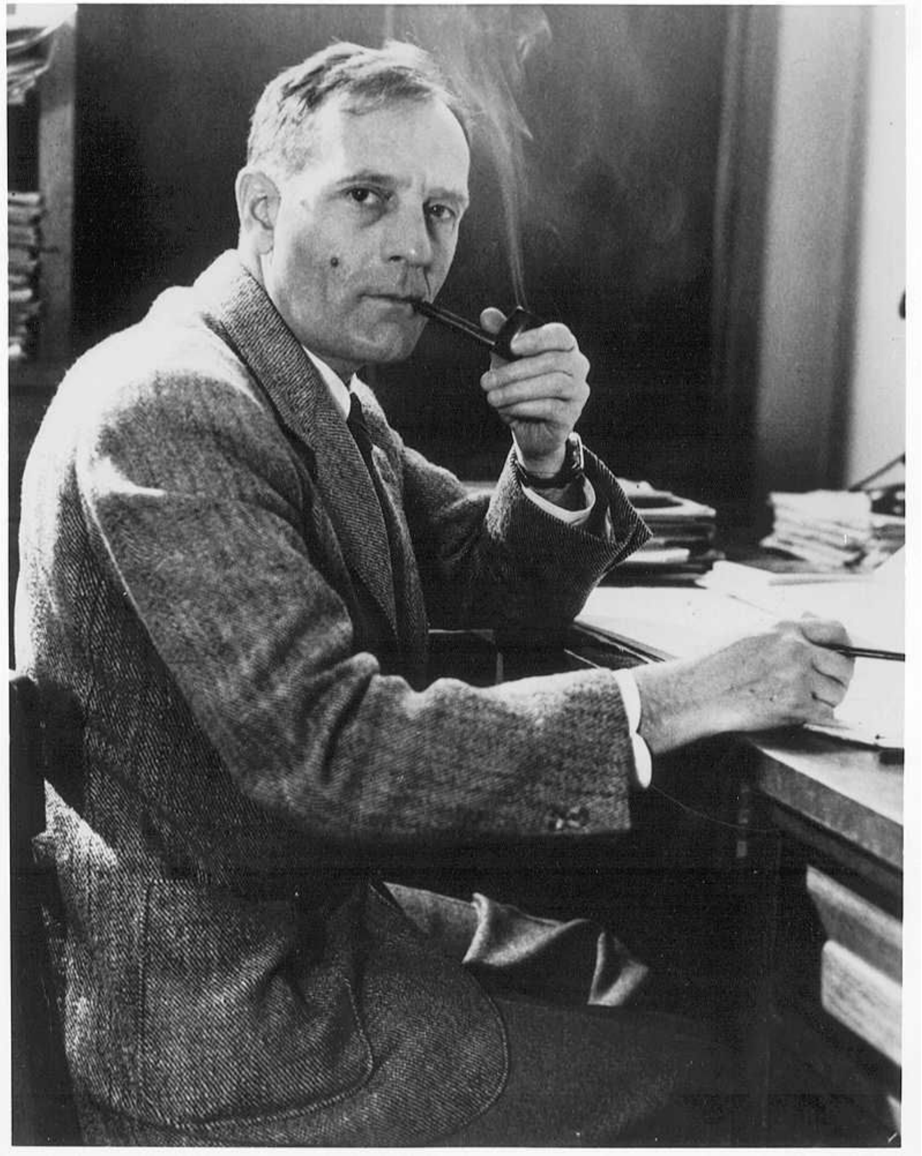

The redshift-distance relation

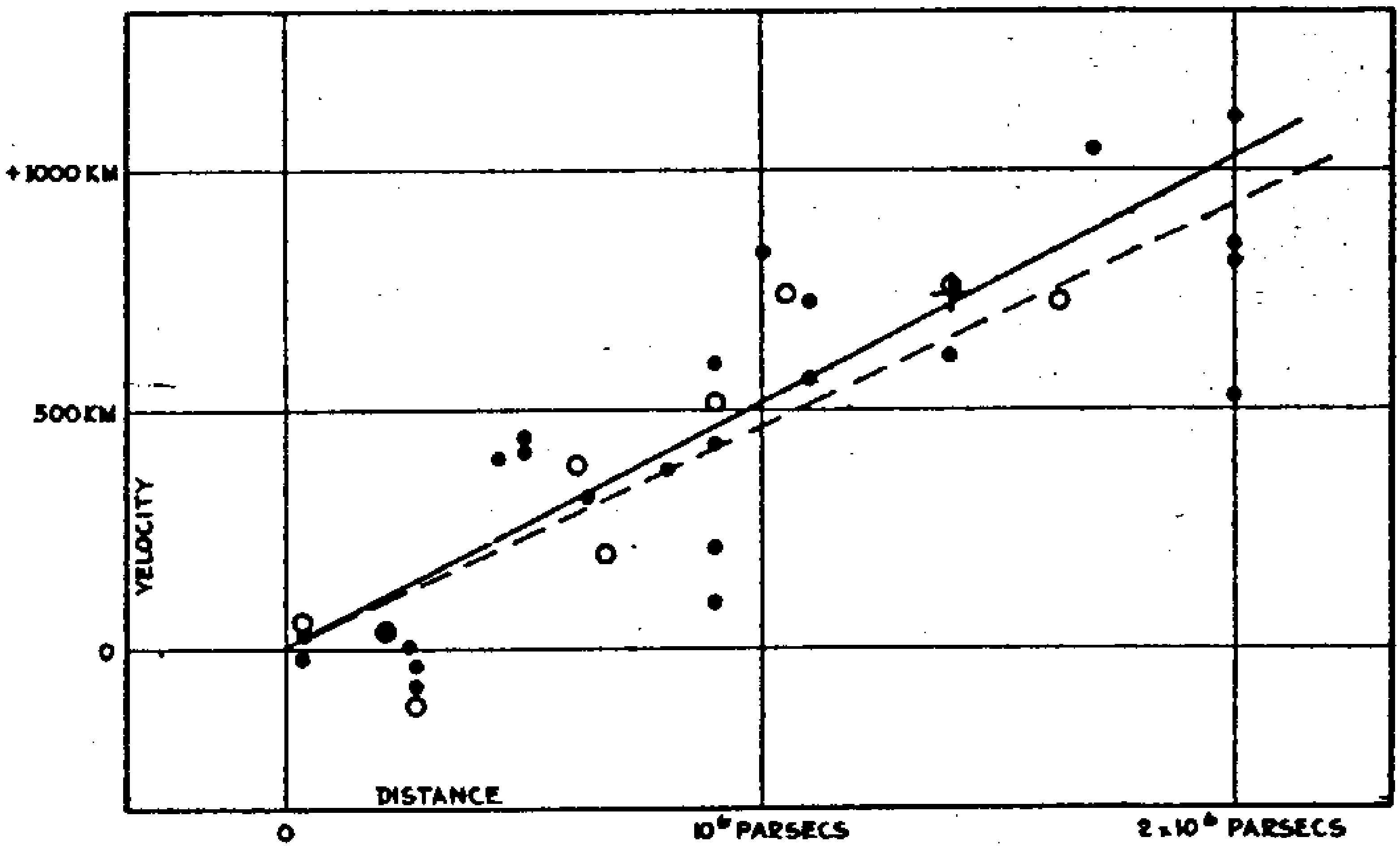

FIGURE 1

Hubble (1938)

A “modern” Hubble diagram

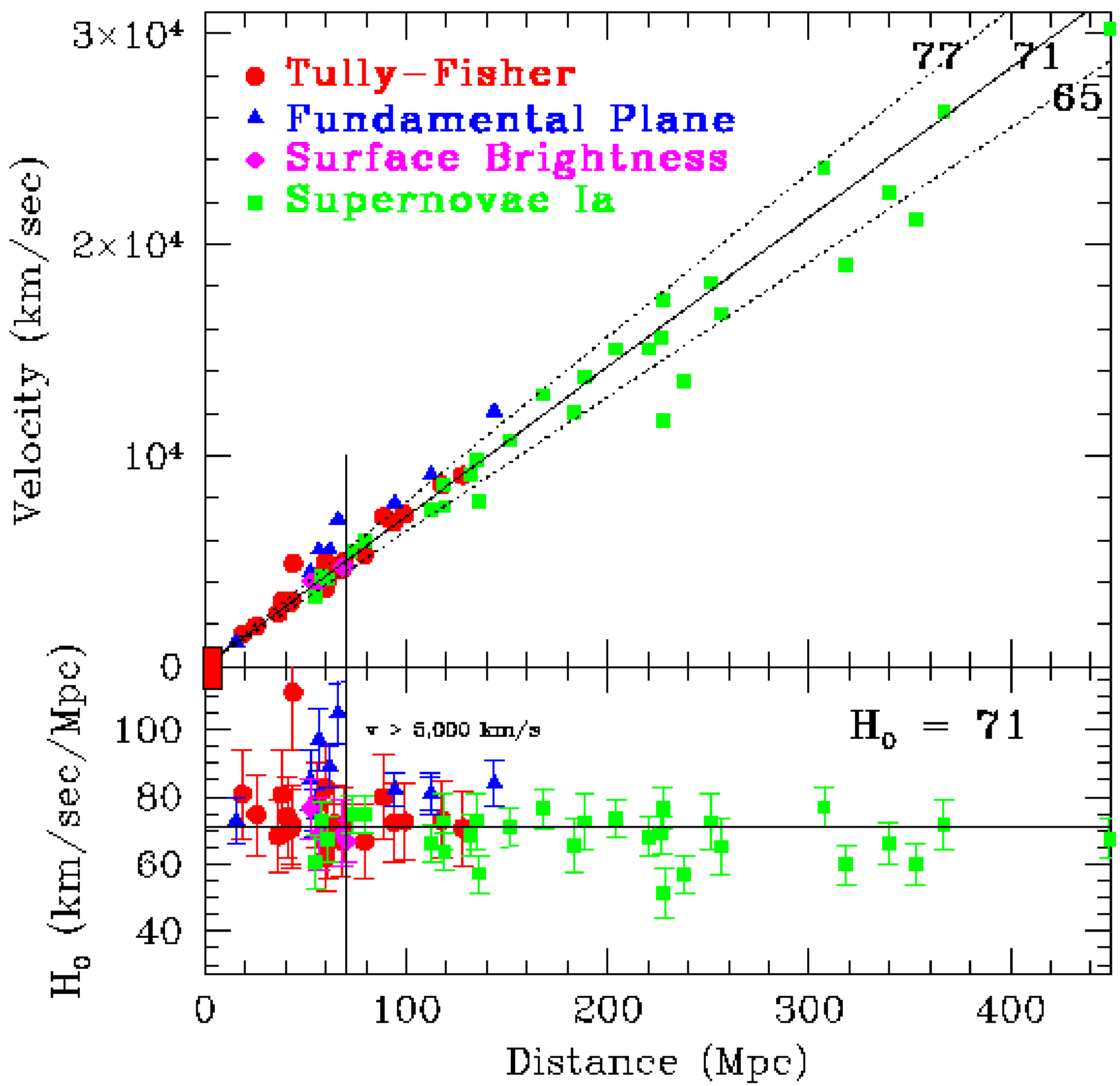

Key results

- Most galaxies are moving away from us
- The recession speed v is larger for more distant galaxies. The relation between recess velocity v and distance d fulfills a linear relation:

$$v = H_0 \times D$$

- Hubble's measurement of the constant H_0:

$$H_0 = 500 \text{ km/s/Mpc}$$

- Today's best fit value (based on Cepheids) of the constant:

$$H_0 = 72 \text{ km/s/Mpc}$$

Why was Hubble so far off?

- Distance measurement based on the period-luminosity relation of Cepheid stars
- What are Cepheids? They are variable pulsating stars

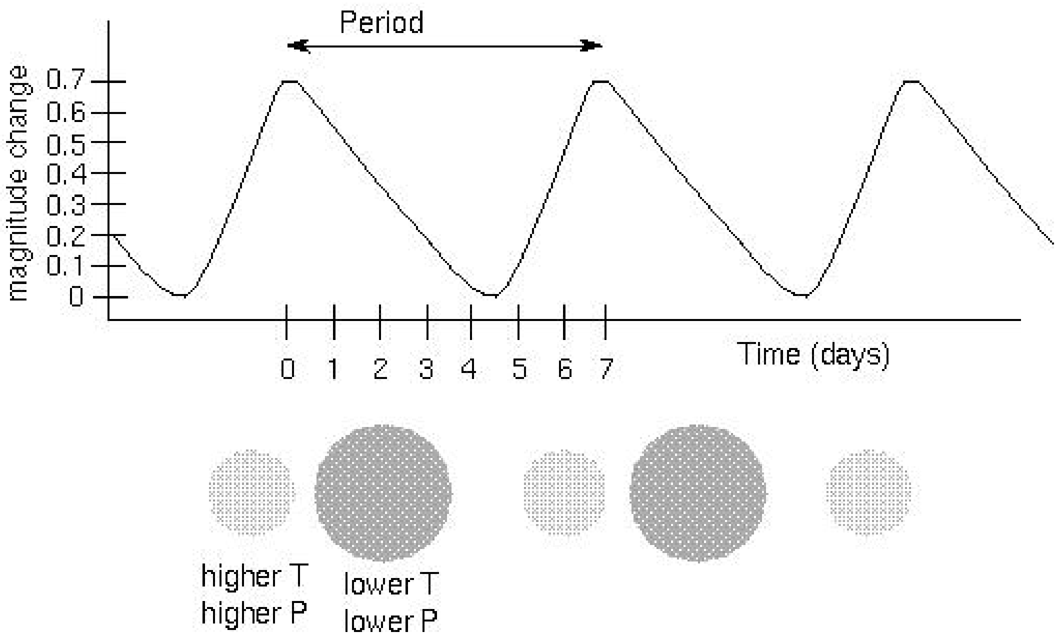

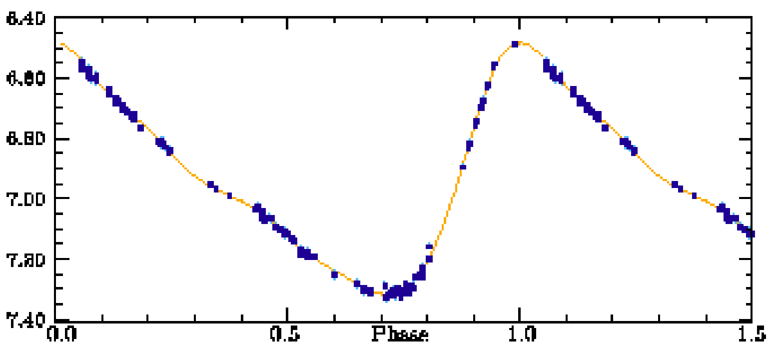

Why was Hubble so far off ?

- There exists a luminosity-period relation for Cepheid stars

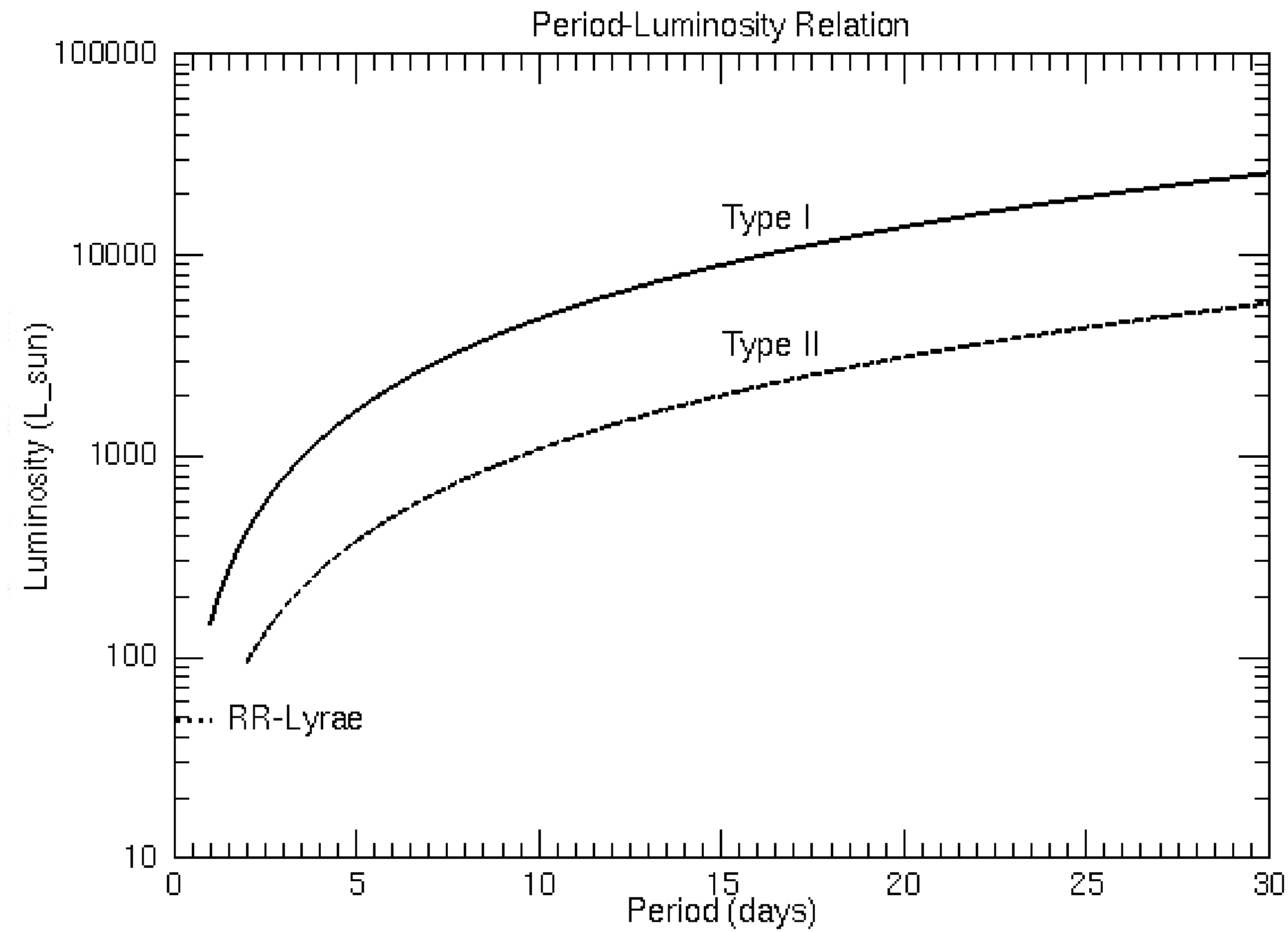

Why was Hubble so far off?

- there are two populations of Cepheids (but Hubble was not aware of that)
  - type I: metal rich stars (disk of galaxies)
  - type II: metal poor stars (halo of galaxies)
  - type II Cepheids ("W Virginis") are less luminous than type I Cepheids ("δ Cephei")

Why was Hubble so far off?

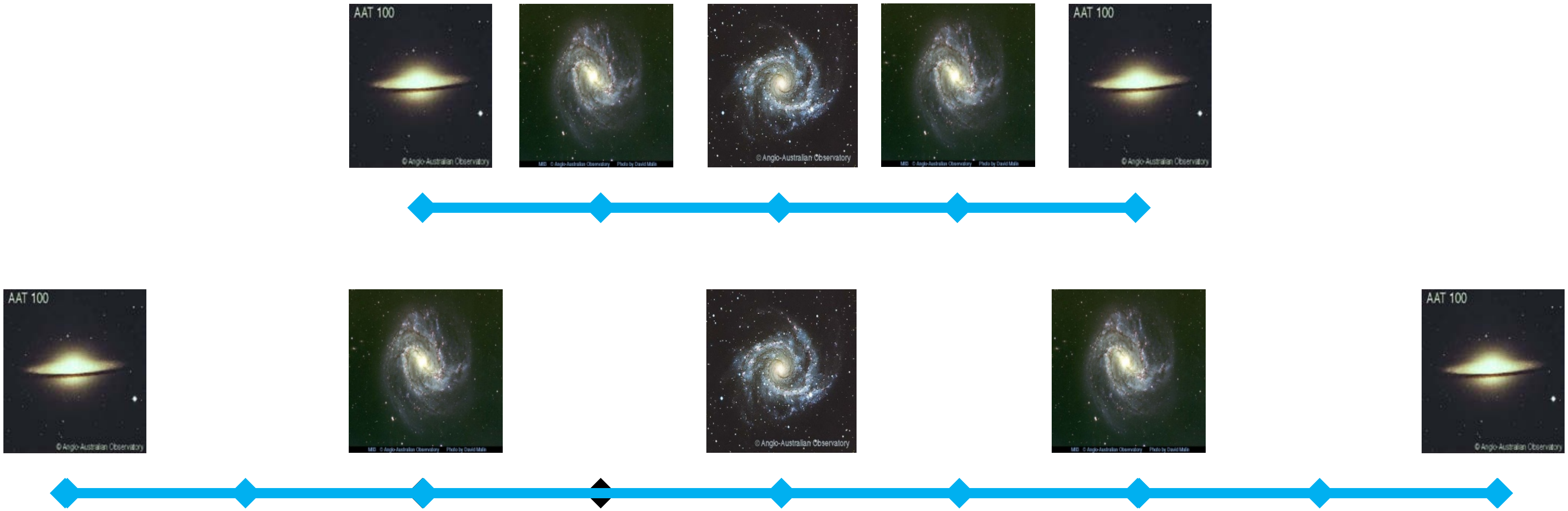

initial distance: 1 length unit
final distance: 2 length units
recess velocity: 1 length unit per time unit

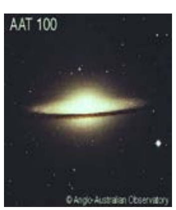

initial distance: 2 length units
final distance: 4 length units
recess velocity: 2 length units per time unit

Why was Hubble so far off?

- Distance scale was calibrated based on type II Cepheids
- Distances to other galaxies were measured using type I Cepheids
- “yard stick” was systematically too small

More about δ-Cephei Stars

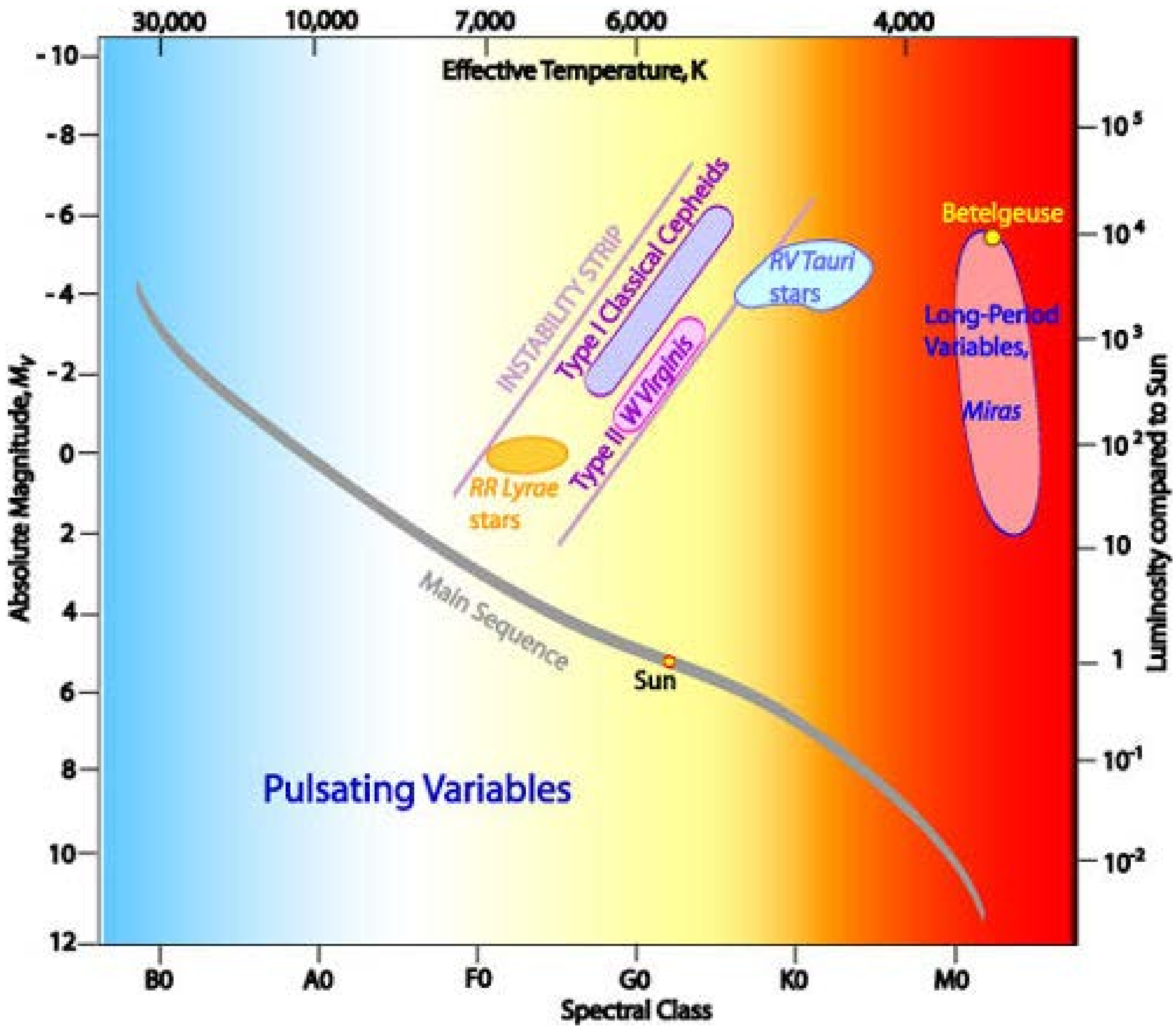

More about δ-Cephei Stars

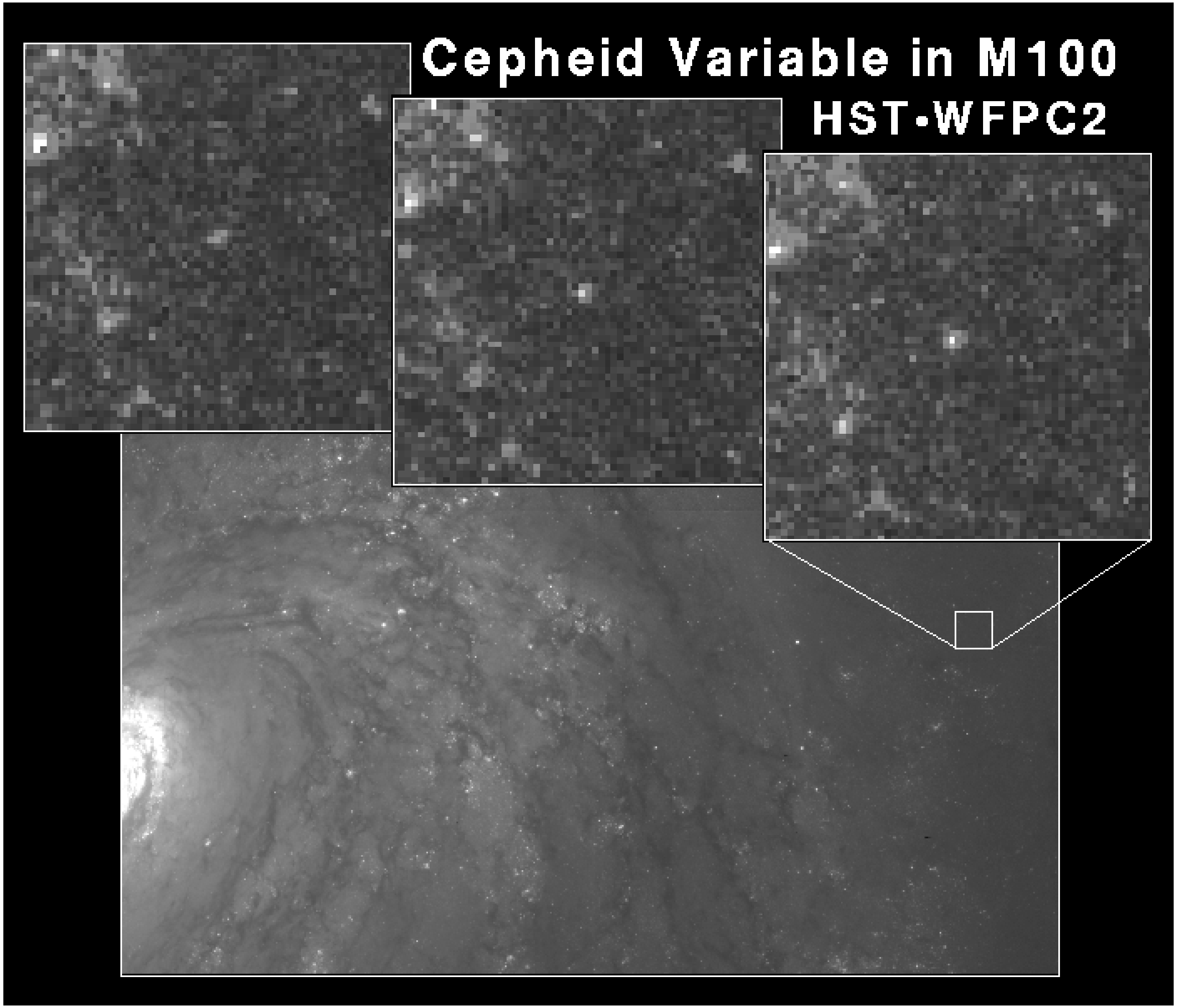

More about δ-Cephei Stars

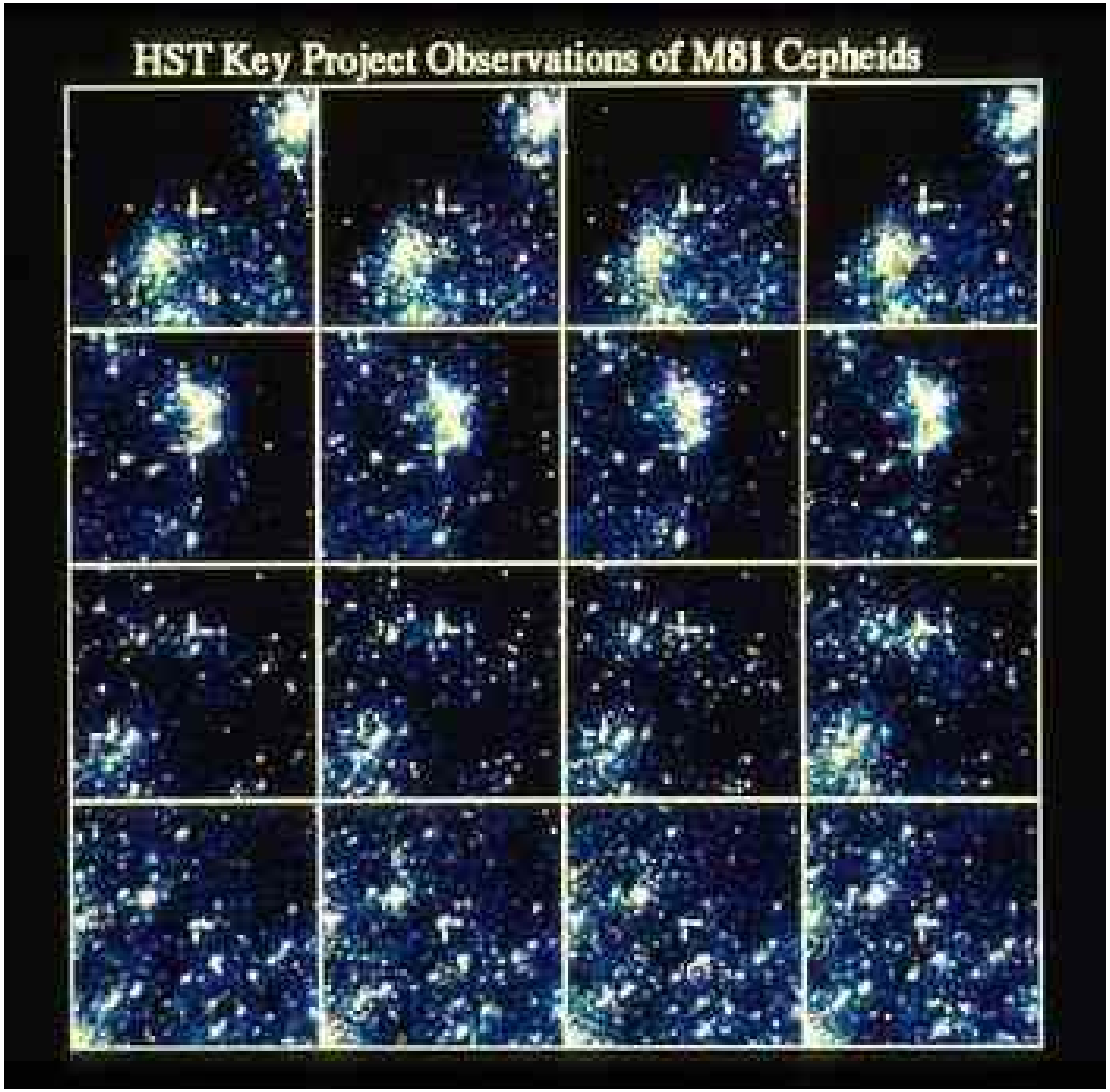

More about δ-Cephei Stars

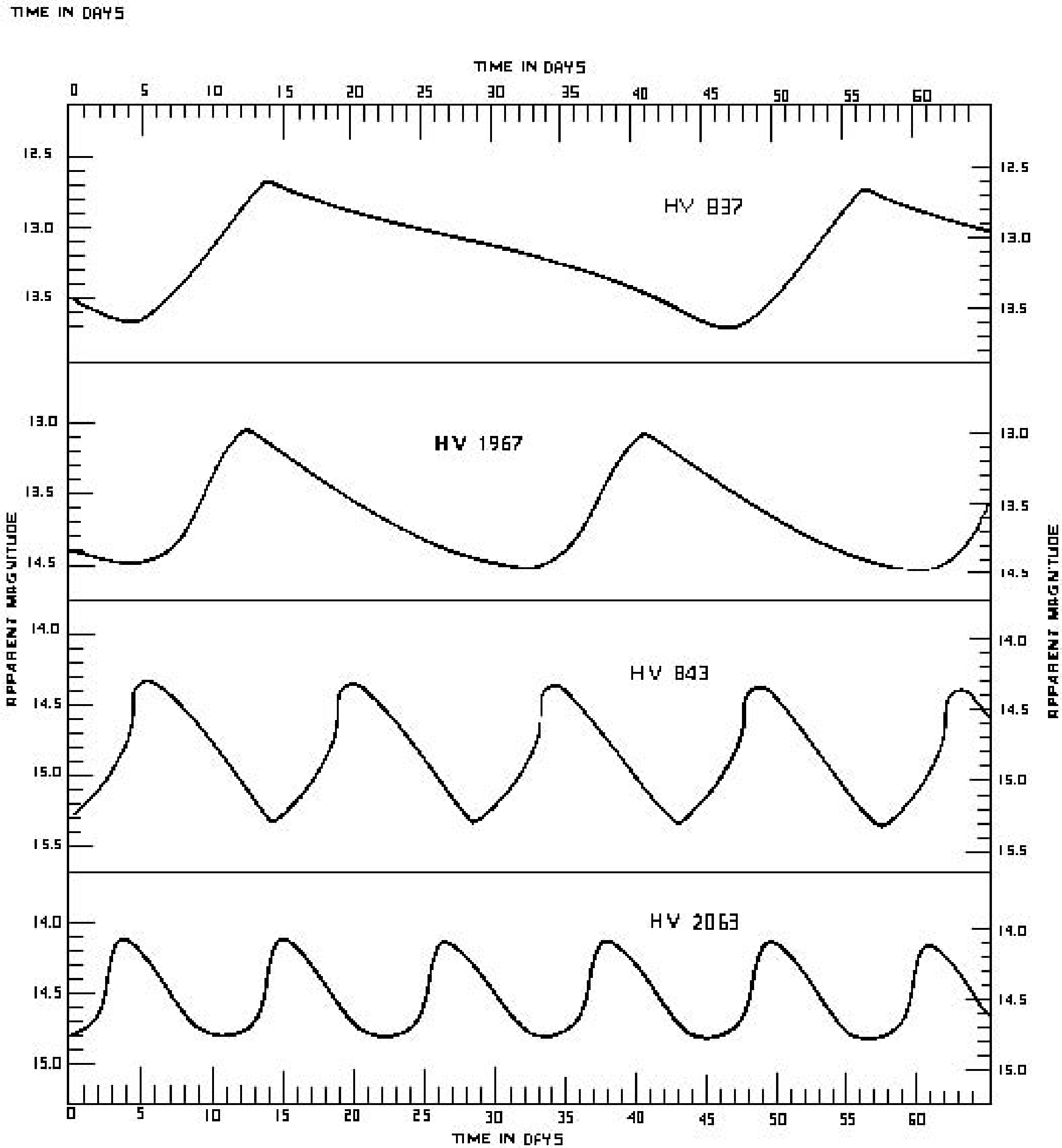

Light-curves :

$$P = 10^{(M-a)/b}$$

$$P_1 - P_2 \approx 0.44^{(M1-M2)/mag}$$

More about δ-Cephei Stars

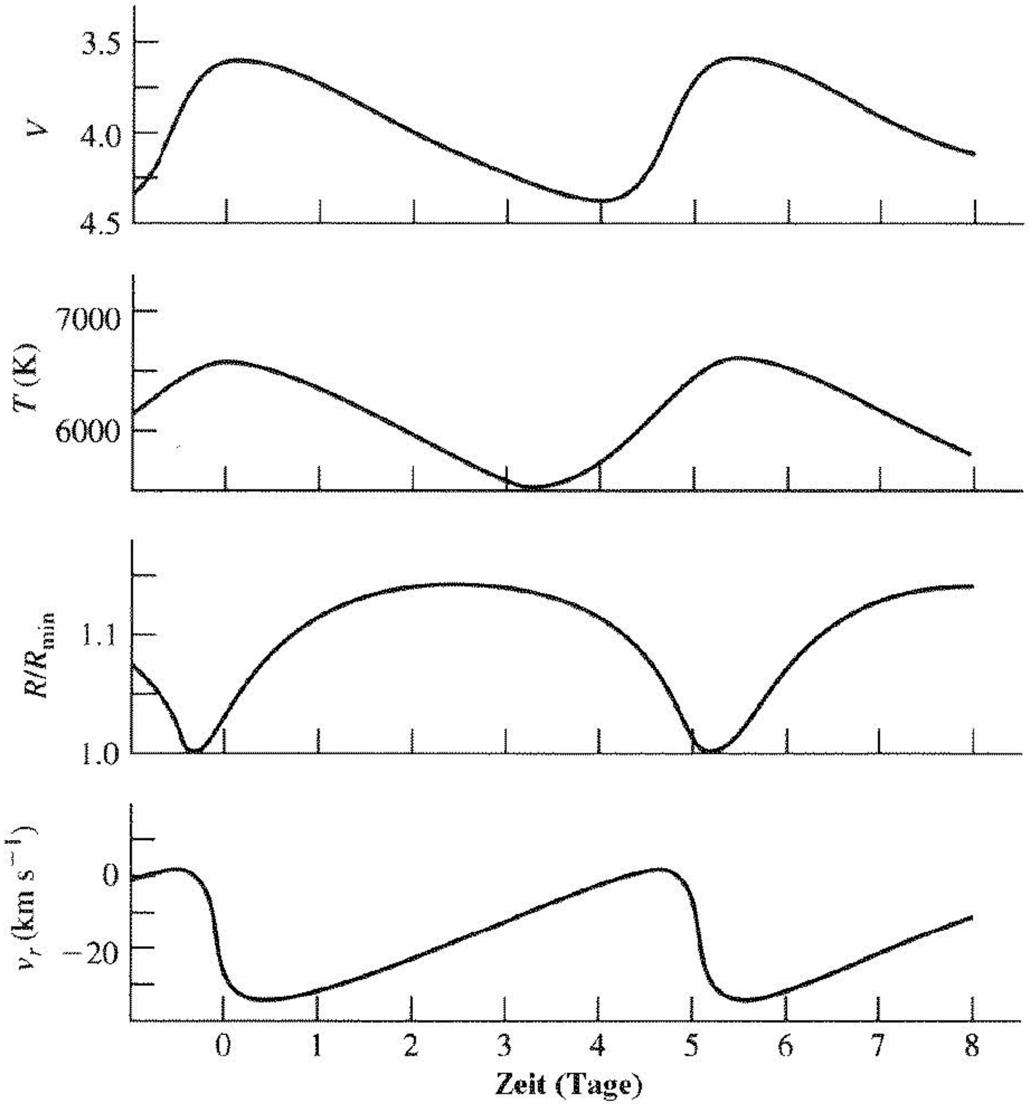

More about δ-Cephei Stars

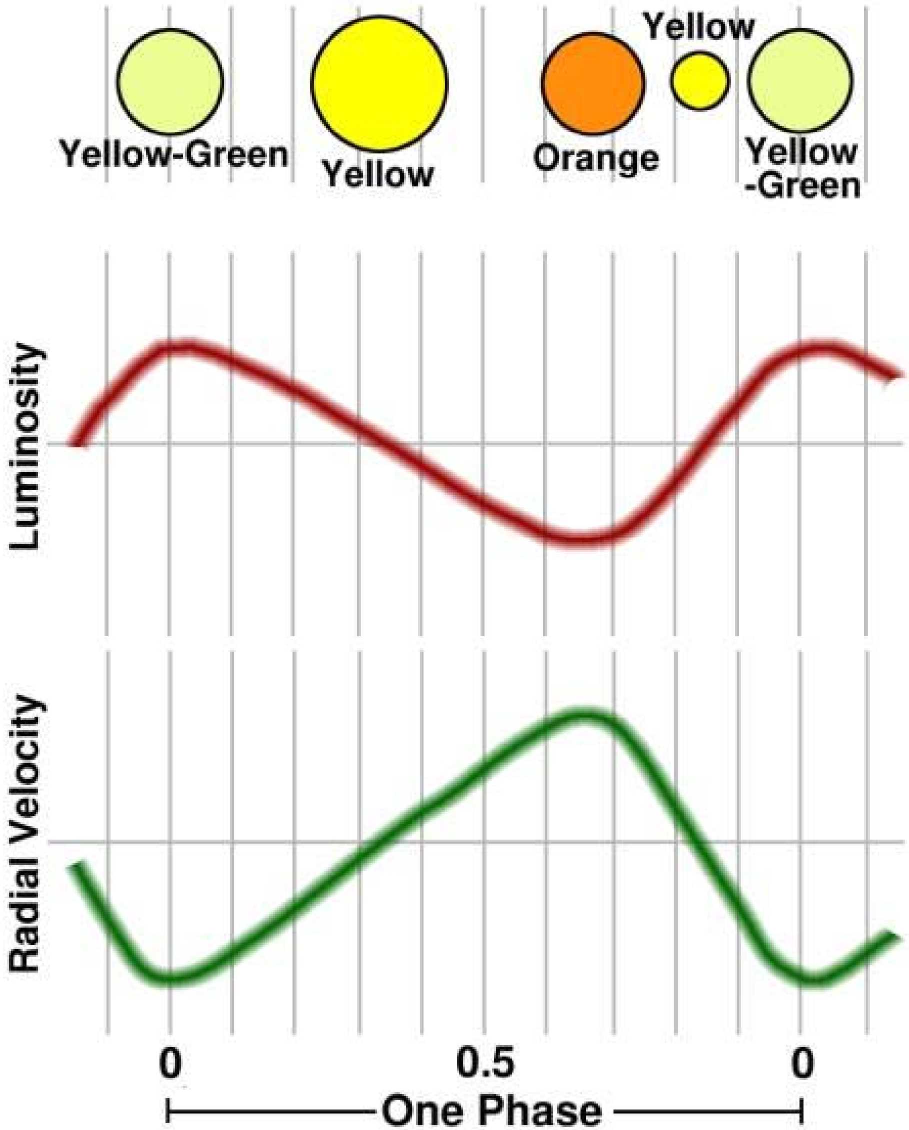

- Use the Hubble diagram (*m-M vs.* log *z*)
  - $m-M=5\log(z)+25+5\log(c)-5\log(H_0)$
- Note that the slope is given here.

- Hubble constant can be derived when the absolute luminosity *M* is known
  - $\log H_0=\log(z)+5+\log(c)-0.2(m-M)$

Hubble constant from SNe Ia

- Calibrate the absolute luminosity
  - through Cepheids
    - ‘classical distance ladder’
      - depends on the accuracy of the previous rungs on the ladder
      - LMC distance, P-L(-C) relation, metallicities
    - HST program (Sandage, Tammann)
    - HST Key Programme (Freedman, Kennicutt, Mould, Madore)
  - through models
    - extremely difficult (but possible!)

Absolute Magnitudes of SNe Ia

SN	Galaxy	m-M	M_B	M_V	M_I	Δm_{15}
1937C	IC 4182	28.36 (12)	-19.56 (15)	-19.54 (17)	-	0.87 (10)
1960F	NGC 4496	31.03 (10)	-19.56 (18)	-19.62 (22)	-	1.06 (12)
1972E	NGC 5253	28.00 (07)	-19.64 (16)	-19.61 (17)	-19.27 (20	0.87 (10)
1974G	NGC 4414	31.46 (17)	-19.67 (34)	-19.69 (27)	-	1.11 (06)
1981B	NGC 4536	31.10 (12)	-19.50 (18)	-19.50 (16)	-	1.10 (07)
1989B	NGC 3627	30.22 (12)	-19.47 (18)	-19.42 (16)	-19.21 (14	1.31 (07)
1990N	NGC 4639	32.03 (22)	-19.39 (26)	-19.41 (24)	-19.14 (23	1.05 (05)
1998bu	NGC 3368	30.37 (16)	-19.76 (31)	-19.69 (26)	-19.43 (21	1.08 (05)
1998aq	NGC 3982	31.72 (14)	-19.56 (21)	-19.48 (20)	-	1.12 (03)
Straight mean			-19.57 (04)	-19.55 (04)	-19.26 (0 6)	
Weighted mean			-19.56 (07)	-19.53 (06)	-19.25 (0 9)	

(Saha et al. 1999)

Nearby SNe Ia

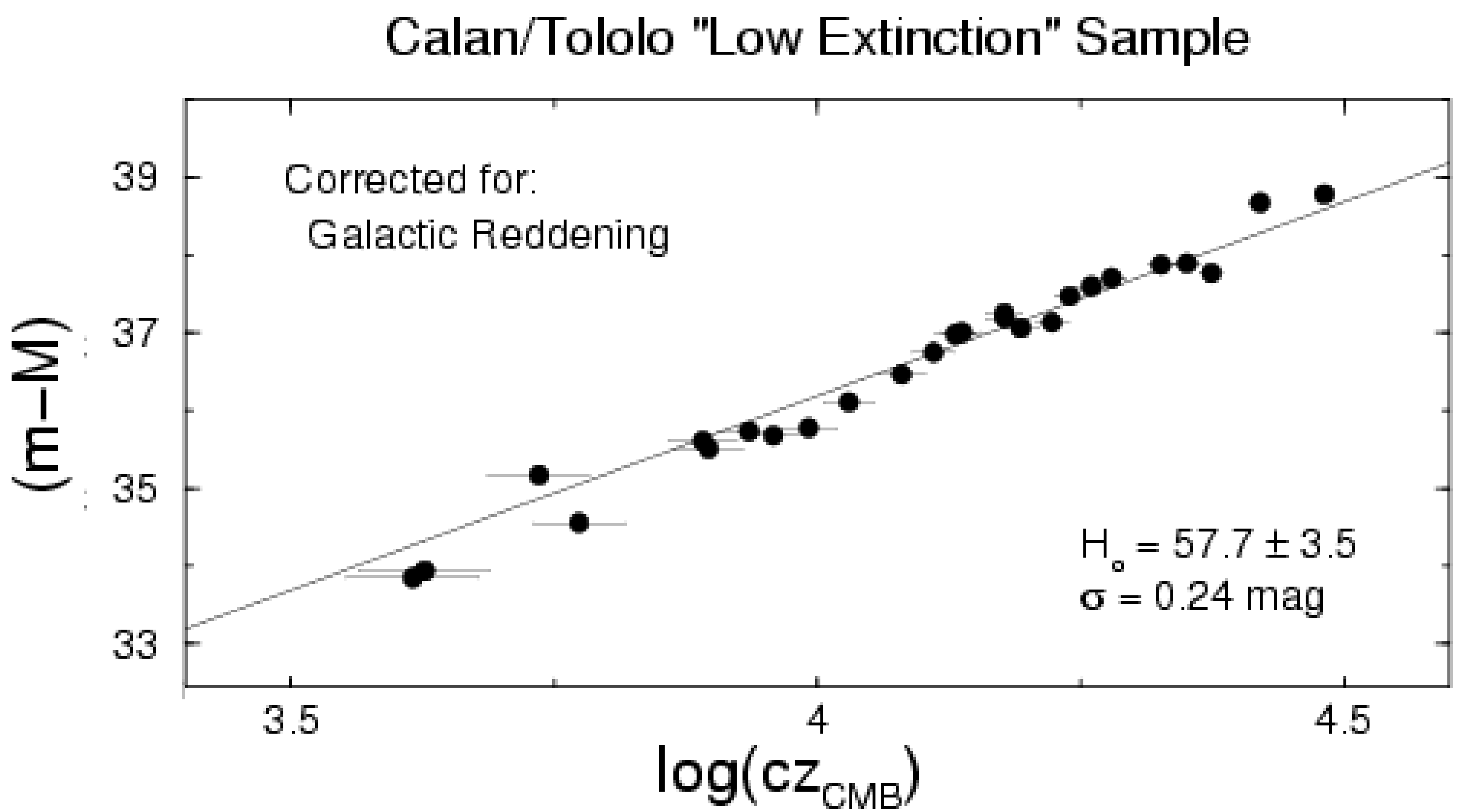

Phillips et al. (1999)

Light curve shape – luminosity

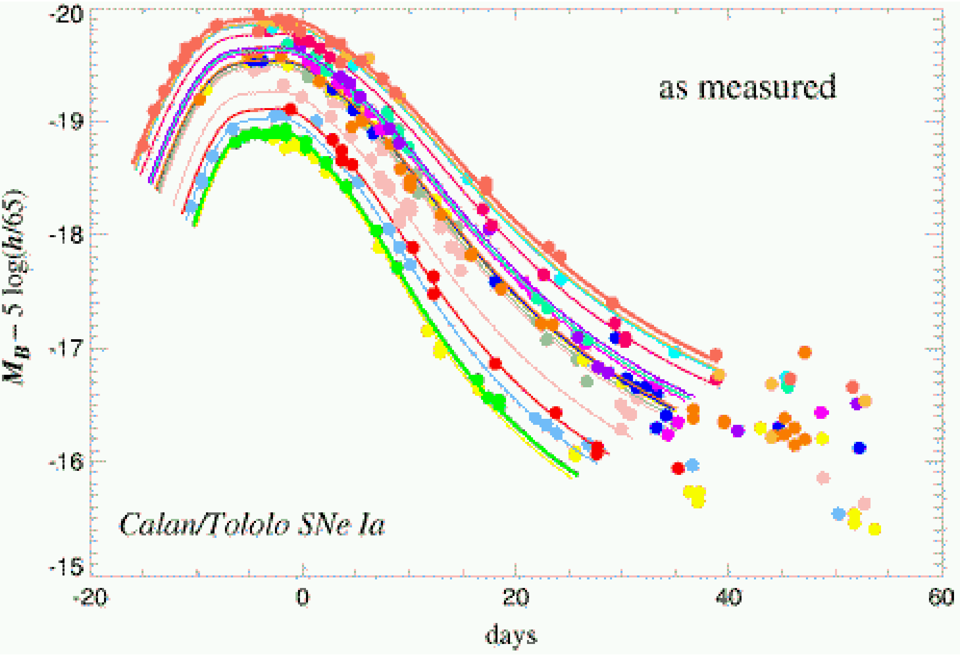

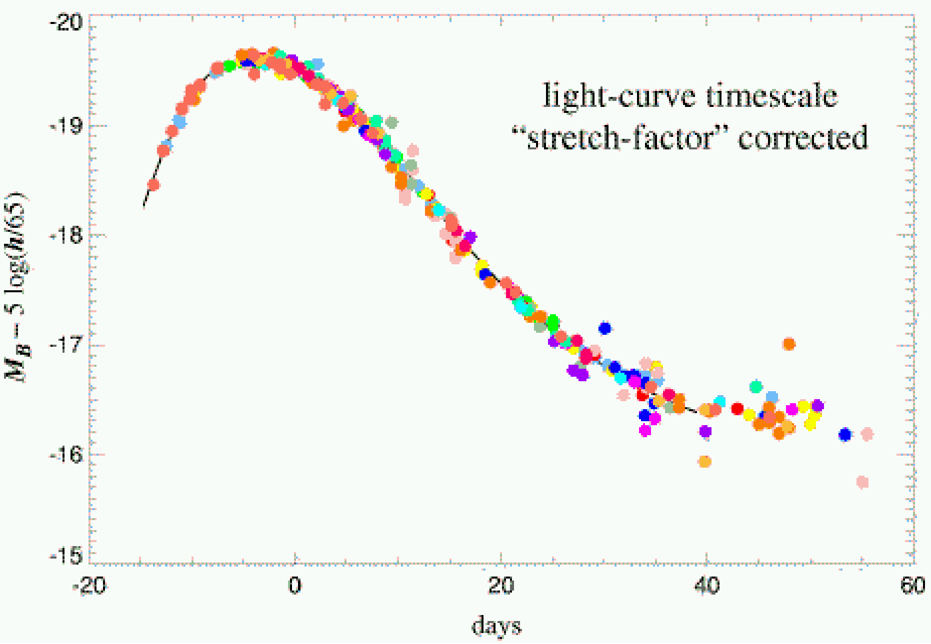

(B-band light curves; Calan/Tololo sample, Kim et al. 1997)

After calibration:: *SNe Ia look like good "standard candles"!*

The nearby SN Ia sample

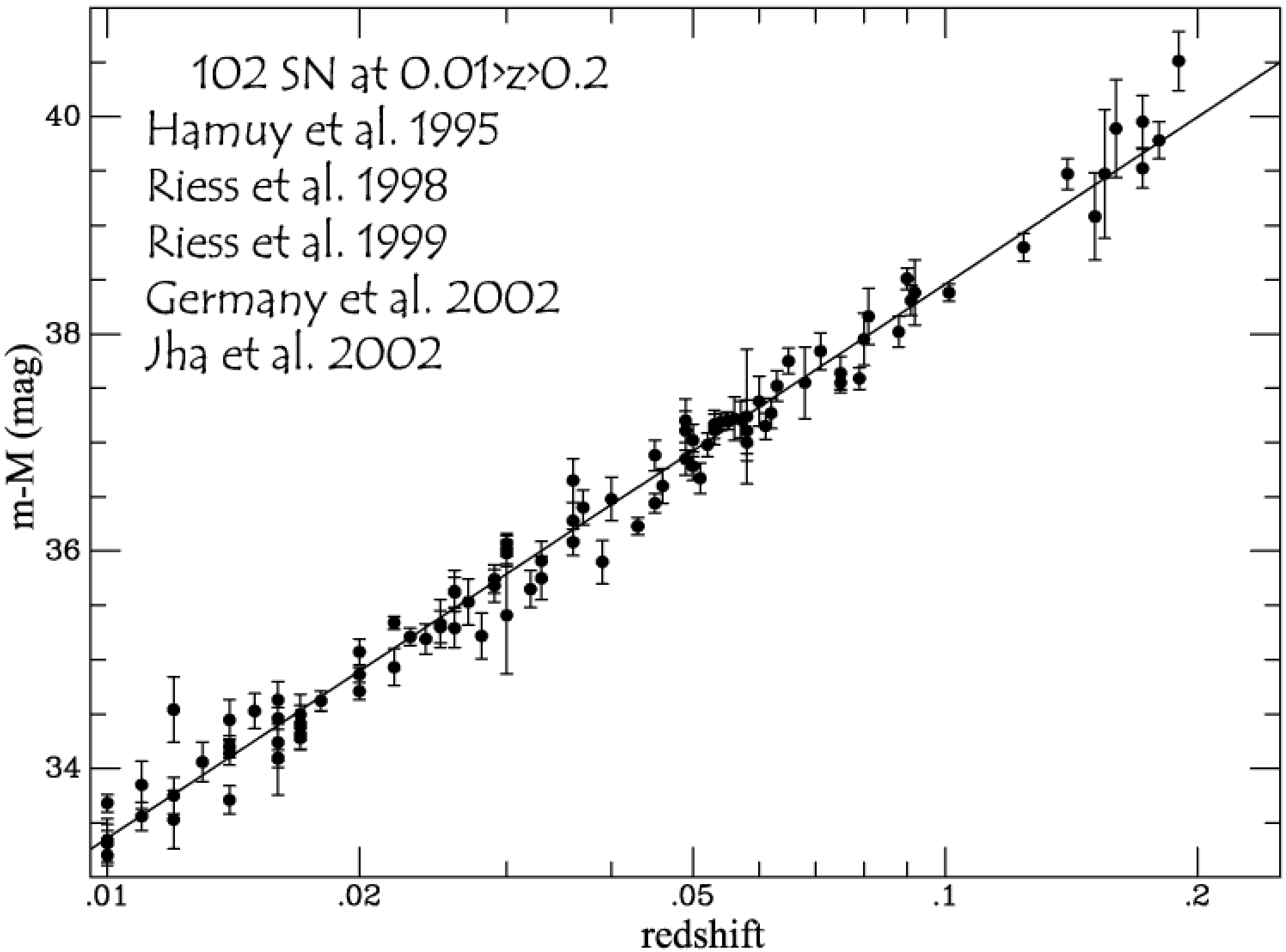

Evidence for good Distances!

Hubble constant from SNe Ia

- Extremely good (relative) distance indicators
  - distance accuracy better than 10%
- Uncertainty in H_0 mostly from the LMC and the Cepheid P-L relation
- Today's best value (Cepheids + SN Ia):

$$\boxed{H_0 = (73.24 \pm 1.74) \text{ km/s/Mpc}}$$

(Riess et al., Astrophys. Journal 826, 31 (2016))

H_0 from CMB

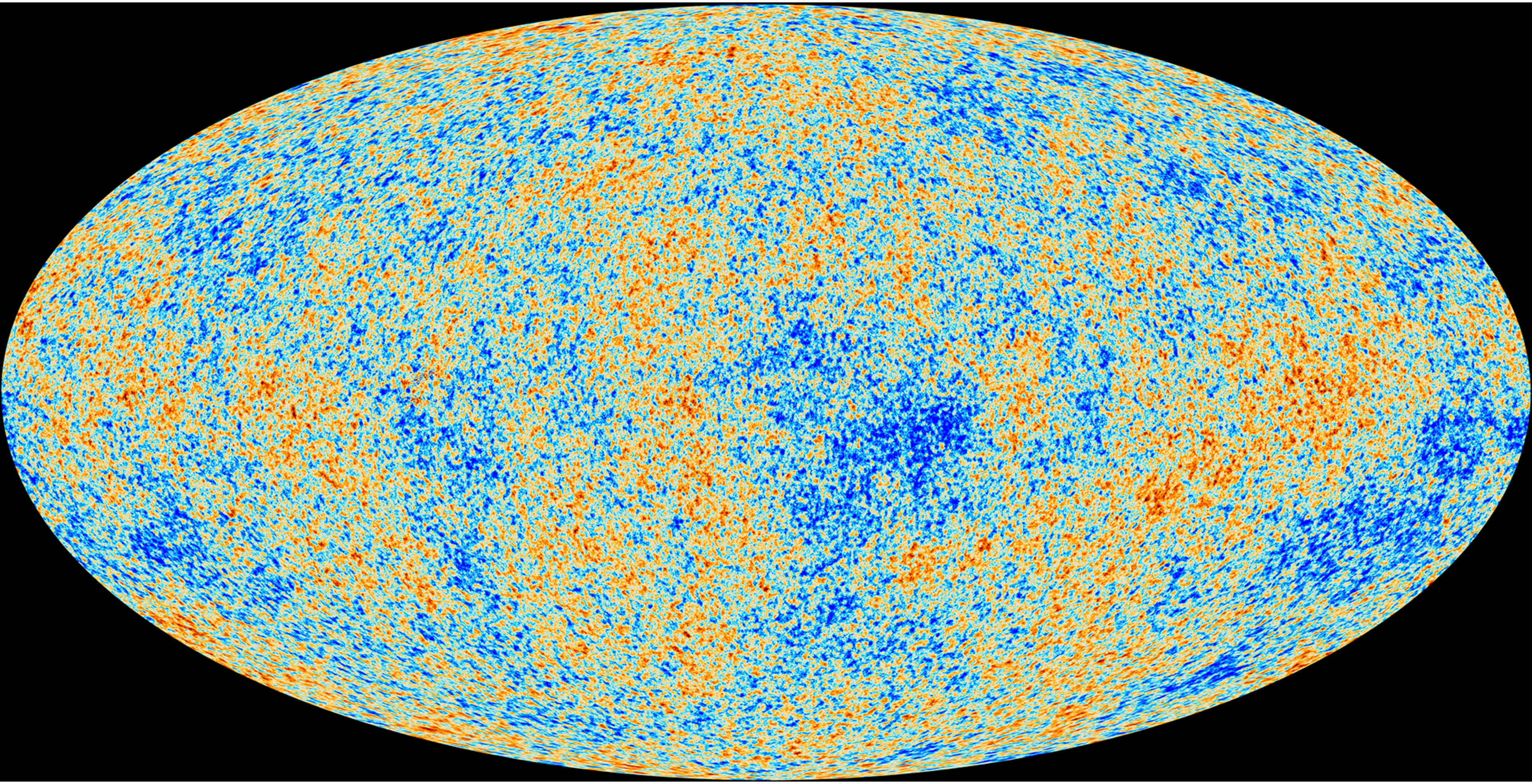

Fit a model to the CMB power spectrum (e.g. ΛCDM) ➡ H_0

Cosmological parameters from Planck

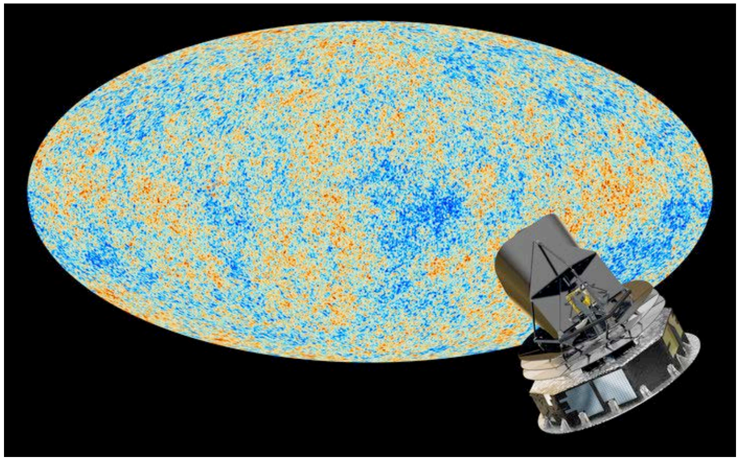

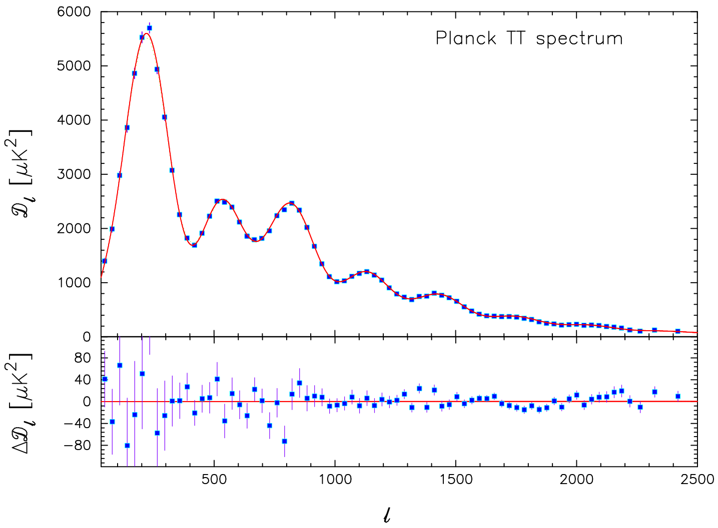

Parameter	Best fit	68% limits
$\Omega_b h^2$	0.022068	0.02207 ± 0.00033
$\Omega_c h^2$	0.12029	0.1196 ± 0.0031
$100\theta_{MC}$	1.04122	1.04132 ± 0.00068
τ	0.0925	0.097 ± 0.038
n_s	0.9624	0.9616 ± 0.0094
$\ln(10^{10}A_s)$	3.098	3.103 ± 0.072
Ω_Λ	0.6825	0.686 ± 0.020
Ω_m	0.3175	0.314 ± 0.020
σ_8	0.8344	0.834 ± 0.027
z_{re}	11.35	$11.4^{+4.0}_{-2.8}$
H_0	67.11	67.4 ± 1.4
$10^9 A_s$	2.215	2.23 ± 0.16
$\Omega_m h^2$	0.14300	0.1423 ± 0.0029
$\Omega_m h^3$	0.09597	0.09590 ± 0.00059
Y_P	0.247710	0.24771 ± 0.00014
Age/Gyr	13.819	13.813 ± 0.058
z_*	1090.43	1090.37 ± 0.65
r_*	144.58	144.75 ± 0.66
$100\theta_*$	1.04139	1.04148 ± 0.00066
z_{drag}	1059.32	1059.29 ± 0.65
r_{drag}	147.34	147.53 ± 0.64
k_D	0.14026	0.14007 ± 0.00064
$100\theta_D$	0.161332	0.16137 ± 0.00037
z_{eq}	3402	3386 ± 69
$100\theta_{eq}$	0.8128	0.816 ± 0.013
$r_{drag}/D_V(0.57)$	0.07130	0.0716 ± 0.0011

The Cosmic Distance Scale H_0

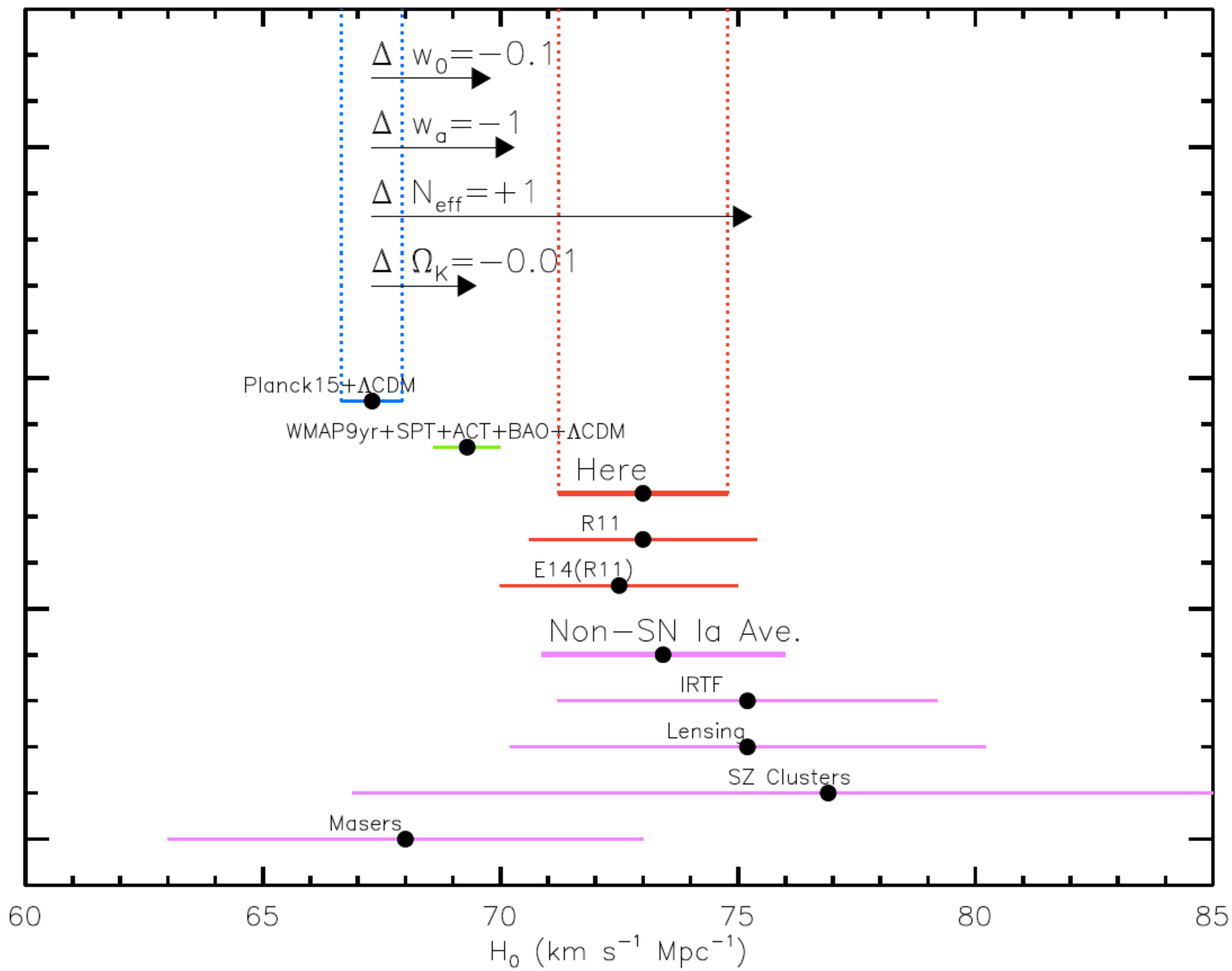

Riess et al., ApJ (2016)

H_0 : What can be wrong?

Cepheids: Calibration? Systematics?

Type Ia supernovae: Systematics?

CMB: Data reduction? Systematics?

Or: "New physics"?

Way out: Use other (independent) methods!